SCANNING ELECTRON MICROSCOPE STUDIES OF CATHODOLUMINESCENCE IN ZnS AND CdS CRYSTALS

by

Subrata Datta

A Thesis Submitted for the Degree of
Doctor of Philosophy of the
University of London

Department of Metallurgy and Materials Science
Imperial College of Science and Technology
London SW7 2BP

October 1977



TO MY MOTHER

FOR MORE THAN CAN BE MEASURED

ABSTRACT

An efficient spectroscopic detection system, developed in this group, for cathodoluminescence (CL) mode scanning electron microscopy (SEM) was used to study the luminescent properties of striated ZnS and CdS crystals in the temperature range 78 to 292K. The system was calibrated so that emission spectra could be obtained in 'absolute' form (ie. number of photon emitted per second versus wavelength).

Structurally complex ZnS platelets, when viewed in the SEM CL mode, reveal very striking local variations in the intensities and positions of both fundamental and impurity CL emission band. It is shown that these variations arise from structural changes, impurity segregation or internal electric field effects or a combination of them.

The peak position and shape of the fundamental or edge (conduction band to valence band recombination) CL band was systermatically studied in ZnS and CdS for different crystal structures, identified from birefingence measurements. The shape and temperature dependence of the "self-activated" (SA) ZnS CL band was also determined.

It is shown that the intensity of the fundamental and SA CL

emission bands can be expressed semiempirically as:

$$L(E) = L(E_o) \exp\left[g(E-E_o)^{\beta} \right]$$

where g and β are shape parameters, L is the intensity, E the photon energy and E_o is the photon energy at the maximum of the band. The temperature dependence of the edge band in hexagonal (2H) CdS and both the hexagonal and cubic (3C) modifications of ZnS as well as the hexagonal and cubic structures of the SA ZnS CL band have been investigated. The results indicated that around the band maximum the shape is Gaussian (ie. $\beta = 2$). However, for the low energy region of the band the shape becomes exponential (ie. $\beta = 1$) and the "Urbach tail" is obtained. In addition the high energy tail was also found to be exponential. Such low energy exponential tails have already been reported for the absorption edge of ZnS, CdS and also in the edge emission band of GaAs. The interpretaion of these results is discussed in relation to the Dow and Redfield (1972) internal electric microfield model for exponential edges. The relevant shape parameters for the edge and the SA CL bands are given.

The vital importance of correction of spectral data for the detection system response is outlined and it is shown that when corrections are applied many discrepancies and misconceptions in the luminescence literature can be eliminated. In particular, the peak of the ZnS "self-activated" band was

observed to shift towards shorter wavelengths (higher energies) with decrease in temperature for corrected spectra but it appeared to move in the opposite direction (to lower energies) when considering uncorrected data.

CONTENTS

		Page No.
ABSTRACT		3
CONTENTS		6
LIST OF FIGURES		10
LIST OF TABLES		17
ACKNOWLEDGEMENTS		18
1.	INTRODUCTION	19
2.	LITERATURE REVIEW	22
2.1	LUMINESCENCE IN II-VI SEMICONDUCTOR COMPOUNDS	22
2.1.1	THE SELF-ACTIVATED (SA) LUMINESCENCE BAND	26
2.1.2	THE SELF-COACTIVATED RED-COPPER LUMINESCENCE BAND	30
2.1.3	LUMINESCENCE DUE TO GROUP IVB ELEMENTS	31
2.1.4	THE GREEN-COPPER (G-Cu) AND THE BLUE-COPPER (B-Cu) LUMINESCENCE BANDS	32
2.2	ELECTRON SCATTERING IN SOLIDS	36
2.2.1	BACKSCATTERED AND SECONDARY ELECTRONS	36
2.2.2	X-RAY PRODUCTION	40
2.2.3	CATHODOLUMINESCENCE SIGNALS	41
2.3	RADIATIVE RECOMBINATION PROCESSES	42
2.3.1	BAND-TO-BAND TRANSITIONS	42
2.3.2	FREE EXCITONS	43
2.3.3	DONOR-ACCEPTOR PAIRS	48
2.3.4	NON-RADIATIVE RECOMBINATIONS	49

		Page no.
2.4	DETECTION OF CATHODOLUMINESCENCE	51
2.5	INTERNAL ELECTRIC FIELDS IN ZnS CRYSTALS	56
2.6	FUNDAMENTAL OPTICAL ABSORPTION	59
2.7	CATHODOLUMINESCENCE EMISSION BAND SHAPE ANALYSIS	60
2.7.1	CONFIGURATION COORDINATE DIAGRAM	61
2.7.2	URBACH'S RULE	68
2.7.3	THE FRANZ - KELDYSH EFFECT	73
2.7.4	THE DOW AND REDFIELD MICROFIELD MODEL	74
2.8	ZINC SULPHIDE CATHODOLUMINESCENCE SPECTROSCOPY	83
3.	EXPERIMENTAL WORK	86
3.1	THE CAMBRIDGE IIA STEREOSCAN SCANNING ELECTRON MICROSCOPE (SEM)	86
3.2	ZINC SULPHIDE AND CADMIUM SULPHIDE CRYSTALS	87
3.3	STRUCTURE DETERMINATIONS FROM BIREFRINGENCE MEASUREMENTS	89
3.4	SAMPLE MOUNTING FOR SEM STUDIES	93
3.4.1	CHARGING EFFECTS	94
3.5	CATHODOLUMINESCENCE DETECTOR SYSTEM	96
3.6	CALIBRATION OF THE CATHODOLUMINESCENCE DETECTOR SYSTEM	106
3.7	THE SEM X-RAY DETECTOR SYSTEM	113
4.	RESULTS AND ANALYSIS	115
4.1	SAMPLE PURITY	115
4.1.1	SEM X-RAY MICROANALYSIS	115

		Page No.
4.1.2	SPECTROCHEMICAL ANALYSIS	117
4.2	LOCAL LUMINESCENCE VARIATIONS IN STRIATED ZnS PLATELETS	117
4.2.1	SYNOPSIS	117
4.2.2	INITIAL CATHODOLUMINESCENCE STUDY	119
4.2.3	FURTHER INVESTIGATIONS OF LOCAL CATHODOLUMINESCENCE VARIATIONS: RESULTS AND INTERPRETATIONS	129
4.2.4	THE POWER OF THE CL SEM TECHNIQUE	152
4.3	COLOUR SYNTHESIS FOR THE PRESENTATION AND ANALYSIS OF SEM CATHODOLUMINESCENCE RESULTS	153
4.3.1	SPECTRAL SENSITIVITY OF THE HUMAN EYE	154
4.3.2	ADDITIVE COLOUR AND SUBTRACTIVE COLOUR FORMATION	155
4.3.3	TERNARY COLOUR MIXTURES USING KODAK "WRATTEN" FILTERS	158
4.3.4	PREPARATION OF BLACK-AND-WHITE CATHODOLUMINESCENCE MICROGRAPHS	164
4.3.5	EXAMPLES OF ZnS COLOUR SYNTHESIS	168
4.3.6	SUMMARY	184
4.4	CATHODOLUMINESCENCE EDGE EMISSION BAND SHAPE ANALYSIS	185
4.4.1	SYNOPSIS	185
4.4.2	RESULTS AND ANALYSIS	186
4.4.3	DISCUSSION	201

Page No.

4.5 SHAPE ANALYSIS OF THE SELF-ACTIVATED CATHODOLUMINESCENCE BAND IN ZnS: Cl CRYSTALS 205

4.5.1 SYNOPSIS 205

4.5.2 RESULTS AND ANALYSIS 207

5. CONCLUSIONS 222

REFERENCES 227

LIST OF FIGURES

Fig. No.		Page No.
2.1	A portion of the periodic table, showing activator, coactivator and host lattice atoms of II-VI compounds	27
2.2	The relation between the different kinds of luminescence bands in ZnS, obtained by varying the concentration of activators and coactivators	34
2.3	Typical electron distribution versus energy graph	38
2.4	Energy-momentum diagram illustrating the difference in band to band recombination in (a) direct and (b) indirect gap semiconductors	44
2.5	Energy band diagrams illustrating various radiative recombination processes in II-VI semiconductors	46-47
2.6	The development of cathodoluminescence collector mirrors	54
2.7	A configuration coordinate diagram showing the ground and excited states of a luminescent centre	63
2.8	Energy bands with penetrating wave functions in a strong electric field	75
3.1	Examples of ZnS platelets seen under crossed polarizers in an optical microscope	91-92

Fig. No.		Page No.
3.2	Electron yield coefficient, Δ (ie the number of electrons emitted per incident primary electron) versus accelerating voltage.	95
3.3	The SEM cathodoluminescence collector unit	99-100
3.4	General view of the SEM and the components of the CL detection system	99-100
3.5	Schematic diagram of the entire CL detector system	101
3.6	A close-up diagram of the light collector sub-system	102
3.7	The quantum efficiency Q (λ) as a function of wavelength for the three basic types of PM	108
3.8	Calibration curve of the cathodoluminescence detector system	112
4.1	Typical X-ray spectrum of a synthetic ZnS platelet	116
4.2	A cluster of ZnS platelets grown at Imperial College: (a) is a secondary electron micrograph (b) a reflected primary micrograph and (c) and (d) are the panchromatic (all wavelength) CL micrograph and the CL spectrum respectively	121-122
4.3	Micrographs of a striated ZnS (350 Type II) platelet where: (a) is a low magnification panchromatic CL SEM micrograph, (b) and (c) are monochromatic (one wavelength) CL micrographs from the area outlined in (a), and were recorded at 420 nm and 523 nm respectively	124-125

Fig. No.		Page No.
4.4	CL emission spectra from the areas marked in Fig. 4.3c: (a) the spectrum from region A and (b) the spectrum from area B	126
4.5	Micrographs of a striated ZnS (227B) platelet: (a) is a low magnification polarized light-micrograph of the whole platelet, (b) is an enlargement of the area outlined in (a) and (c) is a panchromatic CL SEM micrograph. The remaining pictures are monochromatic CL SEM micrographs recorded at the following emission wavelenghts: (d) 328 nm (3.78eV), (e) 334 nm (3.71eV) and (f) 344 nm (3.60eV)	134-135
4.6	The CL edge band emission obtained from the three numbered regions of Figure 4.5(d)	137
4.7	Monochromatic CL SEM micrographs of the same area as in Figure 4.5. (a) at a wavelength of 670 nm (1.85eV) and (b) 685 nm (1.81eV)	139-140
4.8	CL emission spectra from the areas marked in Figure 4.7 (a) the spectrum from region 2 and (b) the spectrum from region 3. The shorter wavelength band is the edge emission (conduction band to valence band recombination radiation). The sharp band at longer wavelengths is due to an impurity activated mechanism	141-142
4.9	CL SEM micrographs of another ZnS platelet (No. 248). (a) is panchromatic and (b) is monochromatic, recorded at 523 nm (2.37eV)	146-147

Fig.No.		Page No.
4.10	Uncorrected and corrected CL emission spectra obtained from the two regions shown in Figure 4.9, (a) is the uncorrected spectrum from cubic region 1 and (b) is the corrected spectrum, (c) is the uncorrected spectrum from 4H polytype region 2, and (d) is that for the same region after correction. The small bands below 350 nm are the intrinsic edge emission bands while the large bands at longer wavelengths are characteristic of impurities	148-149
4.11	(a) Diagram of additive mixtures of three primary colours producing various colours as well as white light (b) Diagram of subtractive colour formation with black in the middle	156
4.12a	A six-step triangular grey scale used for colour balance	160-161
4.12b	The range of ternary colours available with Kodak "Wratten" filters (25-red, 58-green and 47B-blue) and 35 mm colour film (Ektachrome EX-135). The primary colours appear at the apices and the binary mixtures are observed in the centre of each corresponding side of the triangle	160-161
4.13	Transmission curves for the Kodak "Wratten" filters	163
4.14	A CIE (Commission Internationale de l'Eclairage) chromaticity diagram showing the coordinates of the three Kodak "Wratten" filters (dashed triangle)	165

Fig. No.		Page No.
4.15	SEM micrographs of a striated ZnS platelet (350B type II) where (a) is a secondary electron micrograph, (b) is the panchromatic CL SEM micrograph from the same area, (c, d and e) are the three monochromatic separation positives recorded at 430, 530 and 650 nm respectively, (f) shows the uncorrected CL spectrum from this region	170-173
4.16	The CL colour print obtained by sequentially copying the black-and-white micrographs shown in Fig. 4.15c, d and e, through blue, green and red filters respectively. The filter exposure times are given in table 4	175-176
4.17	CL micrographs of another ZnS platelet (No.347) showing (a) a low magnification panchromatic micrograph of the whole crystal, (b, c and d) are the pseudo-monochromatic separation - positives recorded via the blue, green and red Kodak filters respectively; and (e,f,g and h) give the emission spectra (uncorrected) from the various regions as marked in Fig. 4.18a	177-180
4.18	The CL colour micrographs obtained by using the pseudo-monochromatic separation - positives shown in Figs. 4.17 b,c and d (a) was acquired using the filter exposure times given in table 4 and in (b) the exposure times were blue (5/4 sec.), green (1/4 sec.) and red (1/30 sec.) respectively	182-183

Fig.No		Page No.
4.19	Cathodoluminescence edge emission bands of hexagonal structure CdS crystal (a) at 292K and (b) at 78K	187
4.20	Cathodoluminescence edge emission bands of hexagonal structure ZnS (a) at 292K and (b) 78K	188
4.21	Cathodoluminescence edge emission bands of cubic structure ZnS (a) at 292K and (b) at 78K	189
4.22	Plots of the edge emission band data for an hexagonal structure CdS crystal at 292K (cf. Fig. 4.19). The straight line segments in the upper plot show that in the region "G" near the maximum the band has an asymmetic Gaussian form. The straight lines in the lower plot show that in the low energy (LE) and high energy (HE) regions the form of the band is exponential	191-192
4.23	Temperature dependence of the slopes σ_L (low energy region) and $-\sigma_H$ (high energy region) for CdS	197
4.24	Plots of peak position E_p versus coth $(\hbar\omega_{LA}/2kT)$ (dashed line), and E_p versus coth $(\hbar\omega_{LO}/2kT)$ (solid line) where $\hbar\omega_{LA}$ = 0.0185 eV and $\hbar\omega_{LO}$ = 0.038 eV	199
4.25	Plots of half-width H versus coth $(\hbar\omega_o/2kT)$ for both $\hbar\omega_o = \hbar\omega_{LA}$ = 0.0185 eV (dash line) and $\hbar\omega_o = \hbar\omega_{LO}$ = 0.038 eV (solid line). Numbers at points represent temperatures in K	200

Fig. No.		Page No.
4.26	Self-activated cathodoluminescence emission bands, of (a) hexagonal and (b) cubic structure in a ZnS: Cl crystal, both uncorrected and corrected at 292K	209
4.27	Plots of the self-activated emission band data for a cubic structure ZnS: Cl crystal at 78K. The straight line segments show that in the region "G" around the maximum the band has an asymmetic Gaussian form	211
4.28	Plots of the SA emission band for a cubic structure ZnS: Cl crystal at 78K. The straight lines show that in the low energy (LE) and high energy (HE) regions the form of the band is exponential	212
4.29	Corrected (solid) and uncorrected (dashed) self-activated cathodoluminescence bands of cubic ZnS: Cl at room temperature and liquid nitrogen temperature	219

LIST OF TABLES

		Page No.
1.	Typical Spectrochemical Analysis of a number of ZnS platelets	118
2.	Cathodoluminescence edge emission peak energies (E_p) for various ZnS structures at room temperature	130
3.	Room temperature CL peak energies for tin (Sn) activated ZnS (No. 227B)	143
4.	Exposure times for colour composites	166
5.	ZnS Cathodoluminescence (CL) edge emission band shape parameters	154
6.	ZnS Cathodoluminescence (CL)'self-activated' band shape parameters	213

ACKNOWLEDGEMENTS

This thesis describes work carried out at the Imperial College of Science and Technology, University of London, between the period, October 1974 to October 1977 under the supervision of Dr D B Holt.

I am extremely indebted to Dr D B Holt who gave much needed guidance, tuition and continual encouragement during the course of this work. It is probably true to say that his enthusiasm for scanning electron microscope cathodoluminescence is partly responsible for my interest in this aspect of physics.

It is a pleasure to thank Mr P L Giles and Dr B G Yacobi for their many stimulating discussions and valuable assistance in all kinds of ways, through which I have learnt a great deal. To them both I extend my sincere best wishes.

I would like to express my gratitude to the Science Research Council for the financial support given to me in the form of a studentship without which this work would not have been possible.

Finally, special thanks to the photographic section for their help in the preparation of the illustrations in this thesis and to Mr P R Grant, Dr I M Boswarva and Mr J B Steyn for the many informal discussions.

The typing was very kindly completed at short notice by Mrs Prity Datta.

1. INTRODUCTION

The purpose of this project was to investigate the luminescent properties of ZnS and CdS platelets using the scanning electron microscope (SEM) cathodoluminescence (electron stimulated emission) mode.

Striated platelets are one of the characteristic morphologies produced by growth of ZnS by sublimation in a stream of an inert carrier gas. As these platelets are among the best forms in which ZnS is available they have been intensively studied. They exhibit a number of interesting opto-electronic properties, especially the anomalous (high voltage) photo-voltaic effect (section 2.5 and also Merz 1958, Brafman et al. 1964 and Shachar and Brada 1968). The striations are two sets of lines visible to the naked eye. One set run parallel to the original growth direction of the needles on which the platelets form, which is the c-axis of the crystal structures present, and the other set run perpendicular to the c-axis. It is now well established that the set perpendicular to the c-axis are faulted, polytypic bands produced by a martensitic, periodic slip process involving the movement of partial dislocations rotating about a central screw dislocation of large Burgers vector (section 3.2 and the many references given there). The striations roughly parallel to the c-axis are growth steps and are usually referred to in the literature as "linear markings". The various strips

may have either the hexagonal structure (wurtzite - 2H), the cubic structure (sphalerite - 3C) or one of the many polytypic forms.

The work reported here, is a natural extension to some preliminary results obtained in this group by Holt and Culpan (1970) who examined these complex striated platelets using the emissive, conductive and cathodoluminescence (CL) modes of the scanning electron microscope. They showed that the faulted, polytypic striations give rise to contrast in micrographs in all three modes. At that time neither the equipment nor the theory was available to make it possible to arrive at detailed interpretations of these observations. Since then however, an efficient spectroscopic CL detection system employing photon counting and computer data processing has been designed, built and calibrated (see sections 3.5. 3.6 and also Holt et al. 1976 and Steyn et al 1976). The quantitative interpretive theory for the conductive and CL modes for semiconducting materials has also been reviewed (Holt 1974).

A typical CL emission spectrum consists of a number of broad luminescence bands falling within the effective wavelength detection range of 250 to 850 nm (eg. Fig. 4.10 section 4.2.3). Observed emission peaks between 250 and 345 nm in the different structures of ZnS are the fundamental or edge emission band, which arises from conduction band

to valence band recombination (ie. it is an intrinsic phenomenon). The corresponding edge emission band in CdS occurs at 510 nm (see table 5 in section 4.4.2). All bands above (ie. at longer wavelengths than) this fundamental edge are due to impurity luminescence and are considered as extrinsic. Both intrinsic and extrinsic luminescence bands have been investigated and will be reported.

The spatial resolution of the SEM (a few microns) allowed small structurally homogeneous areas from the same platelet to be examined. This was found to be essential as results soon showed gross variations to occur with small displacements over the specimen surface.

2. LITERATURE REVIEW

2.1 LUMINESCENCE IN II-VI SEMICONDUCTOR COMPOUNDS

This thesis is concerned with the electron bombardment excited luminescence properties of CdS and ZnS crystals. These two compounds are members of a larger group known as the II-VI semiconductors. As the name suggests they are formed by a chemical mixture of group IIB and VIB elements of the periodic table. Other semiconductors, Si, Ge and many of the III-V compounds like GaAs, AlP and so on have already found extensive use in solid state electronics industries. Infact calculator displays, electronic wrist watches, solar cells, infra-red detectors and many more devices are inpart, if not entirely, made from these valuable materials. The list would be end-less if civil, military and industrial applications were to be considered.

Naturally the background literature on II-VI semiconductor materials is vast and it is proposed from the start to restrict the luminescence review to that of ZnS, although many of the other compounds in this group behave very similarly.

The luminescence of II-VI's seems to have attracted a great deal of attention since about the mid-nineteenth century. It was about 1866 that Théodore Sidot researching on the crystallization of some metallic sulphides found that his

crystals luminesced. His results were published (Sidot 1866) and formed the first report on luminescent zinc sulphide prepared in a laboratory. The subject received only passing interest until Lenard (1910) reported on the preparation of luminescent ZnS which had till then been rather empirical. However it is worth noting that Verneuil in 1888 proposed that the photoluminescence (PL) of ZnS was due to a foreign luminogen impurity.

Since those early days the available literature on the luminescence properties of II-VI semiconductors has become most formidable. Luckily some excellent reviews have been given by Leverenz (1950), Klick and Schulman (1957), Goldberg (1966) and Curie and Prener (1967) which forms much of the background to this subject.

Amongst the II-VI compounds, ZnS and CdS have been most extensively studied, ZnS for its luminescence properties and CdS for its photoconductive properties. Although these phosphors have been technically developed to perfection and successfully used in cathodo-ray oscilloscope and TV screens, some of the fundamentals of light emission are still far from clear. It is therefore impossible to present a definite and unified picture for the II-VI's as a comprehensive theory does not exist.

It has been established, since the early 1950's, that the II-VI compounds have to be doped by suitable metallic impurities

known as activators to produce luminescence. To increase the solubility a coactivator element has to be added in combination with the activator. Typical activators are group IB elements of the periodic table like Cu, Ag and Au whereas coactivation can be achieved by the addition of either group VIIB elements (Cl, Br, I) or group IIIB elements (Al, Ga, In) (See Fig. 2.1 after Williams 1957).

Furthermore, the incorporation of either coactivator or activator alone, has been shown to be responsible for the characteristic "self-coactivated (red) luminescence" or SCL (Froelich 1953), Aven and Potter (1958) and the well known "self-activated (blue) luminescence" or SAL (Kröger and Hellingham 1948, Kröger and Dikhoff 1950) respectively.

Other less common activators of ZnS are the group V elements (P,As,Sb). For further reading see McKeag and Ranby (1949), Prener (1951) and especially Apple (1959). This group of elements will not be referred to further since they were not present in the samples examined for this work.

There have been relatively small numbers of reports on the luminescent properties of zinc sulphide activated with group IVB elements like Si, Ge, Sn and Pb and also the transition metal impurities (Mn, Fe, Co, Ni). Traditionally Fe, Co and Ni have been regarded as 'killers' of luminescence since they often caused a decrease in visible luminescence without, by

themselves, producing any luminescence within the visible range (Hoogenstraaten 1953).

Kröger and Hellingham (1949), were the first to propose a charge compensation mechanism to explain the luminescence process. They showed that monovalent cation activators (Ag^+, Cu^+, Au^+) replace the divalent cation of the host crystal substitutionally. This results in a deficiency of positive charge, which can be compensated either by the formation of anion vacancies in the crystal or by the incorporation of additional monovalent cations in interstitial positions. Creation of vacancies and interstitials is a highly energetic process and therefore unlikely. However introducing a substitutional halogen ion (Cl^-, Br^-, I^-) to replace the divalent S^{2-} in the lattice leads to the complementary removal of a negative charge.

Analogously, charge compensation could be achieved by the substitutional incorporation of trivalent cations with the usual monovalent activators. For example, Al^{3+} plus Ag^+ replacing 2 Zn^{2+} (see Kröger and Dikhoff 1950). It follows from the considerations above that activation of ZnS with a divalent ion (eg. Mn^{2+}) should require no charge compensating ion. This is known to be the case provided the ion size and bonding properties are not too different from those of Zn^{2+} ion.

Some years later Klasens (1953), Bowers and Melamed (1955)

and also Prener and Williams (1956) showed that activators and coactivators could be considered as acceptors and donors. For elemental semiconductors, Si and Ge, the elements in column VB of the periodic table act as donors, whereas those in column IIIB act as acceptors (Fig. 2.1). Similarly, if column IB (Cu, Ag, Au) and column VB (P, As, Sb) elements were substituted for column IIB (Zn, Cd, Hg) and column VIB(S, Se, Te)elements respectively, these would be expected to behave as acceptors and yield a series of discrete states above the valence band. In the neutral crystal with only these impurities present it is found that the highest state is empty. On the other hand coactivators of column VIIB (Cl, Br, I) and column IIIB (Al, Ga, In) substituted for column VIB (S, Se, Te) and column IIB(Zn, Cd, Hg) elements respectively would have donor properties. This creates a series of discrete levels below the conduction band in which the extra electron is bound.

On excitation, these donor (coactivator) - acceptor (activator) like states act as radiative recombination levels (see Fig.2.5d section 2.3.3).

2.1.1 THE SELF-ACTIVATED (SA) LUMINESCENCE BAND

The nature of centres responsible for the various kinds of luminescence in ZnS and related compounds has attracted a great deal of attention. There is therefore, a large amount of experimental data in the literature that relates to defects in these materials.

I	II	III	IV	V	VI	VII
		Al 13	Si 14	P 15	S 16	Cl 17
Cu 29	Zn 30	Ga 31	Ge 32	As 33	Se 34	Br 35
Ag 47	Cd 48	In 49	Sn 50	Sb 51	Te 52	I 53
Au 79	Hg 80					

Fig. 2.1 A portion of the periodic table, showing activator, coactivator and host lattice atoms of II - VI compounds

A variety of experimental approaches have been used and these include luminescence, optical absorption, photo-conductivity, high-temperature diffusion and electrical transport properties, thermal conductivity, infrared imputity local mode studies, electron paramagnetic resonance (EPR) and so on. Each in turn reflects somewhat different properties of the defects and therefore potentially provides unique information about the centres.

Of all the broad emission bands in ZnS the blue self-activated (SA) luminescence band is the one which is probably the best understood and its atomic nature has been unambigiously elucidated. It is produced in many II-VI compounds by the single incorporation of a coactivator impurity. The peak of this band in ZnS varies anywhere between 450 and 470 nm as the type of preparation and/or the coactivators is changed (Van Gool 1961, Curie and Prener 1967).

The microscopic identification of the centre states that it is a zinc lattice vacancy (Zn^{2+}) paired with a substitutional coactivator (eg. Cl^{-}) donor on an adjacent sulphur site. It has been inferred (Koda and Shionoya 1964, Shionoya 1967) that the acceptor state in the pair emission originates from a Zn^{2+} vacancy with which a coactivator is associated, while the donor state arises from an isolated coactivator (note, donor-acceptor pair mechanisms are discussed in section 2.3.3).

Confirmation of this model has come from polarization of the luminescence, time resolved spectroscopy and correlation of EPR and luminescence (Morehead and Title 1963, Koda and Shionoya 1964, Urabe and Shionoya 1968 and Watkins 1973).

Koda and Shionoya (1964) observed the polarization of the luminescence for Cl-doped cubic ZnS and from this they concluded that the Cl is associated with another simple defect along the <111> axis.

The EPR spectra of the paramagnetic charge state of the SA centre has been investigated by Schneider et al.(1963) and Watkins(1976). The normally diamagnetic centres are converted to the paramagnetic state (ie by trapping a hole or electron) by illuminating the sample at low temperatures with ultraviolet light. It was shown that in all cases, the EPR signal arose from a hole trapped at a S^{2-} ion. The presence of the group VII impurity in the defect has also been established from hyperfine splitting (Schneider et al. 1965).

Also, when the temperature is decreased, the peak energy of the SA band shifts to lower energies (longer wavelengths) with simultaneous decrease in the half-width. Such a spectral shift, which is opposite to that of the fundamental or edge (conduction band to valence band recombination) band gap in this material, is frequently referred to as a characteristic of the blue self-activated luminescence (Schrader and Larach 1956,

Samelson and Lempicki 1962 and Shionoya et al. 1964). Results obtained in the present work indicate that the temperature dependence of the SA luminescence peak position is actually of the opposite sign to this when the observations are corrected for the cathodoluminescence detection system response characteristics, as will be reported later.

2.1.2 THE SELF-COACTIVATED RED-COPPER LUMINESCENCE BAND

The red-copper luminescence (R-Cu) in ZnS arises whenever copper activators are incorporated in the absence of co-activators (Aven and Potter 1958, Shionoya et al. 1962, 1963, 1966b). The emission peak falls in the wavelength range from 670 to 680 nm and shifts towards lower energy (longer wavelength) with decrease in temperature in a similar manner to that of the blue self-activated luminescence band.

The accepted model for this R-Cu centre, states that it is formed by the tight association of a substitutional Cu^{+} ion with a S^{2-} vacancy, which plays the role of charge compensator, at one of the nearest neighbour sites. The luminescence transition takes place from the S^{2-} vacancy level (doubly ionized state of a sulphur vacancy) to the Cu^{+} level. Once again, verification of the model has come from electron spin resonance (ESR) measurements (De Bruin et al. 1964, Sugimoto and Maruyama 1967)

The red-copper luminescence band did not occur in the crystals

examined for this work, however, a knowledge of its properties was necessary when interpreting results in section 4.2.3.

2.1.3 LUMINESCENCE DUE TO GROUP IVB ELEMENTS

Zinc sulphide samples activated by any one of the group IVB elements (eg. Si, Ge, Sn, Pb) all produce very similar emission in the red region of the visible spectrum. This luminescence was investigated by Mita (1965) and Mita and Sugibuchi (1966). Strong photosensitive electron spin resonance (ESR) signals from Si, Ge and Sn activated ZnS was observed by Sugibuchi and Mita (1966) and Sugibuchi (1967). From the small number of experimental reports available it has been concluded that the unexcited luminescence centres are the tetravalent state of these impurities (Pb^{4+}) at substitutional zinc sites, with which no defects are associated. In other words, the impurity ions (having excess positive charge) are perfectly compensated with negatively charged zinc vacancies in the manner outlined by Mandel (1964). The electron transfer between the impurity and the neighbouring sulphur ions has been proposed as a possible luminescence mechanism. Most of the centres excited in this manner can then return to their ground state giving rise to luminescence. It is also possible however, that holes are released from the sulphur ions of the excited luminescent centres to the valence band and are subsequently trapped at hole traps. In such cases the impurity ions become trivalent and are relatively stable. The presence of isolated trivalent ions of tin has been

confirmed by the electron spin paramagnetic resonance technique (Sugibuchi 1967).

Mita (1964) has shown that ZnS: Pb (see review by Shionoya 1967) and ZnS: Sn luminescence are strongly dependent on the firing atmosphere used in preparation and such materials often exhibit both yellow-green and red emission bands. The red band in both Pb and Sn activated ZnS has been observed to shift towards longer wavelengths (lower energies) with a decrease in temperature, and the half-width is also decreased considerably.

Room temperature photoluminescence (PL) emission peak values for cubic (sphalerite - 3C) structure ZnS doped with Sn have been reported by Mita (1964). It is noted that a peak at 680 nm (1.82 eV) found in the present work agrees with Mita and is therefore identified as due to Sn activation (see section 4.2.3 especially table 3).

2.1.4 THE GREEN - COPPER (G-Cu) AND THE BLUE - COPPER (B-Cu) LUMINESCENCE BANDS

Whenever ZnS is fired with copper, as the activator, and a coactivator both green and blue emission bands are obtained. Kröger and Dikhoff (1950) observed that by varying the ratio of copper to coactivator (eg. Al), one or the other of these two bands could be maximized. When the ratio of Cu to co-activator was unity the green band dominated and as the ratio

became greater than unity the blue band increased. The kinds of luminescence centres, created by varying the amounts of activator and coactivator as well as the species, in ZnS have been systermatically investigated by Van Gool (1961). Figure 2.2 summarizes his results.

A wide variety of emission peak positions have been reported in the luminescence literature for these G-Cu and B-Cu bands. However, Van Gool and Cleiren (1960) showed that such a behaviour could be ascribed to changing the coactivator. This idea was taken a step further by Lehmann (1966a) who verified that different coactivators were indeed responsible for the observed peak shifts but also that structural changes had to be considered. That is to say, the emission bands of hexagonal (wurtzite 2H) ZnS: Cu phosphors peak at slightly higher quantum energies (ie shorter wavelengths) than those of cubic (sphalerite - zinc blende - 3C) structure phosphors. Structural changes and their important effects on ZnS cathodoluminescence (CL) edge (conduction band to valence band recombination emission) and impurity emission spectra have been investigated in this present work and will be reported subsequently.

It has transpired from studies of temperature variations of peak positions and half-widths, polarization measurements, time - resolved spectra observations and other related experiments that a donor-acceptor pair mechanism (section 2.3.3) is involved in the case of the G-Cu centre but probably not for the B-Cu (see Shionoya et al. 1963, 1964, 1965, Era et al.

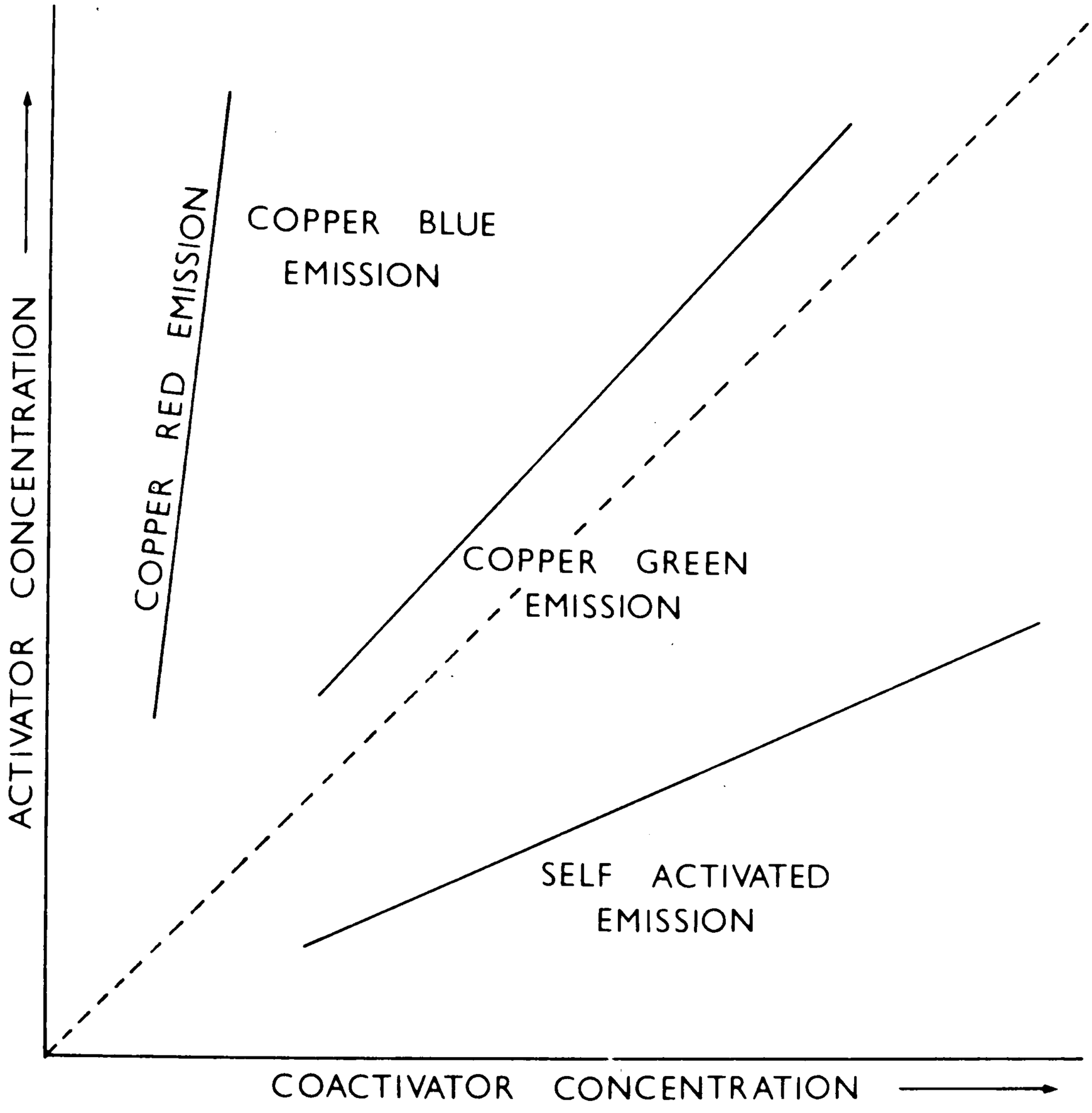


Fig. 2.2 The relation between the different kinds of luminescence bands in ZnS, obtained by varying the concentration of activators and coactivators

1968 a,b, Suzuki and Shionoya 1971 and especially the review articles by Shionoya 1967 and 1970).

For the green - copper emission to occur it is believed to be necessary that electrons are excited to the conduction band from the mono-valent copper level or from the valence band, by initial excitation. These are then captured at the donor (eg. Al^{3+}) levels. Green emission follows by radiative recombination of these electrons with holes trapped at the copper acceptor level and this recombination can occur even in pairs with quite large separation distances (Shionoya 1970). The coactivator (donor) levels are shallow and hydrogenic, whilst the copper level is fairly deep (Shionoya 1967). Experimental results (eg. Shionoya et al. 1964) have shown that with decrease in temperature both the green - copper and blue - copper emission peaks shift towards higher energies (shorter wavelengths), ie. in the same direction as that for the band gap in ZnS.

It is worthy of note, that the blue luminescence of silver activated ZnS (B-Ag) centre follows a similar emission mechanism to that described above (Era et al. 1968a and Lehmann 1966b).

The nature of the blue -copper (B-Cu) centre is still obscure. From the polarization results of Urabe etal (1968) it is thought to be some sort of associated centre. It is probably a substitutional Cu^{+} ion allied to an interstitial Cu^{+} ion, as in the original model proposed by Blick et al.(1961). The emission transition takes place between two localised levels (ie. it is an intra-centre type transition).

2.2 ELECTRON SCATTERING IN SOLIDS

A Cambridge Instruments Stereoscan IIA Scanning electron microscope (SEM) was used as the main experimental apparatus in this investigation. Detailed descriptions of the instrument and its various modes of operation can be found in Thornton (1967), Oatley (1972) and Goldstein and Yakowitz (1975).

A large number of interactions occur when a focussed electron beam falls on a specimen surface, as part of the beam will be backscattered, the rest absorbed. Among the signals produced in this way are secondary electrons, backscattered electrons, characteristic and continuum X-rays, Auger electrons, and photons of various energies. These signals are obtained from specific emission volumes within the sample and are known to be strong functions of electron beam energy, the atomic number of the specimen (Z), etc.

Only a brief summary of these various effects will be presented here since more detailed and rigorous developments of electron-solid interactions can be found in Thornton (1967), Bishop (1974) and Muir (1974).

2.2.1 BACKSCATTERED AND SECONDARY ELECTRONS

The incident high energy electron beam impinging on the solid target undergoes elastic scattering, ie changes of

direction with negligible energy loss, as well as inelastic scattering that is energy loss with usually little change in direction. Elastic scattering is mainly due to the interactions of the electron beam with the nucleus and in this case there is substantial deviation from the initial direction. On the other hand, inelastic scattering is caused by two possible mechanisms, inelastic interaction with the atomic nucleus, and inelastic interaction with the bound electrons and free electrons eg. plasmon losses. All emitted electrons except the backscattered or zero-loss electrons are produced by inelastic processes.

The total electron energy distribution of the emitted electrons with the beam at normal incidence takes the form shown in Fig. 2.3 (Originally from the work of Hachenberg and Brauer 1959). The distribution curve shows three distinct sections.

Region I represents elastically scattered electrons of nearly the same energy as the primary beam. If the incident electrons were backscattered before any inelastic collisions could take place they would have an energy equal to the beam energy. These backscattered or primary electrons are the result of Rutherford scattering or re-emission of electrons from atoms at, or near, the surface of the specimen. The amount of backscattering that takes place increases with increasing specimen atomic number (Heinrich 1965 and Oatley 1972). So if this type of emission is monitored in the SEM it gives atomic number contrast micrographs. The number of backscattered electrons which are emitted from any point on the sample in

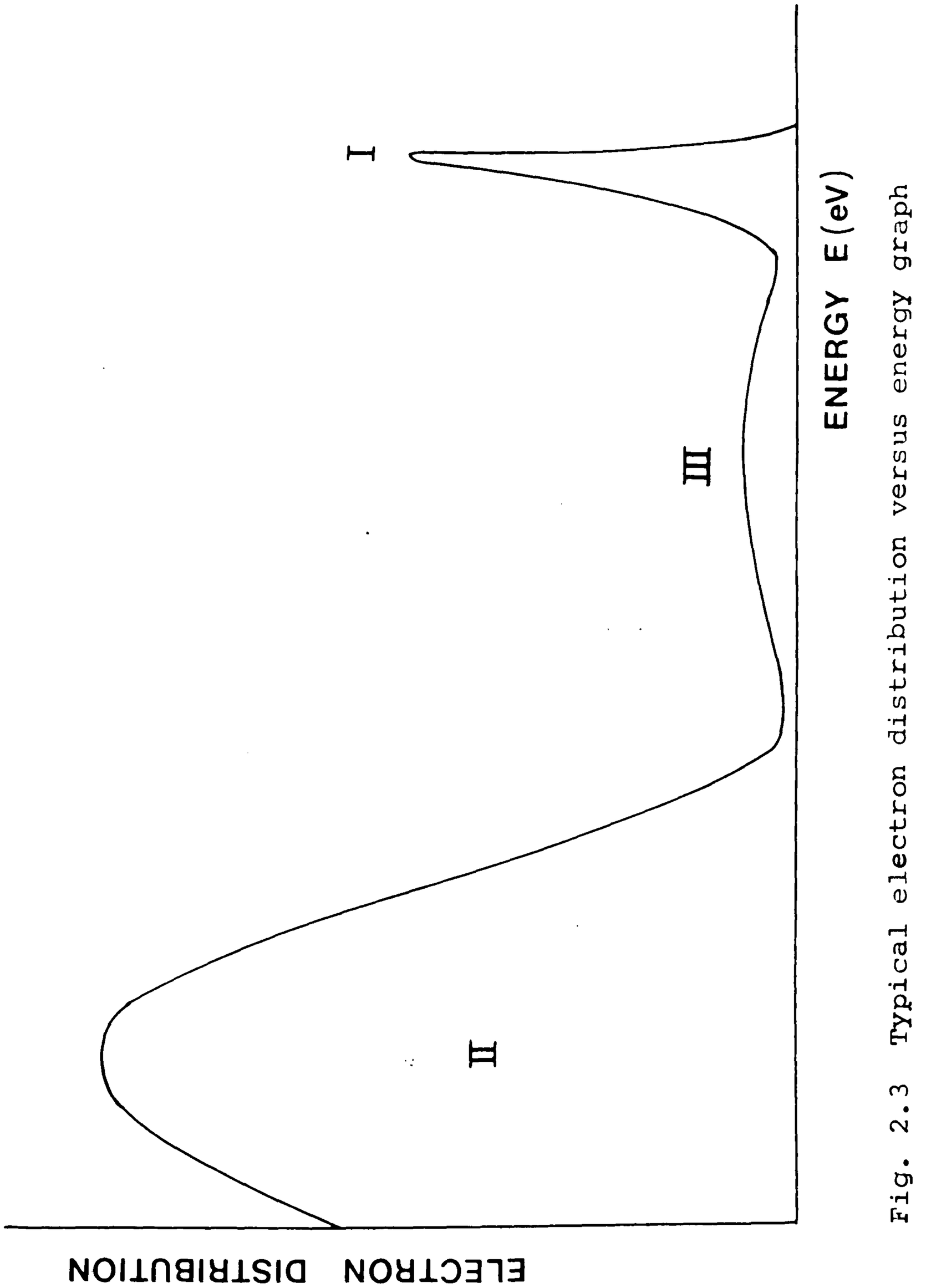


Fig. 2.3 Typical electron distribution versus energy graph

the direction of the SEM electron detector (ie the Everhart - Thornley (1960) detector) is also dependent on the angle between the primary beam, the specimen surface, and the direction of emergence. If the sample is rough the back-scattered electron yield can be selectively absorbed or increased, depending on the beam position. Therefore, the detected intensity of the backscattered electrons is also a function of the sample topography.

The large peak at lower energy, region II, is due to the low energy secondary electrons which are formed as a result of excitation by the high energy primary beam of loosely bound atomic electrons. This type of signal is used in the SEM to image surface topographs and is referred to as the secondary electron signal in the emissive mode (Gopinath 1974). It is the most commonly used mode of SEM operation. The surface barrier of a material determines the peak position and the shape of the distribution in region II. If there is a low potential barrier, the maximum will occur at lower energies. Secondary electron emission is closely related to the incident beam energy, to the number of outer shell electrons, and to the atomic radius.

Finally there is a third group (region III) of electrons with energies corresponding to inelastic scattering. These are called tertiary electrons.

2.2.2 X-RAY PRODUCTION

X-ray emission can occur in one of two main ways, core scattering resulting in the continuous spectrum, and inner shell ionization, which yields the characteristic spectrum. The continuous radiation (Bremsstrahlung or white radiation) forms the background X-ray radiation in the SEM, the intensity of which determines the lowest detectable limit for a particular element.

The characteristic X-rays, which are more important for analysis, are produced whenever a high energy electron of the incident beam removes a K, L or M inner shell electron and leaves the atom in an excited or ionized state. The inner-shell vacancy created is almost instantaneously filled by an electron from an upper energy level, thereby releasing energy. The relaxation of the electron to the inner-shell vacancy may be accompanied by emission of a photon of X-ray radiation. Alternatively, the energy may be absorbed by another electron associated with the atom, and this electron may now have enough energy to escape from the atom. If the latter is sufficiently near the surface, the electron may escape from the solid. It is called an Auger (1925) electron, produced by an Auger process. Auger production is most efficient at low atomic number when statistically an Auger electron is more likely to be emitted than an X-ray photon. Only the X-ray photon emission, resulting in the characteristic X-ray spectrum, will be exploited in the present work.

Since the electrons are quantized, the emitted X-ray photon has a discrete energy which is equal to the difference in energy between the initial and final states of the atom (Barrett and Massalski 1966). Thus the wavelength of the characteristic radiation is unique for any one element (and does not depend on such factors as the primary beam energy). Detection of a characteristic X-ray line therefore indicates that the element is present in the sample.

Bearden (1964) has syste matically tabulated these characteristic wavelenghts and their corresponding energies (KeV), making identification of the various elements simple.

For more detailed introductory accounts of the X-ray mode (microanalysis) technique see Goodhew (1975) and Belk (1974). A more advanced account is given by Wells (1974).

2.2.3 CATHODOLUMINESCENCE SIGNALS

When a solid specimen is irradiated by a beam of electrons part of the beam energy may be emitted as electron-stimulated light which is referred to as cathodoluminescence or CL, whilst the remainder goes towards the production of a number of competing forms of energy. Some of these have already been discussed.

The incident electron beam is thought to excite bound electrons from a lower to a higher excited state. In some

cases in solids, this corresponds to forming an electron hole pair. The excited electron may then spontaneously recombine with the emission of a light photon of characteristic energy.

It will be shown later that cathodoluminescence (CL) spectra can be conveniently divided into extrinsic and intrinsic luminescence. Extrinsic features of CL spectra are those which depend on the presence of impurities in the material (see sections 4.2.2 and 4.5) whereas intrinsic features of CL spectra arise from the energy band structure of the material itself (see section 4.4).

Detailed accounts of the probable mechanism by which energetic electrons produce CL emission have been given by Holt (1974), for semi-conductor type materials and Muir and Grant (1974) and De Mets(1974) for organic materials. Some of these processes will be discussed in the following section.

The cathodoluminescence mode was the most used technique for this work.

2.3 RADIATIVE RECOMBINATION PROCESSES

2.3.1 BAND-TO-BAND TRANSITIONS

There are a number of ways in which the free carriers produced during electron beam excitation can recombine by emitting radiation and in this way dissipate the energy stored in the specimen. One possible process is a band-to-band transitio

in which an electron in the conduction band combines with a hole in the valence band emitting a photon. The energy of the photon ($h\nu$) is equal to the difference in energy between the two bands and therefore, if this emission can be detected it will provide intrinsic (ie fundamental) information about the crystal. The conservation of energy and momentum laws require the transitions to occur only between states of the same k-vector, that is to say 'vertical transitions'. Thus in materials with a band structure similar to that illustrated in Fig. 2.4a, which are known as direct gap materials, the most likely transitions are across the minimum energy gap (E_1-E_2 = E_g). This type of transition has a relatively high probability in such direct band gap materials as ZnS, CdS and GaAs.

There is also the possibility of conserving momentum via the simultaneous emission of a photon and a lattice phonon of suitable wave vector when the electron makes a transition. This is the emission process encountered in indirect bandgap materials like Si, Ge and GaP (Fig. 2.4b). In order to conserve energy the photon emitted must have an energy equal to the difference in energy between the two band states minus the energy of the phonon emitted (ie. $\hbar\omega_p$). The direct process has a higher probability than the indirect process.

2.3.2 FREE EXCITONS

A free electron and a free hole, being a pair of opposite

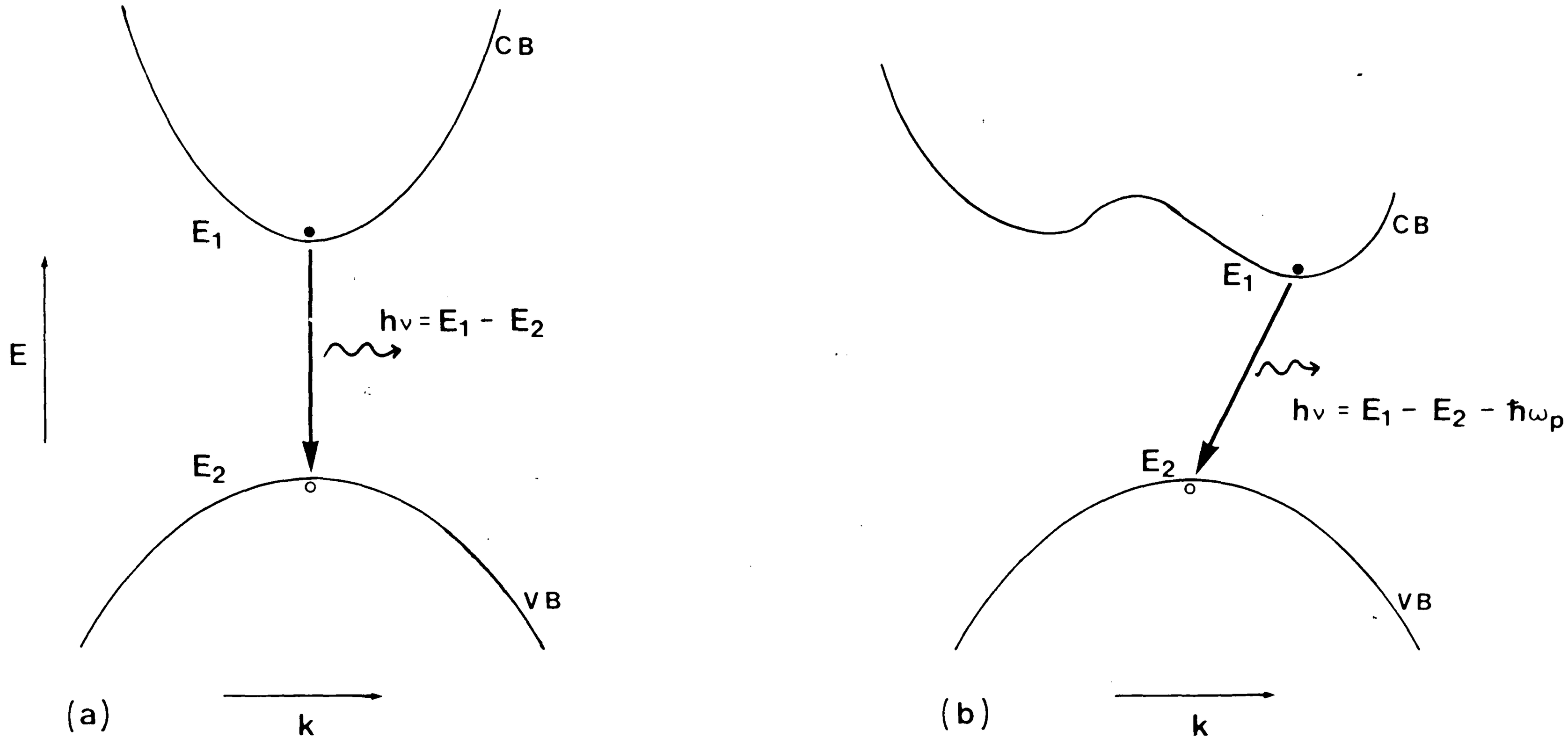


Fig. 2.4 Energy-momentum diagram illustrating the difference in band to band recombination in direct and indirect gap semiconductors:
(a) Direct band to band radiative transition
(b) Radiative indirect transition with phonon participation to conserve momentum

charges, experience a coulombic attraction. Such an interaction can result in an electron and a hole becoming bound together forming an exciton. The free exciton can then wander through the crystal as a mobile associated pair. Due to this mobility the exciton is not a set of spatially localized states. Also, the exciton states do not have a well-defined potential in the semiconductor energy diagram, although it is now fairly customary to use the conduction band edge as a reference level and to make this edge the continuum state (ie.n = ∞). Then the various states of the exciton are represented as shown in Fig. 2.5a, for a direct gap material. It is possible for the electron and hole bound together in an exciton to combine radiatively. This results in the emission of a photon whose energy is equal to the minimum energy gap (E_g) of the material minus the exciton binding energy.

Excitons are essentially an intrinsic phenomenon and represent lowest - energy states for electron-hole pairs. They are formed easily only in the purest of materials and at low temperatures. Moreover, in general, a fraction of the excited electron - hole pairs remain as free carriers occupying band states. These free carriers can then recombine radiatively in a band-to-band transition. Radiative recombination from free excitons has been established experimentally at low temperatures in both direct and indirect gap semiconductors (Queisser and Heim 1974).

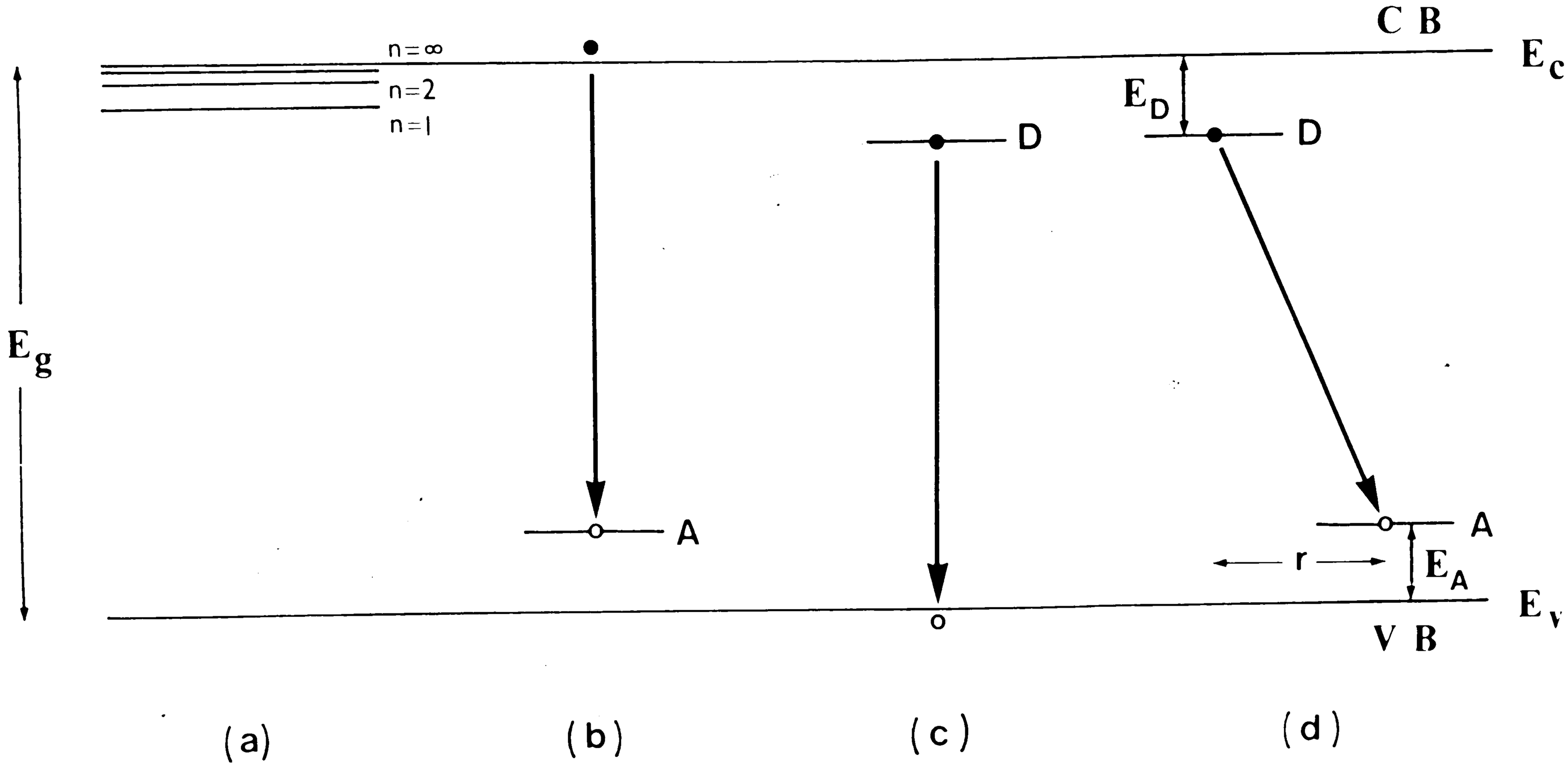
Fig. 2.5 Energy band diagrams illustrating various radiative recombination processes in II - VI semiconductors.

(a) Energy levels for the exciton and its excited states, exciton energy being referred to the edge of the conduction band. Recombination takes place between these exciton states and the valence band.

(b) Radiative recombination of an electron in the conduction band with a hole trapped at a localized acceptor - like level above the valence band (Schön - Kläsen model)

(c) Radiative recombination arising from the recombination of a hole in the valence band with an electron trapped at a donor-like level below the conduction band (Lambe - Klick model)

(d) A donor - acceptor pair transition (r is the pair separation distance, Prener - Apple - Williams model)


C B
E_c
n=∞
n=2
n=1
E_D
D
D
E_g
A
A
r
E_A
E_v
o
V B
(a)
(b)
(c)
(d)

2.3.3 DONOR-ACCEPTOR PAIRS

Real crystals invariably contain impurities and other types of lattice defects. There are several ways in which recombination, involving energy states introduced by these defects can occur as shown in Fig. 2.5 b, c and d.

(a) A centre near the valence band in energy can capture a hole which subsequently combines with a free electron in the conduction band. This is known as the Schön - Kläsens model (Fig. 2.5b).

(b) A free hole can combine with an electron trapped on a centre near the bottom of the conduction band (ie. Lambe - Klick model, Fig. 2.5c).

(c) Finally, interimpurity radiative recombinations of electrons bound to donors with holes bound to acceptors may occur for both remote and close impurity pairs (Fig. 2.5d). This is known as the Prener - Apple - Williams model. The coulomb interaction between donor and acceptor modifies the binding energies so that the transition energy separating the paired states is given by (Williams 1960).

$$h\nu = E_g - E_A - E_D + q^2/\varepsilon r \qquad (1)$$

Where E_D and E_A are the respective ionization energies of the donor and the acceptor as isolated impurities (measured down from E_c and up from E_v respectively as shown in Fig. 2.5d).

The term $q^2/\varepsilon r$ is the amount by which the impurity levels are shifted due to the coulomb pairing interaction inside a medium of dielectric constant ε and r is the donor - acceptor pair separation.

A transition between distant pairs is less probable than a transition between nearer pairs, so the emission intensity should increase as the pair separation distance (r) decreases (Thomas 1968).

Note that since the impurities are localized at discrete sites in the lattice the distance r varies by finite increments thereby providing a possible range of states.

A more complete account can be found in Dean (1969), Elliott and Gibson (1974) and Queisser and Heim (1974)

2.3.4 NON-RADIATIVE RECOMBINATION

An electron-hole pair need not necessarily recombine radiatively. One alternative is the direct conversion of the energy of the transition to heat, by the emission of lattice phonons. Infact, for most transitions photon emission has to compete with the Auger effect, in which the energy released on recombination is immediately absorbed by another free electron which in turn is excited high into the conduction band. Due to a near - continuum of suitable energy states down to the bottom of the conduction band, it is easy

for this 'hot' electron to lose its energy by successive phonon emissions. The Auger transition might be thought to have a lower probability than the radiative electron-hole recombination, because the former requires another electron to be present in the vicinity at the appropriate time before it can occur. On the other hand the 'hot' electron not only receives the released energy but also carries off the momentum of the electron and hole, so that Auger recombination need not be restricted to 'vertical' transition in k-space. This then increases the number of possible transitions.

When impurity centres are involved, then as outlined earlier, recombination usually involves one or more carriers which have been captured and localized in the ground state of a series of impurity levels. In such cases it is often found that the excited states of the impurity centre are sufficiently close together for an electron to transfer non-radiatively from the conduction band to the ground state via the higher levels by a process of phonon emission. The electron can recombine with a nearby hole radiatively or through on Auger process, transferring the energy to a nearby free carrier.

Nonradiative recombination processes will not be dealt with further in this work. For more detailed descriptions see Pankove (1971) and Elliott and Gibson (1974).

2.4 DETECTION OF CATHODOLUMINESCENCE

A wide variety of types of electron beam apparatus are suitable for cathodoluminescence (CL) studies. However, the scanning electron beam instruments are particularly useful since the emitted light can be continuously monitored to form a CL image of the specimen. It was exactly this facility which led Bernard et al. (1959) and Davey (1966) to construct CL detectors for the scanning electron microscope (SEM) and electron microprobe respectively, following the work of McMullen (see Smith and Oatley 1955). The use of a plane mirror to reflect the light emitted from the sample to the detector (ie. a photomultiplier - PM),usually outside the SEM chamber but attached to one of the access ports, was almost universal in the early SEM CL literature. It was with this simple type of CL detector system that Pease and Hayes (1966) first presented total emitted CL (ie. all wavelengths) micrographs of biological specimens. A few years later Williams and Yoffe (1968, 1969a, 1969b) slightly modified the collection system by using a quartz light pipe to collect the luminescence from the specimen and pass it to the photocathode of a photomultiplier tube, the output from which was suitably amplified and used to form an image of the total specimen luminescence. Simultaneously, an image of the specimen was focussed via a quartz lens set in the wall of the vacuum system, onto the entrance slit of a prism spectrometer. The signal from the spectrometer was either

fed to a second photomultiplier tube and amplified, or the luminescence spectrum could be recorded on photographic plates. Monochromatic (one wavelength)scanning micrographs could also be observed or photographed. Their results were for semi-conductor type materials.

It was realised early on in SEM CL investigations that the photomultiplier tube, although an excellent detector of light, could be responsible for spurious CL signals. In a photo-multiplier tube any energy packet over a certain threshold level will cause electron emission at the photocathode and will finally be registered as a signal as if it were a light photon. It is known (Muir 1974) that a proportion of the primary electrons are elastically scattered from the specimen surface and can reach the photomultiplier tube. The PM tube can not distinguish between these high energy primaries and the low energy photons of cathodoluminescence. This produces a confusing background emission (note that X-ray photons can also produce PM noise). Secondly, if the CL intensity is low, as is usually the case in the SEM, then to produce a reasonable CL image on the video screen it is necessary to work at very high PM gain. Doing this obviously amplifies both the PM signal and the noise, and it is quite possible to produce a false CL image. This is why Muir et al.(1971) in an early publication, were able to obtain CL micrographs from metallic samples which were indistinguishable from the backscattered emissive mode micrographs.

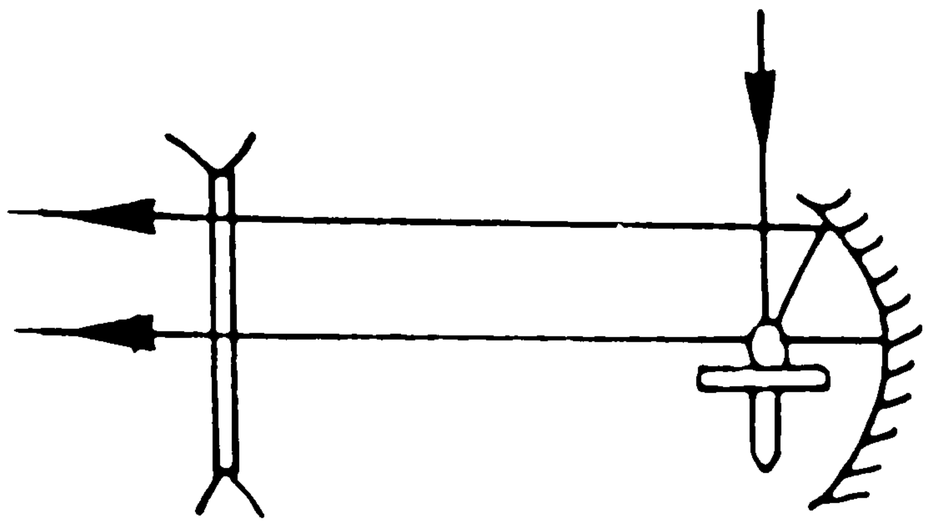
Generally the CL yield from most samples is fairly low and so an essential step has been the development of an efficient light collection system. Only an outline of the CL detector literature is thought necessary since a number of excellent reviews are available, see Thornton (1968), Holt (1974) and Muir and Grant (1974).

Figure 2.6 is a summary of the various devices that have been proposed.

Muir et al. (1971) and others have suggested the use of a partial parabolic mirror placed behind the specimen, This type of arrangement shown in 1, Figure 2.6 collected the luminescence and reflected a collimated beam of light towards the detector provided the specimen was at the focus of the mirror.A variant form of this was used by Jones et al. (1973) to investigate the CL of semi-conductor devices at liquid nitrogen temperature. The design of Bond et al. (1974) was again very similar,except they made use of a more complete parabolic mirror (2 in Fig. 2.6) with a beam hole above the focal point of the mirror. A light collection efficiency of $\sim$ 95% was claimed. All the systems discussed so far had an exit window or lens in line of sight of the specimen. This was a disadvantage, since backscattered electrons could reach it and cause CL in the material of the lens or window.

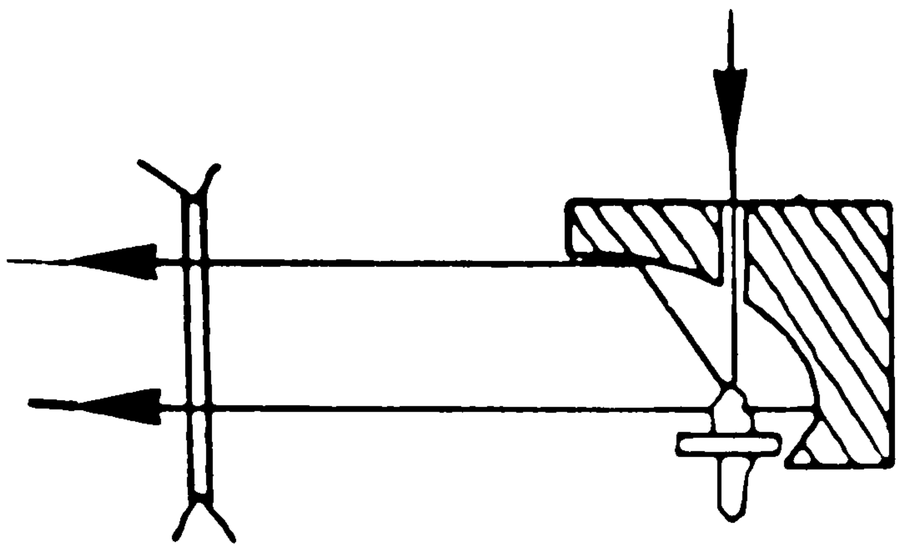
Hörl and Mügschl (1972) and Hörl (1972) described a light collector consisting of a half-ellipsoid of revolution, with

1. Rear parabolic mirror + window



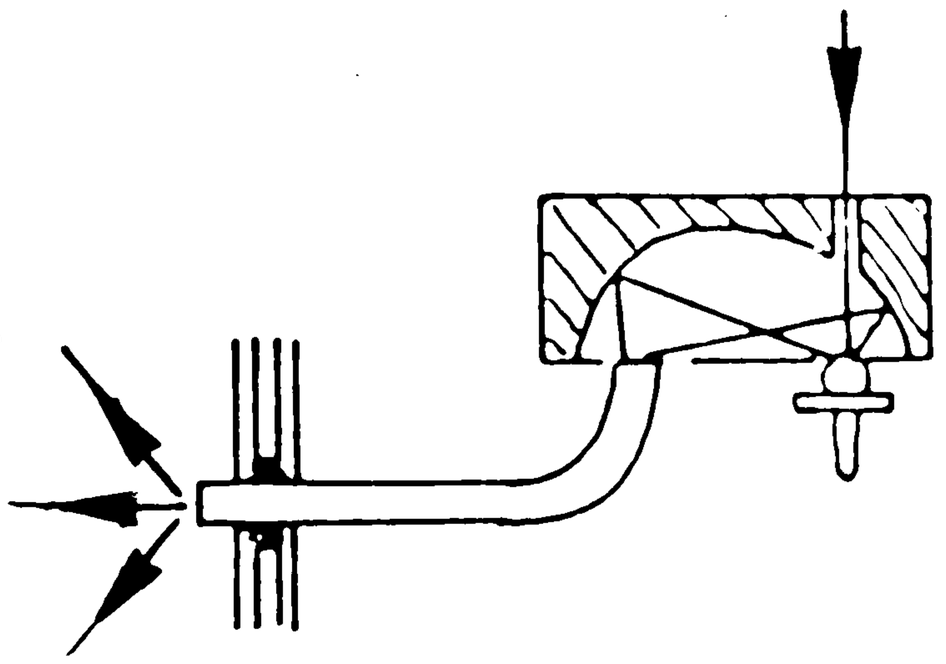
Muir, Grant, Hubbard & Mundell 1971

2. Parabolic mirror with electron beam hole + window



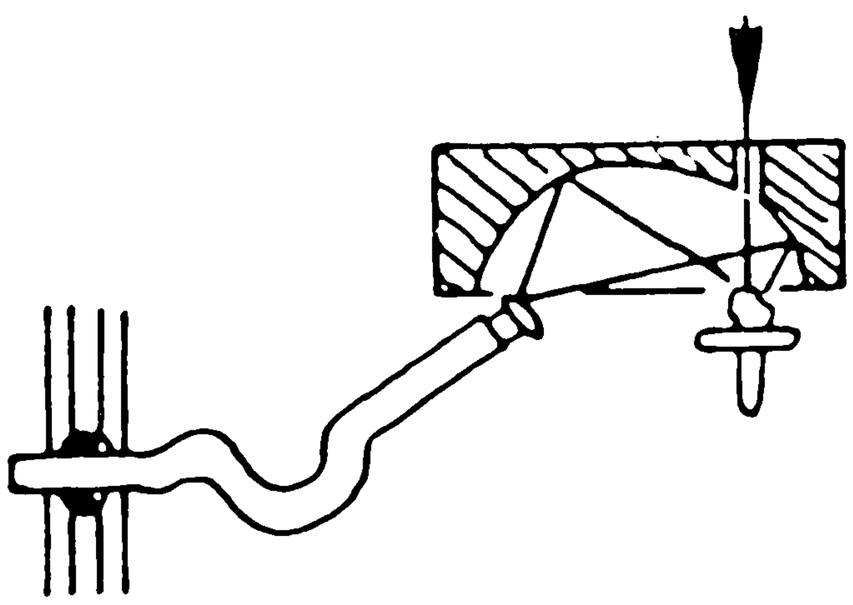
Bond & Haggis 1974

3. Semi - -ellipsoidal mirror + light guide



Hörl & Mügschl 1972

4. Semi - -ellipsoidal mirror + lens + fibre optics



Carlsson & van Essen 1974

Fig. 2.6 The development of cathodoluminescence collector mirrors

its major axis perpendicular to the incident electron beam. The specimen was placed at one focus and the light generated was collected at the other focus by a quartz light guide (3 in Fig. 2.6).

The mirror was made out of epoxy resin and coated with aluminium. Choosing a material of low atomic number (the resin) minimizes the rescattering of electrons. Although the mirror showed good light collecting efficiency there were many optical alignment difficulties to overcome. Especially when the signal had to be passed into other bulky components (eg. monochromators) placed outside the SEM chamber. Furthermore, when the light emerges from the light pipe it is spread over a solid angle of 2 π sr. and hence cannot be passed easily through the slits of a monochromator without a reduction in intensity.

Carlsson and van Essen (1974) replaced the solid quartz light pipe used by Hörl and Mügschl witn a flexible fibre optic light guide thereby overcoming many of the earlier problems of alignment (4 in Fig. 2.6). They also introduced a microscope objective lens infront of the fibre bundle to collimate the CL emission since most light guides have small acceptance angles. The cross-section of the bundle can be changed from circular at one end, to rectangular at the other, to match the monochromator slit dimensions.

The cathodoluminescence light collecting system adopted in

this group is similar to Carlsson and van Essen's design but with some further modifications. For instance the ellipsoidal mirror has been truncated at the second focus, removing an unused section of the mirror, so that good quality secondary and primary electrons as well as CL micrographs can be viewed simultaneously on the video screens of the SEM. The mirror has been constructed as a separate single unit (see section 3.5 Fig. 3.3) which fits into a side port, allowing greater specimen movement. A fuller description of the system used for this work will follow later in section 3.5.

Recently Davidson and Rasul (1977) used an ellipsoidal mirror with its major axis parallel, rather than perpendicular as shown in 3 and 4 of Fig. 2.6, to the direction of the incident electron beam. In this case, the second focus is brought outside the specimen chamber, after passing through a quartz window, by a 45° plane mirror positioned beneath the specimen. They have used this system to study dislocations in both LPE and VPE GaP layers (Rasul and Davidson 1977).

2.5 INTERNAL ELECTRIC FIELDS IN ZNS CRYSTALS

In vapour phase grown ZnS platelets there usually appear a variety of structures (hexagonal, cubic and polytypic bands) all perpendicular to a common c-axis. However, the stacking sequence of the different crystal areas is along the c-axis. Brafman et al. (1964) found that in-spite of polytypism, twinning and one-dimensional stacking

disorders the polar sence (ie the Zn - S - Zn - S sequence) of the [111] axis according to the cubic notation, or c-axis remains constant. Further properties of these striated platelets will be dealt with in section 3.2. The observed striations, which are boundary lines between homogeneous crystal regions, were believed to be some sort of electrical barrier sites giving rise to the well known anomalous photovoltaic effect (APE) in ZnS (Ellis et al. 1958, and Merz 1958). The voltage generated normal to the striations (ie along the common c-axis) when the crystal is illuminated by monochromatic UV light is anomalous in that its magnitude can be many times larger than the potential drop across the energy gap. The latter is the upper limit to photovoltages that can be generated at single barriers such as p-n junctions. Often photovoltages up to several hundred volts per cm along the common c-axis have been reported in ZnS crystals. Also the anomalous photovoltage undergoes several reversals of sign as the wavelength of the illumination is changed across the visible range (Brafman et al. 1964 and Shachar and Brada 1968).

By assuming the existence of intrinsic electric fields, several models were proposed to explain the APE phenomenon Tauc (1959), Hutson (1961) and Neumark (1962). Experimental evidence of internal fields in the direction of the crystallographic c-axis has been obtained by spreading a suspension of TiO_2 powder in silicone oil on ZnS platelets (Brafman et al. 1965).

The electric fields were found to exist both in the dark and under illumination. However they were unable to identify the sense of the electric fields in the different polytypes.

Recent detailed measurements of these internal electric fields are based upon the Franz - Keldysh effect (see section 2.7.3) ie. the electric-field - induced shift of the fundamental absorption edge (Shachar et al. 1970a, Brada et al.1972 and Yacobi and Brada 1974). It has been shown that near the direct absorption edge, if no internal fields are present then $\Delta\alpha$ (the change of the absorption coefficient) is positive and proportional to F^2 (F being the applied external electric field). If however, internal fields are also present then the external voltage either adds to the internal field in which case a positive $\Delta\alpha$ is observed, or acts in opposition to the internal field and then the observed $\Delta\alpha$ may be negative.

The experimental results of Yacobi and Brada (1974) have shown that because of the existence of internal barriers at the boundaries between different crystal (polytype) structures indicated by the striations, see Shachar (1966) and Shachar and Brada (1970), the distributions of the applied field as well as of the internal electric fields are highly inhomogeneous inside the crystal. Also, infering from the magnitude of the observed Franz-Keldysh effect, the highest fields, both intrinsic and extrinsic, were found in the more densely faulted regions of a platelet and not in the uniform

regions. These internal electric fields have now been established as arising from charged dislocation sheets appearing at the interfaces of different structures because of the lattice constant mismatch. The dislocations in one interface are all of the same charge because of the polar character of the common c-axis. The field propagates between two sets of oppositely charged dislocation lines which are preferentially sited at the two boundaries of a polytypic band (Shachar and Brada 1970 and Steinberger et al. 1972). Infact, the nearer the sheets of differently charged dislocations are to each other, the stronger are the expected internal fields as in wider regions a large percentage of the field lines leave the crystal. In the wider regions there are also more photoexcited (or electron-excited) carriers avaliable for charge compensation near the charged sheets of dislocation, thereby effectively neutralizing the internal fields, (Shachar et al. 1971). These internal electric fields are typically of the order 10^5V/cm.

It has been shown by Röppischer (1968) that photoluminescence (PL) in Mn activated ZnS and CdS can be enhanced by the application to the phosphor of an electric field. Results to be presented later in this work (section 4.2.3) have shown that the internal electric fields in these ZnS platelets have a quenching effect on the observed CL emission.

2.6 FUNDAMENTAL OPTICAL ABSORPTION

The most direct and perhaps the simplest method for probing the band structure of semiconductors is to measure the absorption

spectrum. In the absorption process, a photon of a known energy excites an electron from a lower energy (valence band) to a higher energy (conduction band) state. Absorption is expressed in terms of a coefficient α ($h\nu$) which is defined as the relative rate of decrease in light intensity along its propagation path and has typical values in the range 10^5 to 10^6 cm^{-1} in semiconductors. Generally, on the high energy side of this band there is often a smooth fall in absorption over a range of several electron volts. On the low energy side, on the other hand, the absorption coefficient falls more rapidly and may fall by as much as six orders of magnitude within a few tenths of an eV. In semiconductors this low energy boundary of the fundamental absorption is often the most striking feature of the spectrum and is referred to as the absorption edge. The limit of the absorption edge corresponds to the photon energy required to promote electrons across the minimum energy gap (E_g). The edge region often shows some structure, in particular that due to excitons (ie. bound electron-hole pairs see section 2.3.2). Exciton absorption is more pronounced in insulators, particularly in ionic crystals, than in semiconductors, and can lead to strong narrow - line absorption peaks at low temperatures.

2.7 CATHODOLUMINESCENCE EMISSION BAND SHAPE ANALYSIS

The band form of both the optical absorption and emission spectra of semiconductors and insulators has received a great deal of attention; for reviews see Markham (1959, 1966) Klick

and Schulman (1957) and Pankove (1971). Much of the analysis of the optical properties of luminescence centres in solids has followed along similar lines to the theories developed for the luminescence of gases. It has been established that these centres have specific states which can be expressed in atomic spectroscopy notation and that transitions between them lead to absorption and emission. There exists a close analogy between the luminescence spectra of gases and those of solids when inner shell transitions are involved (eg. rare earth doped samples). However, more relavent to this work are the transitions between outer shell states and states of the host lattice, within which the centres are dispersed.

Comparison of the absorption and emission spectra of gases with those of solids shows that they differ in two ways; (1) the spectra of solids no longer consist of lines but broaden out into bands and; (2) the emission bands occur to the low energy side of the absorption bands. This can be understood in terms of configurational coordinate models.

2.7.1

CONFIGURATION COORDINATE DIAGRAM

A convenient quantitative way of expressing optical absorption and luminescent processes is by a configuration coordinate diagram as shown in Fig. 2.7. This type of scheme was first introduced by von Hippel (1936) and since then has found

extensive use because the general form of the diagram is the same for many systems. In such a diagram the ordinate represents the total energy of the defect or entire system for the ground and excited states of the centre and is plotted versus an abscissa which represents the "configurational coordinate", specifying the movement of the ions or electrons from their equilibrium positions.

In Fig. 2.7 the equilibrium position of the ground state occurs at A, from which it is raised to the excited state at B by the absorption of light. Only vertical transitions are allowed in accordance with the Franck-Condon principle. This states that because electrons move much faster than nuclei, an electronic transition occurs so rapidly compared with the vibrational motion of the nuclei that the inter-nuclear separation remains essentially constant during the transition ie. the configurational coordinate is unchanged. Hence optical transitions are vertical in Fig. 2.7 and it is only after a transition is complete that the lattice distorts or "relaxes" so as to minimise its energy. Inspection of Fig. 2.7 then shows that the shift from the absorption to the emission band peak positions arise as follows:-

The centre having reached the excited state at B, the ions of the system relax their energy until a new equilibrium position is established at C. The energy difference between states B and C is compensated by lattice vibrations ie. phonon emission. Once at C, the centre may return to the ground

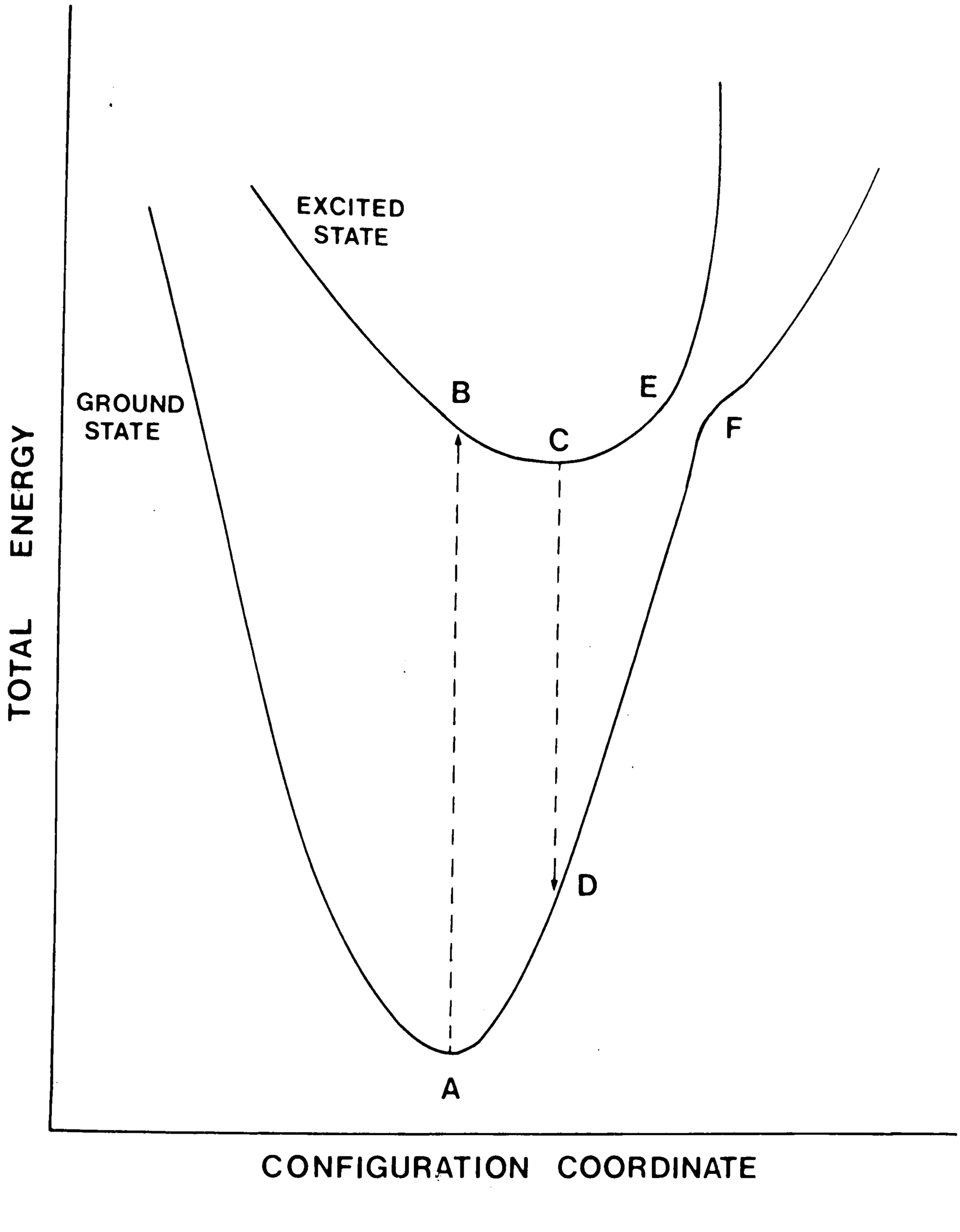


Fig. 2.7 A configuration coordinate diagram showing the ground and excited states of a luminescent centre

state at D by the emission of a photon. The centre finally relaxes from D to A by again giving up energy to the lattice vibrations. In general the weaker binding of the higher level to the centre will produce a shallower excited state well displaced from the ground state minimum. Thus the energy of the emitted photons is usually much smaller than that of the absorbed photons and this difference is known as the Stoke's shift.

Both the curvature of the configurational coordinate plots and their relative displacement along the coordinate axis is determined by the interaction of the particular centre of interest with its neighbouring ions. Obviously, the strength of the interaction also determines the amount of the Stoke's shift observed.

It has usually been assumed (Invi and Uemura 1950, Williams 1951b and Klick 1952) that the physical situation represented by the configuration coordinate model is one in which the ions immediately surrounding the centre all oscillate synchronously in a radial direction from the centre. (This type of oscillation is known as a "breathing" mode of lattice vibration). The coordinate distance then is the distance from the centre to any one of the nearest neighbour ions and the effective mass of the centre is that of the ions surrounding the centre. This assumption most probably is an over-simplification which, however, does not modify the essential ideas.

Using this very general classical configuration coordinate diagram Gurney and Mott (1939) were able to explain the sudden decrease in luminescence efficiency, at high temperatures. This is because a centre in the excited state C can move to a point E, given sufficient thermal energy, and make the small transition to point F associated with the ground state (perhaps with the emission of a low frequency photon) and finally relax to point A by the emission of phonons. In this way the energy of the absorbed photon, which raised the centre from A to B, is infact transferred into heat rather than photon emission and thermal quenching of the luminescence is observed.

The overall generality of the diagram follows from the fact that to a reasonable approximation parabolic energy bands are expected around stable minima, whether considering ion separations in a molecule or the energy levels of electrons near a defect in a solid. In other words for small displacements these systems act like simple harmonic osillators.

Although a classical treatment of the configurational coordinate curves can successfully explain the Stoke's shift between the absorption and emission energies and the high temperature phenomenon of thermal quenching, it fails to describe adequately the low temperature variation in half-width (H) of the absorption and emission bands. It has been shown, Mott and Gurney (1940), that the classical curves predict a variation in band width that is proportional to the square root of the temperature. This form of dependence

is however not observed experimentally at low temperatures, in the absorption and emission spectra of a variety of materials (Johnson and Studer 1951 and Patterson and Klick 1957, give results for KCL: Tl).

It was Schön (1948) who first suggested that the low temperature broad band emission spectra which were observed might be due to zero point vibrational energy associated with the luminescent centre.

Williams (1951 a, b) and Williams and Hebb (1951) using these curves and treating the centre quantum mechanically as a simple harmonic oscillator were able to compute correctly the position and band width of both the emission and absorption bands as a function of temperature.

A quantum mechanical modification of the configuration coordinate curves (or semiclassical Franck - Condon principle) means that the continuous energy distribution curves of Fig. 2.7 can be replaced by a series of equidistant energy levels separated by $h\nu$, where ν is the frequency of the vibrating system. The lowest vibrational level is $h\nu/2$ above the minimum of the classical curve.

As the temperature is reduced, then, a situation is reached in which practically all the excited state centres exist only in the lowest vibrational level. The band shape is then essentially determined by the number of vibrational states at

each ground level. It is known that a large number of quanta can be involved in the process, so a random addition of the vibrational quanta produces a Gaussian shaped distribution of filled states. Consequently the absorption and emission bands are also Gaussian in shape.

Also, as the temperature of a luminescent material is raised, the centres which are in the excited state will exist not only in the ground vibrational state but also in higher vibrational levels. The amplitude will extend over a larger coordinate distance for the higher levels and result in transitions to a wider range of the ground state configuration curve and hence leads to broad bands.

The resulting width of the emission (or absorption) band as a function of temperature has been given by Williams and Hebb (1951) as:

$$H = C \left[(\hbar\omega_o/2k) \coth (\hbar\omega_o/2kT) \right]^{\frac{1}{2}} \qquad (2)$$

where H is the bandwidth in eV, C is a constant, $\hbar\omega_o$ is the "effective" phonon energy, k is Boltzmann's constant, and T is temperature. This equation reduces to Mott and Gurney's expression at high temperature and becomes a constant at low temperature.

A more detailed theoretical treatment of this subject has been given by Markham (1966). Furthermore, some of the assumptions

and approximations involved in the configuration coordinate curve method are discussed by Lax(1952).

The validity of equation (2), has been investigated for the F - centre absorption and emission bands in various alkali halides (Russell and Klick 1956, Konitzer and Markham 1960, Lütz and Gebhardt 1962). In all cases a completely satisfactory agreement was found.

The edge or fundamental (conduction band to valence band transition) emission band data for CdS was shown to follow the above equation (cf. Fig. 4.25 section 4.4) and will be dealt with subsequently.

2.7.2 URBACH'S RULE

The simplest expression for the form of the fundamental optical absorption edge, arising from transitions between the valence band maximum and the conduction band minimum (see section 2.6), is one in which the absorption constant (α) increases with the square root of the photon energy in excess of the gap energy, ie.

$$\alpha(h\nu) = A(E - E_o)^{\frac{1}{2}} \qquad (3)$$

As outlined by Pankove (1971) this expression is obtained by assuming momentum conservation, ie vertical transitions, between parabolic valence and conduction bands. This type

of expression however, is not observed experimentally and can not be considered to represent the shape of the optical absorption or the emission bands in CdS and ZnS (Dutton 1958 and Yacobi et al. 1975).

As mentioned earlier in section 2.7.1, Gaussian band shapes are expected for both absorption and emission bands using the configuration coordinate model, ie. they are of the form:

$$I = I_o \exp\left[\tau^2 (E - E_o)^2\right] \qquad (4)$$

(see Lax 1952, Klick and Schulman 1957 and Markham 1959, 1966 for the detailed analysis). In the case of emission bands, deviations from this form have often been reported but ignored or attributed to insufficient experimental sensitivity eg. by Patterson and Klick 1957. For the fundamental absorption edge the low energy tails are definitely non-Gaussian in shape and can be expressed empirically as a function of temperature and energy as:

$$\alpha = \alpha_o \exp\left[g(E - E_o)\right]; \; g = \sigma/kT \qquad (5)$$

where α is the absorption coefficient; E is the photon energy; α_o, g, σ and E_o (the band gap ie the "edge" photon energy) are all materials constants; and k, T have their usual meaning. This relationship is known as Urbach's rule (Urbach 1953) and

is obeyed over many orders of magnitude of α values in a variety of non-conducting materials, including semiconductors (Dutton, 1958 and Pankove 1965) and a number of alkali halides especially KI (Martienssen 1957 and Haupt 1959). The more detailed measurements and interpretations presented later by Mahr (1962, 1963) using KI diluted in KCl crystals, showed that the exponential spectral dependence of Urbach's rule does not really set in until the absorption coefficient α, has dropped about two orders of magnitude below the peak value. Above this, the spectral dependence was found to be Gaussian in shape. Both ZnS and CdS crystals exhibit exponential absorption edges (Piper 1953, Dutton 1958 and Yacobi et al. 1975).

In covalent semiconductors the absorption tail slope parameter g in equation (5) was found to depend on the concentration and the state of ionization of the impurities (Dixon and Ellis 1961, Redfield and Afromowitz 1967 and Casey et al. 1975). In ionic crystals however, the slope parameter g is a temperature dependent quantity given by $g = \sigma/kT^*$ with an "effective temperature"

$$T^* = (\hbar\omega_o/2k) \coth (\hbar\omega_o/2kT) \qquad (6)$$

where k and T have their usual meanings, $\hbar\omega_o$ is the energy of the relevant phonon and σ is a material parameter (Mahr (1962, 1963).

Numerous attempts have been made to explain the exponential dependence of the optical absorption edge (ie. equation 5) because it seemingly expresses something basic about absorption bands in solids. It is believed, that in general, there are two main reasons for the observed temperature dependence of the optical edge in any semiconductor or insulator. They are (a) the band structure must be a function of the crystal lattice spacing, so that the lattice dilation may be expected to contribute to a change in the absorption edge energy; and (b) contributions arise due to the electron-phonon interaction. Crystal lattice dilation effects in CdS and ZnS (Hohler 1949, Piper et al. 1958 and Yacobi et al. 1975) have been shown to account for at most a 10% change in the absorption edge energy.

Möglich et al. (1940) attempted to explain the temperature dependence of the absorption edge by suggesting that lattice vibrations cause a temperature dependent broadening of the energy levels. However, their calculations predicted too small an effect to explain the experimental results in CdS (Hohler 1949). Later, Radkowski (1948) and Fan (1951) considered the broadening of energy levels as associated with the electron - phonon coupling. Piper et al (1958, 1959) have tried to fit the observed temperature shift of the ZnS absorption edge to Fan's theory and found that too high an effective mass had to be introduced for both electrons and holes. Infact it was concluded, independently of the effective mass assumed, that there remains a temperature dependence > 150K

which can not be explained by either thermal contraction of the crystal or the interaction with optical phonons.

Meijer and Polder (1953) have pointed out that in ZnS there are piezoelectrically active acoustical modes which become relatively more important than the optical modes for electron scattering below 150K.

The experimentally observed temperature behaviour of both LA (longitudinal acoustic) and LO (longitudinal optical) phonons in CdS crystals will be presented in a later section of this work.

A totally different approach was taken by Redfield (1963a,b) and subsequently Dow and Redfield (1972) who studied the effect on the absorption edge of the large random electric fields produced by charged imperfections (including piezo-electrically active phonons) in a semiconductor. The effect is computed on the basis of the internal Franz - Keldysh mechanism (ie. a photon assisted tunnelling between valence and conduction band at photon energies smaller than the energy gap) and leads to exponential tails in the absorption edge. Only this recent unified theory of Dow and Redfield (1972) can be considered as plausible and will be outlined below in section 2.7.4. Although the Dow and Redfield model is far from being universally accepted it has so far, success-fully explained many experimental results including those to be presented in this work.

2.7.3 THE FRANZ-KELDYSH EFFECT

It is well known that an externally applied electric field shifts the fundamental optical absorption edge of a solid to slightly lower energy. This is the Franz-Keldysh effect (and is due to photon assisted tunnelling), (Franz 1958 and Keldysh 1958) and was first observed in silicon (Vavilov and Britsyn 1961). Similar observations have been made in a number of materials (Paige and Rees 1966 and Williams 1960 give for example results for GaAs and CdS respectively).

The Franz-Keldysh mechanism may be understood in terms of quantum mechanical penetration of the wave functions of the band states into the normally forbidden energy gap of a material.

When an electric field ε, is applied to a solid the band edges are tilted. If an electron moves within a band, a distance **x** away from the edge, with constant total energy, then not only will it acquire a kinetic energy ($q\varepsilon x$) but also its momentum will be real. However, if somehow the electron was able to move into the band gap (E_g) maintaining the same constant energy, its kinetic energy would become negative and the corresponding momentum would be imaginary. Thus, the wave function of the electron in the gap is subject to exponential damping. It can be seen, therefore, that in the region of penetration the states at the band edges are effectively broadened exponentially into the gap by an amount

depending on the strength of the applied electric field. In this way, optical interband transitions can be caused by photons of energy $h\nu$, eventhough $h\nu$ is much less than the normal band gap E_g, as illustrated in Fig. 2.8.

Therefore the effect of an electric field is always to reduce the apparent energy of the absorption edge or in other words the tunnelling (ie. penetration) probability is increased. So an ideally sharp, direct, band to band absorption edge aquires a nearly exponential 'tail' at energies less than the band gap E_g.

Redfield (1963a,b, 1964) investigated the way in which an absorption edge may be influenced by the corresponding effect due to naturally occurring internal fields(typically 10^4V/cm) arising from charged imperfection in solids. This internal analog of the Franz - Keldysh effect was used by Dow and Redfield (1972) in their unified theory of Urbach's rule and exponential absorption edges.

2.7.4 THE DOW AND REDFIELD MICROFIELD MODEL

As mentioned previously (section 2.7.2), the Urbach slope parameter g in equation 5 exhibits a variety of forms of dependence on temperature and impurity concentration, being inversely proportional to temperature (at high temperature) in alkali halides and II - VI compounds, but determined by dopant concentration in III - V semiconductors. The exciton

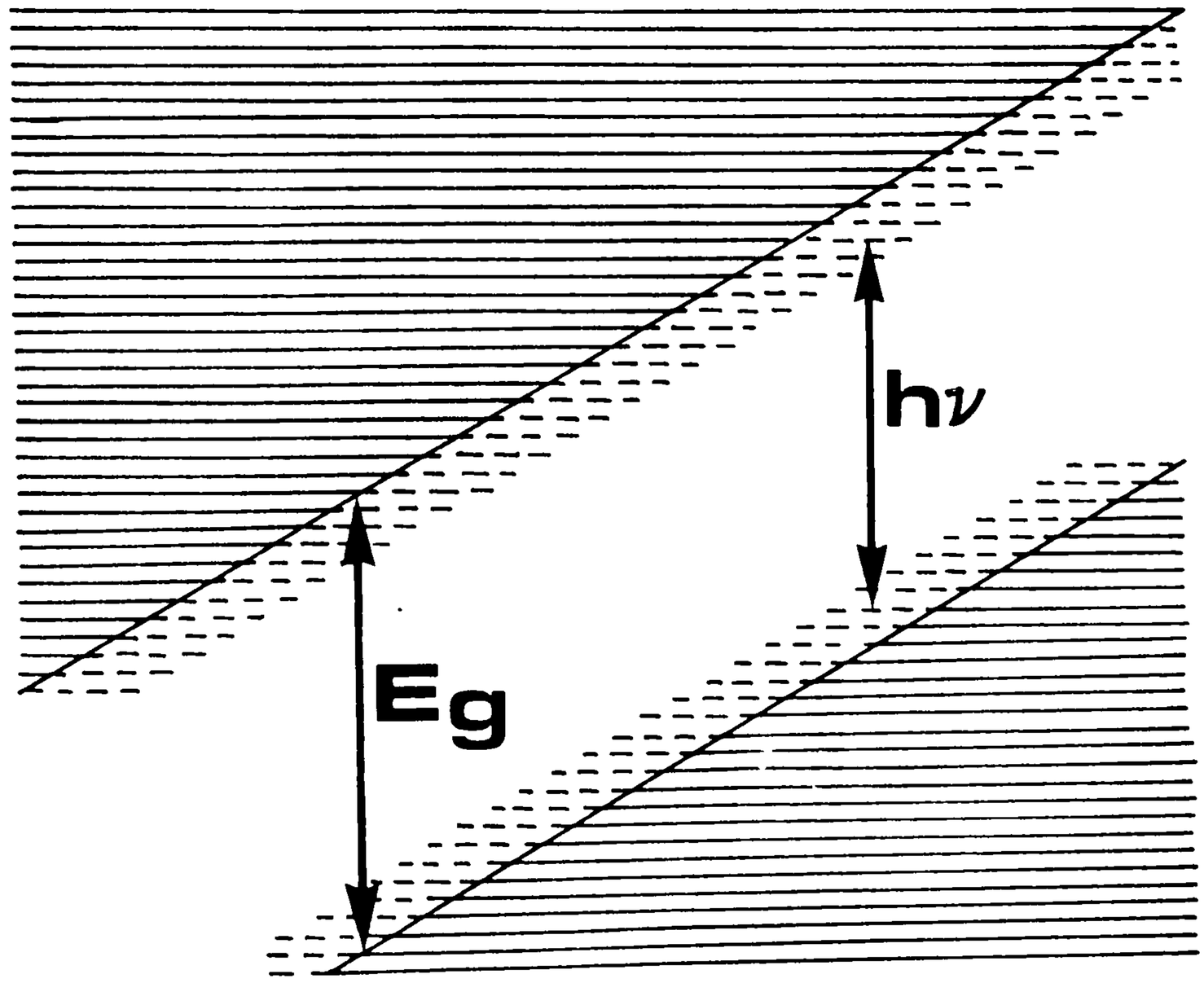


Fig. 2.8 Energy bands with penetrating wave functions in a strong electric field

interaction with phonons (especially LO phonons) has been listed as a primary cause of Urbach's tail in alkali halides (Toyozawa 1959) whereas charged impurities seem to shape the edge of impure GaAs (Redfield and Afromowitz 1967).

There are of course, several different theories which are capable of producing approximately exponential edges caused by either impurities or phonons but none seem to be quantitatively unified.

The presence of exponential edges in both ionic and covalent materials suggest that the physical model should be the same in these non-conducting solids. From this point of view Dow and Redfield (1972) presented a model which is capable of explaining both the exponential form (Urbach tail) and the temperature dependence of the optical absorption edge. It attributes the exponential edges to the internal electric microfield ionization of the exciton,that is field-induced tunnelling of the electron away from the hole as in the Franz - Keldysh mechanism. By internal electric microfields are meant relatively macroscopic fields which extend over many lattice constants, of the order of excitonic radii, and not local fields on an atomic scale. The theory applies to both ionic solids and covalent semiconductors.

The dominent sources of such electric microfields vary from material to material and may be longitudinal phonons, LO and LA,

which produce electric fields through the piezoelectric effect, ionized impurities, dangling bonds, dislocations or other potential fluctuations associated with lattice disorder (Dow and Redfield 1972 and Chopra and Bahl 1972).

The Dow and Redfield (1972) theory is in essence an extension of Redfield's (1963b, 1964) internal Franz - Keldysh mechanism to include the effects of the final-state Coulomb interaction between the optical electron and hole, plus Dexter's (1967) quadratic Stark - shift mechanism to include the electric field broadening of the exciton as well as the shift. It should be noted that neither of the previous microfield theories (ie. Redfield 1963b and Dexter 1967) obtained an accurate exponential spectral shape as an inherent feature. They achieved the exponential shape only by suitable averaging techniques (see Dow and Redfield 1970, 1972).

Experimental support for Dow and Redfield's internal electric microfield model for exponential absorption edges resulting from photon - assisted tunnelling between tails of states induced by Coulomb interaction with charged inpurities was demonstrated by Redfield and Afromowitz (1967). They compared the temperature dependence of the absorption edges in p-type and in compensated GaAs. The state of charge of the impurity and the observed breadth of the edge in the compensated sample were both virtually independent of temperature, whereas the doped sample exhibited increasingly broad edges as the temperature increased and the impurities ionized.

A second experiment by Garrod and Bray (1972) consisted in shooting a pulse of amplified piezoelectric (fast transverse acoustic) phonons down a bar of GaAs and monitoring the domain-induced change in the absorption edge. The resulting edge was exponential and has been termed a piezo-Urbach edge (Dow et al. (1974).

The principal assumption of the Dow and Redfield (1972) theory is that the optical absorption coefficient in the vicinity of the fundamental edge of a real crystal can be expressed as a weighted average of the absorption coefficient $\alpha(\nu, F)$ for excitons in a uniform electric field of magnitude F:

$$\langle \alpha(\nu) \rangle = \int_0^\infty P(F)\, \alpha(\nu, F)\, dF \qquad (7)$$

where P(F) is the probability that there is an electric microfield of magnitude F at the location of the exciton created by the absorbed photon. Dow and Redfield (1972) have calculated this probability P(F), which depends on the details of the source of the microfields. For an ionic crystal, P(F) depends primarily on the electron – optical - phonon coupling constant and the temperature, whereas in a covalent material this probability P(F) mostly relies on the number and spatial distribution of the ionized impurities.

For a Gaussian field distribution, that expected for compensated semiconductors (Morgan 1965) and for the LO phonons in ionic solids (Dexter 1967 and Dow and Redfield 1972),

Dow and Redfield have formulated the probability function P(F) as:

$$P(F) = (2/3\pi \langle F^2 \rangle)^{-3/2} \; 4\pi F^2 e^{-3F^2/2\langle F^2 \rangle} \quad (8)$$

The value of $\langle F^2 \rangle = F_{rms}^2$, ie of the square of the root-mean-square field, can be evaluated from the above equation (8), (Dow and Redfield 1972),

$$\text{ie. } \langle F^2 \rangle = \left[\hbar\omega_{LO} \, q_c^3 \, (\varepsilon_\infty^{-1} - \varepsilon_o^{-1})/3\pi \right] \coth(\hbar\omega_{LO}/2kT) \quad (9)$$

Here $\hbar\omega_{LO}$ is the longitudinal optical phonon energy; ε_o and ε_∞ are respectively the static and optical dielectric constants; q_c is the polaron cutoff wave-vector which is normally of order π/a_L, where a_L is the lattice constant; k and T are Boltzmann's constant and the absolute temperature respectively.

Furthermore, Dow and Redfield (1972) have tried to explain the temperature dependence of Urbach's rule in ionic crystals. The reciprocal of the mean-square value of the field can be expressed as:

$$1/\langle F^2 \rangle = c/\hbar\omega_{LO} \tanh(\hbar\omega_{LO}/2kT) \quad (10)$$

where $C = 3\pi (\varepsilon_\infty^{-1} - \varepsilon_o^{-1})^{-1} q_c^{-3}$

Now equation (10) is rather similar to equation (6) of section 2.7.2.

ie.

$$g = \sigma/kT = 2\sigma_o/\hbar\omega_o \tanh(\hbar\omega_o/2kT) \qquad (11)$$

where, c, σ , σ_o are all constants and $\hbar\omega_o$ is the energy of the relavent phonon participating.

Thus the substitution of $2\sigma_o/c\langle F^2\rangle$ for σ/kT in Urbach's rule $\alpha = \alpha_o \exp\left[g(E - E_o)\right]$ (5); **gives**

$$\alpha = \alpha_o \exp\left[2\sigma_o (E-E_o)/(c\langle F^2\rangle)\right] \qquad (12)$$

So a semilogarithmic plot of the absorption coefficient versus $1/\langle F^2\rangle$ should yield straight lines.

Dow and Redfield calculated the absorption coefficient α from the Elliott theory of optical absorption (Elliott 1957) and found that exact straight lines were not obtained as predicted. The slight deviations were attributed to the rather arbitrary choice for the polaron cutoff q_c, and also because uniform fields have been assumed in the theoretical development of the model. In fact, they (Dow and Redfield 1972) believe that the field should be considered as being quasiuniform over the electron tunnelling distance and not just over an exciton radius as initially assumed.

The principal features of the microfield model are then (1) it is capable of providing a unified explanation of Urbach's edges; (2) it relies on internal quasi-static electric microfields; (3) it involves exciton enhancement of the edge; and (4) it attributes the Urbach broadening to the internal, relative motion of the exciton.

As already emphasized the Dow and Redfield (1972) model is applicable to all types of materials since the exponential shape of the edge as a function of photon energy is insensitive to the type and distribution of the microfields. In other words, the exponential form is a general consequence of internal microfield ionization.

It is reasonable to expect that the fundamental or edge emission band (conduction band to valence band transitions) will also be of a similar form to that of the edge absorption band in these materials. Infact the relation between absorption and emission can be derived from the principle of detailed balance or as it is sometimes known, the Van Roosbroeck - Shockley relation (1954). This states that at thermal equilibrium, the rate of radiative recombination is equal to the rate of optical generation of electron - hole pairs. Using this it is possible to derive the fundamental relation between the expected emission spectrum and the observed absorption spectrum (see Pankove 1971). Casey and Stern (1976) calculated the fundamental emission spectrum of GaAs in this manner from the absorption band and found fair agreement with the experimental

spontaneous edge emission band of p-type material. Dow et al. (1973) showed that the internal electric microfield model could also be used to explain the shape of the low energy tail of conduction band-to-acceptor emission in semiconductor photoluminescence. Recently several papers have reported the occurrence of the external Franz - Keldysh effect in the photo -and electro-luminescence of ZnS (Cingolani et al. 1966, 1967, Vlasenko and Khomchenko 1973) and CdS (Krolevets et al.1974). So it seems that the Dow and Redfield (1972) internal electric microfield model can provide an explanation for the low energy tail of the fundamental emission band of semiconductors.

Experimentally, an exponential variation of the low energy tail of the fundamental edge emission band was observed in GaAs (Casey and Kaiser 1967) and in the photoluminescence excitation spectra of certain chalcogenide glasses (Street et al.1975). In both these cases two very distinct regions of the low energy tail were observed, a higher intensity intrinsic region, and a low intensity region where impurities are important. Casey and Kaiser(1967)found that the slope parameter in the low intensity region of the exponential low energy tail varied in a simple monotonic way with the free carrier concentration. An analogous effect was found in the case of the fundamental absorption edge (Dixon and Ellis 1961, Casey et al.1975).

From the literature reviewed above it seems useful to determine the form of the cathodoluminescence (CL) edge bands (conduction band to valence band recombination emission) in II - VI compounds as it has attracted little attention. Furthermore, it would be interesting to analyse the shape of the low energy tails of these bands and compare it with that of the edge absorption of CdS and ZnS and also with the edge emission results observed in GaAs. Such an analysis is reported in section 4.4 for the case of hexagonal - structure CdS and of both hexagonal - and cubic - structure ZnS.

Shape analysis of a well understood impurity band in ZnS is also reported in section 4.5. This broad impurity band which falls well away from all others in the spectra of the specimens examined here is the well known self-activated ZnS: Cl band.

2.8 ZINC SULPHIDE CATHODOLUMINESCENCE SPECTROSCOPY

Scanning electron microscopy (SEM) spectroscopic cathodolumine-scence (CL) results were first published by Williams and Yoffe, in a study of stacking faults in ZnSe single crystals (Williams and Yoffe 1968, 1969a) and in striated ZnS (Williams and Yoffe 1969b, 1971). They used a quartz light pipe - monochro-mator - photomultiplier (PM) detector system to investigate 'intrinsic' ultraviolet CL from liquid nitrogen cooled platelets of II - VI compounds. By intrinsic it is meant that the

radiation observed consisted of photons having energies with values near to E_g, the energy of the forbidden gap (see section 2.3.1). They showed that in cooled ZnS crystals, the edge emission band contained characteristic bound exciton lines which were ascribed to hexagonal or cubic phase material. The local variations in CL emission in these lines observed over the crystals were related to the crystal defect structure deduced from other experiments such as transmission electron microscopy.

Similar exciton lines were observed at low temperature with the ZnS samples used in this work. However, to obtain a spectrum with good resolution it was necessary to work with the smallest bandwidth available on the monochromator (see section 3.5). Therefore since the CL intensity is low in the region of interest, the SEM beam current had to be increased to obtain a greater emission signal from the samples. Doing this causes specimen charging which is an undesirable effect (see section 3.4.1). Thus it was impossible to investigate further these characteristic exciton lines of ZnS in this present work.

It has long been realised that the emerging PM signal can be utilized in two very distinct modes of operation. These will hereafter be referred to as panchromatic and monochromatic CL micrographs. In the panchromatic mode the whole CL spectrum from the sample is passed to the PM tube and the corresponding image represents the total light signal. For

the monochromatic mode the CL signal is passed through a monochromator and only a limited bandwidth of radiation is allowed to fall on the PM tube.

In some later work, an interesting series of monochromatic SEM micrographs were presented by Yoffe et al. (1973) of ZnSe, ZnS and CdS samples.

Holt and Culpan (1970) used the conductive, cathodoluminescent and emissive modes of the SEM to examine ZnS platelets with striated structures. Their results indicated that not only did stacking faults and polytypic intergrowths correlate with changes in ZnS emission, but also some local variations could be due to inhomogeneous impurity distributions.

The above literature is the only ZnS CL SEM work so far. The results all seem to indicate that local variations in CL emission from structurally complex ZnS platelets may be due to (i) changes in structure, (ii) impurity segregation or (iii) internal electric field effects.

Section 4.2 reports the results of a further investigation of these effects, directed to separating the influences of these three factors.

3. EXPERIMENTAL WORK

3.1 THE CAMBRIDGE IIA STEREOSCAN SCANNING ELECTRON MICROSCOPE (SEM)

The SEM is a multi-mode instrument consisting of an electron optical column and a signal processing and display unit. It is the signal processing facility that gives the SEM its versatility, because almost any form of output from the specimen can be displayed on the video screens.

The backscattered electron, secondary electron, cathodolumine-scence and X-ray modes were mainly used in this work.

A few salient parameters important for SEM operations will be listed here for reference.

Electron Gun Filament	Thermonic 'hairpin' tungsten tip
Beam Energy	1 to 30 KeV
Beam Current	10^{-9} - 10^{-10} A is usually adequate for ZnS CL work
Vacuum	Oil pumped; 10^{-6} Torr
Magnification	20X to theoretically 80KX
Resolution (electron image)	Theoretically ~ 100Å
Specimen Stage	Cambridge Hot/Cold Stage with chromel - alumel thermocouple. Minimum temperature reached was (77 $\pm$ 1) K.

3.2 ZINC SULPHIDE AND CADMIUM SULPHIDE CRYSTALS

The zinc sulphide crystals studied in this work were all obtained from the Hebrew University of Jerusalem, Israel. They were grown by sublimation in the presence of H_2S (Brafman et al. 1964, Alexander et al.1970) or in a mixture of argon and HCl (Shachar et al. 1970b). The crystals were structurally nonuniform, consisting of parallel strips of different birefringence, all perpendicular to the common c-axis. Striated platelets are one of the characteristic morphologies produced by growth of ZnS by sublimation in a stream of an inert gas. These platelets exhibit polytypism which is the ability of a substance to crystallize into a number of different modifications. The phenomenon of polytypism was discovered in SiC by Baumhauer (1912), but since then it has been observed in additional materials like ZnS, CdI_2 and PbI_2 (Verma and Krishna 1966). Since the early 1960's, Professor Steinberger's group at the Hebrew University has systematically studied polytypism in vapour-phase grown ZnS. Infact much of the present knowledge concerning the properties of striated ZnS platelets has been derived from their excellent work as follows.

The striations observed consist of two sets of fine lines, visible to the naked eye. One set runs parallel to the original growth direction of the needles on which the platelets form. This is the common c-axis of the crystal structures present. The other set runs perpendicularly to the common c-axis. It has been well established that the set perpendicular to the

c-axis are polytypic bands produced by a martensitic, periodic slip process involving the movement of partial dislocations rotating about a central screw dislocation of large Burgers vector (Steinberger and Mardix 1967, Alexander et al. 1970 and Mardix et al. 1971). The other fine lines along the c-axis are called linear markings and are due to partially completed layers, secondary growths on the crystal face and so on (Mardix et al. 1968).

The various strips may have either the hexagonal structure (wurtzite - 2H), the cubic structure (sphalerite -3C) or one of the many polytypic forms. The samples examined throughout this work were on average 2 - 8 mm long, 1 - 5 mm wide and 50-100 μm thick.

A number of cadmium sulphide platelets from the same source were also investigated. These were slightly yellow in colour, since the fundamental band gap in this material falls around 2.432 eV (510 nm), as determined in this work. In contrast ZnS is transparent to visible light, having an energy gap in the near ultra-violet region of the electromagnetic spectrum, see table 2 in section 4.2.3 page 130. The CdS crystal were of the wurtzite (hexagonal - 2H) structure and about 100 μm thick.

Other ZnS platelets were obtained from Dr A Custers of the Electrical Engineering Department, Imperial College. These had been grown by sublimation in a stream of argon. The

crystals grew on the walls of a silica tube that had been flame polished to minimize the number of nucleation sites. The ZnS had been purified by pre-firing in argon. The crystals were part of the batch examined previously by Holt and Culpan (1970). However, results this time around were less satisfactory since most of the crystals were found to be heavily faulted. That is to say, the crystal structure in any one platelet changed many times over in travelling a few microns over the surface. Experimental results soon showed that badly faulted regions make quantitative analysis difficult. This aspect will be dealt with subsequently. It is now impossible to say, whether the imperfections were a growth occurance or whether they have been introduced over years of storage. ZnS platelets are all very fragile and crystallographically unstable and undergo structural transformation if handled carelessly. Steinberger and Mardix (1967) have shown that structural transformation can be introduced by applying mechanical stresses. Infact prolonged pressure converts the polytypic bands to sphalerite (3C), as this is the stable modification of ZnS at room temperature.

3.3 STRUCTURE DETERMINATIONS FROM BIREFRINGENCE MEASUREMENTS

The samples investigated were structurally nonuniform, consisting of parallel strips all perpendicular to the common c-axis. The individual strips are very narrow (a few microns) and many of the regions show tilts in their external faces as well (Mardix et al. 1968, Mardix and Steinberger 1970).

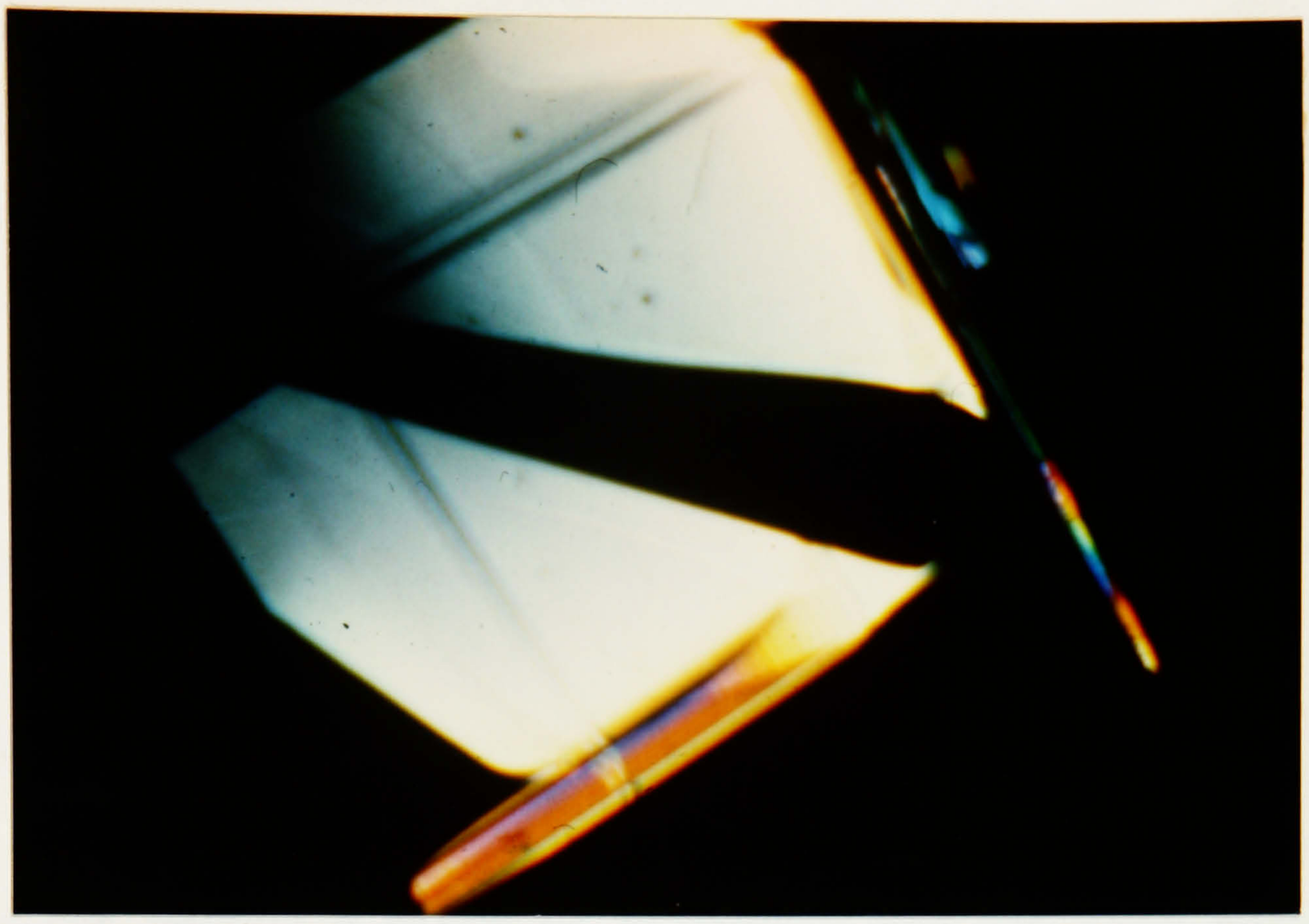
When these synthetic ZnS crystals are viewed between crossed polarizers in an optical microscope, each region appears coloured (Fig.3.1). Changes of colour in the strips perpendicular to the c-axis are due to variations in birefringence from one region to the next. The striations are the boundary lines between areas of uniform birefringence. It was proposed by Baum and Darnell (1962) that the birefringent changes could be associated with the changes in crystal structure. This idea led Brafman and Steinberger (1965, 1966) to correlate X-ray structural analysis with birefringence measurements for several ZnS polytypic bands.

The degree of birefringence is $\Delta n = n_e - n_o$, where n_e and n_o are the extreme values of the refractive index. Also, $\Delta n = t/d$ in which t is the optical path difference and d the crystal thickness.

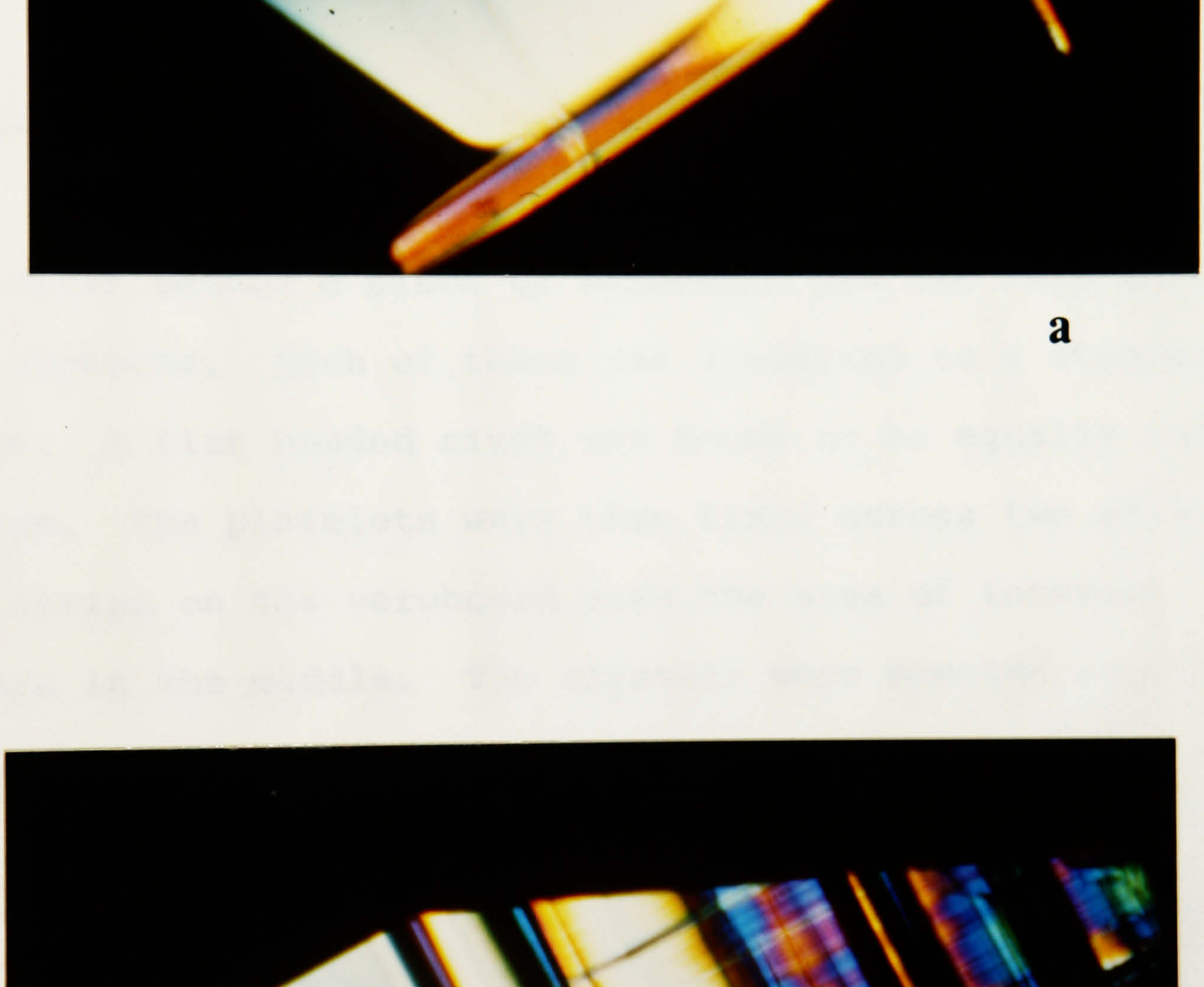
By measurement of Δn, the crystal structure of any desired area of a crystal could then be identified. To do this the experimental value for Δn (degree of birefringence) was compared with the table of values for different polytypes given by Brafman and Steinberger (1966).

Most common of all the structures was the cubic (3C), which could be found as wide uniform bands in many of the platelets. The hexagonal (2H) structure (wurtzite) usually occurred in the thinnest crystals and often had subsidary hexagonal "flags" growing out of the plane of the parent crystal. These hexagonal

Fig. 3.1 ZnS platelets seen under crossed polarizers in an optical microscope
(a) Two hexagonal crystals with a few thin cubic regions
(b) Another platelet showing a number of polytypic bands as well as linear markings along the common c-axis



a



b

Fig 3.1

areas, if mistreated, soon showed fine lines due to martensitic transformation, on otherwise uniform bands. Less common, but still more frequent than the other polytypes was the 4H structure. All the higher order polytypes of which there are a great many (Kiflawi et al. 1972 and Steinberger et al. 1973), are extremely rare.

3.4 SAMPLE MOUNTING FOR SEM STUDIES

Two methods of sample mounting were utilized.

In the first method a piece of veroboard was cut into small square sections. Each of these was araldited to a standard SEM stub. A flat headed rivet was found to be equally suitable as a stub. The platelets were then fixed across two adjacent copper strips on the veroboard with the area of interest somewhere in the middle. The crystals were mounted so that the polytypic bands were parallel to the copper strips. A small drop of colloidal silver paint at each end of the crystal not only attached it to the copper strips but also provided good thermal and electrical contact with the base. The veroboard was made just big enough to allow soldering of wires, away from the crystal, onto the copper strips. One of the wires was needed to provide an earth connection on the SEM specimen stage, thereby preventing electrical charging.

In the second method, the crystal was secured directly onto a flat copper plate. This type of attachment was better when using the cold-stage facilities of the SEM.

Using a soft brush for handling was the only way to prevent these delicate platelets from shattering.

3.4.1 CHARGING EFFECTS

Charging may occur whenever poor electrical conductor type materials are examined in the SEM. It can be identified by the irregular flashes appearing on the viewing screen whilst scanning the sample. An overall gradual image degradation also usually takes place. In severe cases the electron beam can be deflected off the specimen. The charging can sometimes be avoided by reducing the electron accelerating voltage and/or beam current so that the electron emission from the surface can balance the rate of arrival of electrons in the beam. However, this can often cause a reduction in resolution. The manner in which electron yield coefficient Δ , defined as the number of electrons emitted per incident electron, varies with beam voltage is shown in Fig.3.2. The shape of this curve is found to be very similar for a large variety of materials (Hachenberg and Brauer 1959). Operating the electron microscope with the incident beam voltage (V_b) approximately equal to either of the two crossover voltages (V_1 and V_2) will eliminate charging because these are the voltages for which the electron yield is unity.

Another way to overcome charging is to use a thin conductive coating (eg aluminium) on the specimen surface (see Echlin and Hyde 1972). Coating is obviously unsuitable for cathodo-luminescence work as it will inhibit light emission from the sample.

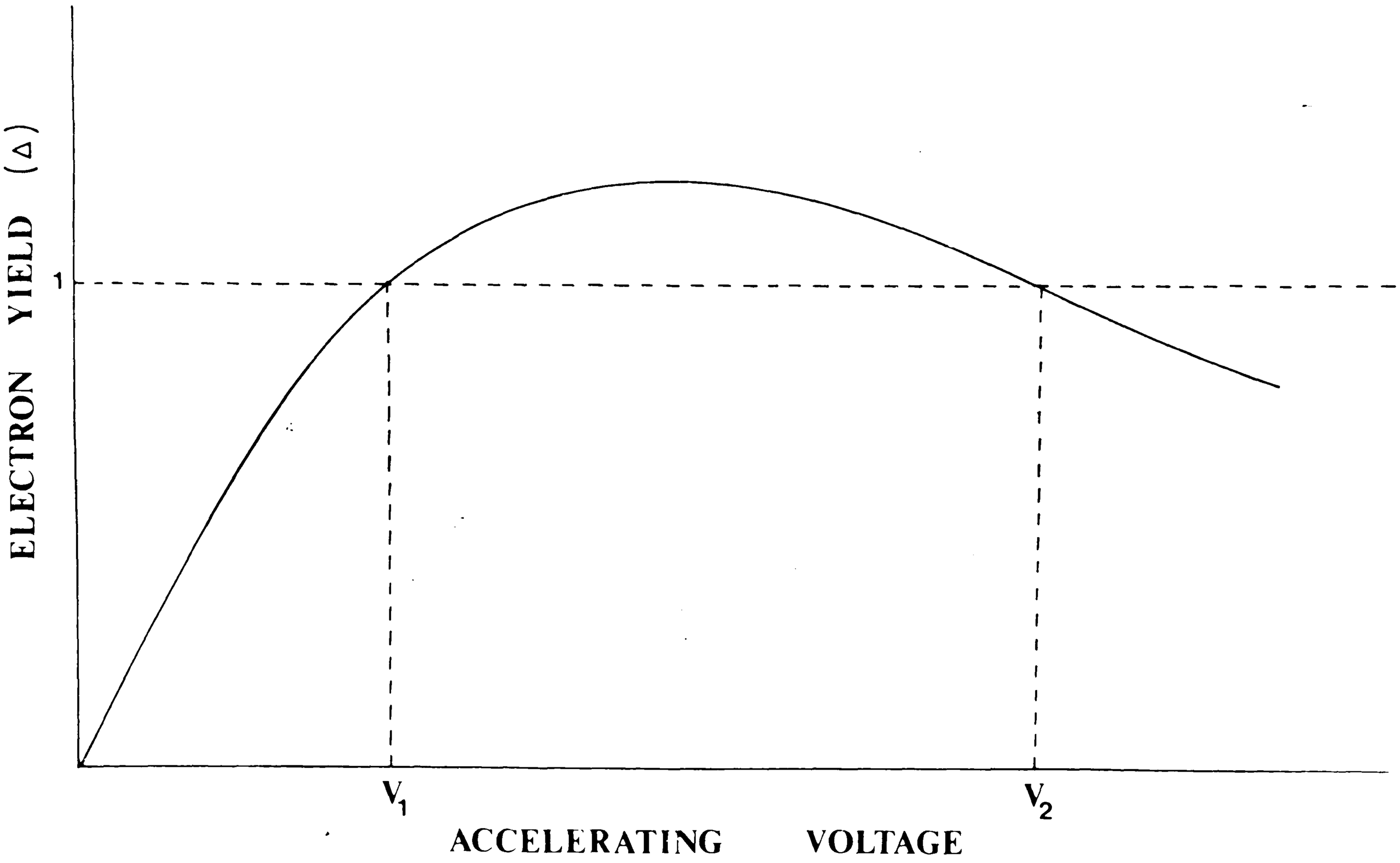


Fig. 3.2 Electron yield coefficient, Δ (ie the number of electrons emitted per incident primary electron) versus accelerating voltage. The two voltages at which the yield is unity are known as the first (V_1) and second (V_2) crossover potentials

Most of the crystals used in this work showed little charging provided there was a good earth connection through which the surplus electrons from the specimen surface could be dissipated. However, in the more severe cases a compromise between final spectral resolution and charging had to be made, since reducing the beam current reduces the CL emission which in turn produces a poor quality spectrum. It is also helpful to scan more slowly (frame and line time) so that the specimen leakage current has a much longer time to remove the excess charge.

3.5 CATHODOLUMINESCENCE DETECTOR SYSTEM

A Cambridge IIA Scanning electron microscope (SEM) fitted with an efficient spectroscopic light detection system was used for cathodoluminescence (CL) emission measurements. Basically the CL detector system consisted of a semi-ellipsoidal light collection device (Fig.3.6) feeding a grating mono-chromator, cooled photomultiplier (PM) tube with an S20 response and a photon counter as shown in Fig.3.5. The output of the photon counter could either be fed via a video amplifier to a display C R O screen to produce both mono-chromatic (one wavelength) and panchromatic (all wavelength) CL micrographs or stored in a multichannel scaler for later computer processing (Fig.3.5).

The possibility of analytical CL mode SEM has been a field of active research at this college for many years. This interest has led to the development of the present CL system (Mark 4) since a satisfactory SEM CL attachment is still not

available commercially. Over a period of years the design of the CL system has been optimised by careful selection and matching of such parameters as mirror size, ellipticity (ε), fibre optic bundle diameter and area of the monochromator entrance slit as well as selecting various monochromators with differing transmissive efficiency (E) - (see publication by Steyn et al. 1976).

Although a number of people have been involved in the building of the system most of the credit must go to J B Steyn (Department of Metallurgy and Materials Science) and P L Giles (Department of Geology) for the present arrangement. (See Muir et al. 1971, Muir and Holt 1974, Holt et al. 1975 and Steyn et al. 1976).

The semi - ellipsoidal mirror light collector (Fig. 3.6) was cast in araldite and coated with aluminium as in the Hörl and Mügschl and Carlsson and Van Essen systems (see section 2.4 page 51). Steyn et al. (1976) have shown that the collection efficiency of a semi - ellipsoid varies with its eccentricity, ε, where $\varepsilon^2 = 1 - b^2/a^2$ (a and b being lengths of major and minor axes). Also it has been shown that for a point source a mirror of $\varepsilon = 0.75$ collects 85% of the light whereas a mirror of $\varepsilon = 0.4$ collects about 40%. However, at magnifications below X 1,000 where source size is not negligible, the lower eccentricity mirror becomes relatively more efficient since it collects light from a larger focal spot or scanned area.

A mirror of the latter type ($\varepsilon = 0.4$) was used throughout this work.

Figure 3.3 shows the CL collector unit. The mirror on the left is placed within the SEM chamber under the final aperture lens but over the specimen. Alignment of the collector can be achieved by means of the bellows (right of Fig. 3.3). This allows for X - and Y - directional mirror movements from outside the chamber. The whole unit fits into the 90° port of the SEM chamber and is marked as E in Fig. 3.4.

The electron beam passes through a small aperture in the mirror onto the sample placed at one focus of the mirror (F_1). A diagram of the entire CL system is shown in Fig. 3.5, with a close-up view of the light collector (ie ellipsoidal mirror - lens - quartz fibre bundle) sub-system given in Fig. 3.6. The geometry of a semi-ellipsoid enables all the luminescence emitted by the specimen to be collected by a quartz fibre (Schott - UV) optic light guide placed near the second focus (F_2). A spectrosil lens placed with its principal focus at the second focus of the mirror provided a beam of collimated light at the input of the fibre bundle (Fig. 3.6). The cross - section of the fibre bundle was altered along its length, from circular to accept the collimated beam from the lens, to rectangula to match the entrance slit of the monochromator. The flexible quartz light guide transmits the CL from the mirror, through a vacuum seal, into a grating monochromator placed outside the chamber. A narrow range of wavelengths then fall on the photomultiplier.

Fig. 3.3 The SEM Cathodoluminescence Collector Unit

Key:

M = Mirror

B = Bellows

LG = Fibre Optic Light Guide

Fig. 3 4 General view of the SEM and the components of the Cathodoluminescence detection system

Key:

A = Cambridge IIA SEM Controls

B = SEM Electron Column

C = Hot/Cold Specimen Stage

D = X-Ray Detector Cryostat

E = Cathodoluminescence Attachment

F = Monochromator

G = Photomultiplier and Cooled Housing

H = Monochromator Stepper Motor

I = MCA

J = Power Pack for X-Ray Detector

K = Teletype and Computer Facility

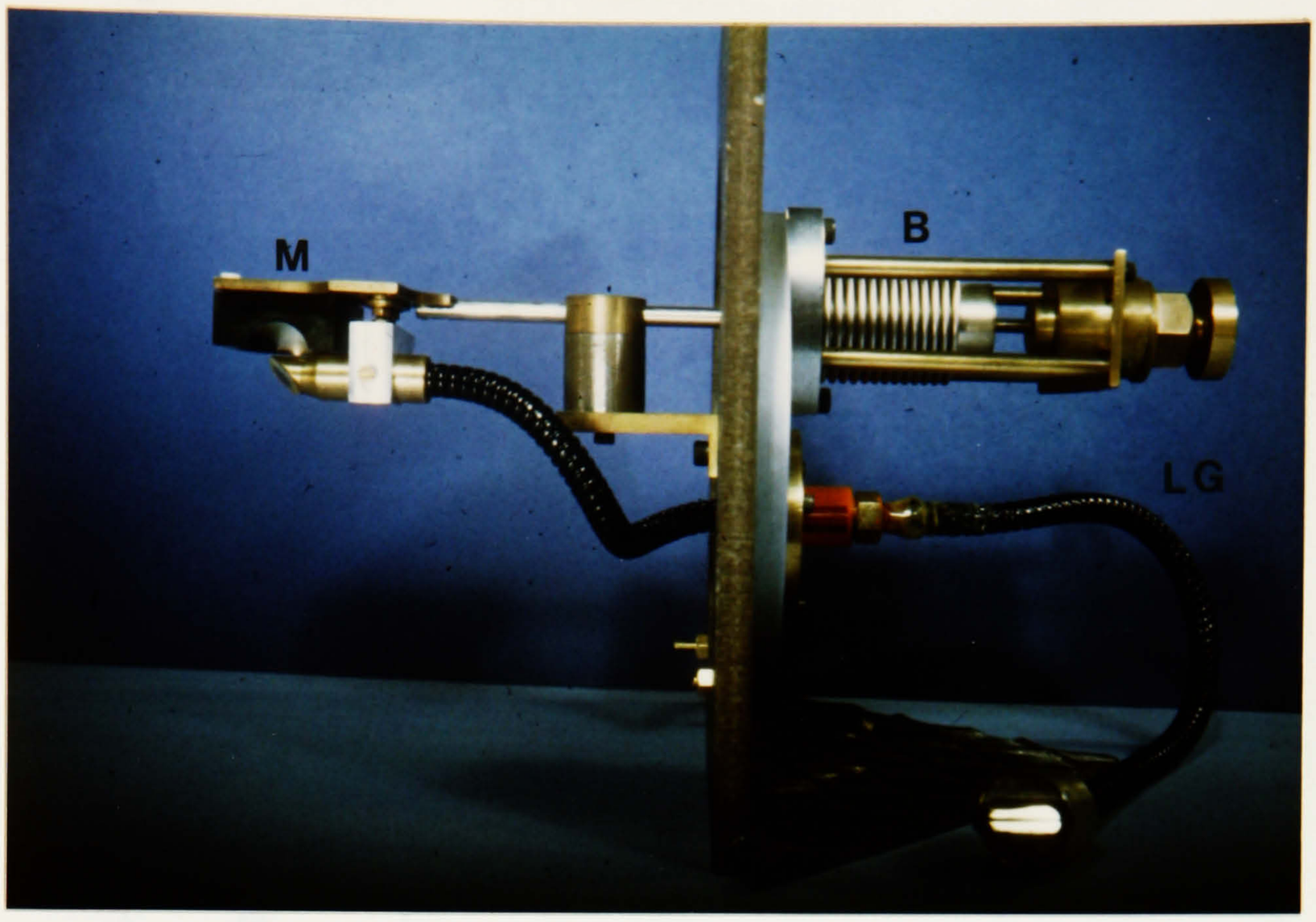


Fig 3.3

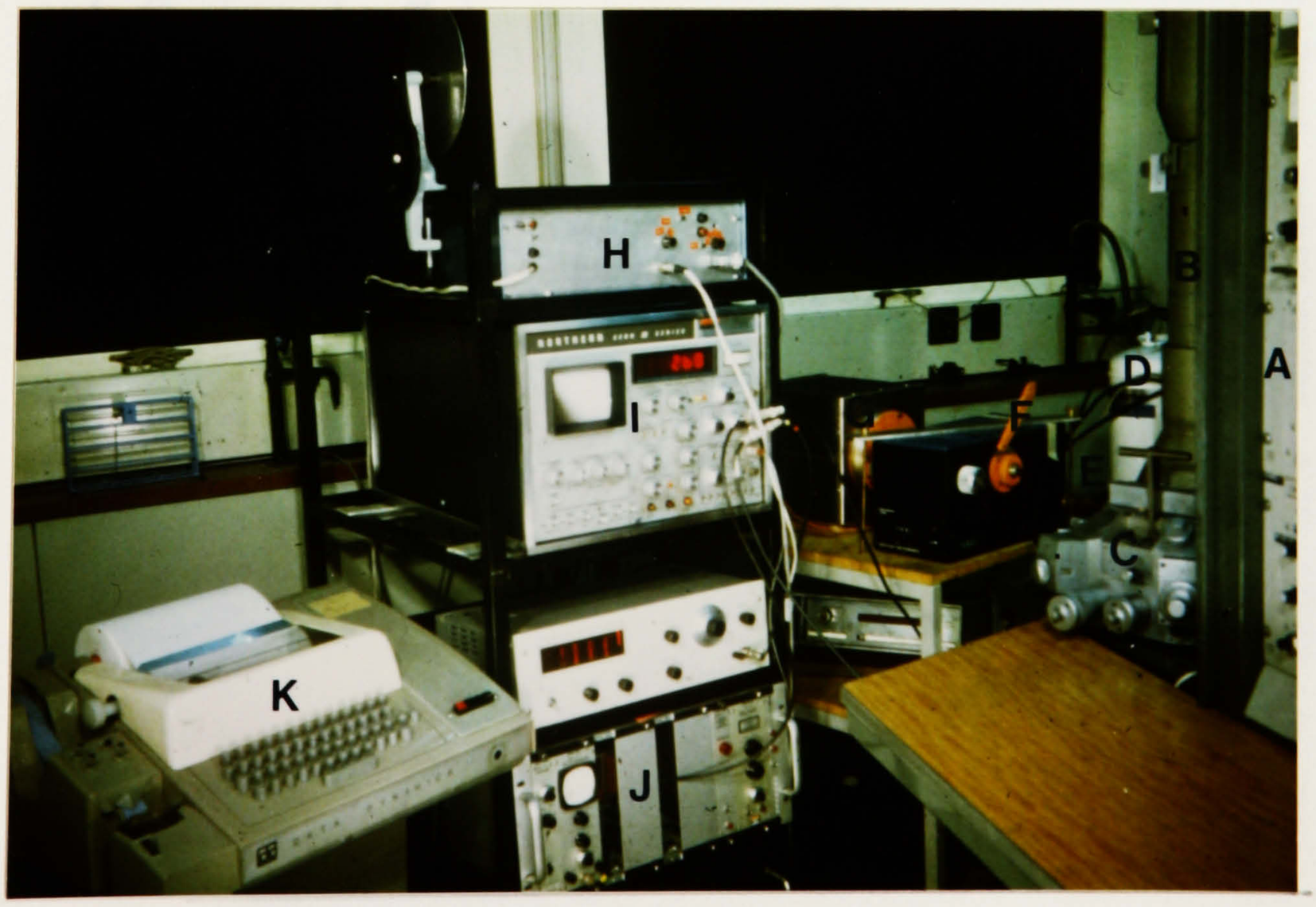


Fig 3.4

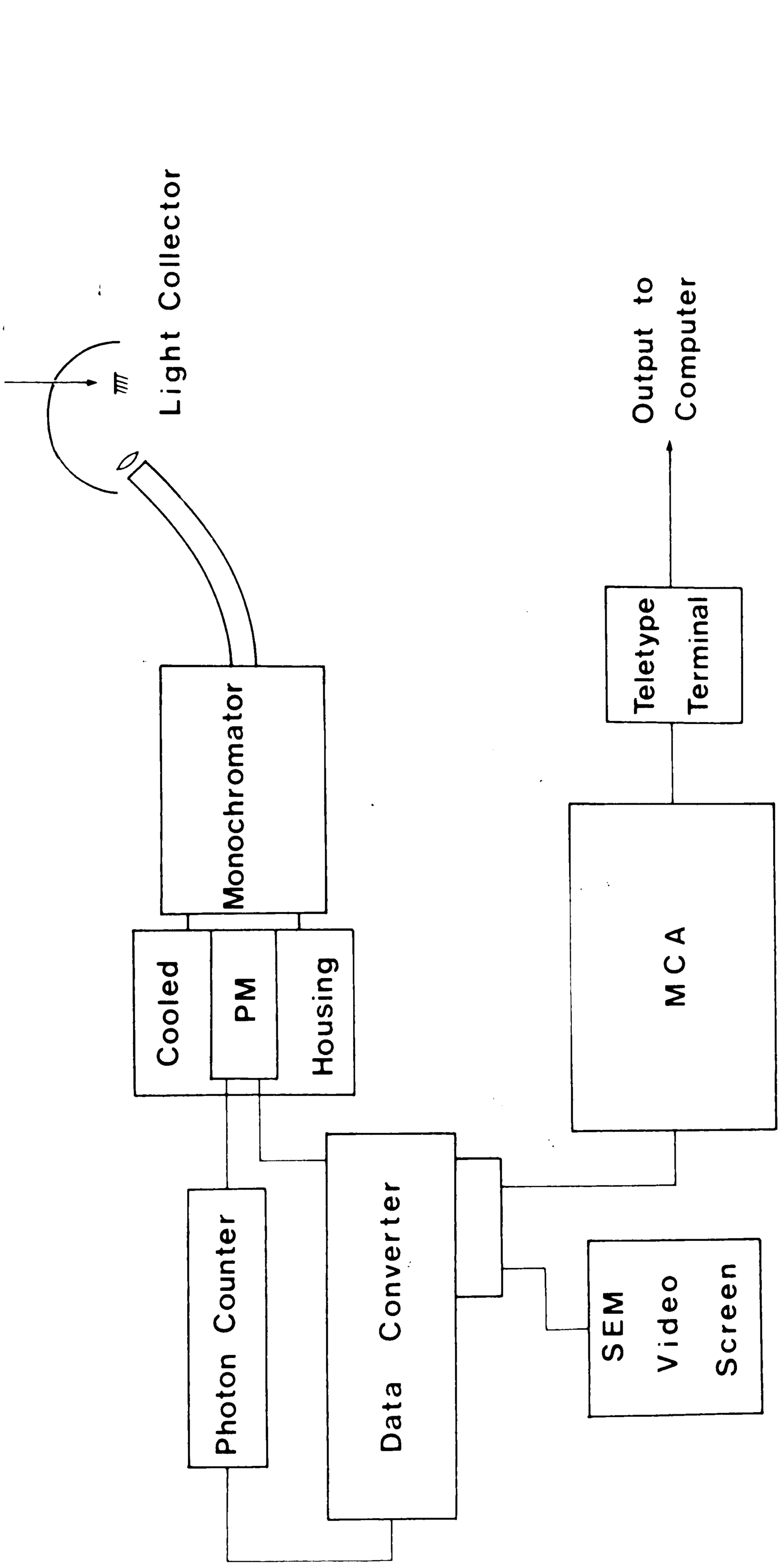


Fig. 3.5 Schematic diagram of the entire Cathodoluminescence detector system

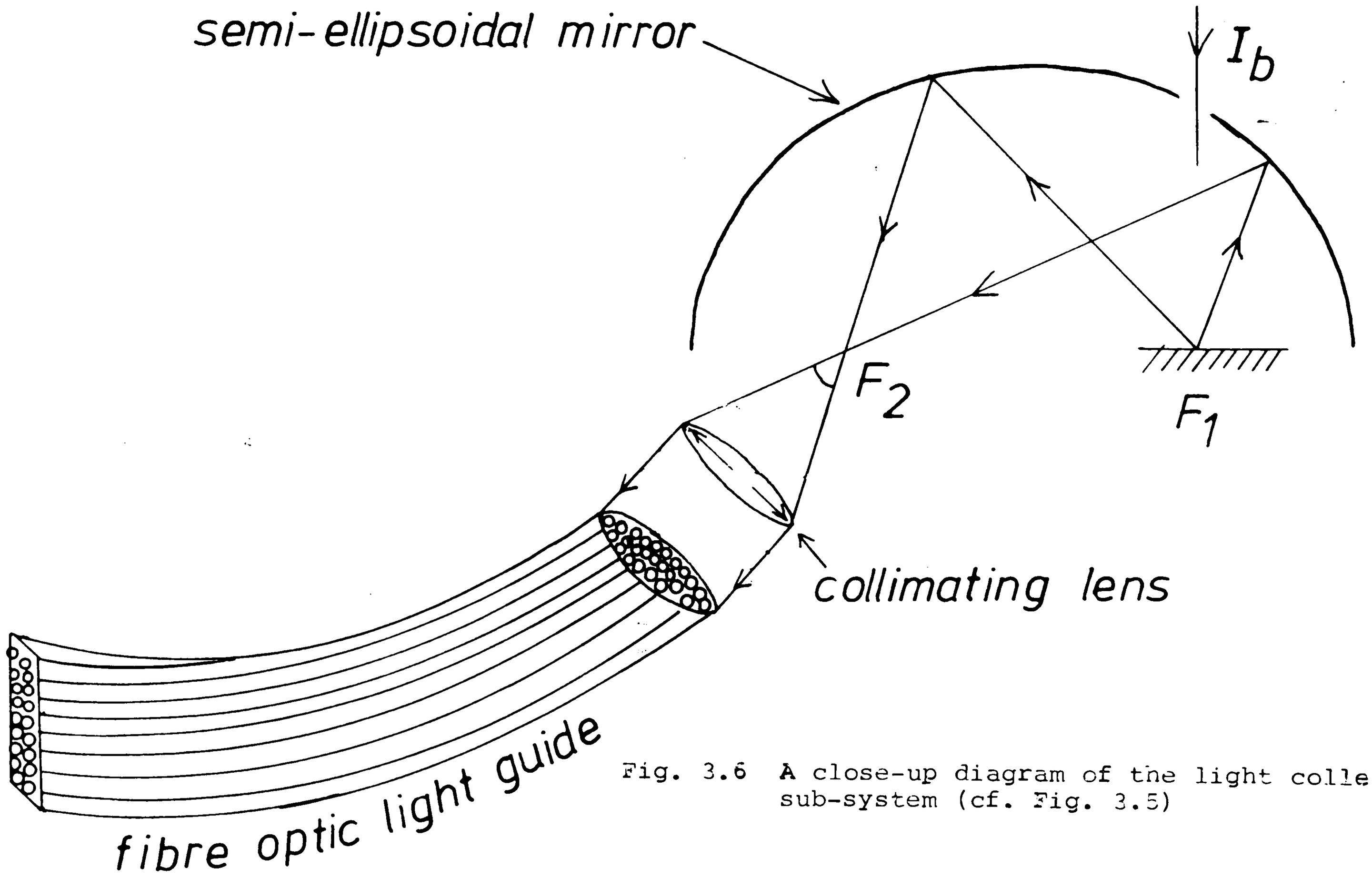


Fig. 3.6 A close-up diagram of the light collector sub-system (cf. Fig. 3.5)

The monochromator was a Bentham Instruments, model number CF 44 VM of aperture f/4. Its optical arrangement was that of a symmetrical Czerny - Turner mounting (Thorne 1974). It was also fitted with a set of four interchangeable slit widths (0.25, 0.5, 1 and 2 mm).

An EMI 9558 QA photomultiplier (PM) tube with extended S20 response was mounted at the exit of the monochromator and maintained at a constant cathode potential of - 1250V. A light tight shutter, and a four position filter holder were included between the monochromator and PM tube. The shutter minimizes the risk of inadvertent exposure of the PM tube to ambient light. The filter holder contained three Wratten filters (Kodak Ltd Nos. 47B(blue) 58(green)and 25(red). These were used in the colour synthesis technique to obtain colour photographs of the CL emission in the SEM at high magnification (see section 4.3 page153 of this work).

The photomultiplier background noise and its origin must be carefully scrutinized because this eventually determines the lowest detectable light level. In all PM tubes the noise, electrical and dark current, is what presents the basic limit on the accuracy of measurements. Electrical noise occurs because the signal arriving at the photocathode is a beam of photons which are randomly distributed with time. The PM tube being an excellent amplifier does not smooth out these statistical fluctuations in the input signal. The problem is minimized by operating the tube according to the makers specifications.

The inherent dark current on the other hand occurs due to thermionic emission. To reduce this the PM tube was maintained at - 40 $\pm$ 2C in a refrigerated chamber (Products for Research type TE - 149 TS - RF) which was shielded against magnetic and radiofrequency fields. For the same reason the effective photocathode area was decreased to 6 mm by an EMI permanent focusing magnet. This produces fields in the vicinity of the photocathode which prevents spurious electrons from the outer sections from reaching the first dynode and thereby restricts this component of the dark current from appearing in the PM output.

The signal from the cooled PM tube was fed to a photon counter (SSR Instruments - amplifier/discriminator). This is a pulse counting circuit which can discriminate and reject some of the pulses which from their height and spacing are known to be noise. That is, a threshold level is set which passes genuine pulses originating in electrons emitted by the PM photocathode. Signals arising from spurious electron emission from later dynodes in the PM tube undergo amplification but produce pulses of smaller amplitude. The threshold level of the photon counter is set to reject these pulses. In addition pulses due to photocathode emission are not square but have an amplitude which varies over the pulse length. This can result in two peaks in a single pulse being counted separately. The photon counter discriminator level can eliminate these signals as well. A discussion of photon counting technique can be found in Oliver and Pike(1968) and Foord et al. (1969).

The output of the SSR Instruments 1120 photon counter is a pulse train the rate being proportional to the number of incident photons arriving at the photocathode of the PM tube. The pulses are mismatched for direct coupling to the multi-channel height analyser (MCA) since this only recognises TTL (transitor transitor logic) pulses of 0.1 μs or longer duration whereas the photon counter produces ECL (emitter coupled logic) pulses of 20ns duration. To overcome this difficulty an ECL/TTL converter (Motorola 1012S) and a pulse stretcher, lengthening the pulses to about $\sim$ 1 μs was used as an intermediate step (Fig. 3.5). The signal could then be passed to a Northern Scientific Instruments, Econ II (NS - 710) MCA operated in the multichannel scaler mode and run synchronously with the monochromator stepper motor. The information from the scaler, which had 1024 discrete memory channels, was passed directly into the Imperial College Computer Centre (ICCC) computer for data processing or /and stored on paper tape via a Data Dynamics teletype terminal. Alternatively the photon counter signal can be passed to one of the simultaneously scanned video screens of the SEM to produce monochromatic (one wavelength) or panchromatic (all wavelengths) CL micrographs.

Operation of the CL detector system is simply a matter of aligning the mirror within the SEM chamber so that the electron beam falls normally onto the sample, choosing suitable scan raster times and magnifications, and selecting the required values of the bandwidth of the monochromator, the stepper

motor scan speed and the MCA dwell time. A spectrum can then be recorded over the range from 250 to 850 nm by activating one switch.

To obtain the true CL emission spectrum, the calibrated fraction of the photons emitted which give rise to a counted pulse in the detector, as a function of wavelength, was stored in the computer and used to correct all raw count-rate data. Both the uncorrected and corrected spectra were obtained from the ICCC computer in the form of a microfilm as well as a printed output.

More complete descriptions of the CL system have already been published by Giles (1975) and Steyn et al. (1976).

The CL calibration procedure will be dealt with in the next section.

3.6 CALIBRATION OF THE CATHODOLUMINESCENCE DETECTOR SYSTEM

Two types of CL system calibration are necessary. In the first the wavelength scale of the monochromator should be regularly checked using for example the mercury lines from a low pressure Hg lamp. Corrections can be made by adjusting the symmetrical Czerny - Turner optics, however this is best left to the manufacturer.

Secondly, the total response function (QEF) of the CL detector at different wavelengths throughout the required wavelength range must be determined. The observed count rate obtained from the detector system can be written (Steyn and Holt 1973) as:

$$R(\lambda) = Q(\lambda)\ E(\lambda)\ F(\lambda)\left\{1-A(\lambda)\right\} N(\lambda) \qquad (13)$$

Where Q is the photomultiplier (PM) quantum efficiency that is the ratio of the number of PM pulses produced to the number of photons incident on the photocathode per unit time; E is the transmissive efficiency which is the fraction of photons incident at the monochromator input which emerges from the output slit, and F is the fraction of emitted photons that are collected and transmitted to the monochromator. N is the quantum yield; that is the number of photons of wavelength λ generated per second in the material and (1-A) is the fraction of those photons which escape from the specimen so that A is the fraction lost internally due to self-absorption, internal reflection etc. All these factors vary with the wavelength λ of the cathodoluminescence.

Figure 3.7 gives the quantum efficiency of a number of basic types of photomultiplier photocathodes as a function of wavelength. An S20 type PM tube was considered suitable due to its extensive wavelength range compared to the S11 or S1, although the efficiency falls fairly rapidly in going from the blue to the red end of the visible spectrum. The

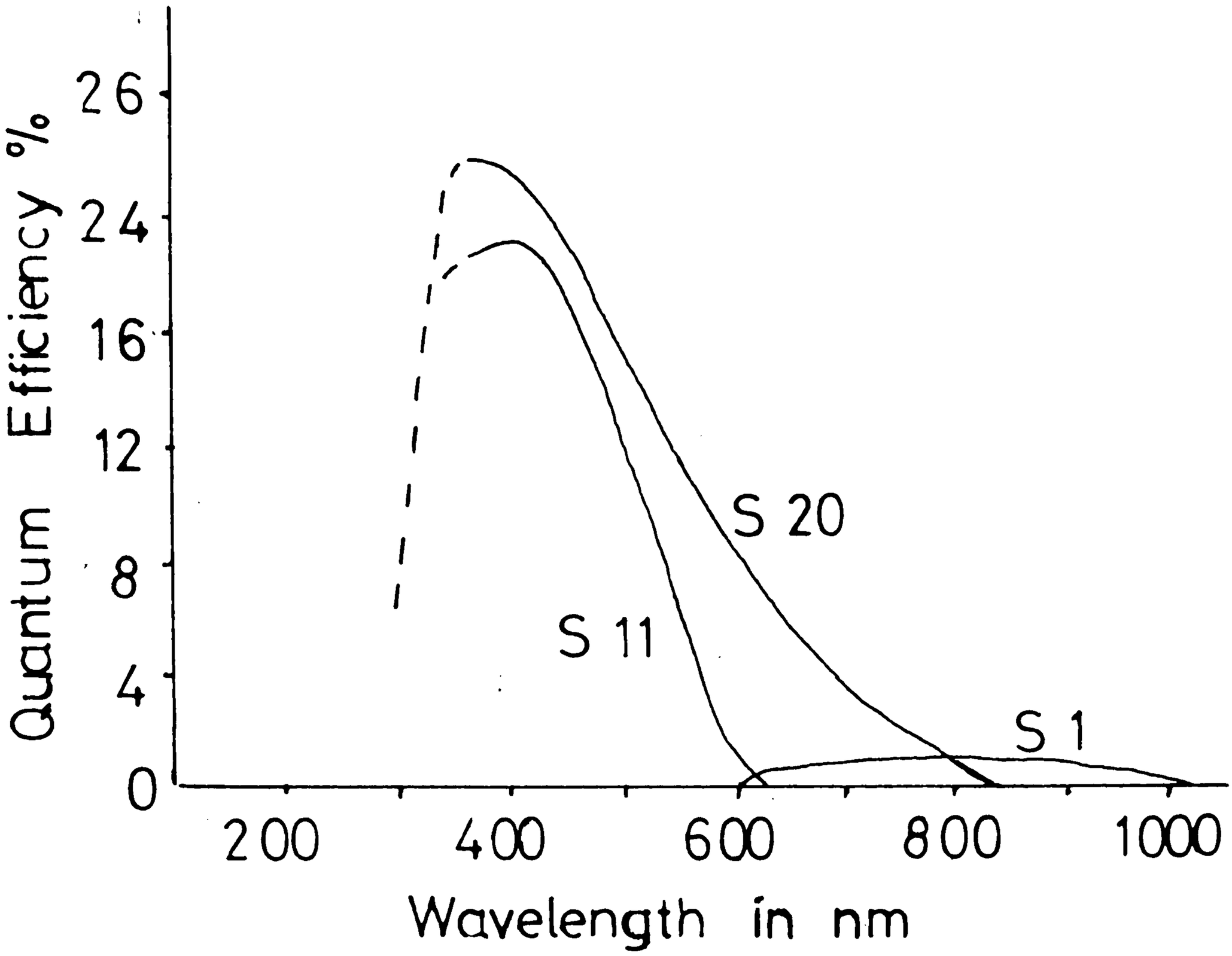


Fig. 3.7 The quantum efficiency Q(λ) as a function of wavelength for the three basic types of PM

calibration was designed to correct for this behaviour and other instrumental losses encountered by the emitted photon between generation at the specimen and its eventual detection as a counted pulse on the multichannel scaler.

A description of the salient features of the calibration will be presented below but a fuller account can be found in Steyn and Holt (1973) and especially Steyn et al. (1976). The present, Mark 4 CL detector system (as shown in Fig. 3.5 section 3.5 page 96.) was calibrated with the kind help of Phill Giles (Department of Geology) who also wrote the computer programs required to process the data.

The CL detector system was calibrated using a quartz windowed, halogen filled, tungsten standard lamp. A calibration curve supplied with the lamp gave the filament equivalent black-body temperature in terms of the current flowing through it. Knowing the filament temperature the rate of photon emission $N(\lambda)$ in a bandwidth $\delta\lambda$ at wavelength λ can be calculated by Planck's black-body radiation equation. This is given by,

$$N(\lambda) = (C_1 \lambda^{-4}/hC) \left\{(\exp C_2/\lambda T) - 1\right\}^{-1} \delta\lambda \qquad (14)$$

Here C_1 and C_2 are known respectively as the first and second radiation constants, h is Planck's constant and C is the velocity of light. In addition $\delta\lambda$ was set equal to the value for the monochromator at the relavent slit width, eg $\delta\lambda$ = 1.30 nm when the slit width W = 0.25 mm in the case of the Bentham Instruments

(CF 44) monochromator

If $N(\lambda)$ = number of photons at λ, $\delta\lambda$, T leaving the source and $N'(\lambda)$ = number of photons incident on the slit then,

$$N'(\lambda) = (N(\lambda)\ A/R^2)\ W_f L_f \qquad (15)$$

is the photon rate entering the fibre bundle. L_f and W_f are the standard lamp filament dimensions, A is the area of the monochromator entrance slit and R is the distance between the filament and fibre bundle aperture.

Thus having calculated the photon rate at the fibre bundle aperture using equations 14,15, the transmission factor is obtained by comparing this value with the pulse rate recorded by the detector.

In other words the monochromator - photomultiplier - photon counter response factor $Q(\lambda)\ E(\lambda)$ is given by

$$Q(\lambda)\ E(\lambda) = \frac{\text{Number of photons counted}}{\text{Number of photons incident on the entry slit}}$$

Note, that since from previous determinations (Steyn et al. 1976) the collection efficiency $F(\lambda)$, of the ellipsoidal mirror was found to be 40% throughout the wavelength range, this value

was taken as determined. In the same paper it was indicated that the attainable collection efficiency was affected by mirror aberrations. Such aberrations arose due to the limited precision available for machining the brass ellipsoids from which the mirrors were cast. It was concluded however, that the actual collection efficiency $F(\lambda)$, of the mirror currently in use ($\varepsilon = 0.4$), approached the value computed by ray tracing methods.

The total instrumental response factor, QEF, of the CL detector system is shown in Fig. 3.8. This performance factor data was stored in the computer as a nine term polynomial and used to correct the observed count rate spectrum to obtain the true CL emission spectrum. In Fig. 3.8 the rapid fall in efficiency from the blue to the red ends of the visible spectrum is mainly a property of the photomultiplier photocathode (Q).

To record a standard lamp emission spectrum the monochromator stepper motor was started only after a stabilized current, I, was passing through the lamp filament. The current was controlled manually using a simple d.c. resistive circuit. Since the number of photons emitted varies exponentially with temperature (T), variations in I and hence in T can lead to relatively large errors in the measured performance factor (QEF) of the detector system. The magnitude of these errors were investigated by Steyn et al. (1976) by repeating the calibration procedure several times using different slit widths, ie different resolutions. It was observed that variations in

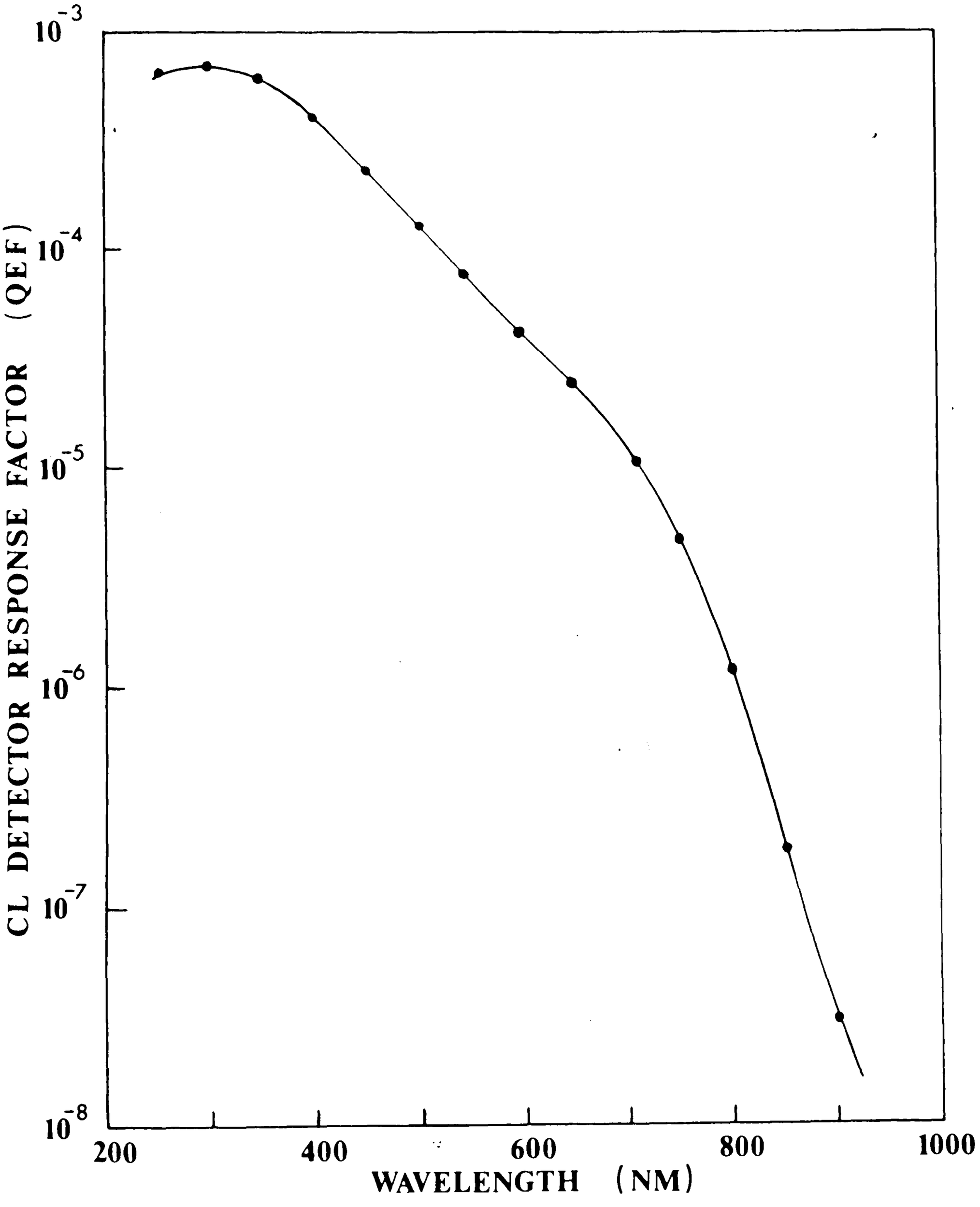


Fig. 3.8 Calibration curve of the Cathodoluminescence detector system. The detector response factor is the proportion of photons emitted from the specimen that results in a pulse in the photon counter (= QEF in equation 13 section 3.6)

T from one run to the next caused variations in the results which all fell within the limits of the calculated errors. Furthermore it is believed that the calibration procedure only gives the correction factor QEF, with an accuracy of perhaps $\pm$ 10% to 20%.

Problems due to scattered light not directly from the filament, and stray light within the monochromator had to be considered also. The former was combated by recording a spectrum with the filament obscured, and subtracting this spectrum (formed by unwanted scattered light) from the calibrated spectrum. The latter problem of stray light is more difficult to deal with and could only be estimated. This is caused by light scattering within the monochromator, which allows light to by-pass the grating. Monochromators of the type used have stray light levels of about 0.01%.

3.7 THE SEM X-RAY DETECTOR SYSTEM

The SEM was also fitted with an Ortex 7000 series energy-dispersive X-ray spectrometer (Gedcke 1974). The detector consisted of a lithium - drifted silicon diode, operated at liquid nitrogen temperature for optimum performance. In this, X-ray photons pass through a beryllium window and cause ionization of the biased Si (Li) detector. This produces charged pulses of magnitude proportional to the energy of the incoming X-ray photons and these therefore can be discriminated as representative of the chemical element of the X-ray emitting

atom in the specimen. The number of such pulses is proportional to the number of incident photons of a particular energy. Each pulse is then amplified and passed to the multichannel height analyser (NS-710), which is shared with the cathodoluminescence (CL) system. This unit is capable of deciding which of the 1024 channels, each representing a different X-ray energy, the pulse should be registered in, thereby giving a simultaneous microanalysis of a wide range of elements.

An excellent bibliography of the energy - dispersive X-ray technique can be found in Yakowitz (1974).

Most of the active part of the X-ray detector is housed within the cryostat(white cylinder labelled as D in Fig.3.4) with the associated voltage supply and discrimination obtained from the units at the bottom of the main instruments panel marked as J in Fig.3.4. The final X-ray spectrum can either be recorded photographically from the display cathode ray tube (CRT) of the MCA, or read out onto a chart recorder.

4. RESULTS AND ANALYSIS

4.1 SAMPLE PURITY

The purity of these ZnS platelets were checked by spectrochemical analysis and X-ray micronanlysis in the SEM. Although the samples were thought to be of high purity, and probably represent the best form in which ZnS is presently available, they still contained various uncontrollable impurities. The concentration of these impurities varied from one growth run to the next and sometimes from sample to sample from the same growth run, as will be shown below.

4.1.1 SEM X-RAY MICROANALYSIS

X-ray analysis provides a method by which very small volume's of a specimen can be analysed for elemental composition extremely rapidly and non-destructively, by detecting the characteristic X-rays emitted from a specimen bombarded with sufficiently energetic electrons in the SEM (see section 2.2.2) as already discussed. The detection limit for impurities is only about one part in 10^4 at best however.

By careful positioning of the electron beam raster on the platelet, X-ray spectral analysis of the region of interest can be obtained. One such typical spectrum of a ZnS platelet is shown in Fig.4.1.

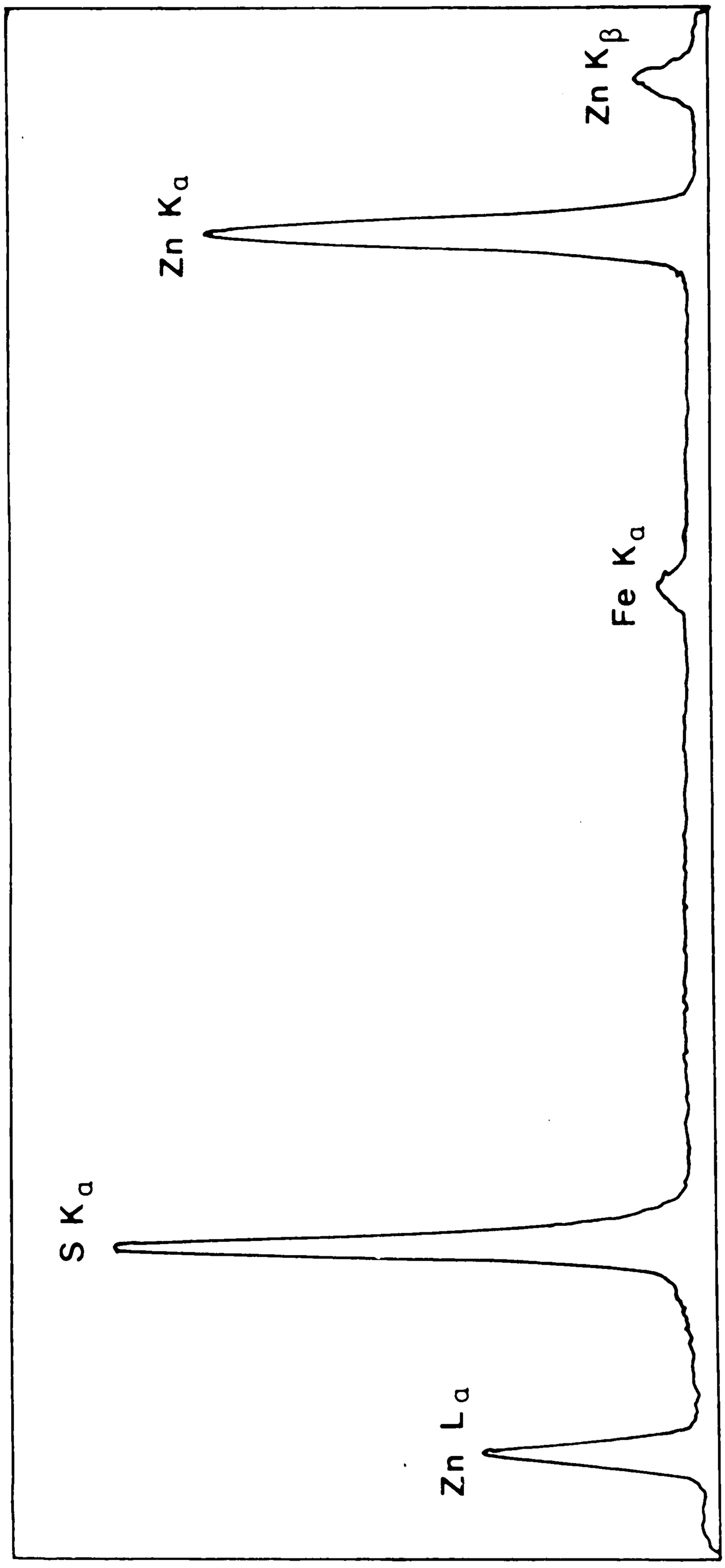


Fig. 4.1 Typical X-ray spectrum of a synthetic ZnS platelet

It can clearly be seen that all the peaks except one are due to the elements, zinc and sulphur. The small K_α iron peak occuring at about the middle of Fig.4.1, was later identified as being due to X-ray emission from the SEM pole pieces. Since no further impurity peaks could be identified from X-ray micro-analysis in these specimens, it was abandoned in favour of spectrochemical analysis.

4.1.2 SPECTROCHEMICAL ANALYSIS

The spectrochemical analysis facilities of the Analytical Services Laboratory at Imperial College and the Weizmann Institute of Science, Israel, was used to examine a number of these crystals. A compilation of the data obtained from both laboratories is presented in table 1, which shows the type and amount of each impurity present. Although this method is of high accuracy it is in essence destructive in nature. The results however have helped to identify a number of CL emission bands as will be outlined later.

4.2 LOCAL LUMINESCENCE VARIATIONS IN STRIATED ZnS PLATELETS

4.2.1 SYNOPSIS

Structurally complex ZnS platelets, when viewed in the SEM CL mode, show striking local variations in cathodoluminescence. It is believed that this arises from structural changes, impurity segregation, or internal electric field effects or a combination

TABLE 1

TYPICAL SPECTROCHEMICAL ANALYSIS OF A NUMBER OF ZnS PLATELETS

ELEMENT	SAMPLE 1	SAMPLE 2	SAMPLE 3	SAMPLE 4
Silver (Ag)	1-10 ppm	5 ppm	1-10 ppm	~1 ppm
Aluminium (Al)	<10 ppm	5 ppm	~10 ppm	10-100ppm
Calcium (Ca)	-	< 1 ppm	-	-
Copper (Cu)	1-10 ppm	1-10 ppm	~10 ppm	1-10 ppm
Iron (Fe)	~10 ppm	~10 ppm	~10 ppm	1-10 ppm
Magnesium (Mg)	1-10 ppm	~1 ppm	~10 ppm	1-10 ppm
Manganese (Mn)	1-10 ppm	-	1 ppm	-
Lead (Sb)	<10 ppm	-	5 ppm	~5 ppm
Tin (Sn)	<10 ppm	-	5 ppm	-
Silicon (Si)	~1 ppm	5 ppm	1 ppm	~1000 ppm
Titanium (Ti)	<1 ppm	-	-	-

ppm - parts per million

of these effects. The peak position and shape of the fundamental or edge (conduction band to valence band recombination emission) CL band for different crystal structures, identified from birefringence measurements, was determined. In this manner the crystal structures of homogeneous regions of a platelet, which were too small for accurate birefringence measurements, could theoretically be determined from the positions of their characteristic edge CL emission bands. The variation of the peak positions of certain impurity bands was determined as a function of crystal structure. Observations showed that heavy faulting causes CL quenching (ie a decrease in the emitted intensity) from a number of such areas. Intense electric field effects are thought to be responsible. The existence of high fields has already been well established in these ZnS crystals (Shachar et al.1970a, Brada et al. 1972 and also section 2.5). Evidence for the preferential segregation of impurities was also seen in a number of cases and will be presented.

The vital importance of correcting the raw emission spectral data for the varying response of the detector system is emphasised, since emission band heights, peak positions and shapes are markedly altered.

1.2.2. INITIAL CATHODOLUMNESCENCE STUDY

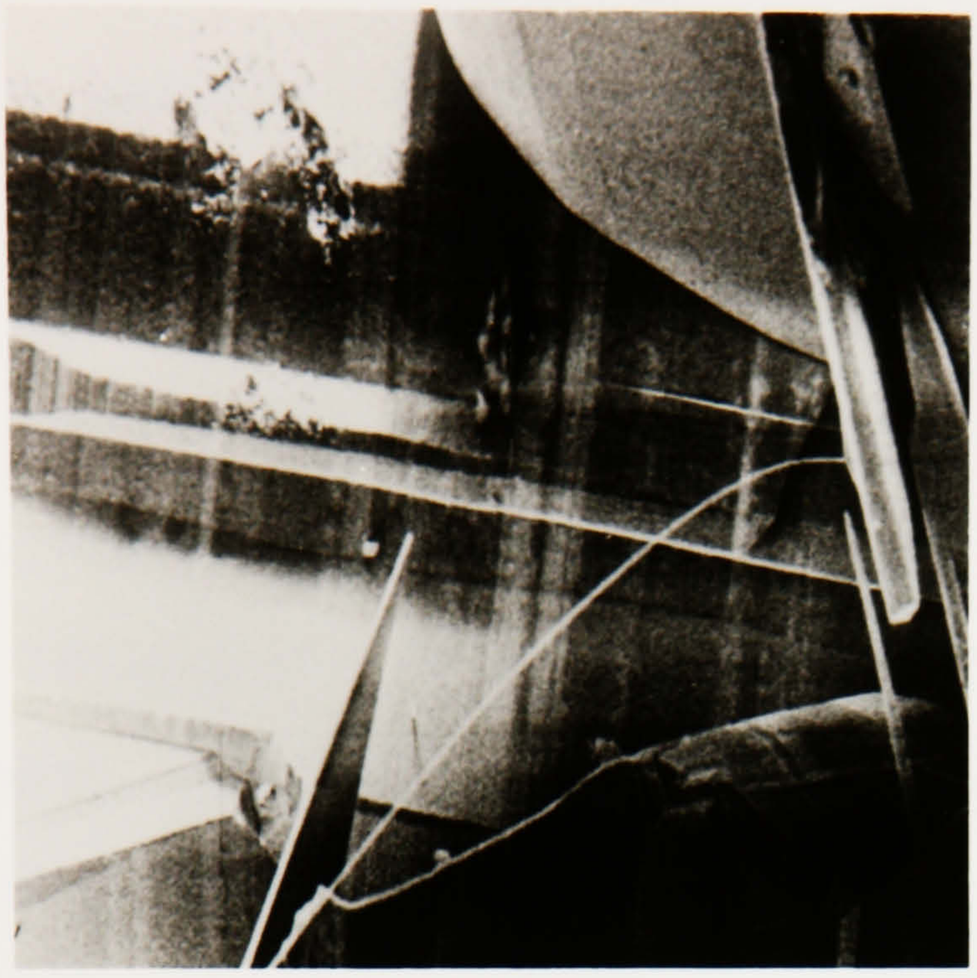
At the start of this work the CL detector system developed in this group was nearing completion. It was infact the third version of the detector and consisted basically of the components

shown in Fig. 3.5. There were however, a few differences between the earlier (3rd) and later (4th) forms of the detector; the monoch romator used at the start of this work was a Spex Minimate, the photomultiplier (PM) tube was neither cooled nor did it have magnetic focussing to reduce the dark current and a glass fibre light guide was used. Furthermore, at that time there was no direct computer access to the ICCC computer centre.

This short section is essentially an introduction, as preliminary results indicated that further modifications to the CL detector system was necessary which in turn provided more analytical cathodoluminescence (CL) results from these structurally complex striated ZnS platelets.

Figure 4.2 shows one such platelet grown by the Electrical Engineering Department, Imperial College. It grew as a cluster of platelets as can clearly be seen from the topographical micrograph (ie that produced by secondary electrons), Fig.4.2a. The atomic number contrast micrograph (reflected primary electron emission) is shown in Fig. 4.2b for comparison. Fig.4.2c, d are the panchromatic (all wavelengths) CL micrograph and the CL spectrum respectively. The panchromatic picture is made up of light and dark bands which run perpendicular to the common c-axis. The spectrum shows only one broad emission band peaking at 527 nm, which from the luminescence literature can be identified as the green copper (G-Cu) band (see section 2.1.4) and will be discussed later. The noise in the CL spectrum (Fig.4.2d) arose from the dark current component of the PM tube. Many of

Fig. 4.2 A cluster of ZnS platelets grown by the Electrical Engineering Department at Imperial College: (a) is a secondary electron topographical micrograph (b) a reflected primary micrograph and (c) and (d) are the panchromatic (all wavelength) CL micrograph and the CL spectrum respectively. The area represented is approximately 660 μm wide with the crystal c-axis in the direction of the arrow as shown in (c). The micrographs were produced by using a beam voltage of 30 KeV.



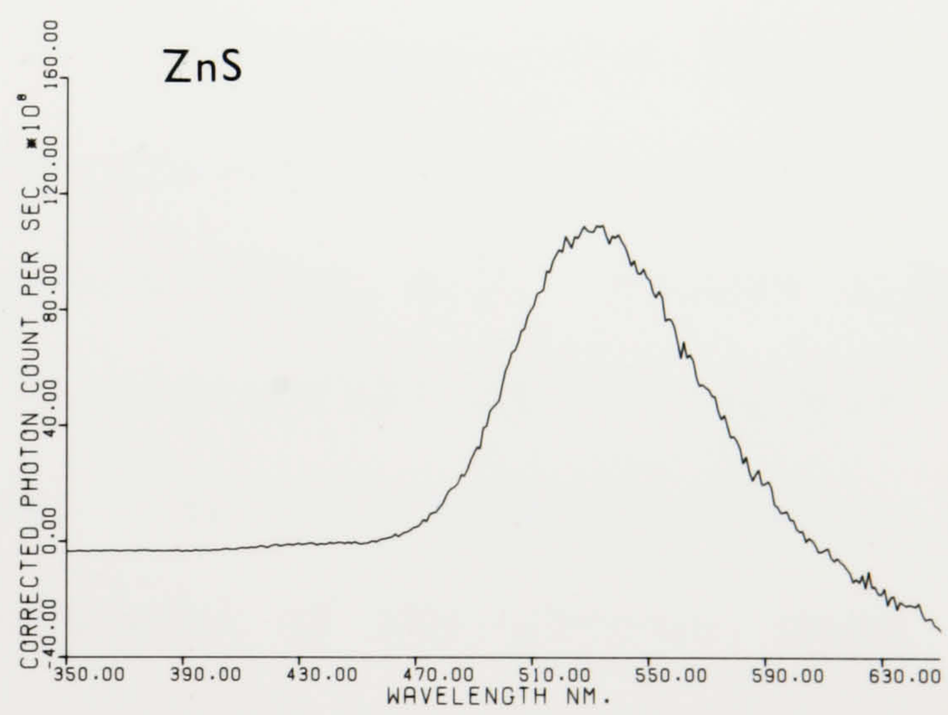
b



a



c


ZnS
CORRECTED PHOTON COUNT PER SEC ×10⁶
160.00
120.00
80.00
40.00
0.00
-40.00
350.00
390.00
430.00
470.00
510.00
550.00
590.00
630.00
WAVELENGTH NM.

d

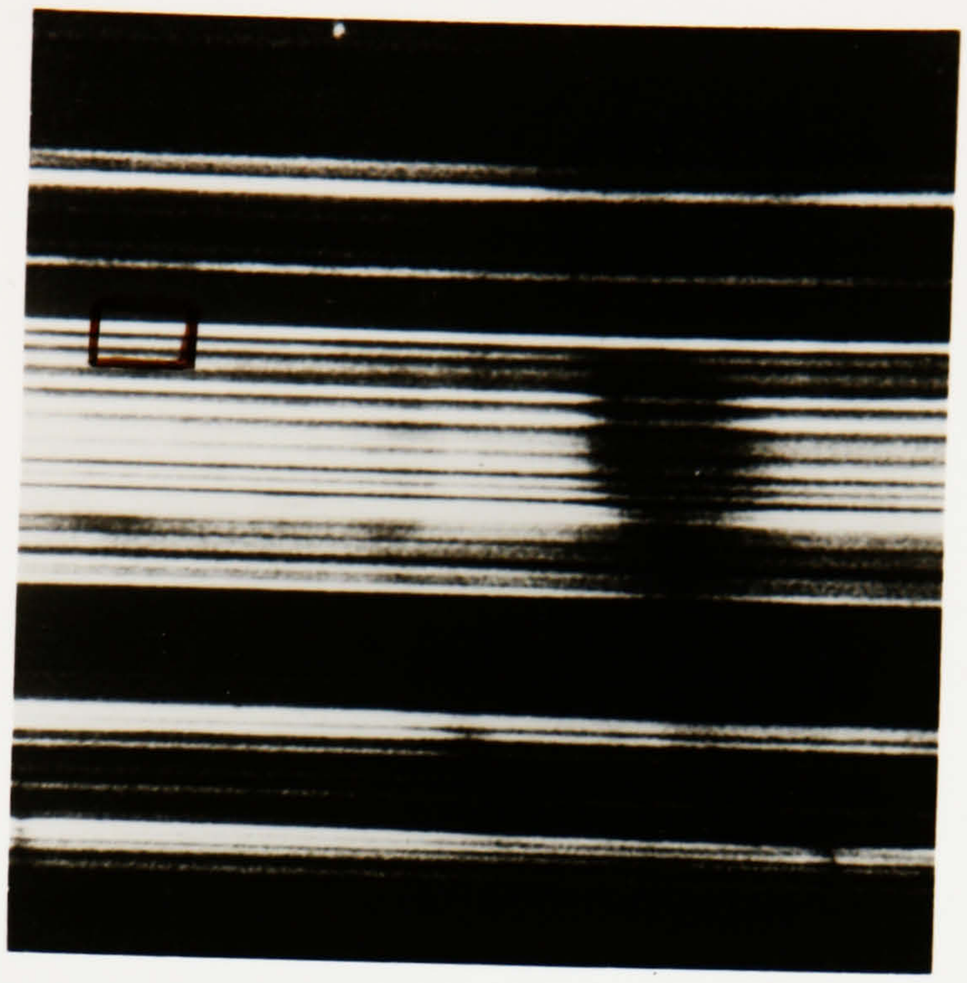
Fig 4.2

the samples investigated in this group of platelets were found to be heavily faulted as already outlined in section 3.2.

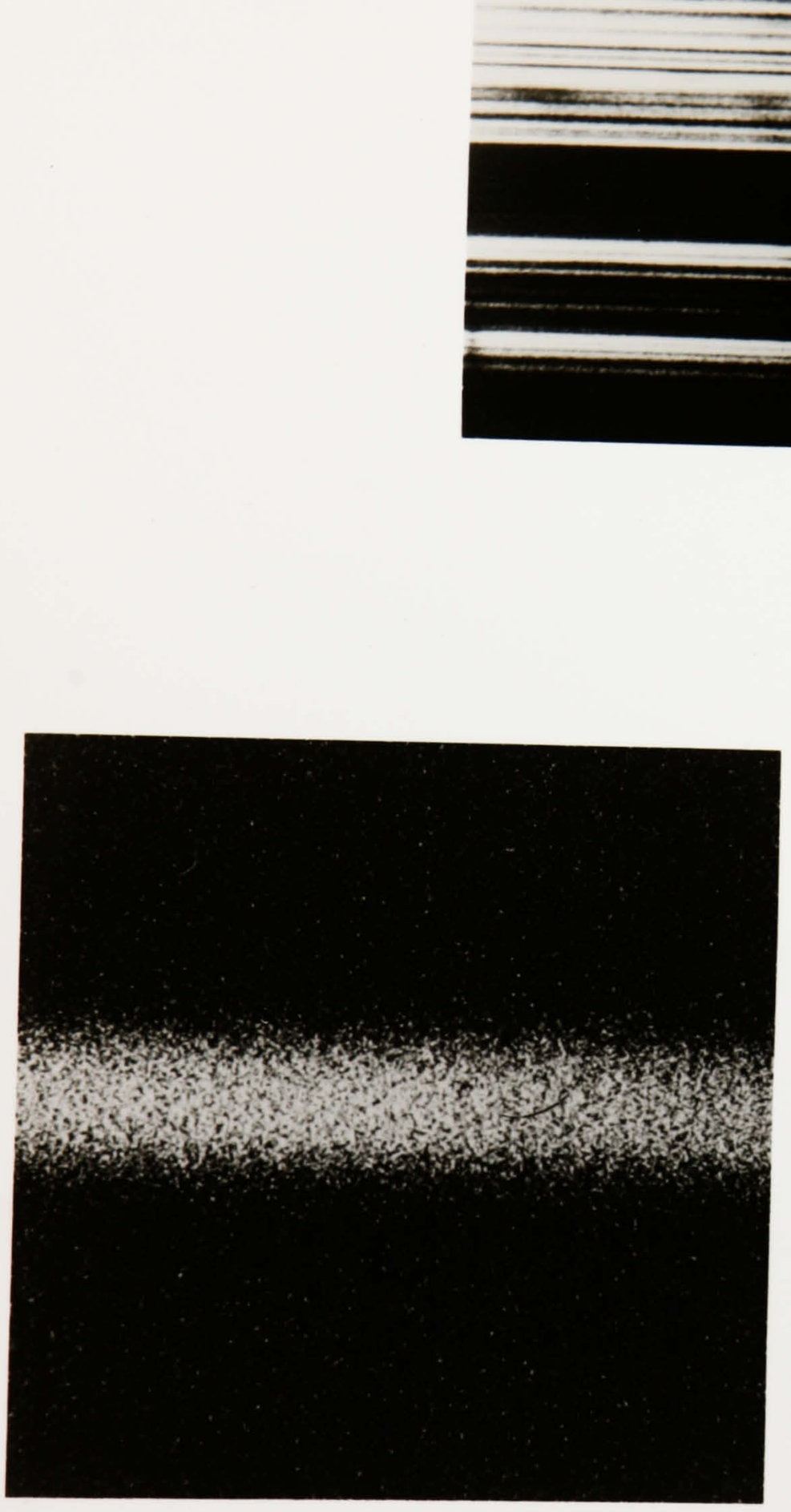
Specific impurity segregation effects when they do occur, are not always obvious. The problem becomes more difficult if the area being investigated has already undergone a large degree of structural transformation in a short distance along the c-axis. This was the case with most of the Imperial College grown platelets. Whenever this type of heavy crystal faulting occurs, slight variations in the CL emission from the many thin regions become hard to separate from the general and usually much stronger CL background.

Preferential localised impurity luminescence was first observed in the Jerusalem grown platelets, these were generally found to be less structurally faulted. The results from one such specimen, ZnS - 350 Type II, are shown in Fig. 4.3. Figure 4.3a, is a panchromatic (all wavelength) CL micrograph of the sample with the area of interest delineated. The high magnification monochromatic (one wavelength) micrographs of the choosen area are given in Figs. 4.3b,c. They clearly show localized luminescence from two nearly adjacent regions of the crystal. By using the limited area scan facilities of the SEM it was possible to acquire equal volume spectra from the middle of the two areas marked A and B, which are separated by approximately 12 μm, see Fig. 4.3c. The corrected spectra are shown in Figs 4.4a,b and correspond to regions A and B respectively. The luminescence bands observed are thought to arise from impurities and to be the blue-copper (B-Cu) band at 457 nm and the green -

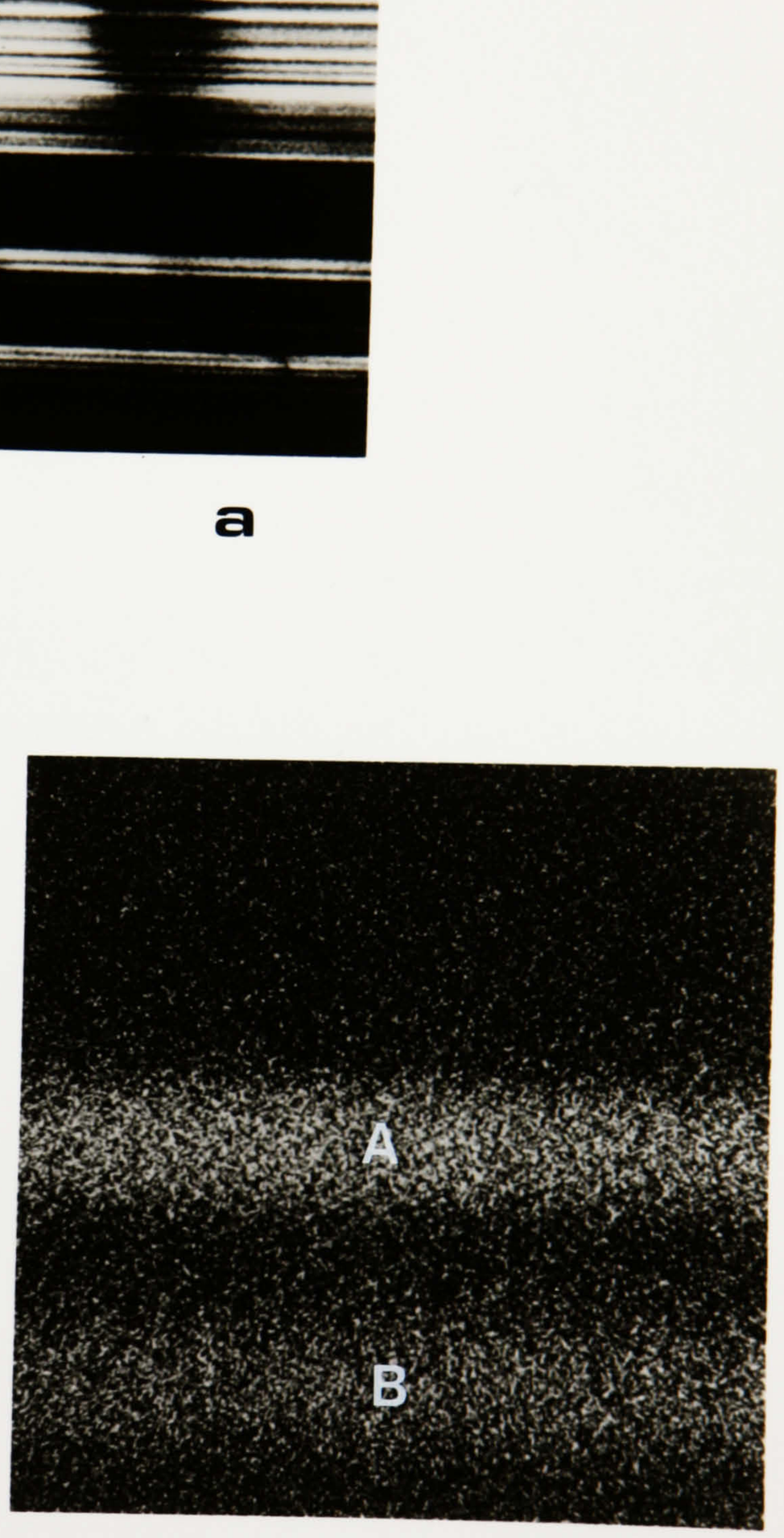
Fig. 4.3 Micrographs of a striated ZnS (350 Type II) platelet with the common c-axis running vertically: (a) is a low magnification (80X) panchromatic CL SEM micrograph, (b) and (c) are high magnification (1600X) monochromatic (one wavelength) CL SEM micrographs from the area outlined in (a). The monochromatic CL micrographs were recorded at the following emission wavelengths: (b) 420 nm and (c) 523 nm from an area approximately 56 μm wide



a

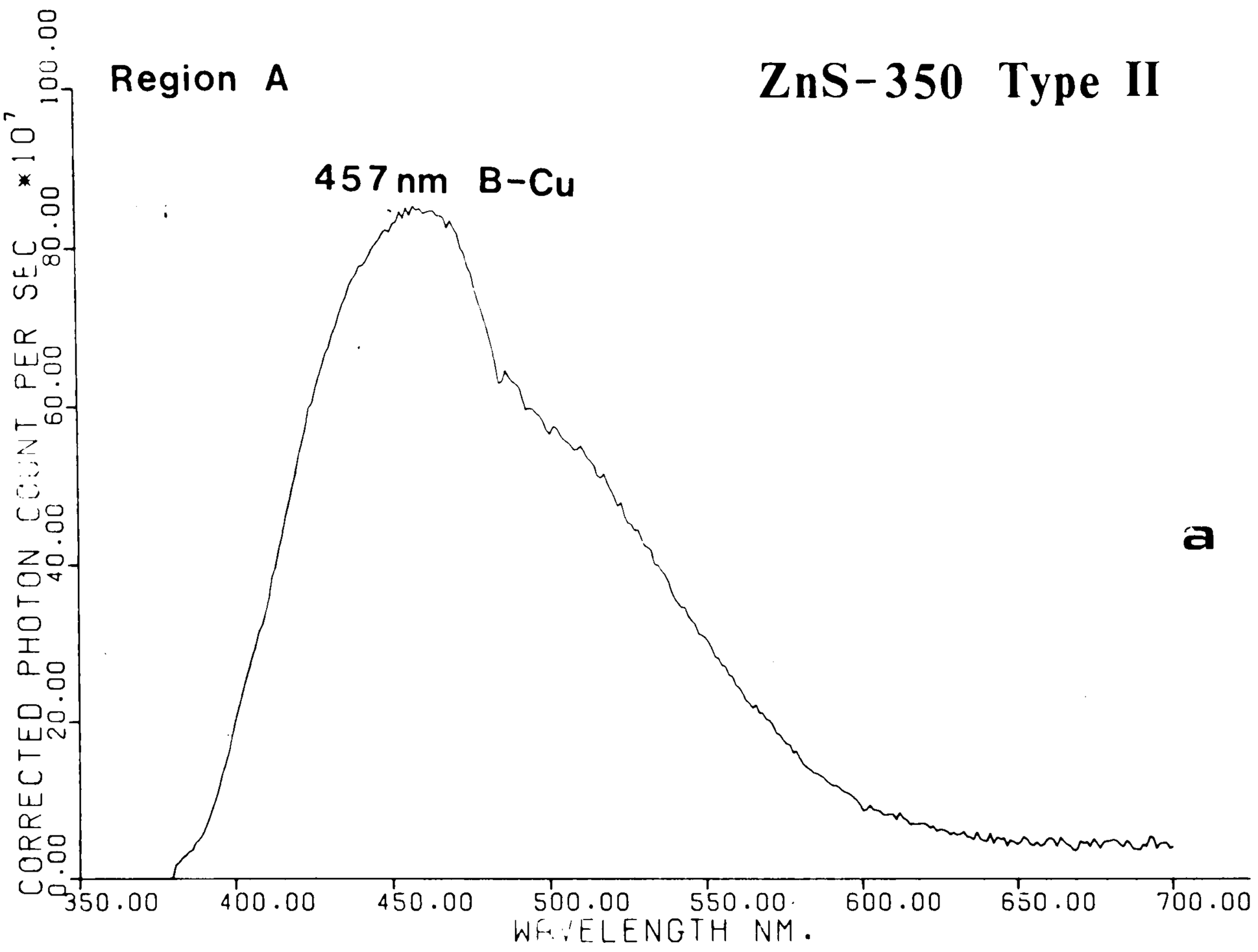


b



c

Fig 4.3



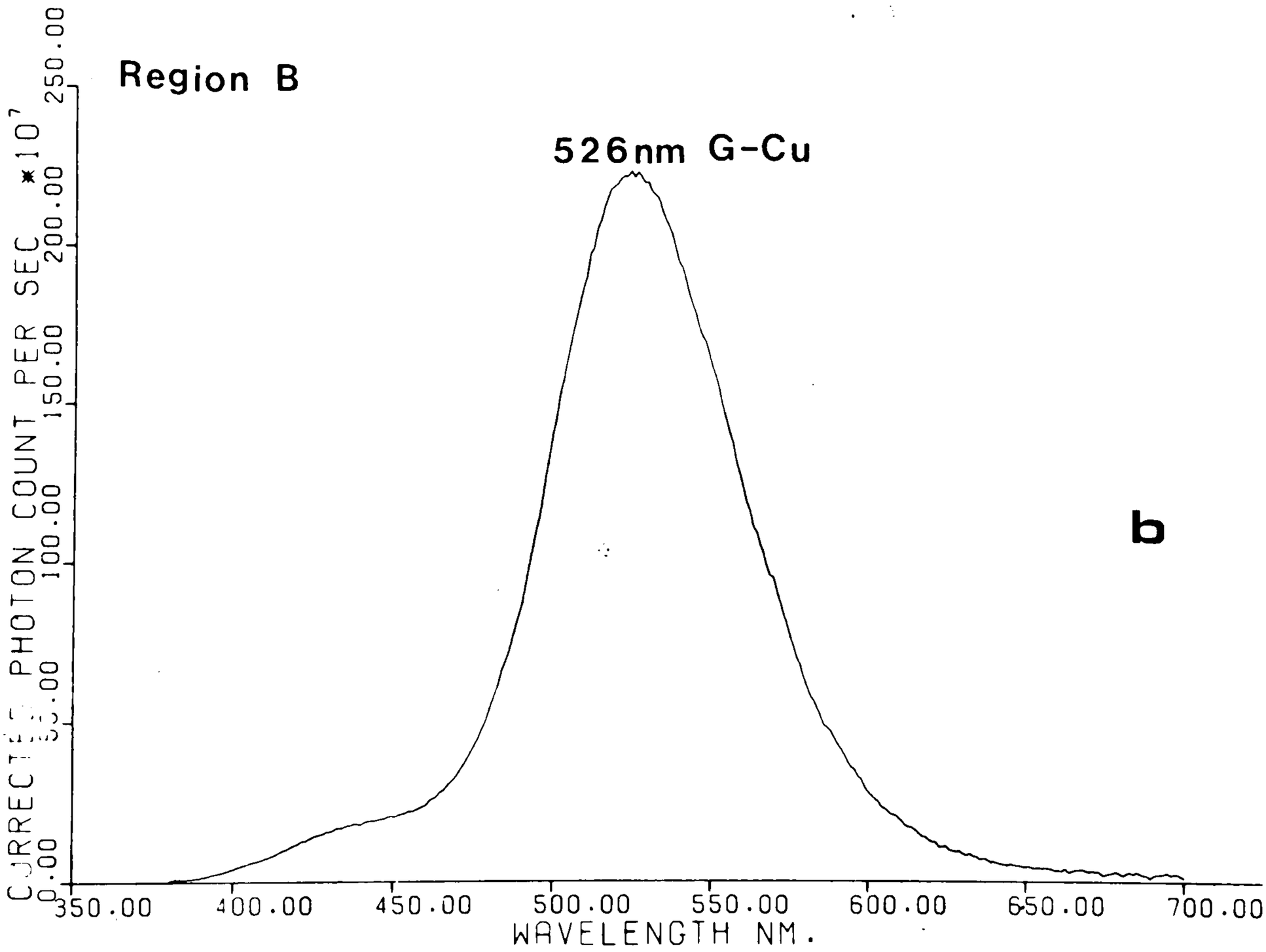


Fig. 4.4 CL emission spectra from the areas marked in Fig. 4.3c: (a) the spectrum from region A and (b) the spectrum from area B.

copper (G-Cu) band at 526 nm. These peak values for ZnS agree closely with the luminescence literature values (Curie and Prener 1967). It is already well known that when Cu is added as the impurity activator with a coactivator like Cl or Al in ZnS both green and blue luminescence bands can be produced (see section 2.1.4). Furthermore, depending on the activator - coactivator ratio either of these two bands can be maximized so that the G-Cu band predominates when the ratio in unity and the B-Cu band when the ratio becomes greater than unity (Kröger and Dikhoff 1950, Van Gool et al. 1960, Van Gool 1961).

The spectrum in Fig. 4.4a shows that region A (as defined in Fig. 4.3c) of the sample emits mostly the B-Cu luminescence, which suggests that the copper (ie activator) concentration is larger here than in region B where the G-Cu band prevails (Fig. 4.4b). This variation in luminescence between the two copper bands can be understood in terms of Fig. 2.2 section 2.1.4, where the relationship between the activator concentration to the coactivator concentration has been plotted for ZnS.

In retrospect, the evidence given in Figs. 4.3 and 4.4 suggests preferential impurity segregation rather than luminescence variations due to structural changes or internal electric field effects. All these effects will be more fully discussed in the next section. However it is best to point out here that the observed shift in peak position of 69nm in going from region A to region B can not be attributed to structural changes and/or internal field effects. This is

because the results following in the next section will show that changes in crystal structure between the two extreme limits of hexagonal (2H) and cubic (3C) modifications in ZnS produce only about 8nm wavelength difference (see table 2 section 4.2.3 and also table 5 section 4.4.2). Also internal electric fields, if present, would only decrease the luminescence intensity but would not contribute to the peak shift (see section 4.2.3 and especially Fig 4.6).

As a direct consequence of these earlier experiments, a number of alterations were found to be necessary before more quantatitive CL measurements could be performed. These were the addition of (1)a PM tube refrigeration housing unit, (2) photocathode magnetic focussing and (3) a quartz fibre light guide. The first two improvements helped to reduce the inherent PM dark count by a factor of 10^2 to about 3-5 counts per second. The quartz fibre increased the wavelength range of the CL-system since glass does not transmit in the ultra-violet region. The 'edge' emission (conduction band to valence band transition) in ZnS occurs in the near ultra-violet region of the electromagnetic spectrum.

The overall response factor (QEF) of the final CL system (Mark 4) was an order of magnitude better than the value found in calibration of the earlier (Mark 3) system as reported by Steyn et al.(1976). The count rate, R, of the photon counter is the product $R = QEF \left\{1-A\right\} N$ (see Steyn and Holt 1973), where Q is the PM tube quantum efficiency and falls rapidly

in going from the blue to the red end of the visible spectrum. E is the transmissive efficiency of the monochromator which peaks at the blaze wavelength, F the fraction of photons leaving the specimen which are delivered by the collector to the monochromator entry slit, and $\{1-A\}$ the fraction of the photons generated in the specimen, N, which escape. (A is the internal loss fraction due to self-absorption, etc.). All these factors are a function of wavelength. An account of the calibration work can be found in section 3.6 page 106.

The results to be presented hereafter were all obtained using the final (Mark 4) system as shown schematically in Fig. 3.5. The crystals used, both ZnS and CdS, were all from the Hebrew University of Jerusalem as they were of a better structural quality than the others available here.

4.2.3 FURTHER INVESTIGATIONS OF LOCAL CATHODOLUMINESCENCE VARIATIONS:RESULTS AND INTERPRETATIONS

Many structurally homogeneous hexagonal wurtzite (2H), cubic sphalerite (3C) and 4H polytype regions were choosen from over three dozen striated ZnS platelets for the investigation of local cathodoluminescence (CL). As already explained, a typical platelet consists of numerous areas which differ from each other in birefringence and therefore in crystal structure (see section 3.3). Corrected room temperature values for the energy of a photon at the peak (E_p) of the CL edge emission band (arising from conduction band to valence band transitions) from the selected areas are given in table 2.

TABLE 2 CATHODOLUMINESCENCE EDGE EMISSION PEAK ENERGIES FOR VARIOUS ZnS STRUCTURES AT ROOM TEMPERATURE

CRYSTAL STRUCTURE	E_p (eV)
Hexagonal (Wurtzite)	3.740 (331 nm)
4H Polytype	3.706 (335 nm)
Cubic (Sphalerite)	3.657 (339 nm)

To record emission spectra the monochromator was scanned through the selected wavelength range by means of a stepper motor (section 3.5 page 96). This rotates the diffraction grating, stopping for a selected time at wavelengths separated by intervals which are much smaller than the bandwidth of the monochromator. Varying the stepper motor speed (for which there are six positions) varies the wavelength interval between two consecutive spectral points. Throughout this section the monochromator bandwidth was set at 5 nm whilst the spectral points obtained were 1.25 nm apart. The computer graphics terminal however, draws straight lines between two experimental points. So a "ragged" spectrum is an indication of the spread in experimental points which obviously leads to errors. The reproducibility of the values given in table 2 was found to be surprisingly consistent from one experimental run to the next. Infact, disagreement only occurred whenever very fine fault lines were found imbedded in what was originally thought to be a pure region of a structure. All emission spectra were obtained by working at 30 KeV with beam currents of 10^{-9}-10^{-10} A

Brafman and Steinberger (1966) showed that the various regions of a striated ZnS platelet differ from each other in the stacking sequence of the basal planes. The difference can be characterized by a single structure parameter β , which is the percentage of the close-packed planes which are in a hexagonal nearest - neighbour environment. So the numerous strips can be classified as having a certain percentage of hexagonality β which is 100% for wurtzite (2H), 50% for

polytype 4H and 0% for sphalerite (3C). The many higher order polytypes known to exist in ZnS all fall between the values for the cubic and the 4H structures. To account for the structural properties of these ZnS platelets Shachar et al. (1970a) have proposed a rough classification into four categories. Type (I) platelets are basically crystals of hexagonal (2H) structure with regions containing only a very narrow range of lower β values. Type (II) platelets are crystals with a wide range of values of β including regions of 2H structure. Type (III) and (IV) platelets are crystals which contain only regions of low β structures. Furthermore Brafman and Steinberger (1966) have shown that the ZnS absorption edge shifts linearly with the percentage of hexagonality β. It therefore seems reasonable, to expect the 4H polytype CL edge emission peak to have a value of E_p that is intermediate between the values of the two extreme structures (3C and 2H) in table 2. Recently Morozova et al. (1974) reported CL edge emission data for a number of ZnS structural forms. The values given in table 2 are generally in good agreement with their's. Differences arose, as a spectral correction procedure has been used in this work which allows for the fall with increasing wavelength in the fraction of the photons emitted, that are detected, over the wavelength range from 250 to 850 nm (see section 3.6 which deals with the CL calibration).

In the literature, local cathodoluminescence variations have been attributed to (i) structural changes or to (ii) impurity segregation or to (iii) internal electric field effects.

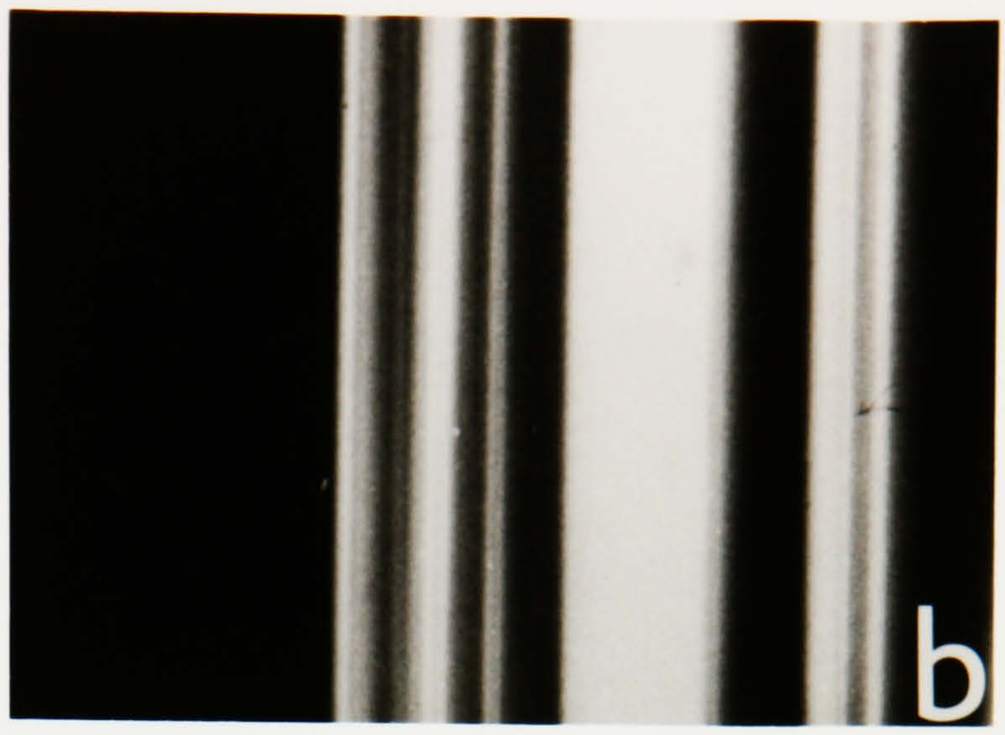
The following results will give evidence of the influence of all these three factors. Structural changes are easiest to identify from birefringence measurements as already explained. Figure 4.5a shows a typical ZnS platelet (No.227B) taken under crossed polarizers in an optical microscope. The polytypic bands running perpendicular to the polar c-axis of the crystal and some linear markings parallel to the c-axis can clearly be distinguished. Regions containing linear markings have been avoided when taking spectra. An enlargement of the delineated area, in which CL measurements were made, is given in Fig.4.5b. Three regions were selected for study. Region 1 was a heavily faulted cubic area, region 2 a 4H polytypic band and region 3 a broad unfaulted cubic band. Due to the intrinsic nature of the edge emission, recording at wavelengths between 325 nm and 345 nm at room temperature probably eliminates serious impurity perturbations. Care was however needed in interpreting results since in the following sections, it will be shown that analysis of the shape of the edge emission band in ZnS revealed two distinctive exponential regions in the low energy side of the band (see section 4.4). The lower of the two exponential sections is believed to be influenced by both impurity concentration and temperature.

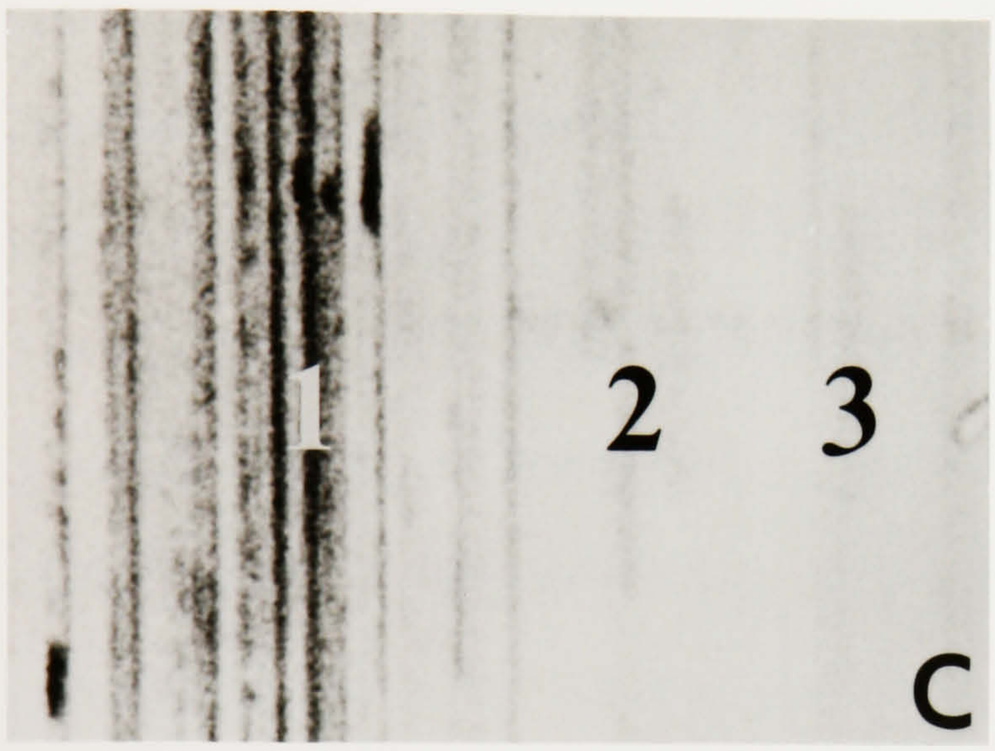
The remainder of Fig.4.5 is made up of (c), panchromatic and (d,e,f) monochromatic CL micrographs recorded at the emission wavelengths of 328 nm (3.78eV), 334 nm (3.71eV) and 344 nm (3.60eV) respectively. The area represented is about 308 μm wide.

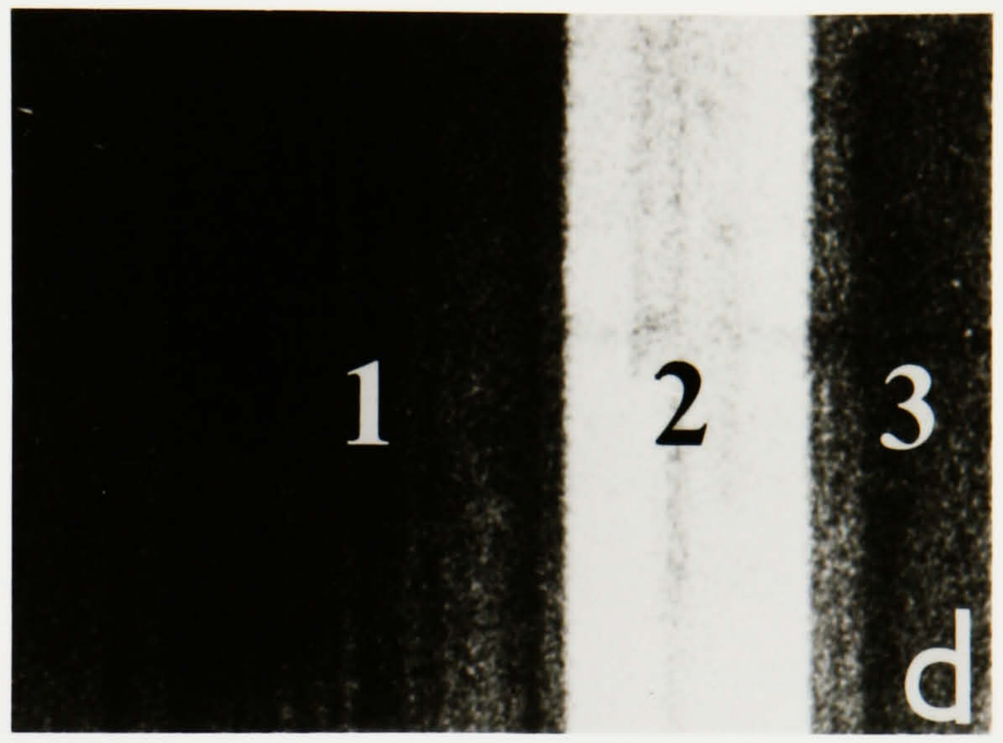
Fig. 4.5

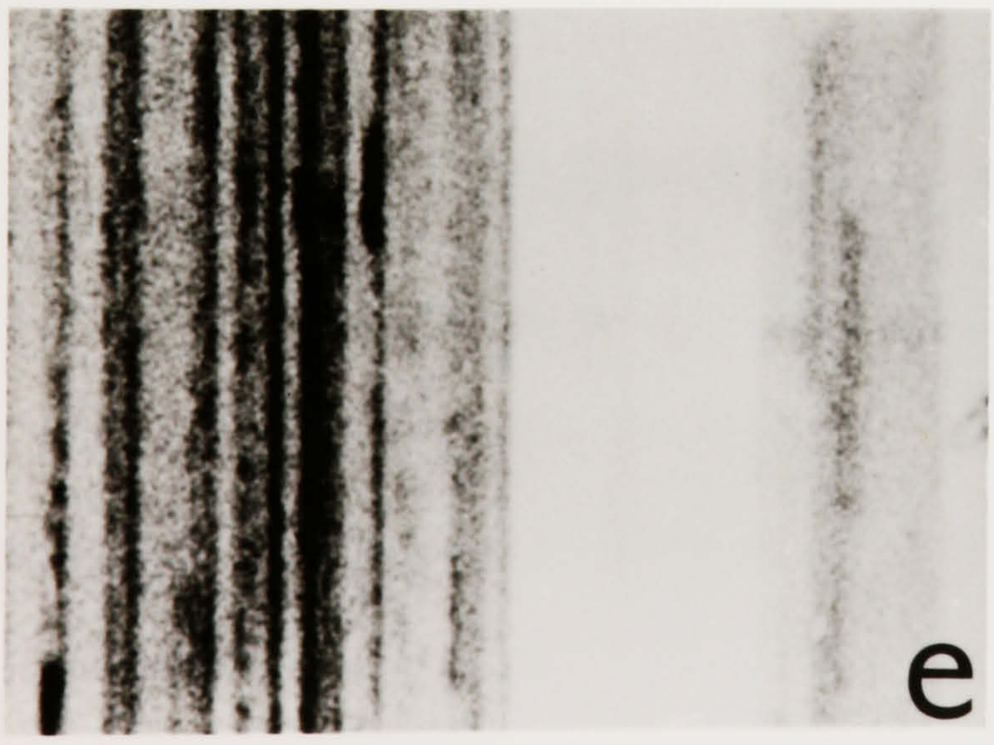
Micrographs of a striated ZnS (227B) platelet with the common c-axis running horizontally. (a) is a low magnification polarized light - micrograph of the whole platelet, showing the polytypic bands running vertically. The remaining micrographs are all of the area in the rectangle outlined in the centre of the platelet. (b) is an enlargement of the area outlined in (a), (c) is a panchromatic CL SEM micrograph. The remaining pictures are monochromatic CL SEM micrographs recorded at the following emission wavelengths: (d) 328nm (3.78eV), (e) 334 nm (3.71eV) and (f) 344 nm (3.60eV). The width of the area represented by the CL micrographs (c), (d), (e) and (f) is 308 μm.











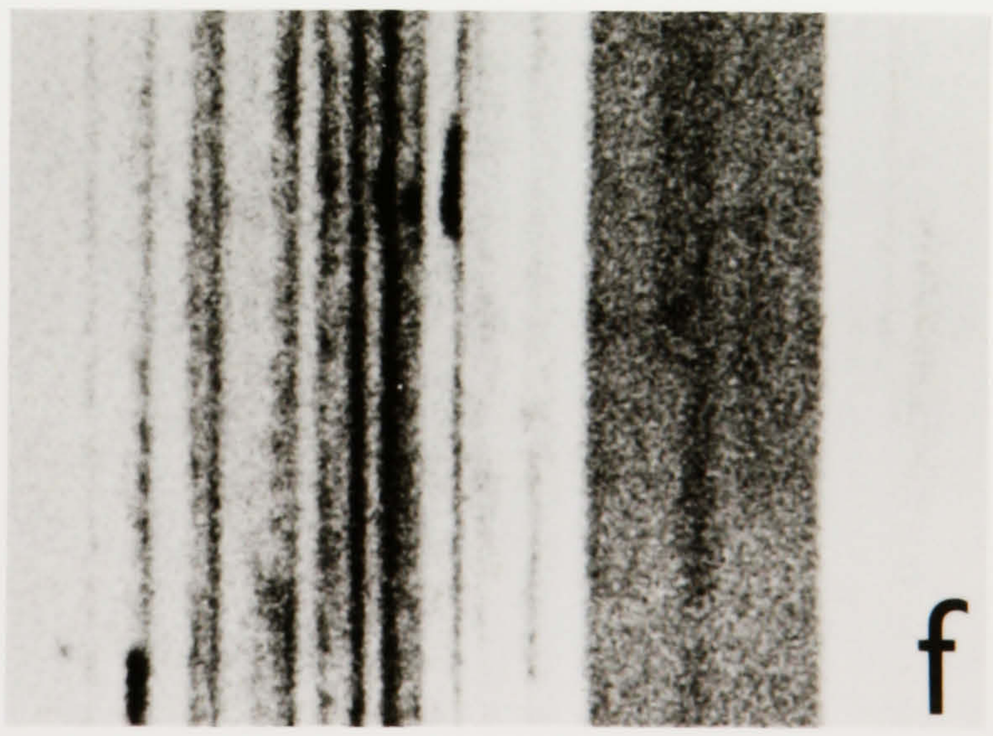


Fig 4.5

The changes between the micrographs are considerable as would be expected because each structure has an unique edge peak emission value, table 2, and depending on the wavelength used as signal for the micrograph, regions appear light or dark. An interesting feature is region 1, where little or no emission occurs at any wavelength as was shown by spectral analysis. It is worth comparing this behaviour with that of the second broader cubic region 3, especially in the micrograph Fig. 4.5f. By suitably magnifying and taking spectra from one of the dark lines, in region 1, it was found to emit low intensity cubic edge emission. For correlation of relative photon emission from the three regions, equal volumes of each type of structure were examined under identical SEM conditions. The results presented in Fig.4.6 show marked quenching of the CL emission to occur in region 1 as compared to region 3 which has the same cubic structure. This reduction in CL luminescence can be attributed to internal electric fields see section 2.5 page 56. The existence of strong macroscopic internal fields, which are dependent on structure, has been thoroughly established in these ZnS platelets (Shachar et al. 1970a, Brada et al. 1972). These fields occur due to charged sheets of dislocations (Shachar and Brada 1970, Steinberger et al. 1972), which occur whenever there is a lattice - constant misfit between adjacent crystal structures. Fields with strengths up to 10^5 V/cm occur in the more densely faulted regions of a platelet (Yacobi and Brada 1974). Without the help of CL spectra (Fig.4.6), the CL SEM micrographs on their own give very little indication of field quenching.

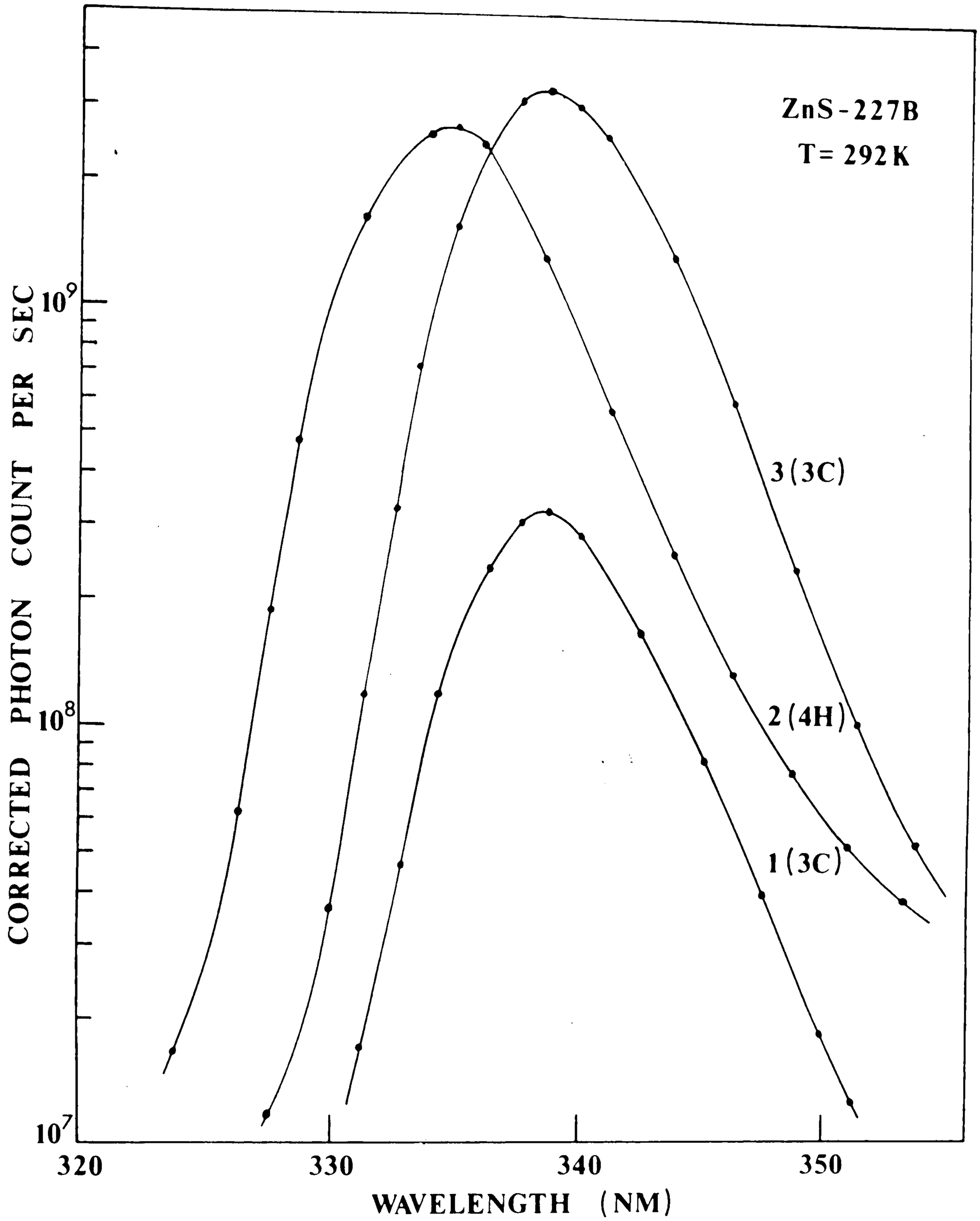


Fig. 4.6 The CL edge band emission obtained from the three numbered regions of Figure 4.5(d).

Confirmation that electric fields were indeed responsible for the reduced emission from region 1 was only possible due to the spatial resolution of the spectroscopic CL mode of the SEM.

Using the same sample area, local variations in impurity activated CL was also investigated. The monochromatic CL SEM micrographs shown in Fig. 4.7 were taken (a) at a wavelength of 670 nm (1.85eV) and (b) 685nm(1.81eV). The CL emission spectra from the areas marked in Fig. 4.7 are presented in Fig. 4.8, where (a) is the spectrum from region 2 and (b) the spectrum from area 3. The emission spectra consists of two relatively sharp bands well separated in wavelength (Fig. 4.8). The one at shorter wavelength (higher energy) is due to the edge emission (c.f. Fig. 4.6) whilst the other is an impurity band. From spectrochemical analysis, section 4.1.2 table 1, it was known that a number of impurities, in varying amounts, are always present in these platelets. The value of this particular impurity band peak energy E_i(eV) is given in table 3 from which it can be seen that there is a shift towards lower energies (longer wavelengths) in going from region 2 (4H polytype) to region 3 (cubic). This behaviour taken together with the fact that the ratio of E_p (for edge emission) to E_i (for impurity emission) remains constant suggests that the same impurity is responsible for the observed red luminescence band in both structures. Therefore region 2 in Fig. 4.7a, appears bright because this micrograph was recorded using a photon energy near the impurity band peak E_i(eV) for the 4H polytype but the relative brightness

Fig. 4.7

Monochromatic CL SEM micrographs of the same area as in Figure 4.5: (a) at wavelenght of 670 nm (1.85 eV) and (b) 685 nm (1.81 eV). The width of the area represented in these two micrographs is approximately 294 μm with the polar c-axis of the crystal running horizontally.

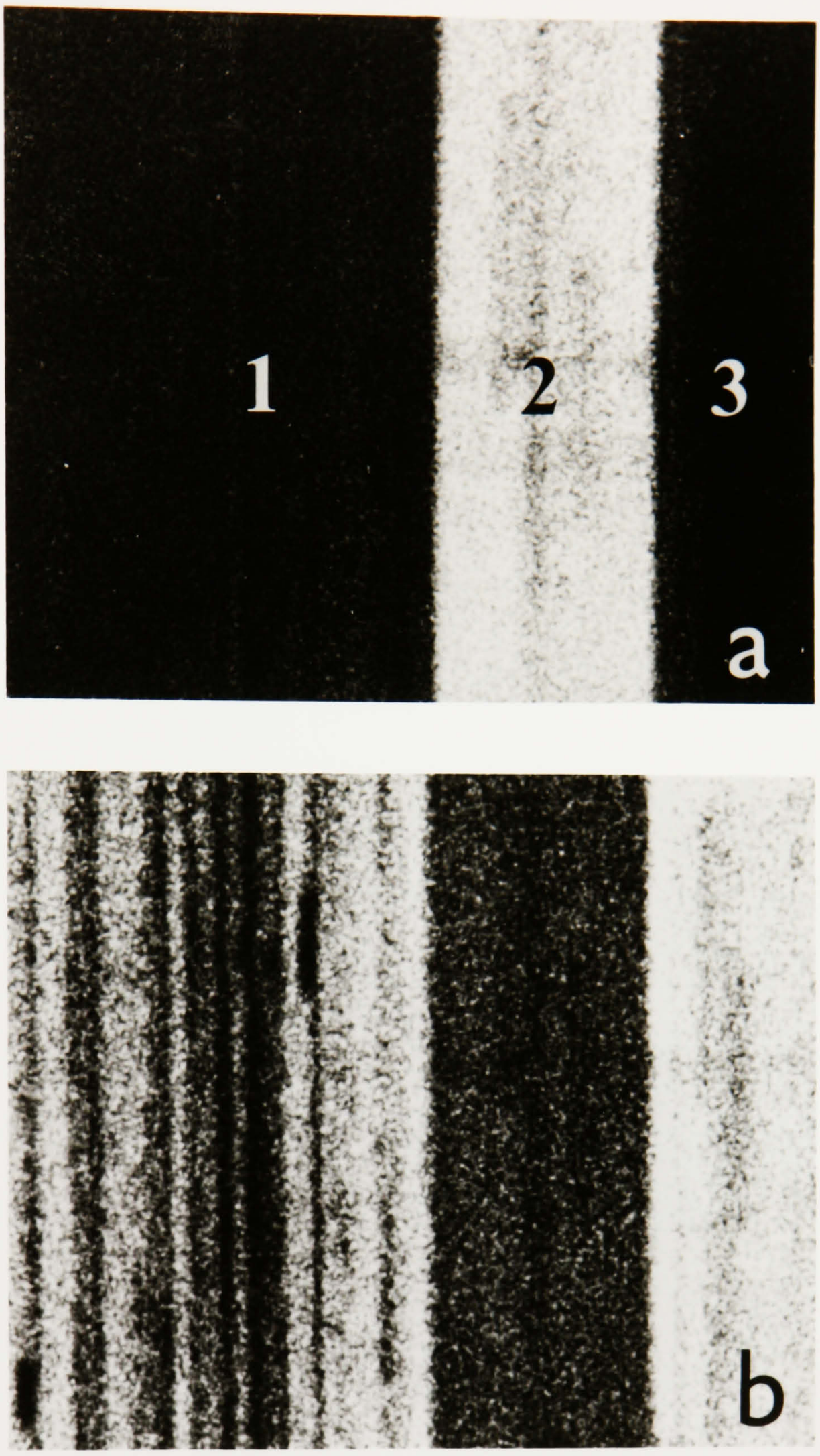
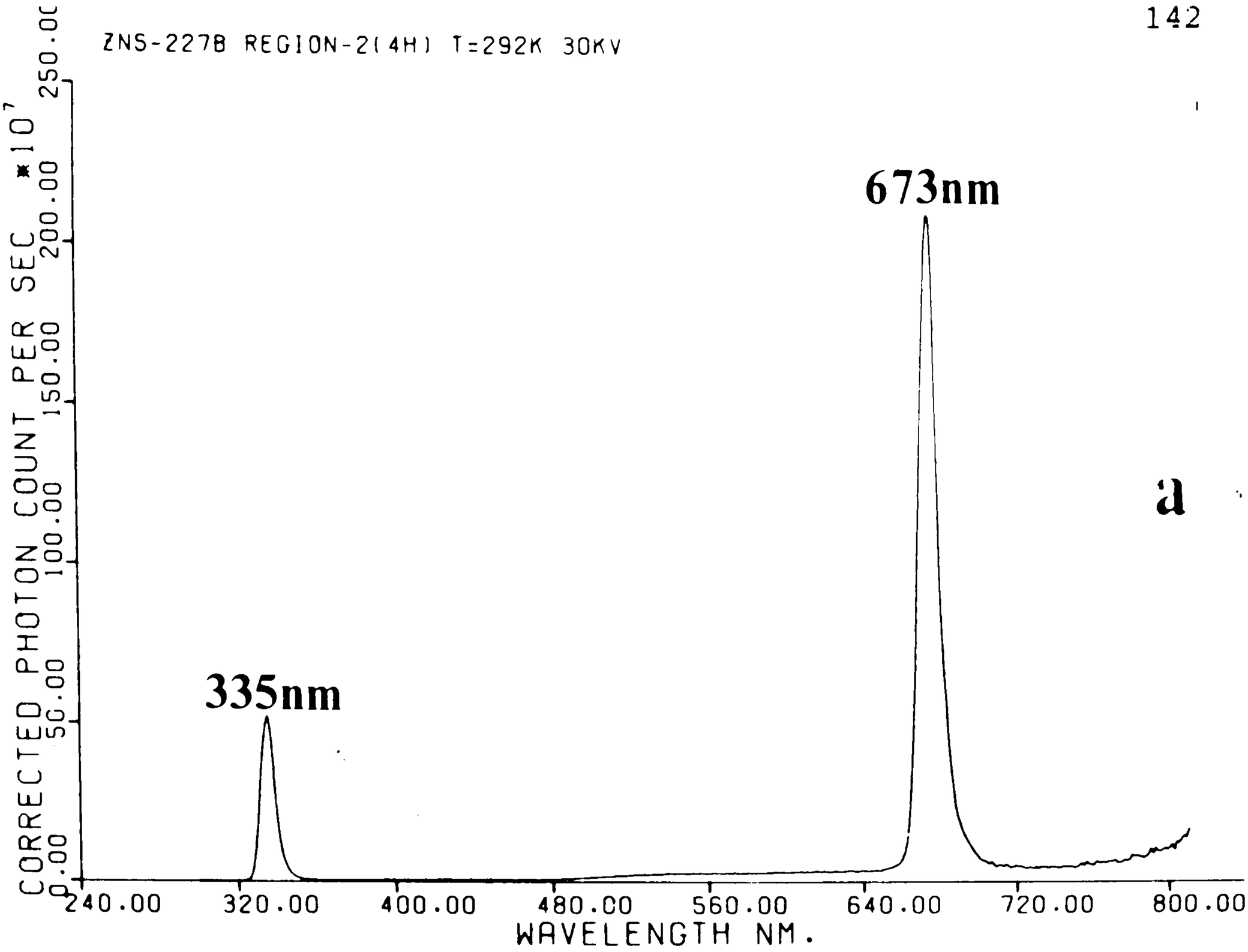


Fig 4.7

Fig. 4.8

CL emission spectra from the areas marked in Figure 4.7 (a) the spectrum from region 2 and (b) the spectrum from region 3. The shorter wavelength band is the edge emission (conduction band to valence band recombination radiation). The sharp band at longer wavelengths is due to an impurity activated mechanism.


ZNS-227B REGION-2(4H) T=292K 30KV
CORRECTED PHOTON COUNT PER SEC *10^7
0.00
50.00
100.00
150.00
200.00
250.00
673nm
335nm
a
240.00
320.00
400.00
480.00
560.00
640.00
720.00
800.00
WAVELENGTH NM.

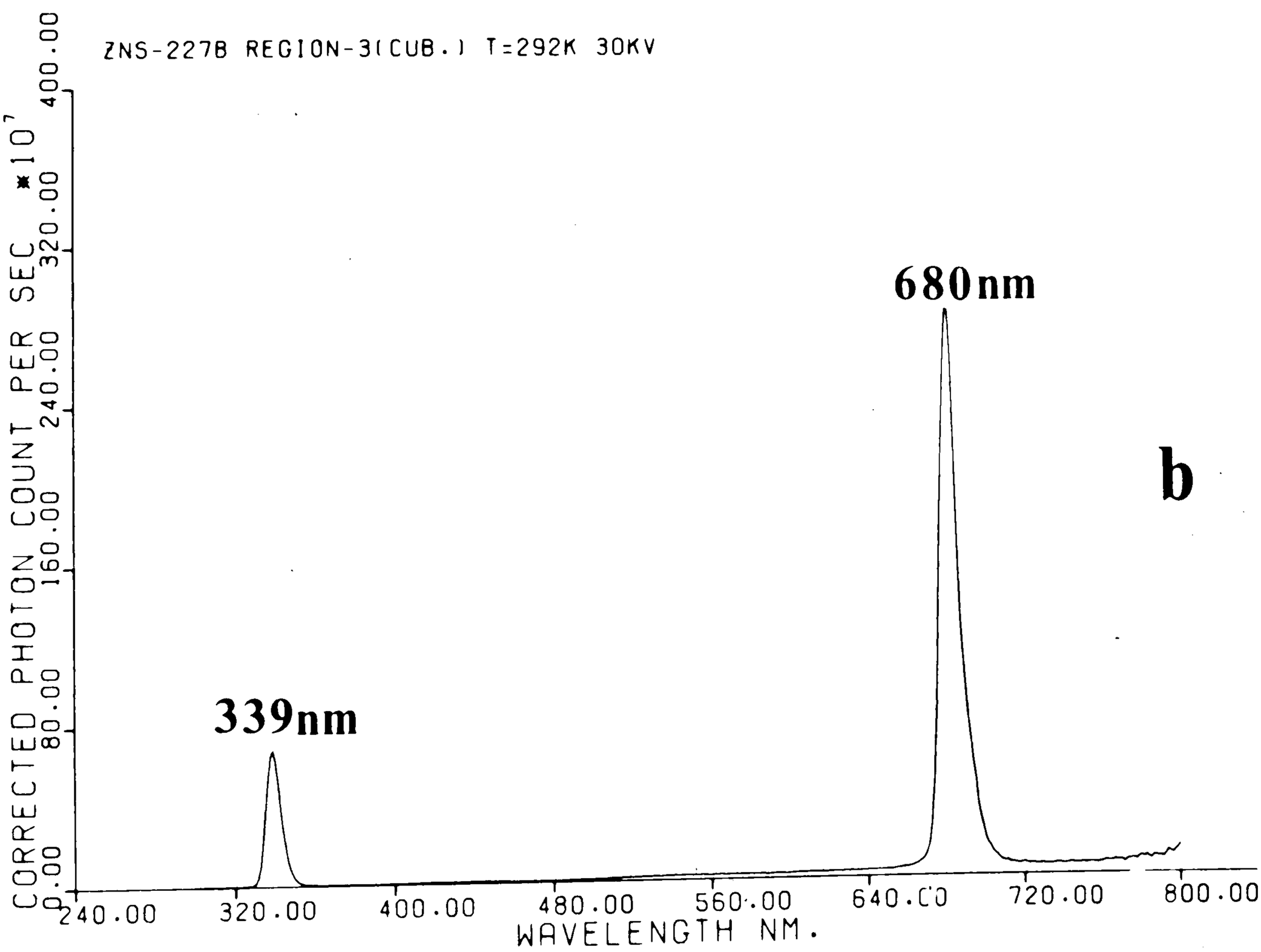

ZNS-227B REGION-3(CUB.) T=292K 30KV
CORRECTED PHOTON COUNT PER SEC *10^7
0.00
80.00
160.00
240.00
320.00
400.00
680nm
339nm
b
240.00
320.00
400.00
480.00
560.00
640.00
720.00
800.00
WAVELENGTH NM.

Fig 4.8

TABLE 3 ROOM TEMPERATURE CATHODOLUMINESCENCE PEAK ENERGIES FOR TIN (Sn) ACTIVATED ZnS (No.227B)

CRYSTAL STRUCTURE	E_i (eV)
4H Polytype	1.842 (673 nm)
Cubic (Sphalerite)	1.823 (680 nm)

soon moves to region 3 in Fig. 4.7b, as the wavelength recorded moves towards the cubic impurity peak value. Since the impurity band is intense and well defined, local CL contrast changes greatly over just a few wavelength resolution intervals of the detector system. Internal electric field quenching of region 1 was also observed for this impurity band.

To identify the impurity responsible for the observed red band in this crystal, the spectral measurements were compared with data in the luminescence literature. Red emission bands in ZnS, falling in the wavelength range 670 to 680 nm, have been produced by copper and tin impurities as explained earlier in sections 2.1.2 and 2.1.3. There are two factors which make red - copper (R-Cu) luminescence unlikely in this case. (a) For R-Cu emission to occur there must be no coactivation from the group IIIB or VIIB elements (Shionoya et al. 1966b), otherwise the emission occurs in another wavelength range. However, aluminium (group IIIB) is known to be present in these platelets (see table 1) from spectrochemical analysis. (b) The usually reported half-width value for R-Cu emission at room temperature, 0.65eV, is larger by something like an order of magnitude than the half-widths of the impurity bands from this sample (eg those in Fig. 4.8).

It therefore seems more probable that the red band can be assigned to tin activation. Infact the peak emission position reported by Mita (1964) for tin - activated cubic ZnS agrees with that given in table 3.

Finally, an example of preferential impurity segregation perpendicular to the c-axis was found in another platelet (ZnS - 248). Using the data given in table 2, structurally homogeneous regions were choosen by means of edge emission observations. In this way it was established that regions 1 and 2 (Fig. 4.9) in ZnS - 248 were cubic (3C) and 4H polytypic structures respectively. Birefringence measurements were later taken to check the CL structure determinations.

The panchromatic and monochromatic CL micrographs for the sample (ZnS - 248) are shown in Fig. 4.9a and 4.9b respectively. The wavelength used to record the monochromatic micrograph was 523 nm (2.37 eV). Selected area spectra (uncorrected) from the two structures involved are given in Figs. 4.10a and 4.10c with the corrected spectra in Fig. 4.10b and 4.10d respectively.

The impurity emission characteristics of the two areas are very different even though the two regions are adjacent and the spectra were taken from areas that were only about 60 μm apart in the two structures. The panchromatic CL micrograph, Fig. 4.9a, is best described as the result of the combination of the two uncorrected spectra. The intense luminescence in region 1(cubic) is due to the broad impurity band peaking on the uncorrected spectrum of Fig. 4.10a at 523 nm (2.37eV). This band is however, missing in the adjacent 4H structure (c.f. Figs. 4.10a,c which are uncorrected).

Fig. 4.9

CL SEM micrographs of another ZnS platelet (No. 248): (a) is panchromatic and (b) is monochromatic, recorded at 523 nm (2.37 eV). The polar c-axis runs horizontally and the area represented is 178 μm wide.

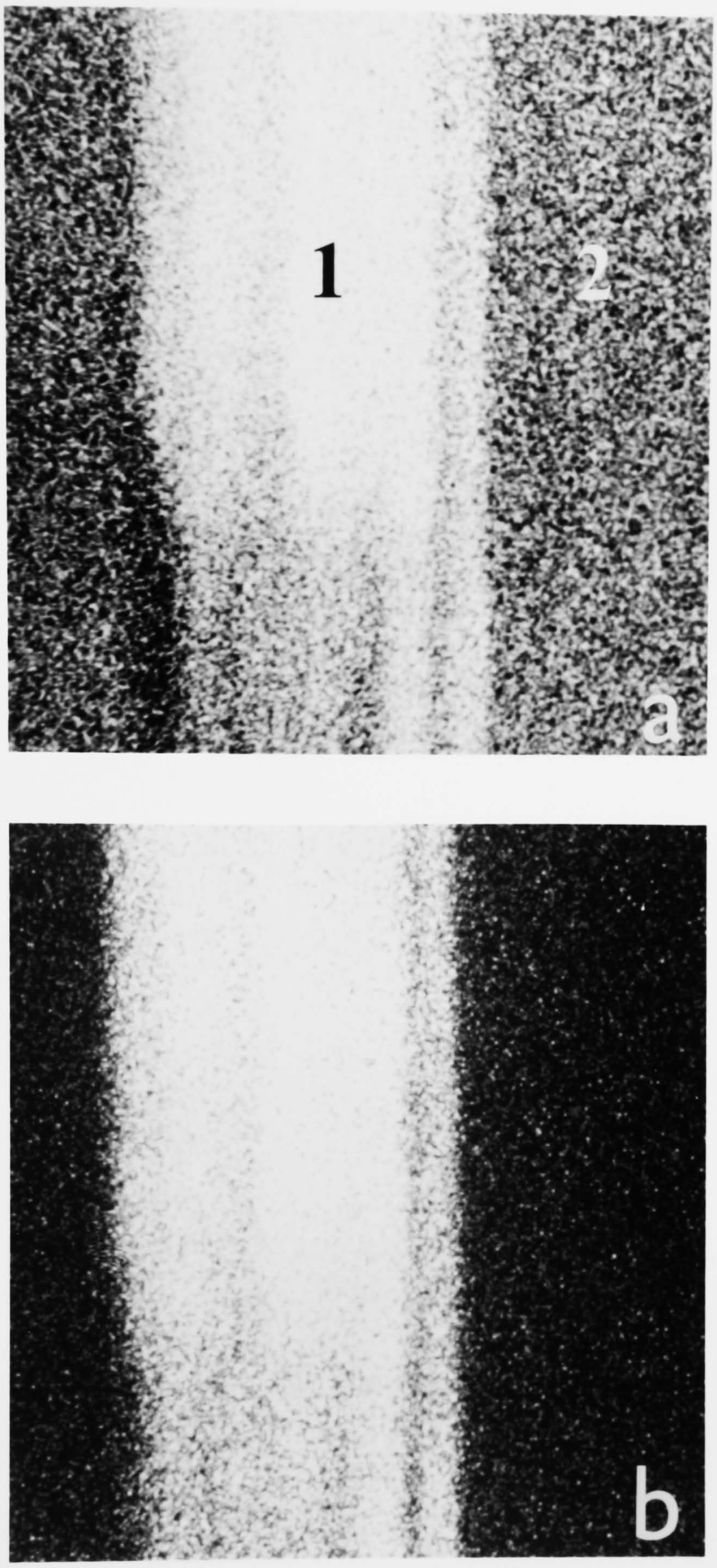


Fig 4.9

Fig. 4.10

Uncorrected and corrected CL emission spectra obtained from the two regions shown in Figure 4.9. (a) is the uncorrected spectrum from cubic region 1 and (b) is the corrected spectrum. (c) is the uncorrected spectrum from 4H polytype region 2, and (d) is that for the same region after correction. The small bands below 350 nm are the intrinsic edge emission bands while the large bands at longer wavelengths are characteristic of impurities.

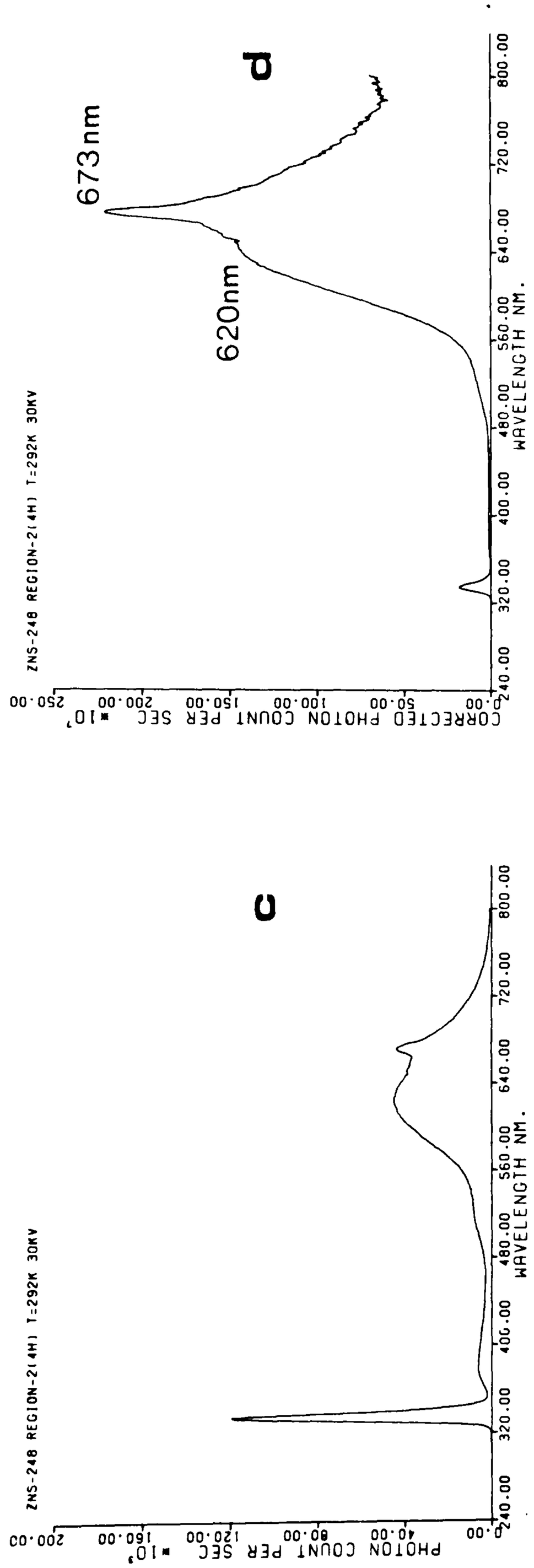

d
673nm
620nm
534nm
523nm
b
c
a
ZNS-248 REGION-2(4H) T=292K 30KV
ZNS-248 REGION-1(CUB.) T=292K 30KV
CORRECTED PHOTON COUNT PER SEC *10³
WAVELENGTH NM.
240.00
320.00
400.00
480.00
560.00
640.00
720.00
800.00
0.00
50.00
100.00
150.00
200.00
250.00
40.00
80.00
120.00
160.00

Fig 4.10

Note that Fig. 4.9b, was obtained by using the raw count rate at the uncorrected peak wavelength as video signal. Thus Fig. 4.9b shows that in the ZnS platelet an impurity segregated in the region of the crystal of one structure in preference to the other. Note, that the relative brightness of different areas in a panchromatic micrograph alone is not proof of segregation. On correction, the impurities present in the two areas are infact found to be of equal emission strengths. This makes the panchromatic CL micrograph (Fig. 4.9a) unreliable as an indicator of impurity segregation since both regions should, but do not, appear as bright bands of different emission wavelengths. Equally, the monochromatic CL micrograph must be interpreted with caution. For example, Fig. 4.9b was taken at 523 nm (2.37 eV) which corresponds to the peak energy value of the uncorrected impurity band (Fig. 4.10a), whereas the corrected band maximum is at 534 nm (2.32 eV), Fig. 4.10b.

Even if on-line computer corrected spectral data were available, to obtain corrected monochromatic micrographs, it might still be necessary sometimes to work at wavelengths off the corrected peak. This is in order that the experimental (raw) count rate may give a sufficiently high signal strength in relation to the noise in the detector - display system to obtain good quality pictures.

In Figs. 4.10 (a,b,c and d) the edge emission is the band with the shortest wavelength in each case. The various impurity bands have been identified from their peak position and

half-width values as before. The 523 nm (uncorrected ie. 2.37eV) emission band in region 1 (cubic) is the well known green-copper (G-Cu) luminescence which occurs when ZnS is copper activated with aluminium as the coactivator (see section 2.1.4). Even taking account of the spread in results for the G-Cu band in the luminescence literature, there is still a discrepancy between the peak value reported above and those usually given. There seem to be three contributory factors which could produce this discrepancy. Firstly, the emission results of Lorenz and Orton (1970) for samples of InP, GaAs and many III - V ternary alloys, show that the CL and photoluminescence (PL) modes of excitation do not produce identical emission spectra. They found that PL produced emission bands with their peaks at greater wavelengths than did CL. Similar conclusions can be drawn from the work of Norris et al. (1973) who used ZnS and CdS specimens. Secondly, the dependence of the green-Cu CL luminescence on the concentration of aluminium and copper was investigated by Kawai et al. (1974). A shift of peak wavelength was observed with an increase in concentration but their results are further complicated by their use of polycrystalline samples. Thirdly, the forgoing results have clearly demonstrated that structural changes can produce large changes in the spectra for small displacements over the specimen surface.

The disagreements in peak position of the extensively studied G-Cu luminescence band reported in the literature are also probably an effect of changing the initial PL excitation wavelength (Grasser et al. 1971) as well as using different

PM tubes of varying quantum efficiencies without correcting for this.

The sharp impurity peak at 673 nm (1.84eV) (Fig. 4.10d) from region 2 (4H polytype) in Fig. 4.9 is believed to be due to tin activation. This peak position agrees with the value given in table 3 (Fig. 4.8a) for the earlier ZnS - 227B sample. There is in addition a poorly resolved shoulder appearing at 620 nm (2.0eV), the identity of which is unknown.

4.2.4 THE POWER OF THE CL SEM TECHNIQUE

A number of important features make the CL SEM technique attractive. Firstly, the spatial resolution (from one to a few μm, depending on the luminescent efficiency of the material and on the beam current and voltage consequently required) is sufficient to separate the effects of phase changes or impurity segregation. Secondly the spectral resolution and the range of wavelengths that can be detected covers both structure-dependent bands, eg the edge band, and impurity - dependent bands. Thirdly, corrected spectra are reproducible and, at least in principle, theoretically interpretable.

It might be thought that monochromatic CL micrographs recorded using an impurity activated wavelength as signal could be at least semiquantitatively interpreted as displays of the concentration of the impurity varying from point to point as they are in the case of electron probe microanalysis micrographs.

This is not possible in general because the height of the peak is not the only thing that changes from place to place. The position of the peak E_i(eV) in general shifts with changes in the crystal structure and with changes in concentration of the impurity. Two regions with the same concentration of the same impurity can therefore appear as bright and dark due to the peak occuring at the recorded wavelength in one region and right away from it in the other, as for example for the Sn peak in Fig. 4.7, due to a change in structure. Alternatively two regions with very different concentrations of the same impurity could appear equally bright due to a change in peak height being compensated by a shift of the peak relative to the recorded wavelength.

4.3 COLOUR SYNTHESIS FOR THE PRESENTATION AND ANALYSIS OF SEM CATHODOLUMINESCENCE RESULTS

It is an easy matter to provide a series of black-and-white SEM monochromatic (one wavelength) CL micrographs as a permanent record of the luminescent characteristics of a specimen (like those presented in the previous section).

The comparison of areas occupied by the various impurities is normally carried out by visual assessment of a number of black-and-white photographs, each showing the distribution of a single element activating emission at pre-selected wavelengths. This type of appraisal requires training and experience, and with many of these complex platelets it is

difficult to extract the maximum amount of available information from a set of such photographs. The problem of identification becomes more acute when two or more luminescent impurities occur in a single location. The previous section 4.2.3 has already exemplified these difficulties.

In this respect it is believed that colour photography can be especially useful in delineating complex luminescent areas and presenting the information in an aesthetically pleasing manner. The creation of the same visual sensation of colour as would have been obtained by examining the original subject directly was the goal of CL colour synthesis and the results obtained will be presented in this section.

The method of colour separation has already found extensive use in identifying mixed structural phases in electron probe X-ray microanalysis (Jones et al. 1966 , Lennartz and Laffolie 1967 and Goldstein and Yakowitz 1975). In the above cases, however, colours are selected arbitrarily to represent a certain element and mixed colours then indicate the presence of superimposed elements.

4.3.1 SPECTRAL SENSITIVITY OF THE HUMAN EYE

The human eye responds to radiant energy which if expressed in terms of wavelength in air, ranges from approximately 380 nm to 760 nm. Its sensitivity is not uniform for all wavelengths, nor does a curve representing its relative

response at one illumination level express its relative sensitivity for all other illumination levels. However, the sensitivity of the eye is a maximum in the central region of the visible spectrum (~ 550 nm) at all illumination levels, falling off rather sharply towards the blue and red extremes. But at high levels of illumination the peak of sensitivity, as well as the entire relative sensitivity curve, is shifted towards the yellow-green in comparison to the position of the curve representing the eye sensitivity at low levels of illumination where the peak is in the blue - green. For further reading on human colour perception see Sheppard (1968) and Rose (1973).

4.3.2 ADDITIVE COLOUR AND SUBTRACTIVE COLOUR FORMATION

A wide range of colours can be obtained by adding relatively few basic primary colours in varying proportions. The trichromatic theory of colour vision is based on three primary colours which are red, green and blue. None of these primaries can be obtained from mixing the other two.

If three circular beams of white light are directed onto a screen but pass first through red, green and blue filters respectively, then the combination of red and green produces yellow, green and blue produces cyan (sky colour) and blue and red produces magenta (pinkish). The three primary colours add to make white as shown in Fig. 4.11a.

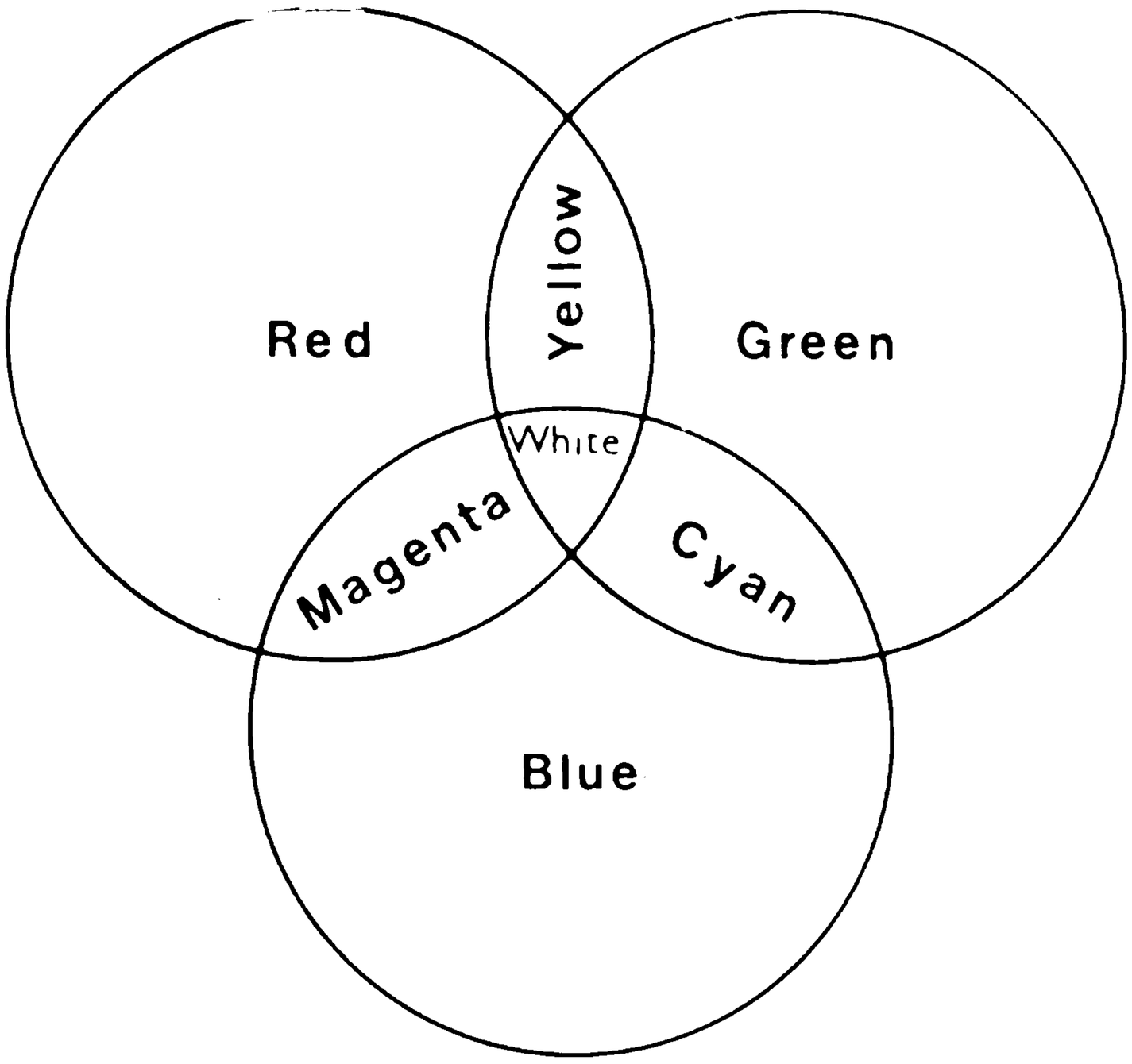


Fig. 4.11a Diagram of additive mixtures of three primary colours producing various colours as well as white light

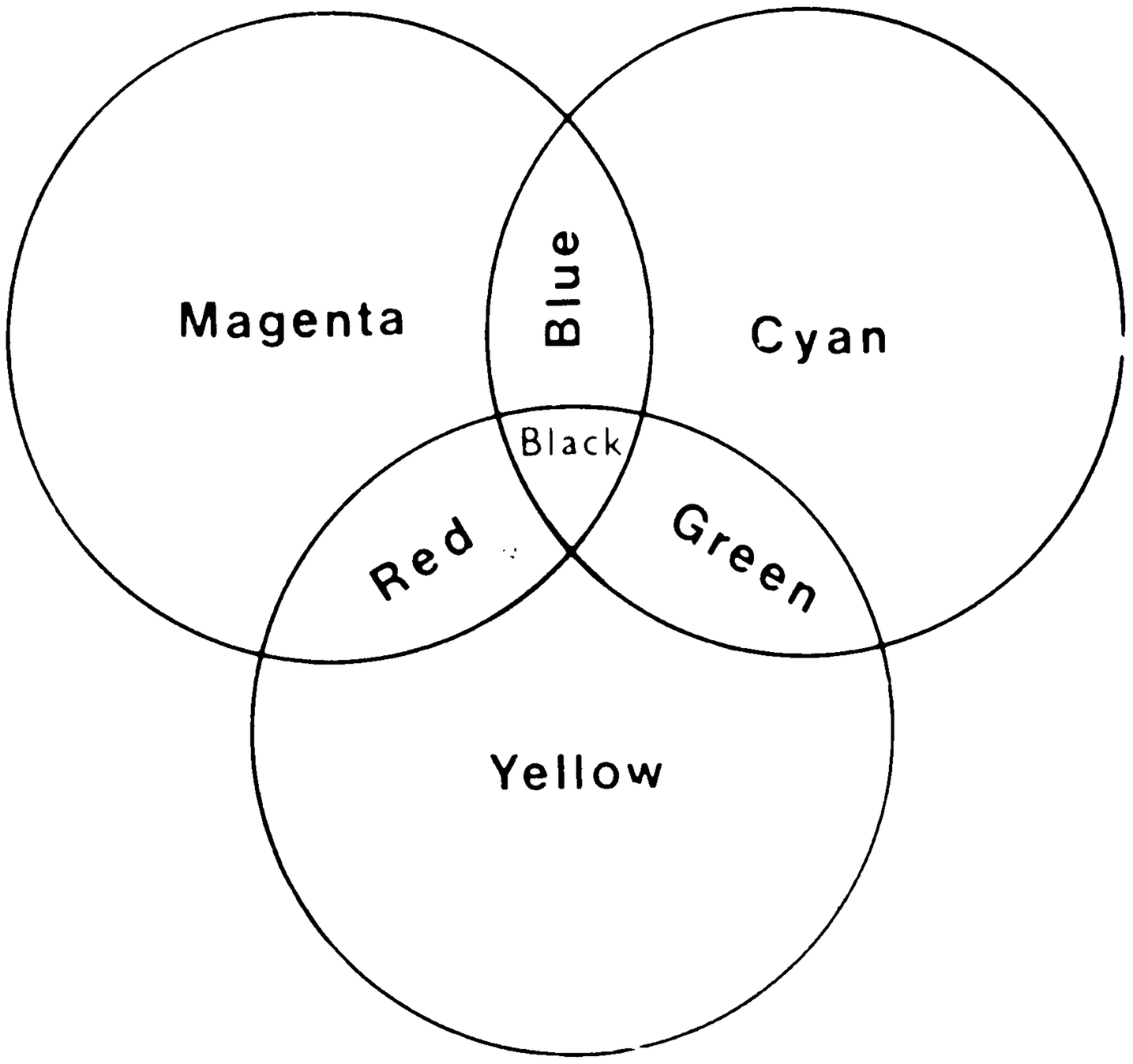


Fig. 4.11b Diagram of subtractive colour formation with black in the middle

The intermediate colours yellow, cyan and magenta can be considered as consisting of white light minus blue, red and green respectively. The colour resulting from omitting a single primary from white is called the complement of that primary or secondary colour.

Various other colours (ternary) can also be produced by the additive combination of these primary colours in varying proportions. Thus, the addition of green to red will produce orange, yellow or yellow-green, depending upon the relative intensity of the green to the red. Likewise, the mixture of green and blue produces various blue-greens and the combination of red and blue can yield all variations of magenta.

Colours can be obtained also by subtracting light of a certain wavelength from white light. A yellow filter transmits red and green and absorbs blue. In other words, yellow is minus blue, it contains all the colours of the spectrum except blue. If a yellow filter is placed on a white paper or in front of a source of white light, and then over this a magenta filter which absorbs green light, as in Fig. 4.11b, only red light will be reflected or transmitted to the observer. Similarly, a combination of cyan and yellow filters produces green as the yellow absorbs the blue and the cyan the red, leaving only the green. A blue may be obtained through a combination of magenta and cyan filters. Thus the three primaries red, green and blue as well as other colours, can equally be produced by subtracting colour from white by means of cyan, magenta and yellow colorants.

4.3.3 TERNARY COLOUR MIXTURES USING KODAK 'WRATTEN' FILTERS

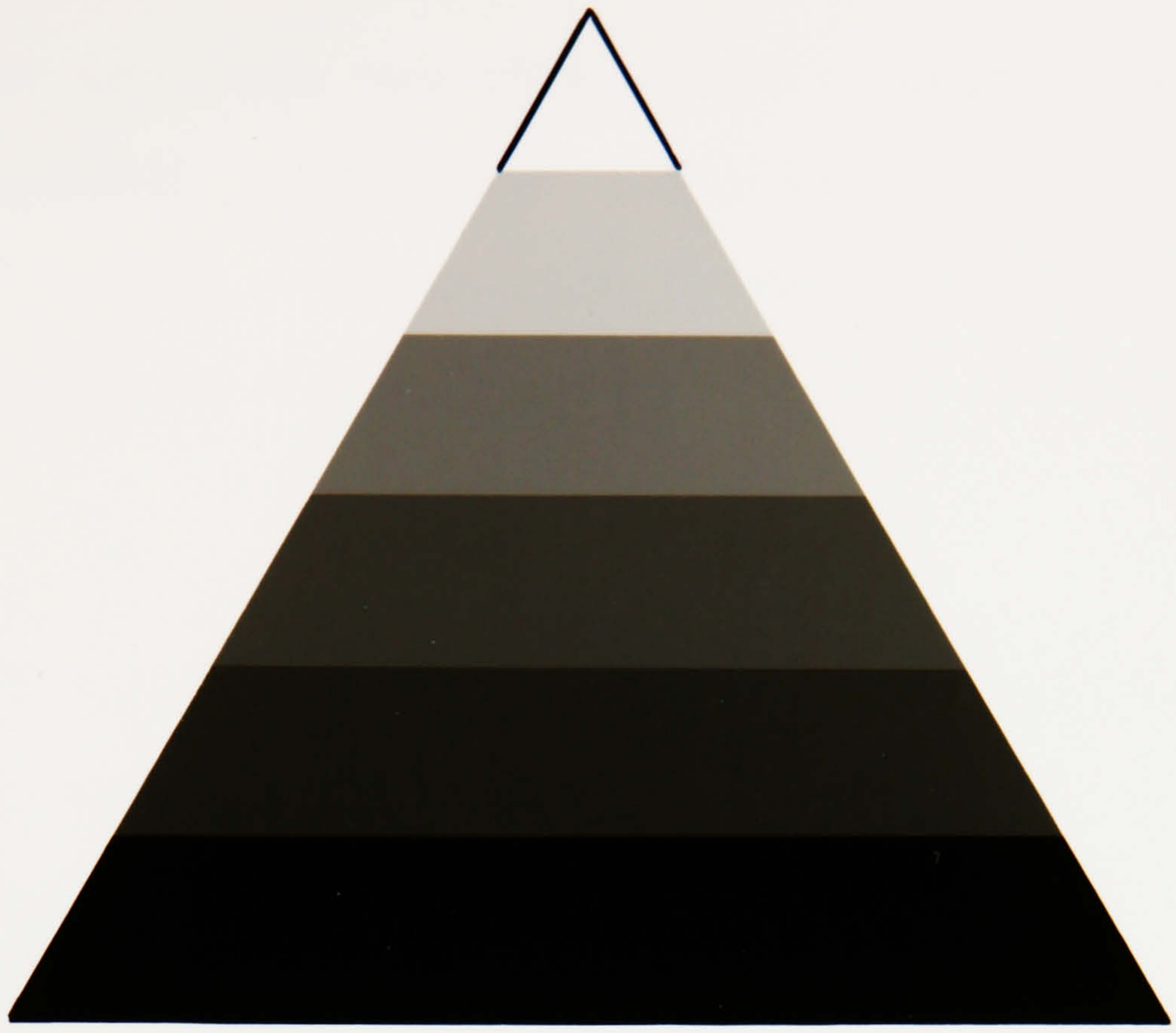
The process of colour synthesis consists of copying sequentially black-and-white CL micrographs onto colour film via the primary filters. Due to the characteristics of the human eye, it can not unequivocally interpret mixtures of more than three components, thus the choice of red, green and blue filters. Colour film like the human eye is also based upon the three primaries and can only resolve combinations of them. The use of more than three primaries leads to colour blends of the same chromaticity (ie hue, saturation and lightness). Examples of this have been given by Jones et al. (1966) and Bennartz and Laffolie (1967). Hue is that quality of sensation according to which an observer is aware of differences of wavelengths of radiant energy. Saturation is the quality of sensation by which an observer is aware of different purities of any one dominant wavelength. Lightness is that attribute of visual sensation by which one surface is judged to reflect a greater or smaller proportion of the incident light than another.

The SEM cathodoluminescence micrographs used throughout this work, could never be considered as purely black-and-white but contained all shades of grey. Therefore, in preparing composite colour photographs, the ternary mixtures of the primaries resulting from such black-and-white pictures must be considered.

The ternary colours can best be shown in the following way. A 6-step grey scale (Fig.4.12a) was prepared and cut into an equilateral triangle having white as an apex and black along a base. Standard 24-step grey scales are commercially available from Kodak Limited. However, such 6-step scales are easily devised and give satisfactory results with minimal cost. The triangle was successively photographed between red, green and blue filters, having been rotated 120° between each exposure. The colour triangle produced by this method is shown in Fig. 4.12b, where the primary colours appear at the apices and the binary mixtures yellow, magenta (pinkish) and cyan (sky colour) can be observed in the centre of each corresponding side of the triangle. Ternary colour mixtures, including grey, are seen in the interior of the triangle. If the grey scale steps were increased (ie greater than 6) then a more extensive range of colours would have been produced (as shown by Yakowitz and Heinrich 1969). A triangle of this type is designed to control the relative quantities of red, green and blue falling on the film. Proper balance of colour is achieved when the addition of the three exposures on the black-and-white pictures yields a neutral grey on the colour picture, using a particular set of filters. This criterion was satisfied by obtaining a colour picture of the equilateral grey scale, adjusting the exposure time for each filter until the photograph showed a neutral grey in the middle, Fig. 4.12b. Changing the exposure time for a given filter changes the colour balance. Note, also that choosing a specific filter set defines an entire range of colours for a given film.

Fig. 4.12a A six-step triangular grey scale used for colour balance

Fig. 4.12b The range of ternary colours available with Kodak "Wratten" filters (25-red, 58-green and 47B-blue) and 35 mm colour film (Ektachrome EX-135). The primary colours appear at the apices and the binary mixtures yellow, magenta (pinkish) and cyan (sky colour) are observed in the centre of each corresponding side of the triangle



a



Fig 4.12b

The light source used was two 150W (240V), tungsten filament Mazda (Thorn Limited) "household" light bulbs. A set of Kodak 'Wratten' colour - separation filter numbers 25(red), 58(green) and 47B(deep blue) provided the most satisfactory results.

The intermix of colours obtained using this particular set of filters gave intrepretable as well as good quality colour, see Fig. 4.12b. The superimposed curves representing the wavelength versus transmission characteristics of the three primary filters are drawn in Fig. 4.13. Also for consistency, colours need to be defined more accurately than simply by analogy with familiar objects. To the human observer, colour can be considered as having three attributes which are hue, saturation and lightness. Colour specification data must also take into account the psychological reactions of the human observer. There have been many experiments, notably those of Wright (1928) and Guild (1931), which have tried to standardize human colour perception. The compilation of the various experimental data forms the basis of a recommendation by the International Commission of Illumination for a widely accepted standard psycho-physical system of colour specification. It has created a "standard" observer that will always give the same response to the same stimulus. This is known as the C.I.E. system (Commission Internationale de l'Eclairage). The C.I.E. has also defined three artificial light sources that are easy to reproduce and whose energy distributions are precisely known. They are known as standard illuminants A, B and C. Illuminant A is a gas-filled tungsten

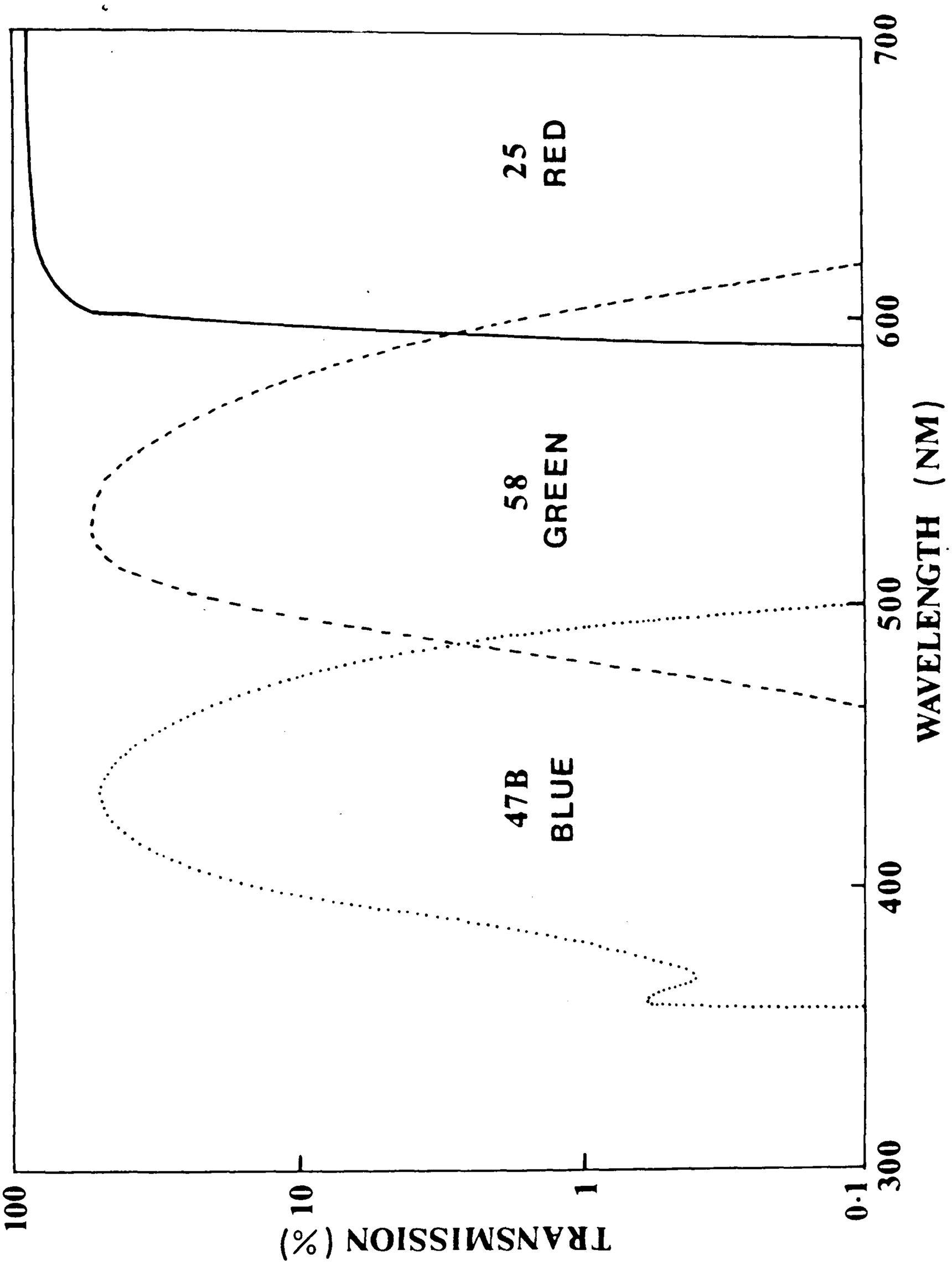


Fig. 4.13 Transmission curves for the Kodak "Wratten" filters

lamp operating at a colour temperature of 2854K, and its radiation is characteristic of an ordinary 150-watt incandescent lamp. Illuminants B and C consists of Illuminant A with appropriately defined filters. Illuminant B is similar to the direct light of the sun, while C is similar to an overcast sky or a mixture of sun and blue sky. Under ordinary conditions an observer in an environment illuminated by any of these standards will perceive as white (or grey) radiation whose spectral distribution is that of the illuminant. Furthermore the C.I.E. have agreed that the exact colour quality of a stimulus can be uniquely defined on a chromaticity diagram provided the illuminant is designated. Such a diagram is reproduced here for completeness and the chromaticity coordinates (x,y), as given by Kodak Limited, for the three filters are plotted in Fig. 4.14. Detailed derivation of this diagram is discussed by Murray (1952) and Sheppard (1968).

The Kodak 'Wratten' filters, series numbers 25, 58 and 47B, being the most suitable, were used to prepare all the illustrations given in this work (Figs. 4.16 and 4.18). Table 4 gives the exposure times for each filter when using Kodak Ektachrome - X (EX-135) colour film with ASA rating of 64. Originally, Polaroid colour film (type 48) was used but the expense made a change to 35 mm film desirable.

4.3.4 PREPARATION OF BLACK-AND-WHITE CATHODOLUMINESCENCE MICROGRAPHS

It has been suggested by Jones et al. (1966), Lennartz and

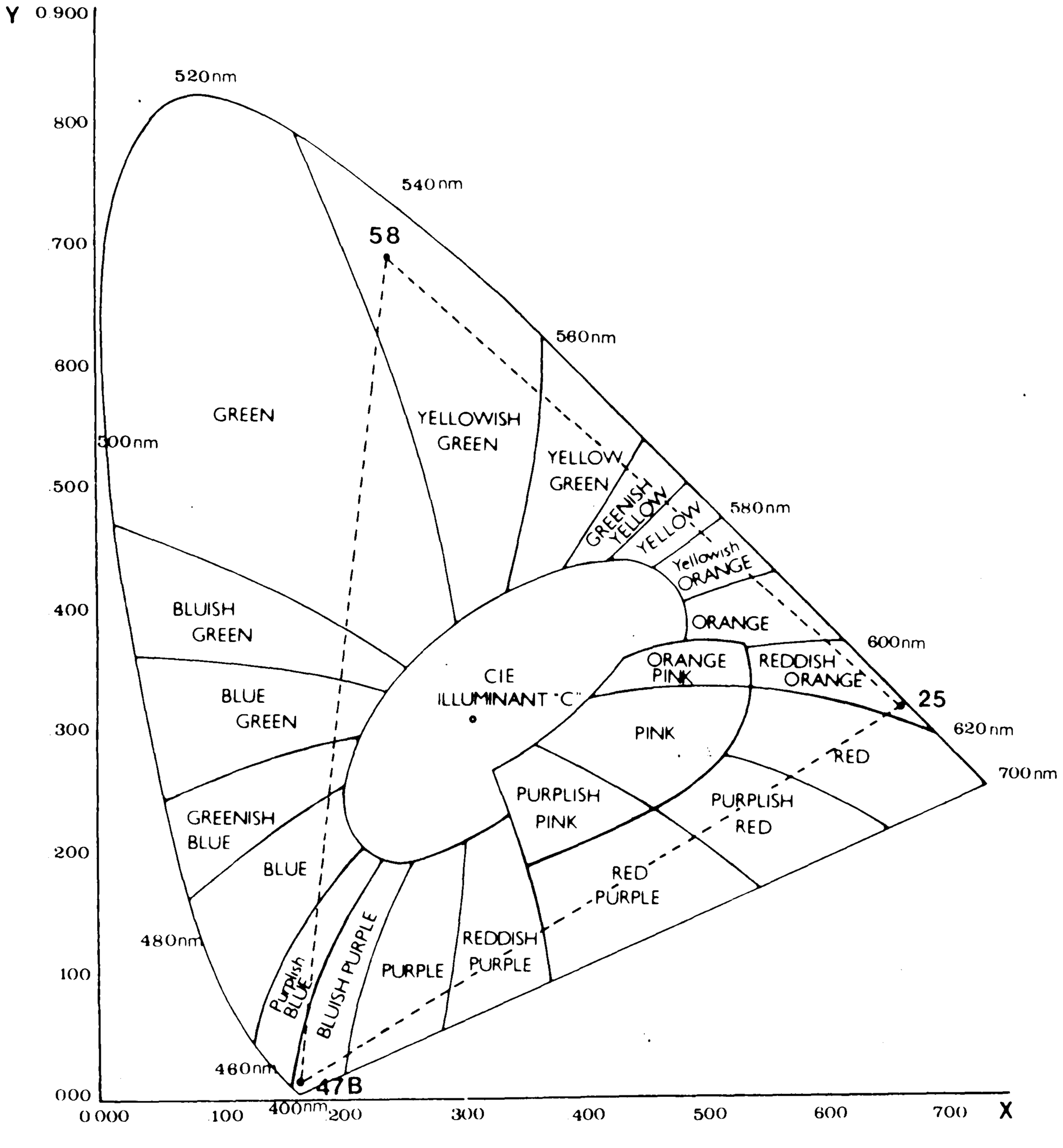


Fig. 4.14 A CIE (Commission Internationale de l'Eclairage) chromaticity diagram showing the coordinates of the three Kodak "Wratten" filters (dashed triangle)

TABLE 4 EXPOSURE TIMES FOR COLOUR COMPOSITES

KODAK WRATTEN FILTER SET NUMBER	COLOUR	EXPOSURE TIME (SEC)
25	Red	1/60
58	Green	1/4
47B	Blue	5/4
LIGHT SOURCE: Two 150-watt light bulbs placed 12 in. apart and 7.5 in. diagonally above the subject. Camera 7 in. above prints. Lens setting f5.6		

Laffolie (1967) and Goldstein and Yakowitz (1975), that electron micrographs in colour can be obtained in one of three ways. These are, (a) by using a conventional colour television display system, or (b) three individual signals are recorded sequentially, changing filters between exposures. Or (c) by preparing customary black-and-white scanning images and then using them as colour-separation positive prints, with appropriate filters, to make colour prints.

All illustrations given in this section were obtained by using method(c), since this required only a little modification of the available apparatus.

A typical set of black-and-white monochromatic (one wavelength) CL micrographs, as in Fig. 4.15c, d, e, were initially (ie using Mark 3 of the CL system as outlined in section 4.2.2) obtained by setting the monochromator (a Spex minimate in this case) at 430, 530 and 650 nm respectively. These wavelengths represent the peak at which the selected Kodak 'Wratten' filters, 47B (Blue), 58 (Green) and 25 (Red) have their respective maximum transmission values as given by Fig. 4.13.

In the latter CL arrangement (Mark 4, section 3.5 and section 4.2.2) the three separation filters were incorporated into the entrance slit of the monochromator. This set-up enabled a similar series of panchromatic (all wavelenghts) micrographs, interposed by the filters, to be recorded like those in Fig. 4.17b, c and d. They are in essence pseudo-monochromatic

because the colour filters have typical halfwidth values of about 100 nm (Fig. 4.13), thereby allowing a greater spread of wavelengths to pass through giving a micrograph of higher overall intensity. In other words, it is less selective in wavelength then those obtained via the monochromator. It must be said however, that the final colour picture using either method (Figs.4.16 and 4.18 respectively) gave equally satisfactory results although the pseudo-monochromatic micrographs were preferred.

Results have shown that the success of this technique depends upon a number of related factors.

(a) The quality of the black-and-white images must be of the highest photographic standards before these seperation - positives can be copied onto colour film via the filters.

(b) The characteristics of the light source, the film and the selected set of filters must be property balanced as detailed previously in section 4.3.3.

(c) Care should be taken that the specimen position with respect to the SEM scan does not change between exposures, due to electrostatic charges (see section 3.4.1) or mechanical displacements. Similar steps to prevent movement during colour copying were also necessary.

4.3.5 EXAMPLES OF ZnS COLOUR SYNTHESIS

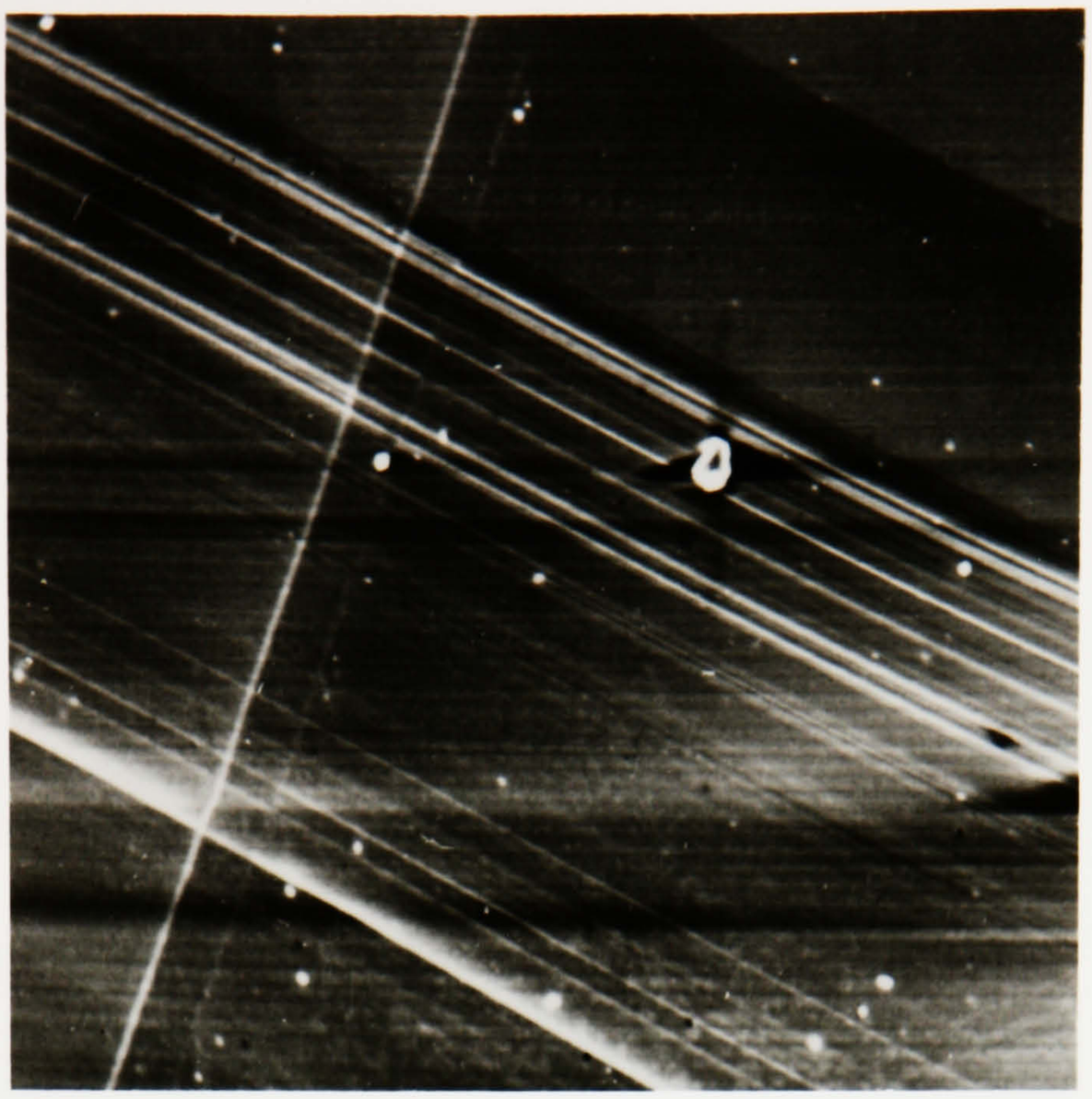
A striated platelet, ZnS - 350B, known to have good emission characteristics, was selected for the first colour synthesis

illustration (Fig. 4.16). Figure 4.15a, shows a secondary electron micrograph in which the choosen area was approximately 590 μm wide and Fig. 4.15b is the panchromatic (all wavelength) CL emission micrograph of the same area. The three monochromatic (one wavelength) black-and-white separation positives Fig. 4.15c, d, e, were obtained at 430, 530 and 650 nm respectively. They were printed using identical exposure times, otherwise the various emission intensities as well as any special features can be artificially altered in the printing process.

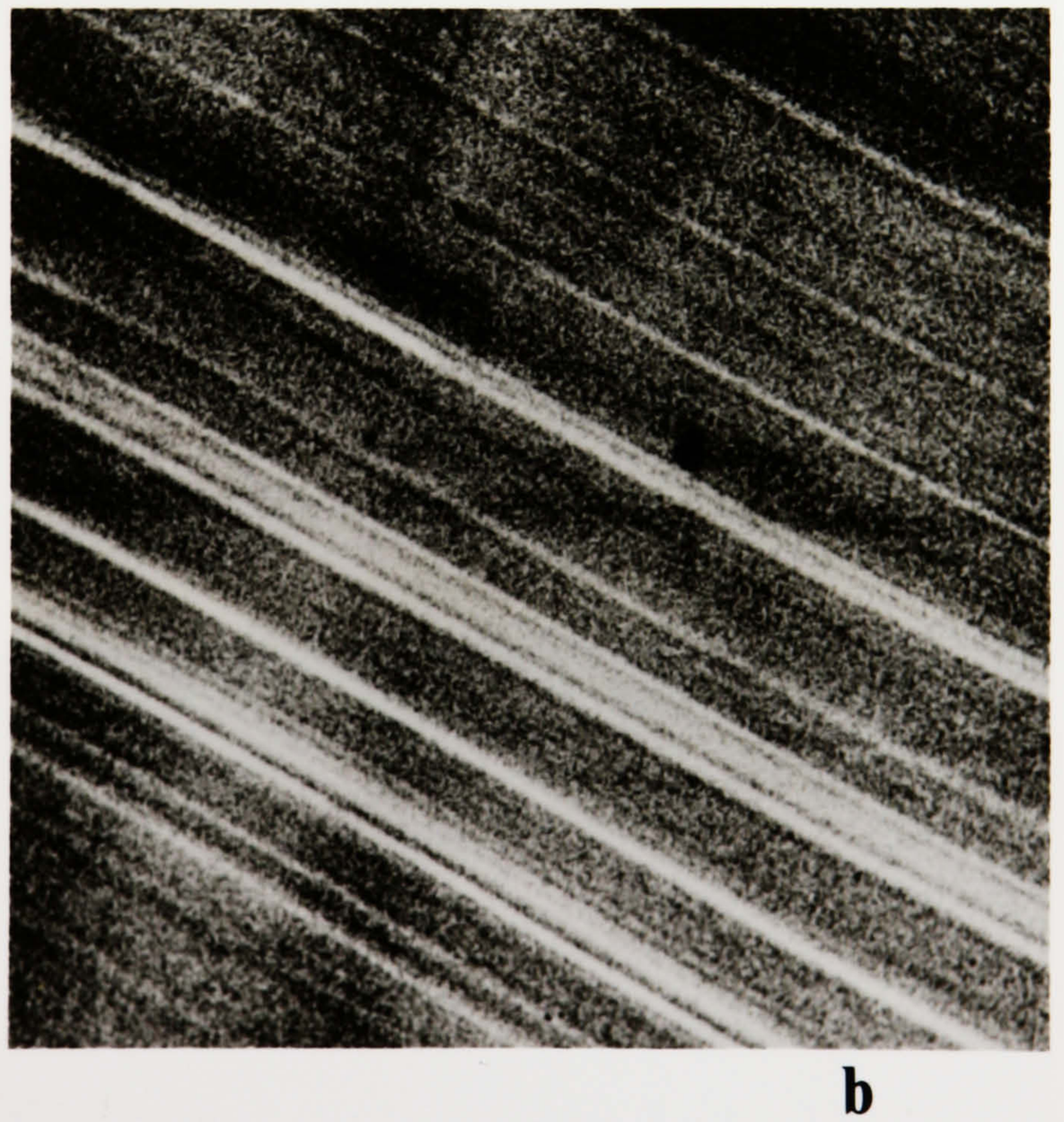
As discussed in section 4.2.3 page 129, care needs to be taken when interpretating SEM CL micrographs as they represent the raw photon count rate data picture. That is to say, it has not been corrected for the CL detector response factor (QEF), which is known to fall rather rapidly when going from the blue to the red ends of the visible spectrum (see section 3.6 page106 and particularly Fig. 3.8). A large contribution to this curve arises from the way in which the photomultiplier quantum efficiency Q(λ), varies with wavelength as shown in Fig. 3.7 page 108. For this reason, only uncorrected spectra will be presented because they correlate with the final colour composites.

The dust particle seen to the right of middle in the micrographs (Fig. 4.15) served as a convenient registration mark when copying Figs. 4.15c, d, e, with appropriate filters, to produce the final colour composite given in Fig. 4.16. The CL spectrum of the area is presented in Fig. 4.15f and shows

Fig. 4.15 SEM micrographs of a striated ZnS platelet (350B type II) with the common c-axis of the crystal running perpendicularly to the bright bands in (b). The crystal area represented by the micrographs is approximately 600 μm wide: (a) is a secondary electron micrograph showing topographic features, (b) is the panchromatic CL SEM micrograph from the same area, (c, d and e) are the three monochromatic separation positives recorded at 430, 530 and 650 nm respectively, (f) shows the uncorrected CL spectrum from this region. The peak at shorter wavelength is the blue-copper band whilst the other (longer wavelength) is due to the green-copper activation of ZnS.

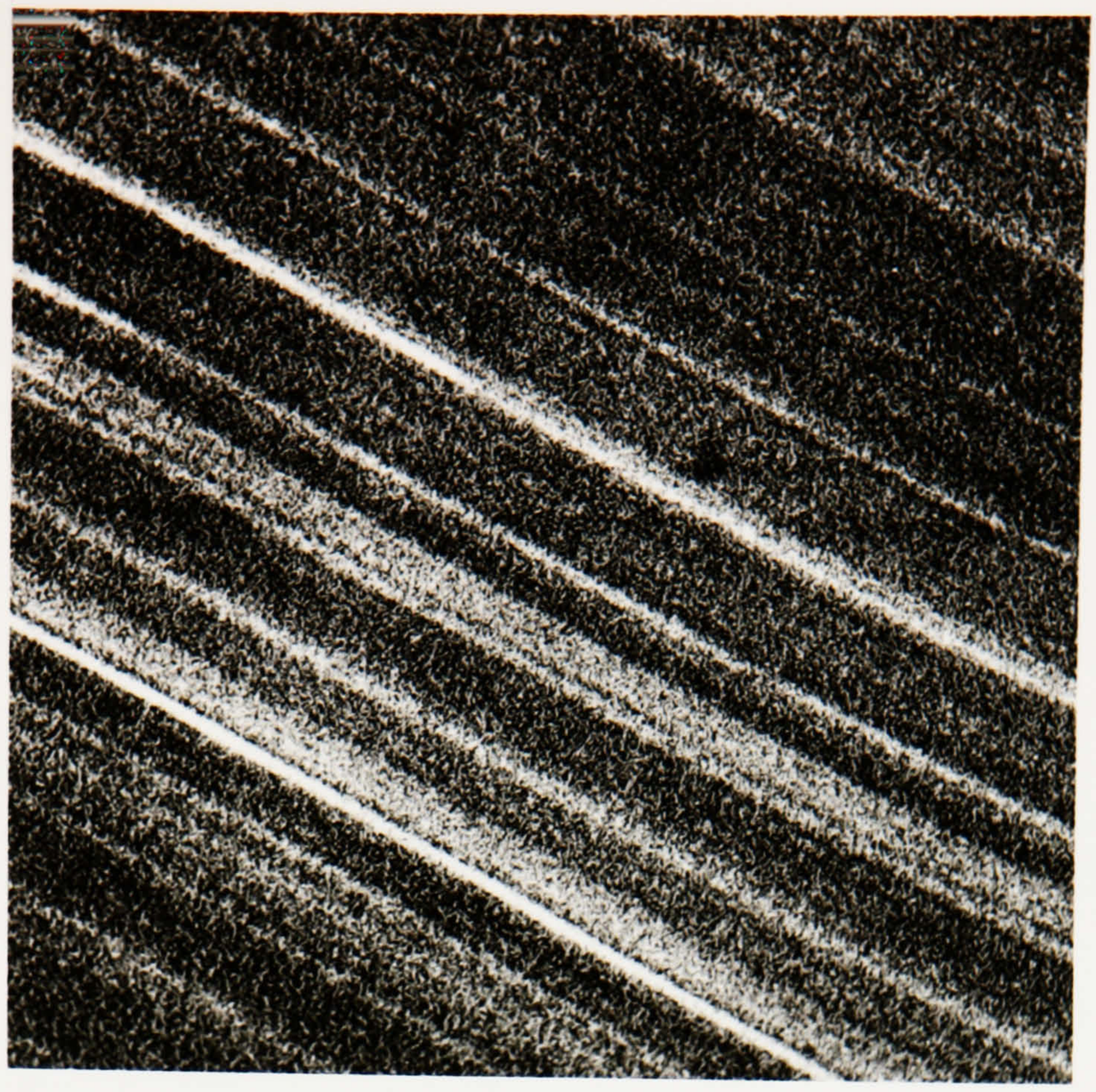


a

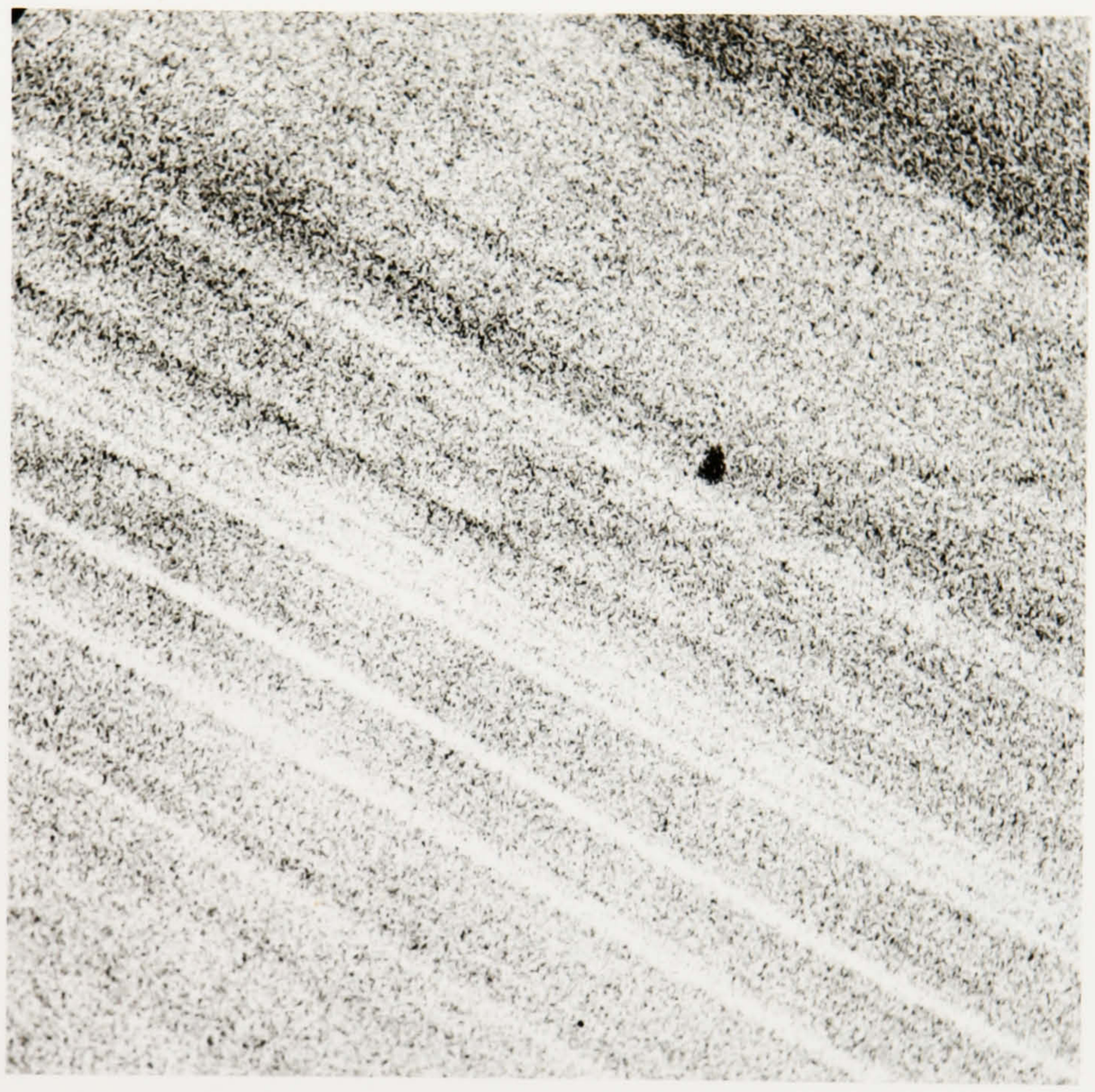


b

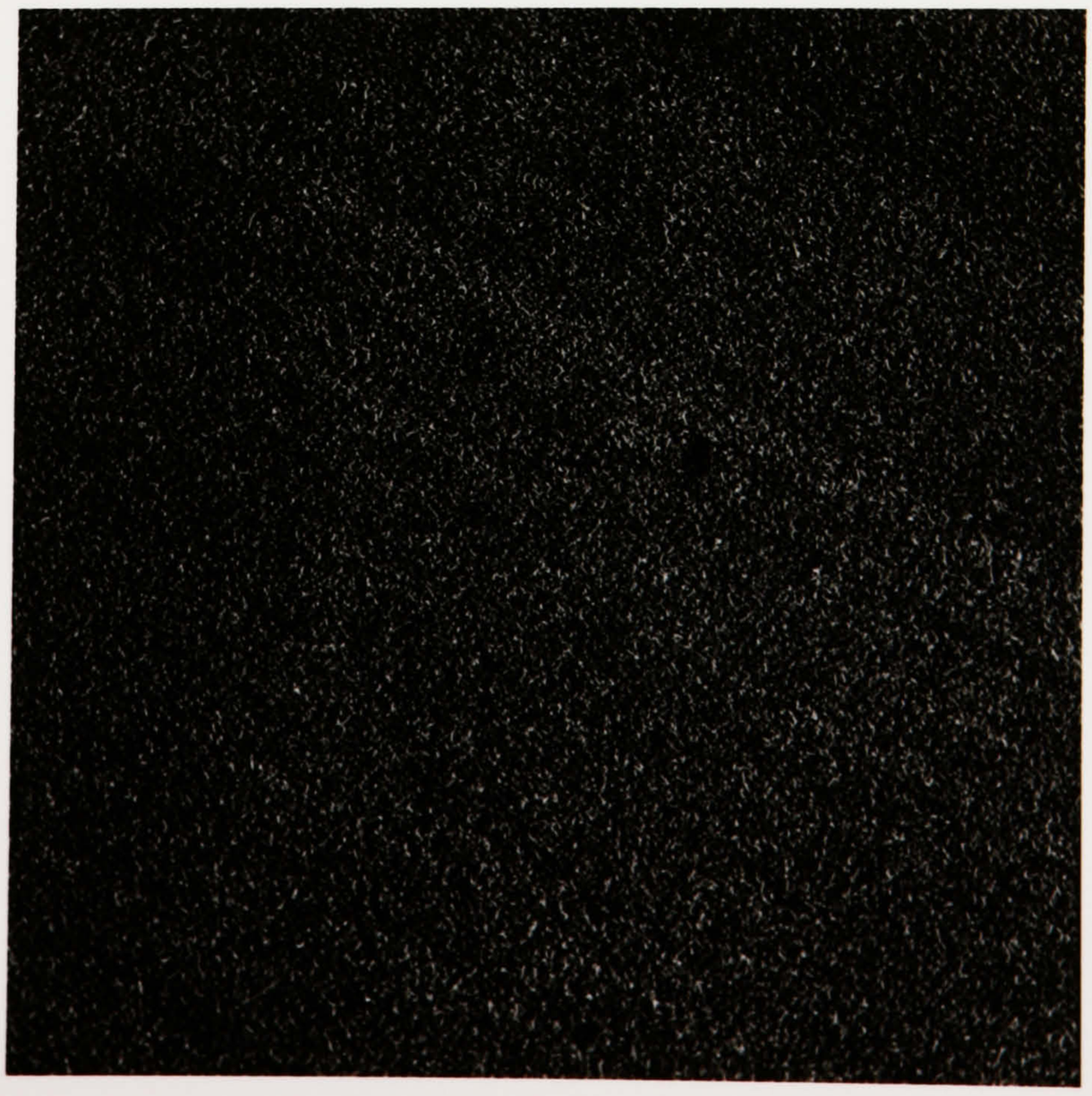
Fig 4.15



c



d



e

Fig 4.15

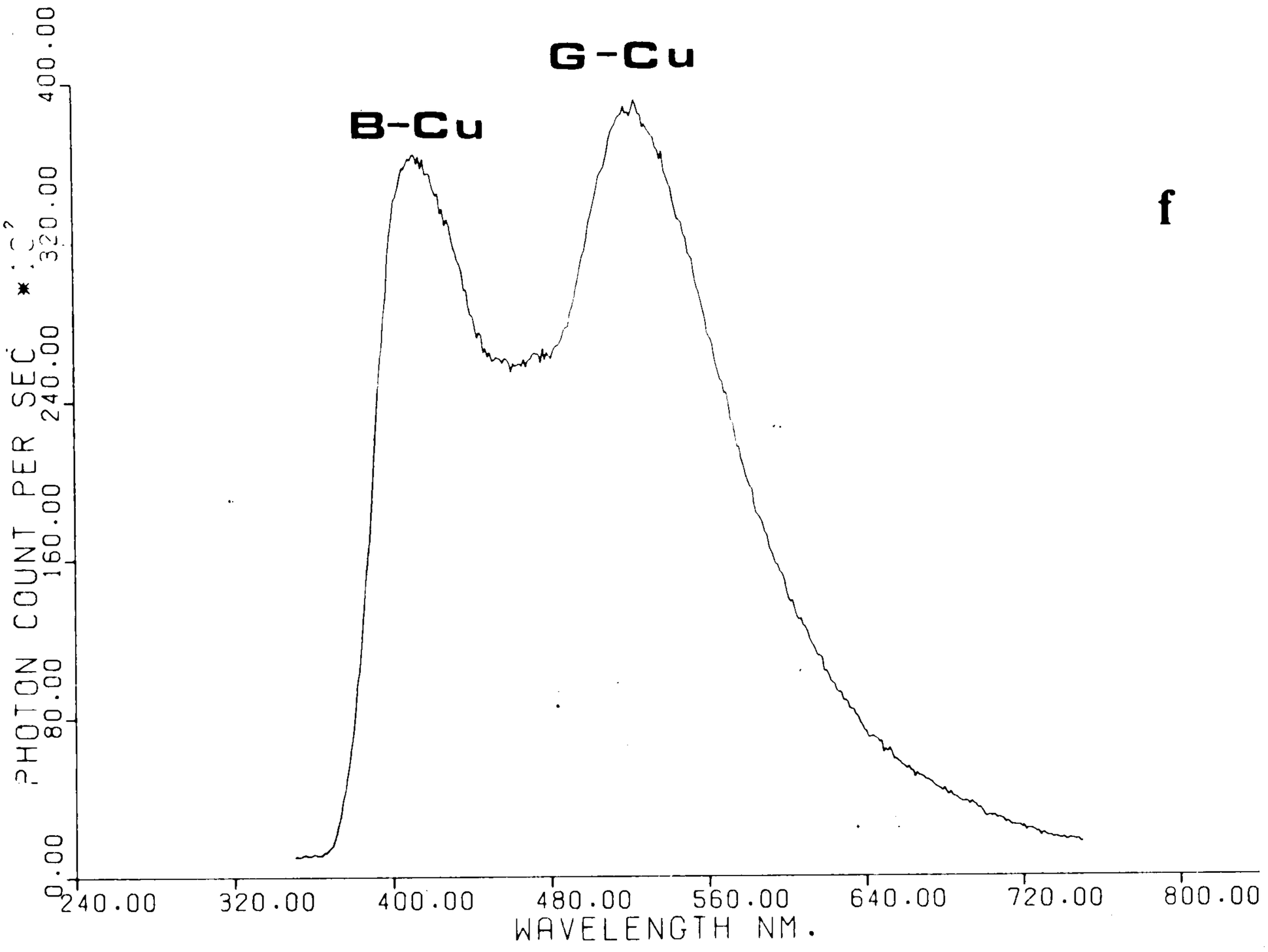

G-Cu
B-Cu
f
400.00
320.00
240.00
160.00
80.00
0.00
PHOTON COUNT PER SEC
240.00
320.00
400.00
480.00
560.00
640.00
720.00
800.00
WAVELENGTH NM.

Fig 4.15

two broad impurity bands well separated in wavelength. They have been identified in the manner already discussed in section 4.2.2 as arising from blue copper (412 nm) and green copper (521 nm) activation of ZnS. The colour print (Fig. 4.16) immediately highlights the prominence of certain features which would otherwise have required a careful appraisal of the remaining black-and-white SEM micrographs and the emission spectrum given in Fig. 4.15 (ie a, b, c, d and f).

The method of colour synthesis can be especially useful when dealing with ZnS platelets that show complex emission characteristics involving a number of different luminescent bands. One such typical example, Fig. 4.18 a and b, were obtained by transfering the three pseudo-monochromatic CL black-and-white separation-positives Figs. 4.17 b, c and d photographed originally via the blue, green and red Kodak filters respectively onto colour film using the same sequence of filters. Again, the three separation - positives were given identical exposures to ensure that each print (Fig. 4.17 b, c and d) was a true intensity representation of the observed uncorrected emission. A low magnification panchromatic CL micrograph of the specimen with the area of interest outlined is presented in Fig. 4.17a. The width of the crystal area investigated was approximately 1470 μ m. The first of the two colour micrographs shown in Fig 4.18a was taken with the exposure times listed in table 4 (ie that required for colour balance of the Kodak filters). Results show that in Fig. 4.18a the area to the bottom left-hand corner of the micrograph seems to emit more intensely than the surrounding regions. The original black-and-white

Fig. 4.16 The CL colour print obtained by sequentially copying the black-and-white micrographs shown in Fig. 4.15 c, d and e, through blue, green and red filters respectively. The filter exposure times are given in table 4.

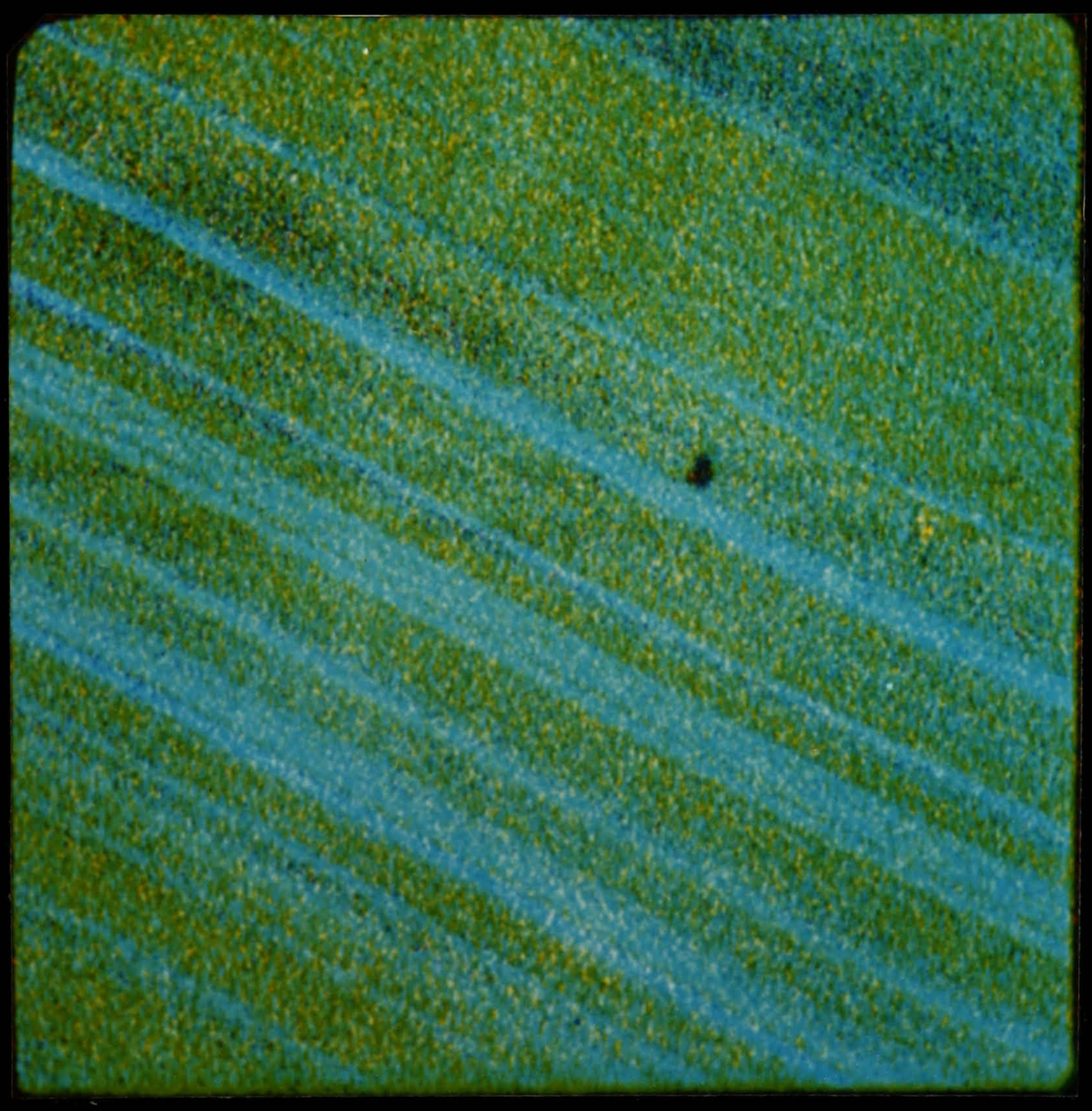
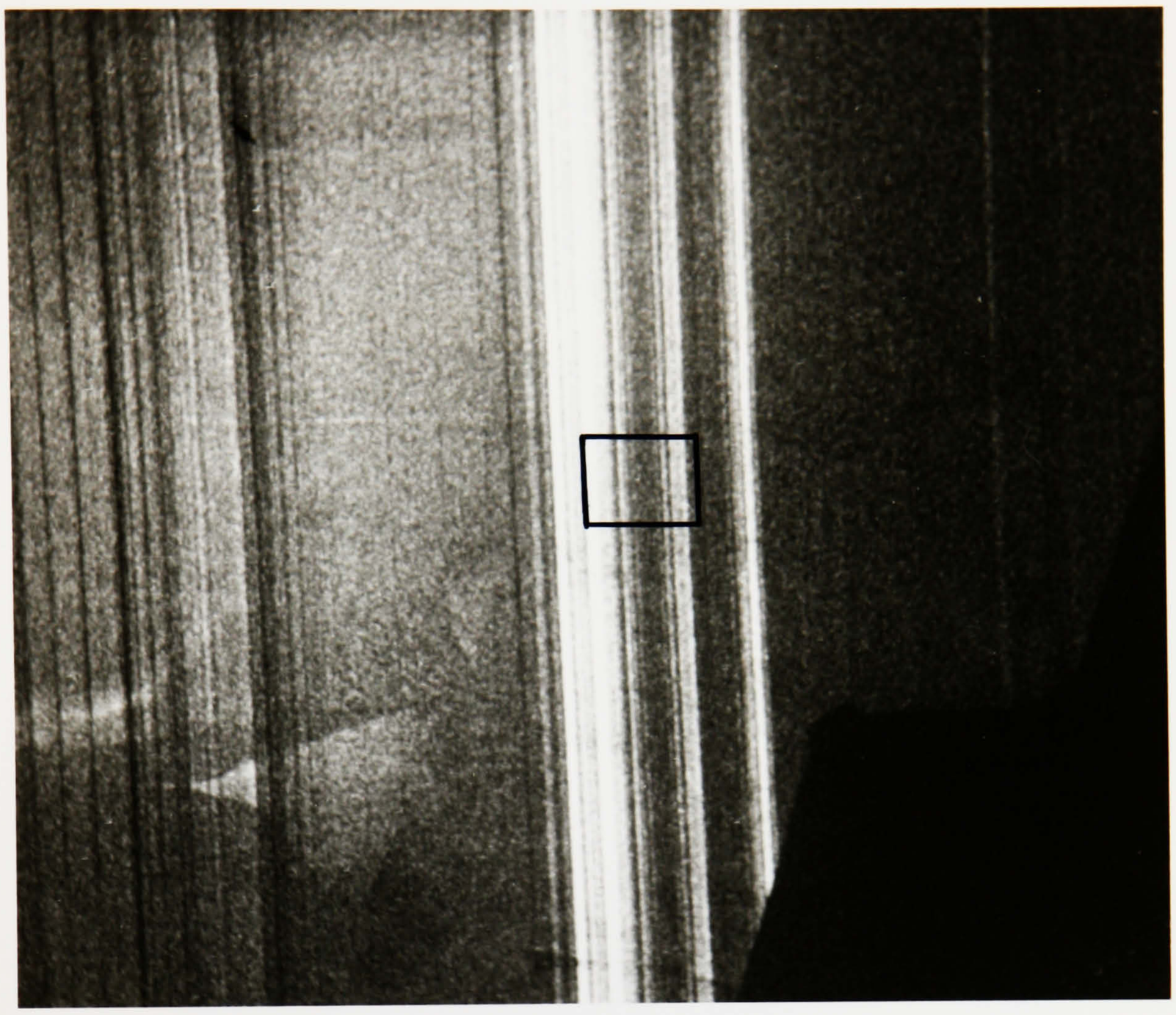


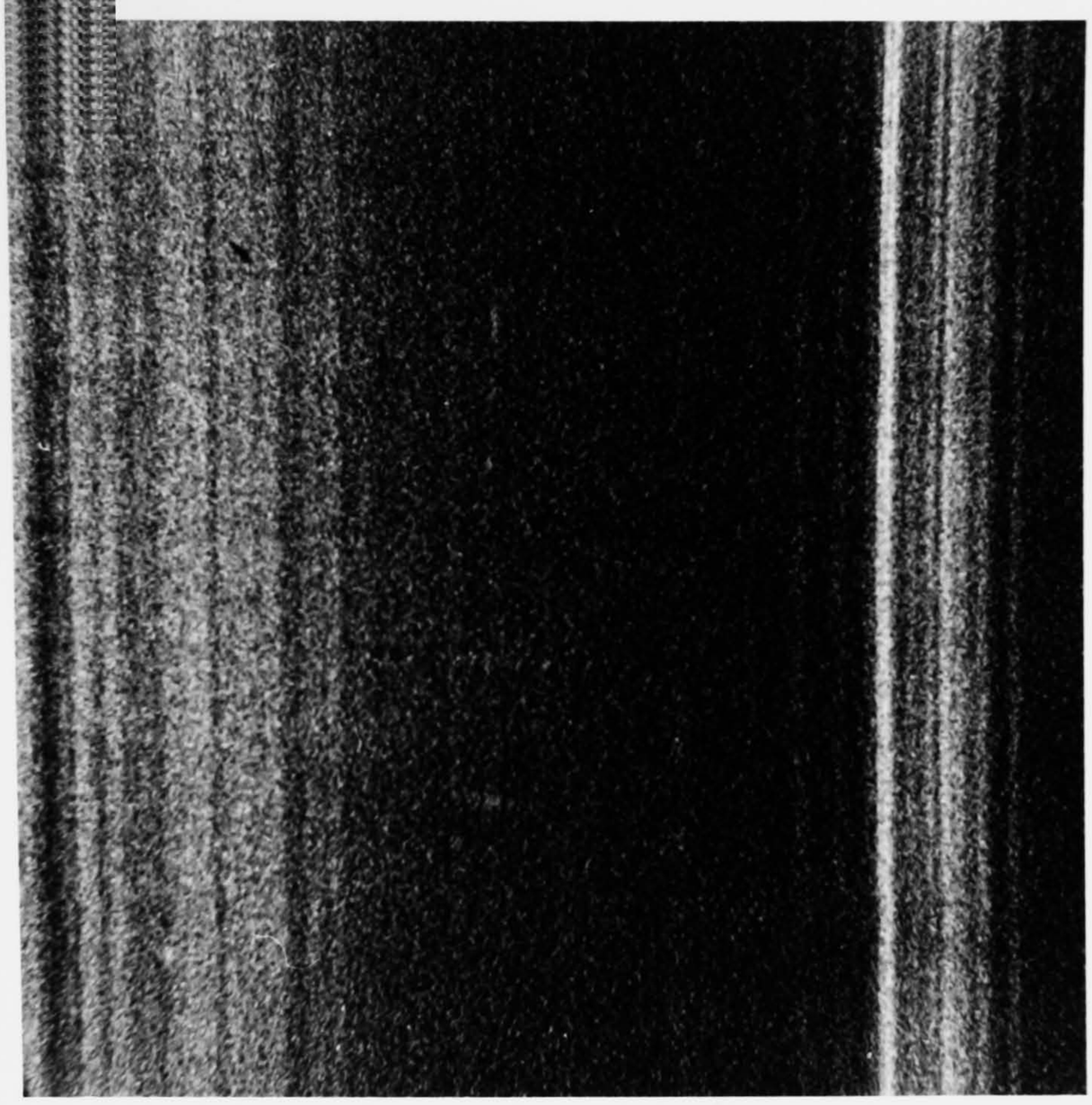
Fig 4.16

Fig. 4.17 CL micrographs of another ZnS platelet (No.347) with the common c-axis running horizontally (a) is a low magnification panchromatic micrograph of the whole crystal. The remaining CL micrographs are all of the area in the rectangle outlined in the centre of the platelet; (b, c and d) are the pseudo - monochromatic separation - positives recorded via the blue, green and red Kodak filters respectively and (e, f, g and h) give the emission spectra (uncorrected) from the various regions as marked in Fig. 4.18a. The area represented by the pseudo-monochromatic micrographs (b, c and d) is 588 μm wide.

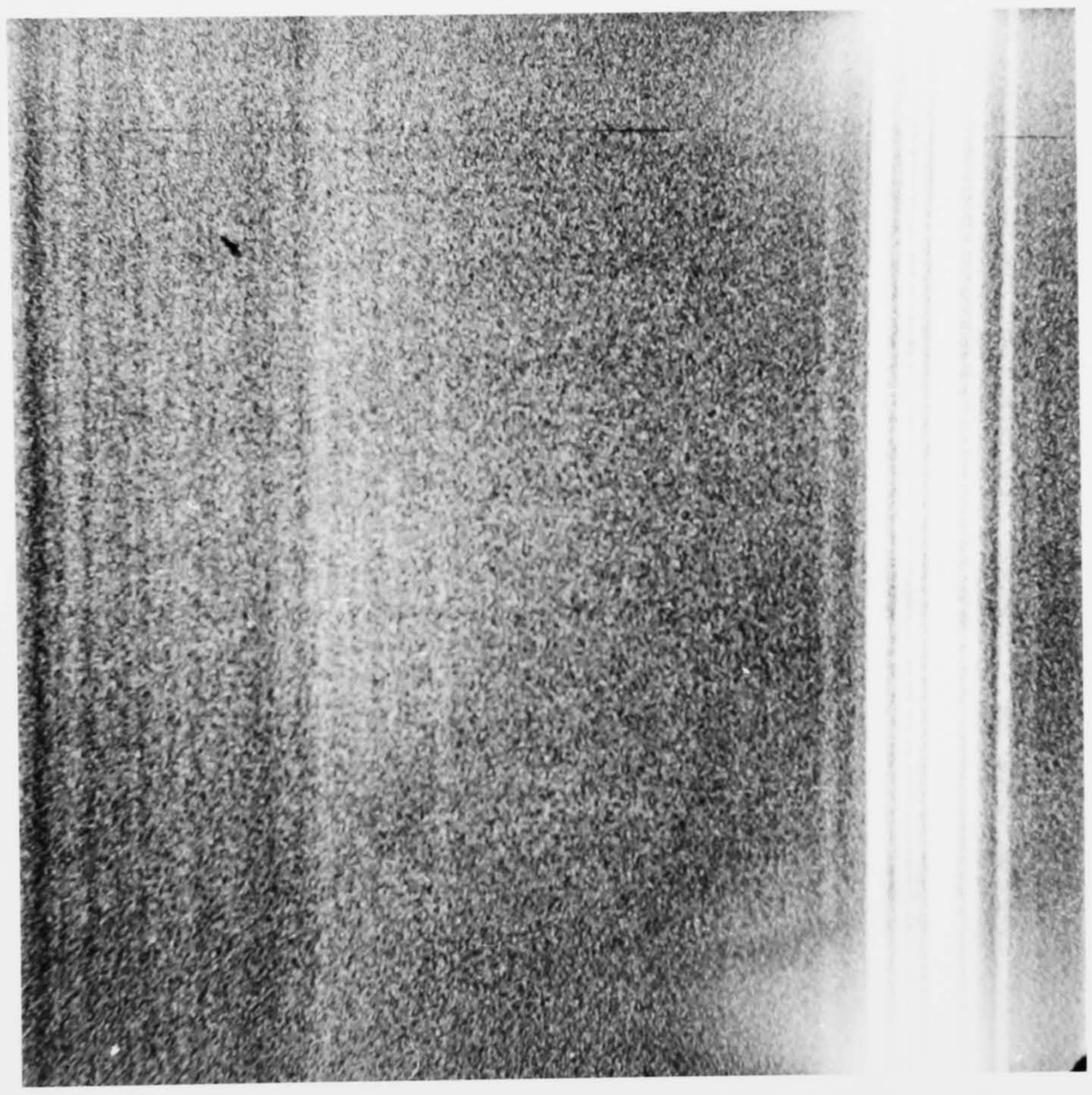


a

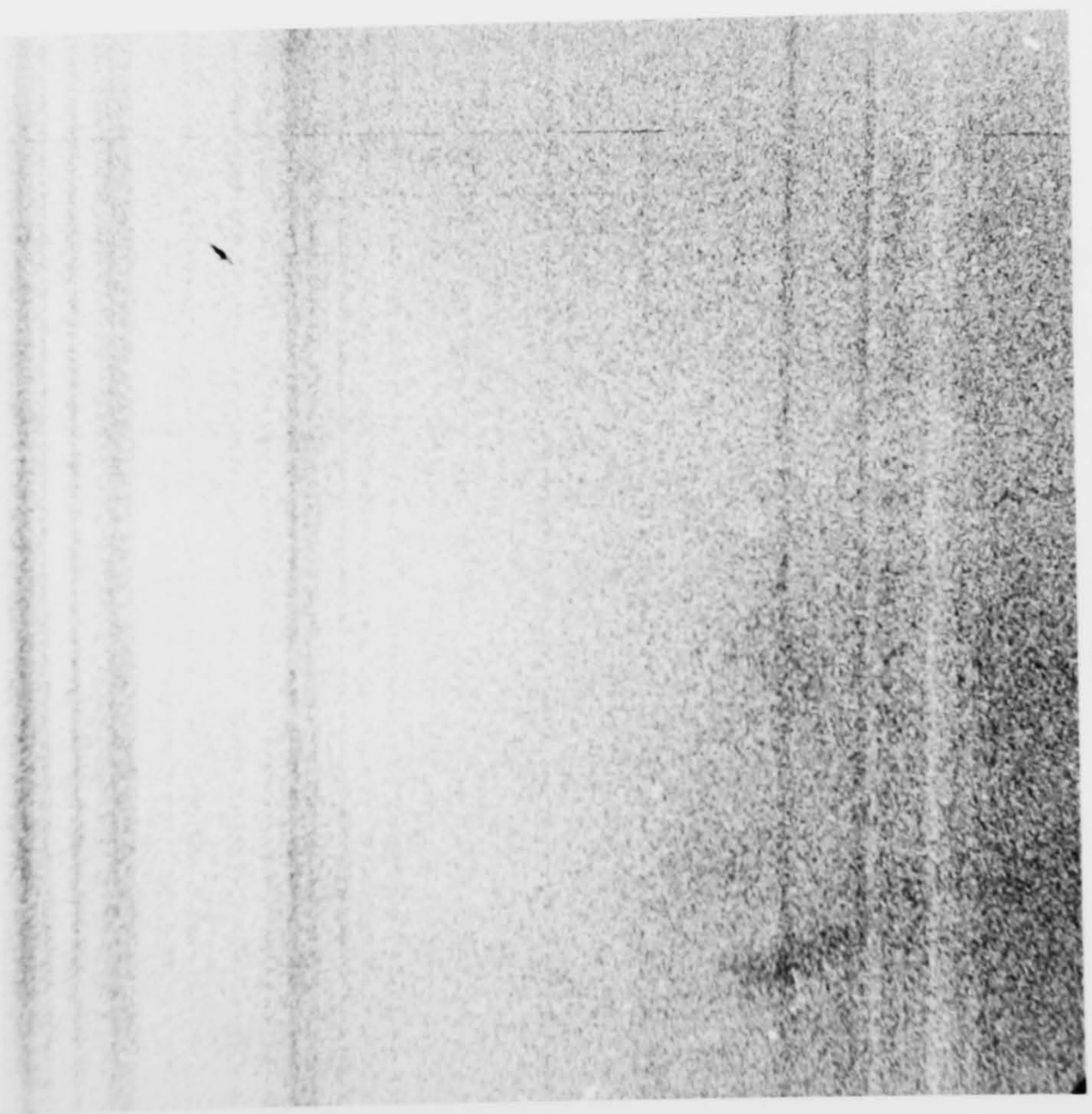
Fig 4.17



b

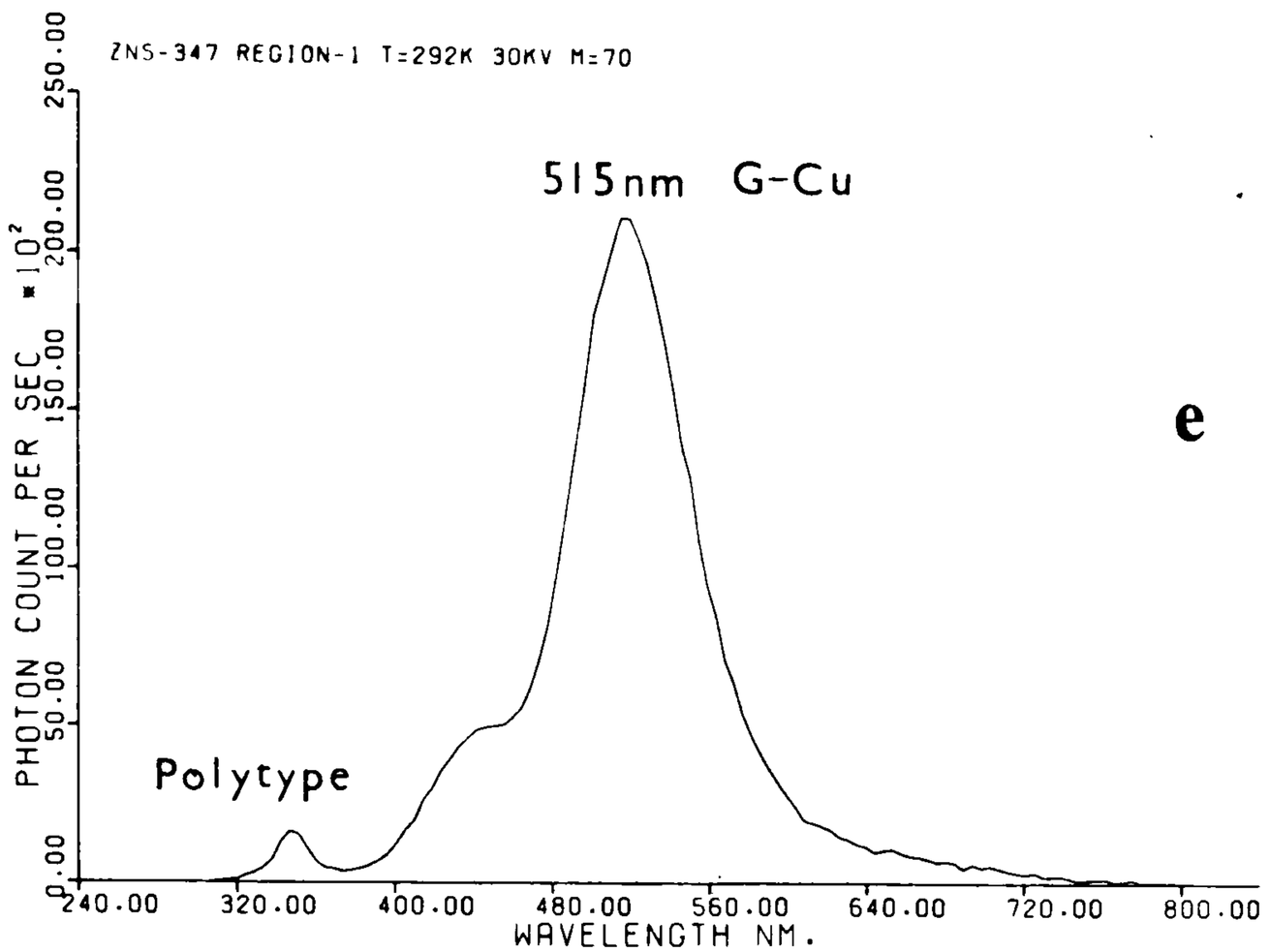


c

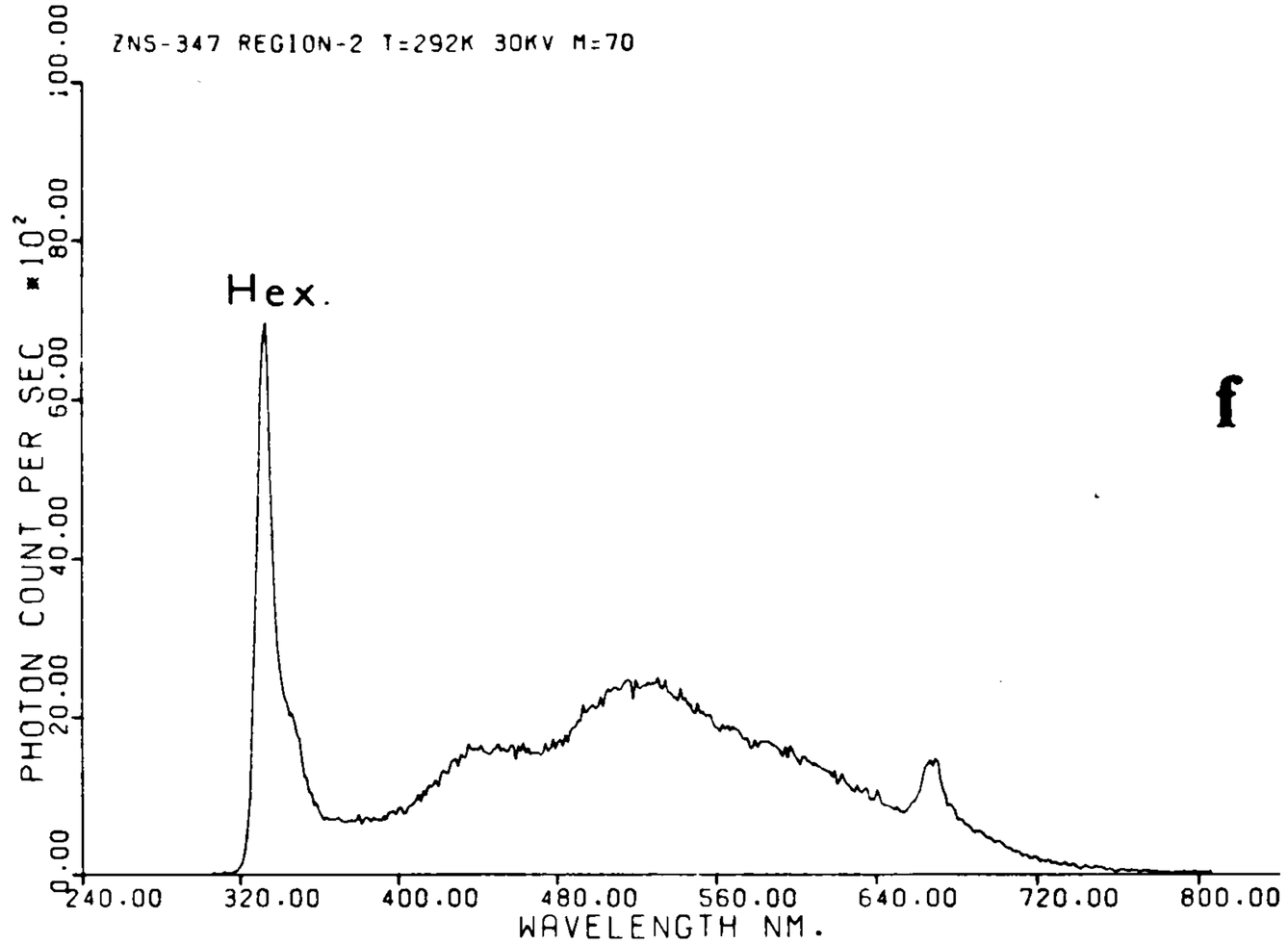


d

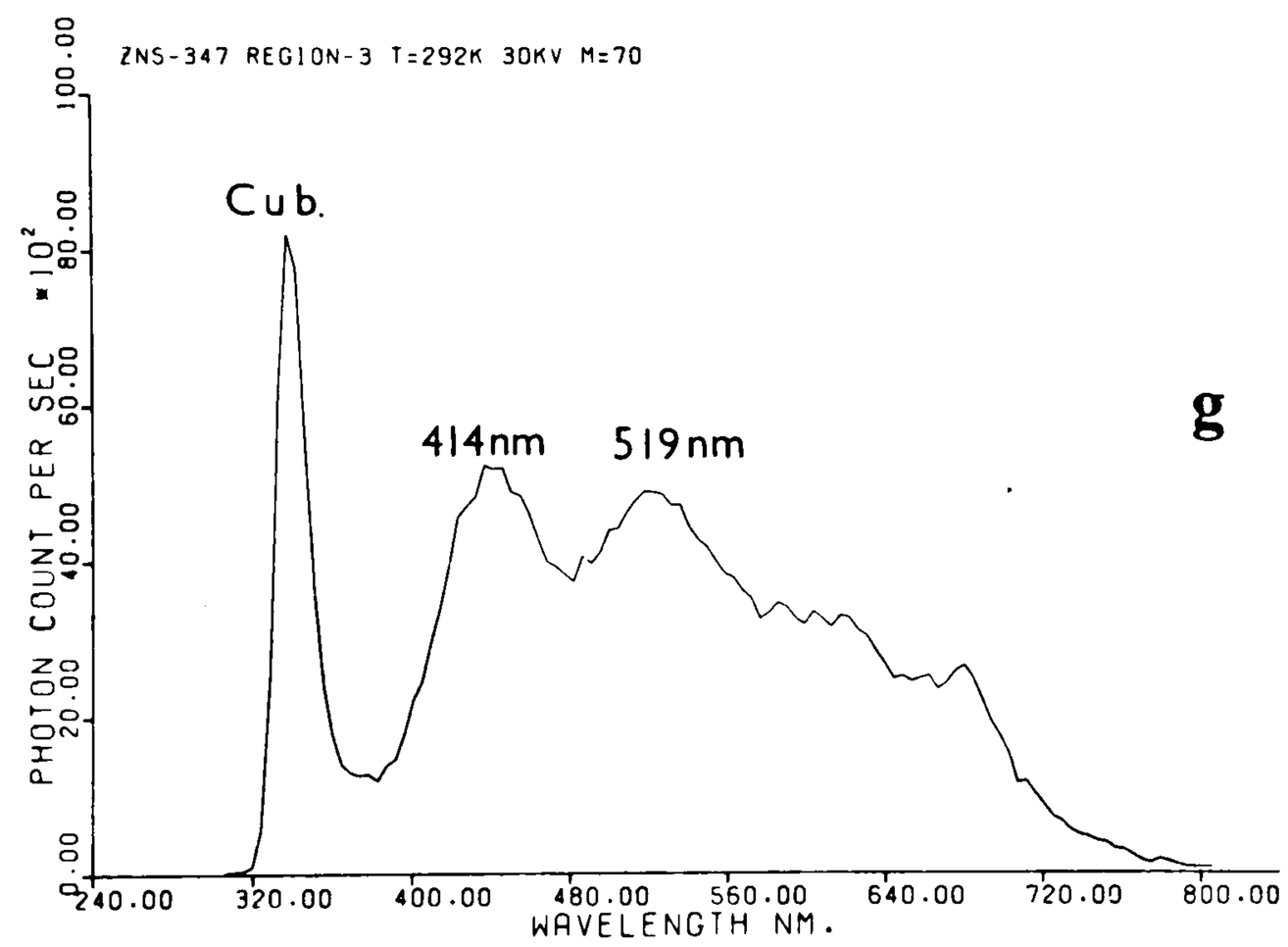
Fig 4.17


ZNS-347 REGION-1 T=292K 30KV M=70
515nm G-Cu
Polytype
PHOTON COUNT PER SEC *10²
WAVELENGTH NM.
0.00
50.00
100.00
150.00
200.00
250.00
240.00
320.00
400.00
480.00
560.00
640.00
720.00
800.00

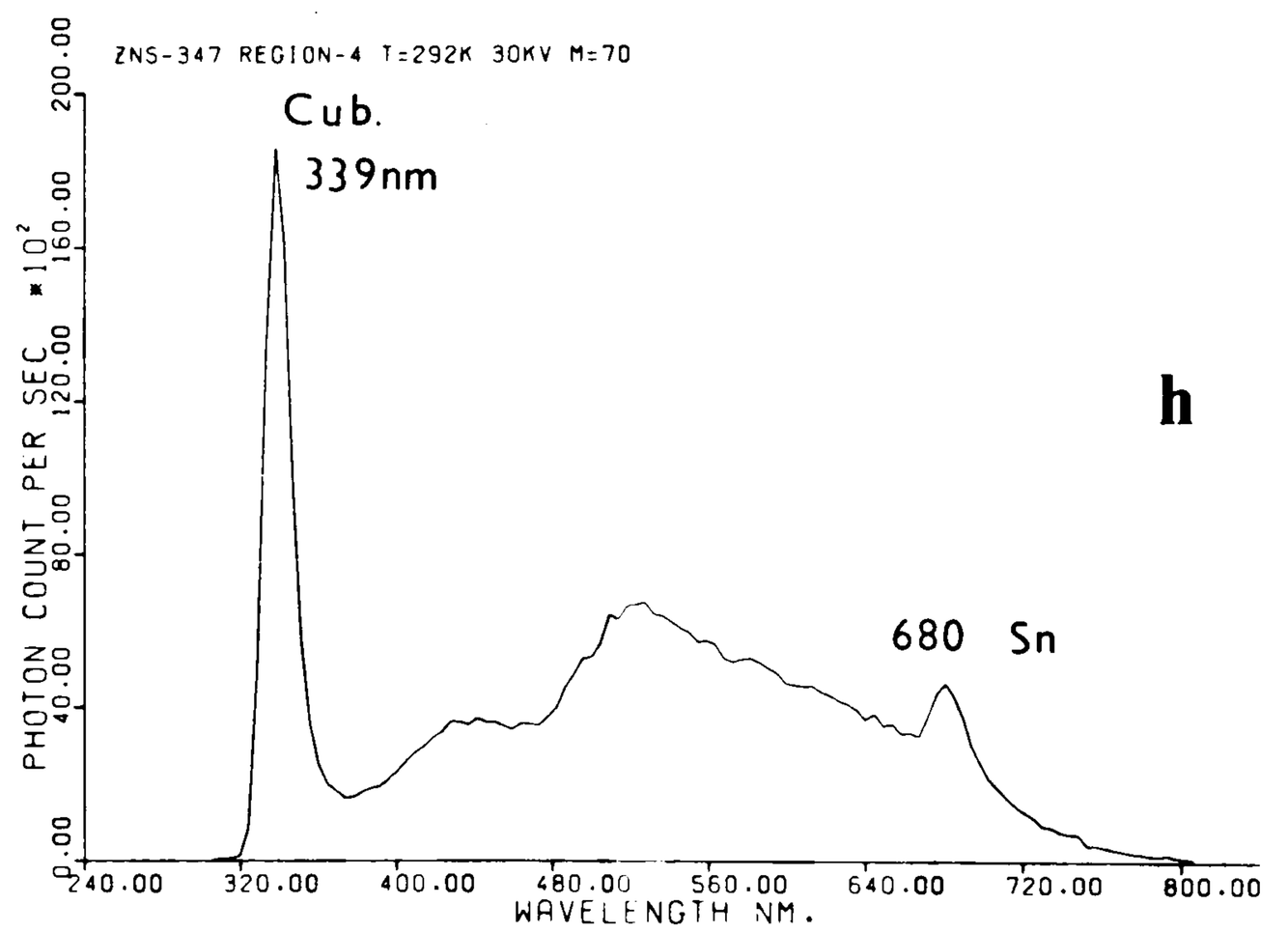
e


ZNS-347 REGION-2 T=292K 30KV M=70
Hex.
PHOTON COUNT PER SEC *10²
WAVELENGTH NM.
0.00
20.00
40.00
60.00
80.00
100.00
240.00
320.00
400.00
480.00
560.00
640.00
720.00
800.00

f


ZNS-347 REGION-3 T=292K 30KV M=70
Cub.
414nm
519nm
PHOTON COUNT PER SEC *10²
WAVELENGTH NM.
0.00
20.00
40.00
60.00
80.00
100.00
240.00
320.00
400.00
480.00
560.00
640.00
720.00
800.00

g


ZNS-347 REGION-4 T=292K 30KV M=70
Cub.
339nm
680 Sn
PHOTON COUNT PER SEC *10²
WAVELENGTH NM.
0.00
40.00
80.00
120.00
160.00
200.00
240.00
320.00
400.00
480.00
560.00
640.00
720.00
800.00

h

Fig 4.17

micrographs (Fig. 4.17 b, c and d) give no indication of this behaviour, however. It is believed that although the Kodak filters were matched for colour balance (section 4.3.3), the initial negatives from which these prints (Fig. 4.17b, c and d) were taken could have been of a poorer photographic quality (ie arising from incorrect contrast and brightness settings on the SEM photographic screen). The nature of this colour print can be considerably improved upon by altering the filter exposure times from those given in table 4. Figure 4.18b is an example of this where the blue, green and red exposure times were 5/4, 1/4 and 1/30 sec respectively (cf table 4). Although Fig. 4.18b gives a better description of the crystal luminescence it is however, incorrect in colour composition.

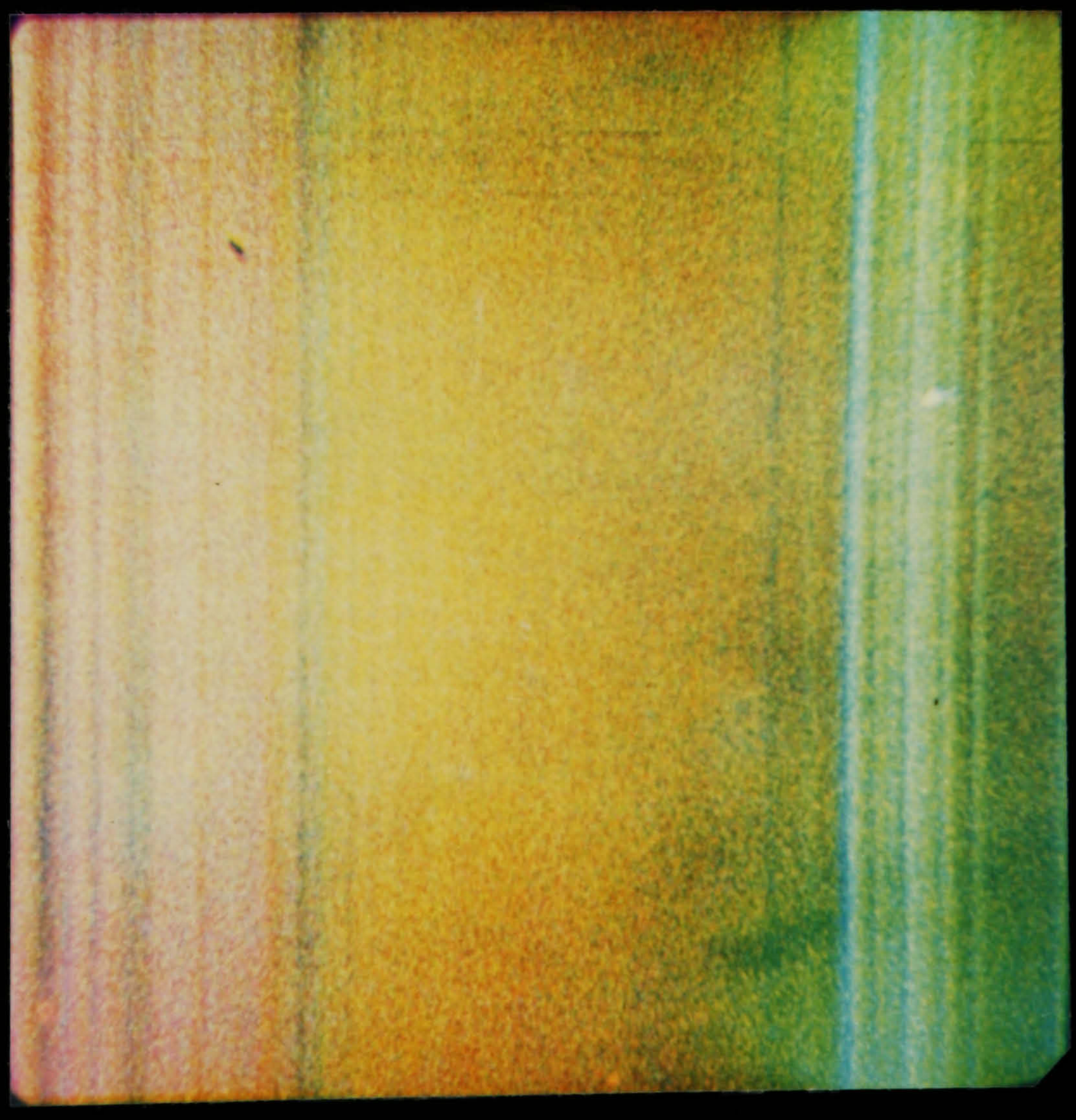
Emission spectra (uncorrected) from the various regions (as marked in Fig.4.18a) of this ZnS platelet are reproduced in Figs. 4.17 e, f, g and h and clearly show that a number of different impurities, in varying proportions, are involved in the observed luminescence. Wherever possible, the peak wavelength of each emission band and its probable origin is indicated on the spectrum. Since a quartz fibre bundle light guide was available during this work (Mark 4 of the CL system, see section 4.2.2), the luminescence band at the lowest wavelength in each case was the intrinsic or edge emission band. This is the recombination emission due to conduction band to valence band transitions in the crystal. By comparing the edge peak (E_p) wavelength values with those given earlier

Fig. 4.18 The CL colour micrographs obtained by using the pseudo-monochromatic separation - positives shown in Figs. 4.17 b, c and d.

(a) was acquired using the filter exposure times given in table 4, and in (b) the exposure times were blue (5/4 sec), green (1/4 sec) and red (1/30 sec) respectively.



a



b

Fig 4.18

in table 2 section 4.2.3 page 130, the four crystal regions were identified as being, region 1 - a polytype, region 2 - hexagonal (2H) and region 3 and 4 - cubic (3C) structures respectively. In the case of Figs. 4.17 e, f, g and h, successive spectral points were obtained every 4.5 nm with a monochromator bandwidth of 10 nm and a fast stepper motor speed. Such settings are only suitable for qualitative work because the spectra obtained have many sharp edges.

The final colour composite (Fig. 4.18a) correlates fairly accurately with the observed regional emission spectra (ie those of Figs. 4.17 e, f, g and h). Once again the colour synthesis gives an instant visual assessment of the luminescence complexity encountered in this specimen, which would otherwise have required careful analysis of a number of black-and-white monochromatic CL micrographs as well as related spectra, to obtain the same amount of information.

Note, that due to the process of colour printing Figs. 4.12b, 4.16 and 4.18a, b have all lost some colour brilliance which is regrettably unavoidable.

4.3.6 SUMMARY

In conclusion, the method of colour synthesis can be used successfully to present SEM CL data in a conveniently compact as well as meaningful manner. The cost of preparing colour composities routinely is minimal and requires little previous

experience once the choosen filter set has been properly matched for colour response. The importance of good quality black-and-white positives and their subsequent alignment during colour copying must again be emphasized otherwise the final colour picture can be a little deceptive (c.f. Figs. 4.18a and b).

Finally the results presented in sections 4.2 and 4.3 suggest that the only way to arrive at a reliable interpretation is to obtain the corrected "absolute" CL emission spectrum and interpret the information it contains as a preliminary to the recording for analytical purposes of any CL micrographs. An iterative procedure may in some cases be necessary, using the first micrographs to select significant areas for spectral "point or scanned area" analysis followed by the recording of further micrographs.

4.4 CATHODOLUMINESCENCE EDGE EMISSION BAND SHAPE ANALYSIS

4.4.1 SYNOPSIS

In this section the form of the cathodoluminescence edge emission (conduction band to valence band recombination emission) or fundamental band has been investigated between liquid nitrogen and room temperature. It is found that the intensity of the edge emission can be expressed semiempirically

as: $$L(E) = L(E_o) \quad \exp \left[g(E-E_o)^{\beta} \right],$$

where g and β are shape parameters, L is the intensity, E the photon energy and E_o is the photon energy at the maximum of the band. The temperature dependence of the edge band in hexagonal CdS and both the hexagonal and cubic structures of ZnS have been measured. Results have indicated that around the band maximum $\beta = 2$, ie the shape is Gaussian. However, for the low energy region of the band $\beta = 1$, ie the shape becomes exponential and the Urbach tail is obtained. In addition the high energy tail of the edge emission band is also exponential. Such low energy exponential tails have been reported for the absorption edge of CdS and ZnS and in a wide variety of other semiconductors and insulators and also in the edge emission band of GaAs. The interpretation of these results is discussed in relation to the Dow and Redfield (1972) internal electric microfield model for exponential edges (section 2.7.4).

4.4.2 RESULTS AND ANALYSIS

Typical, corrected, edge CL spectra of hexagonal CdS and of both hexagonal and cubic ZnS at 78K and at 292K are given in Figs. 4.19, 4.20, 4.21 respectively. The spectra show intensity enhancement with a decrease in temperature in each case and this it is believed results from the temperature variation of the radiative lifetimes, an effect which has

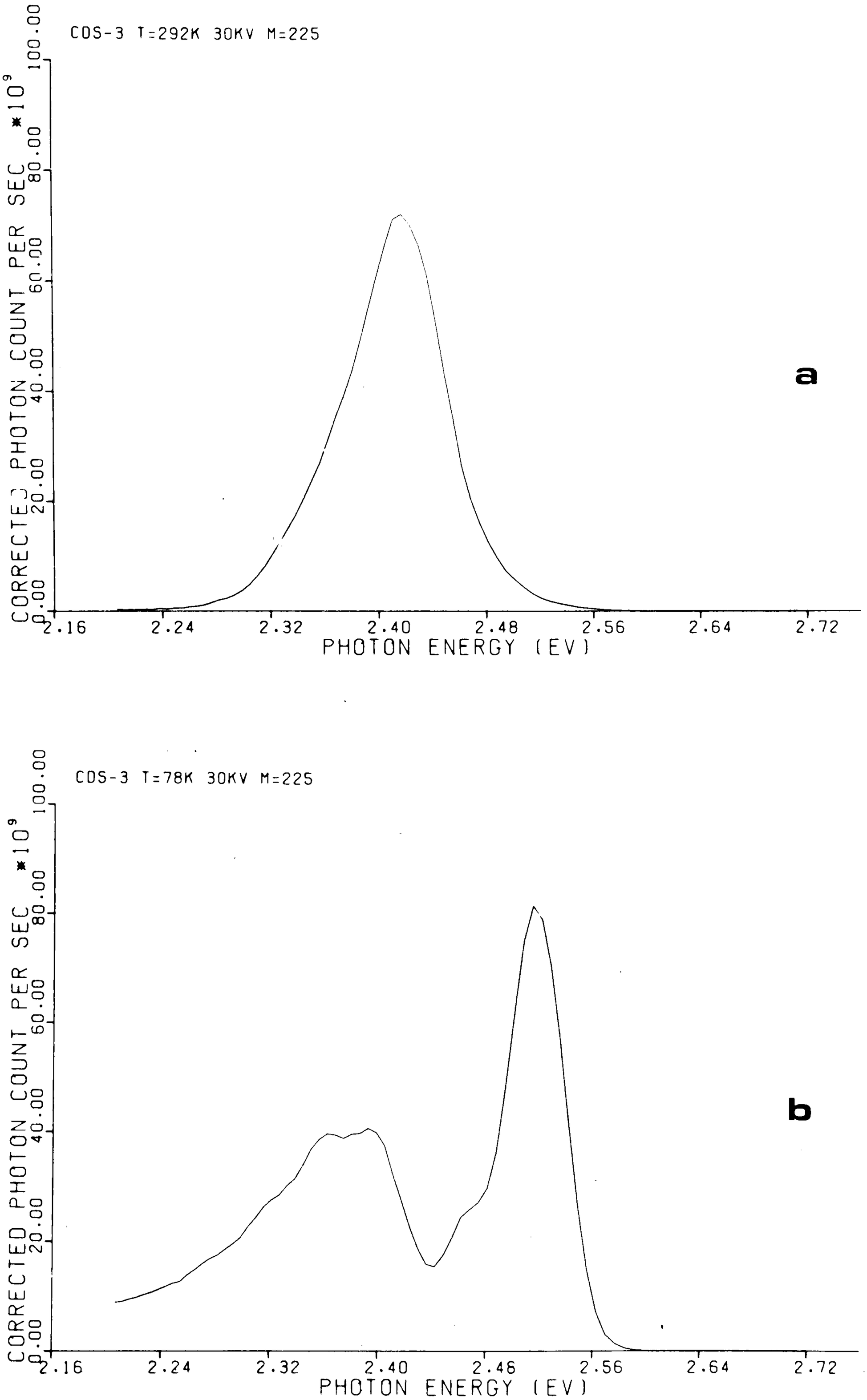


Fig. 4.19

Cathodoluminescence edge emission bands of hexagonal structure CdS crystal (a) at 292K and (b) at 78K.

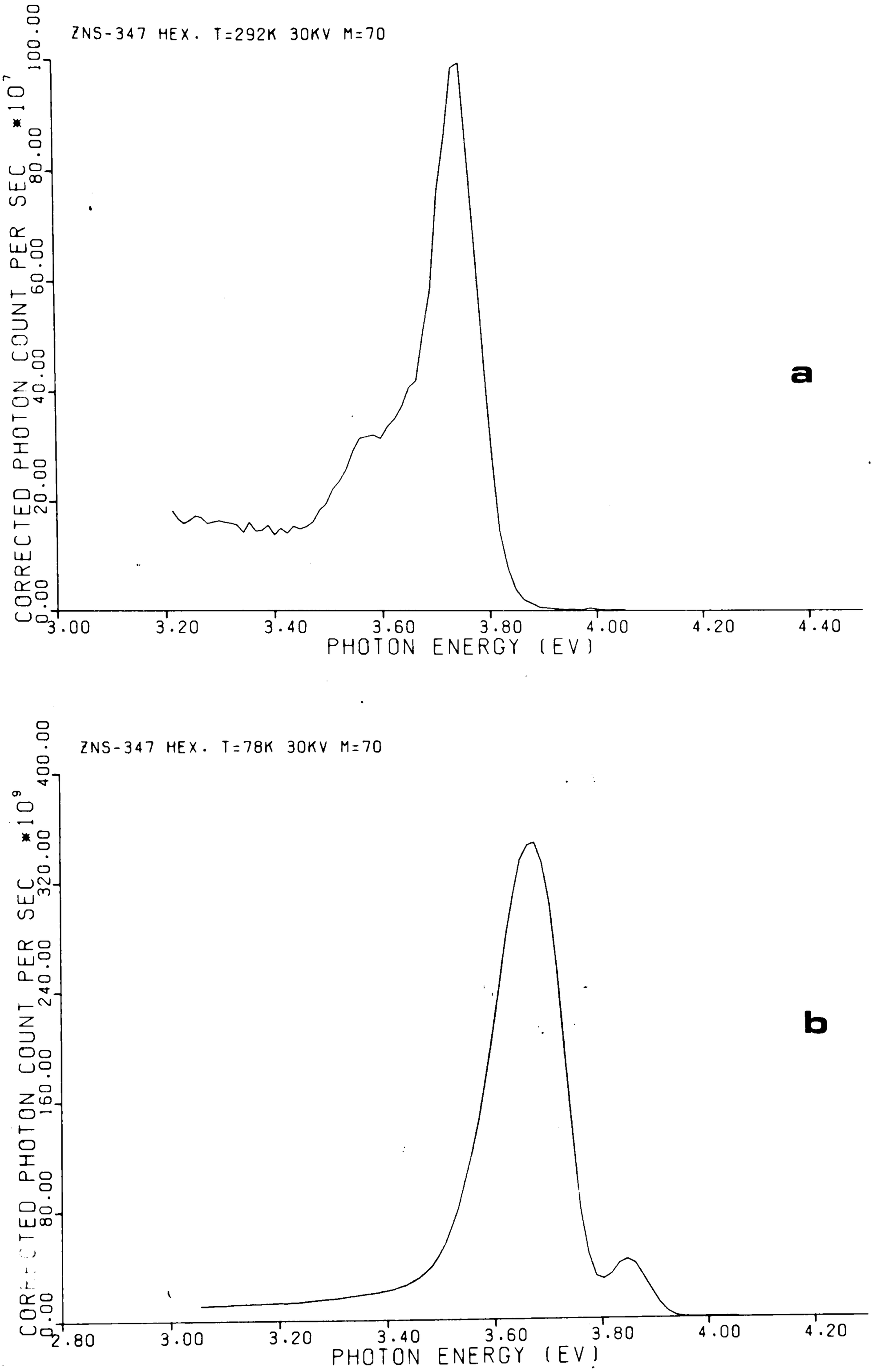


Fig. 4.20

Cathodoluminescence edge emission bands of hexagonal structure ZnS (a) at 292K and (b) 78K.

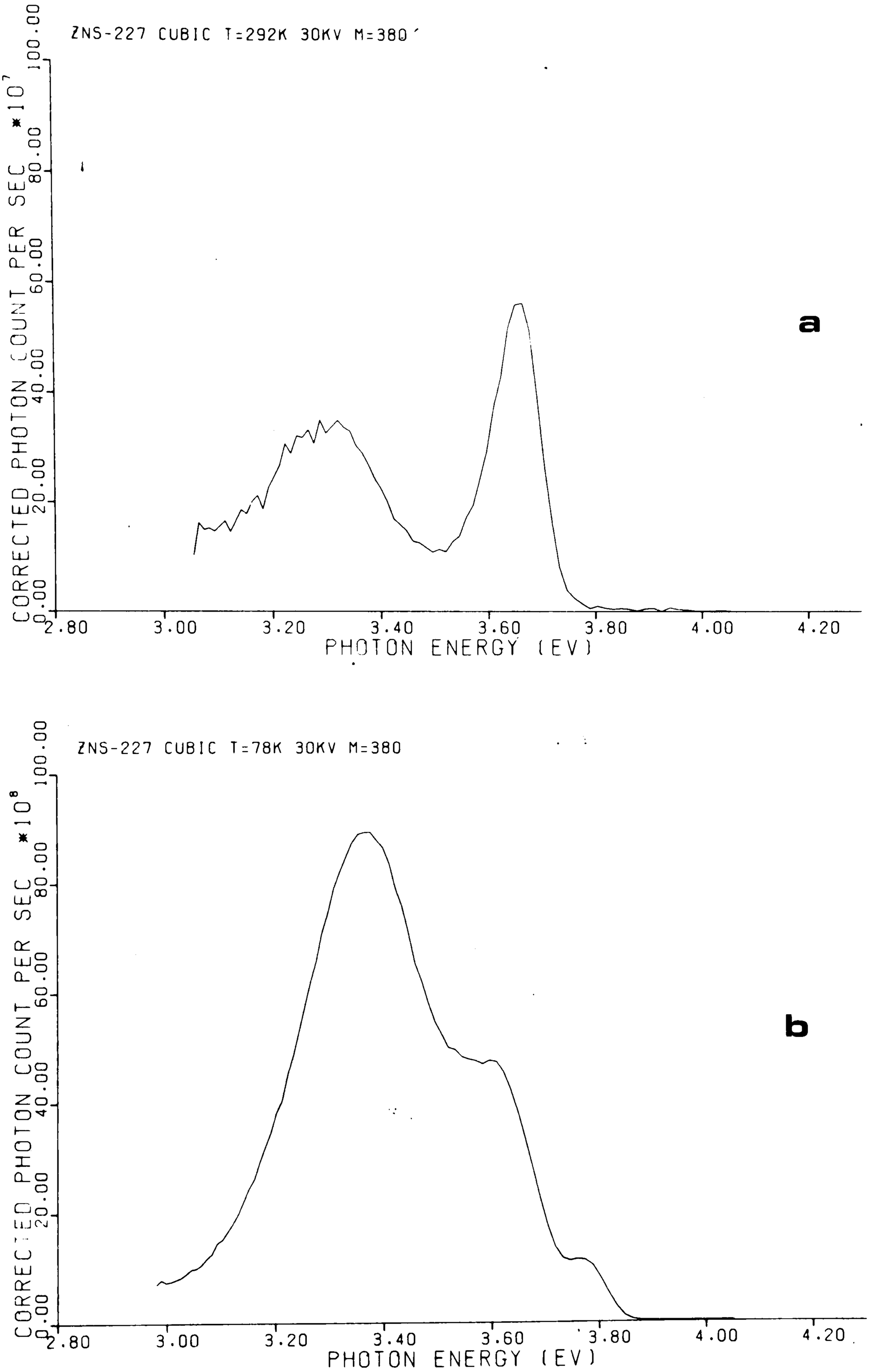


Fig. 4.21

Cathodoluminescence edge emission bands of cubic structure ZnS (a) at 292K and (b) at 78K

recently been discussed for direct gap materials by Jones et al. (1974).

Section 2.7.1 page 61 has already detailed the way in which the configuration coordinate model leads to a Gaussian shaped emission band. Experimentally however, a low energy exponential tail is often observed (see section 2.7.2 page 68).

It is proposed here that the two forms can both be represented by a simple semiempirical equation as follows:

$$L(E) = L(E_o) \quad \exp \left[g(E - E_o)^{\beta} \right] \qquad (16)$$

where L is the intensity, g and β are shape parameters which differ from one region of wavelength in the band to another, E and E_o are the photon energies at any wavelength and at the band maximum respectively. Figure 4.22 illustrates the case for CdS which has been plotted to find where the shape is Gaussian by plotting ln (L/L_o) versus $(E - E_o)^2$ and where it is exponential by plotting ln (L/L_o) versus E. The straight line segments shown in the upper plot of Fig. 4.22 indicate the range of the two asymmetric Gaussians around the maximum and this range has been labelled G (for Gaussian). The lower plot of ln (L/L_o) against E exhibits three straight line segments corresponding to the occurrence of three exponential regions of the band. One is the high energy (HE) tail of the band, and two exponential sectors occur in the low energy (LE) tail of the edge emission band. The high intensity sector of the low-energy (LE) tail probably arises from band-to-band

Fig. 4.22

Plots of the edge emission band data for an hexagonal structure CdS crystal at 292K (c.f. Fig. 4.19). The straight line segments in the upper plot show that in the region "G" near the maximum the band has an asymmetric Gaussian form. The straight lines in the lower plot show that in the low energy (LE) and high energy (HE) regions the form of the band is exponential.

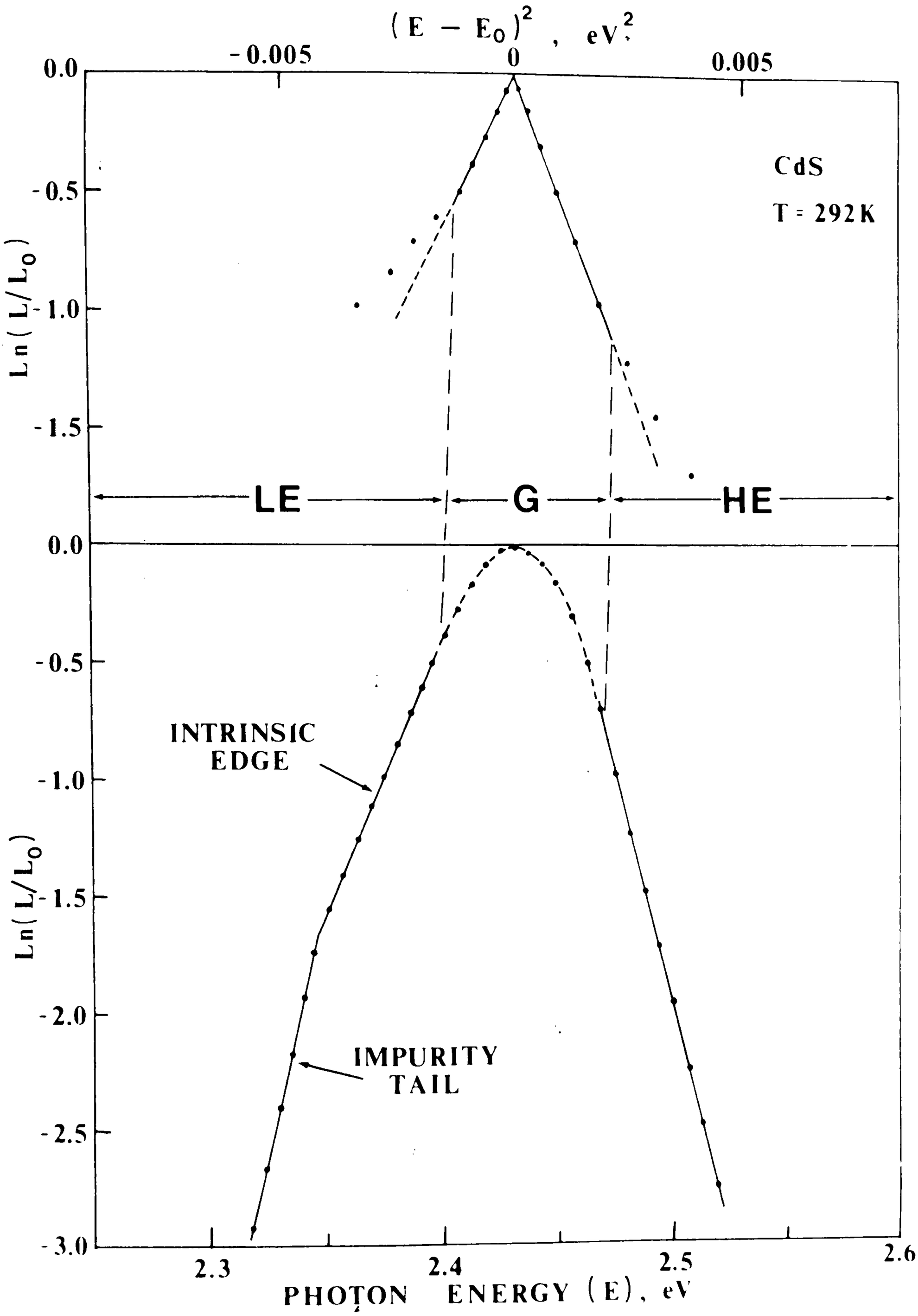

$(E - E_0)^2$, eV^2
-0.005
0
0.005
0.0
-0.5
-1.0
-1.5
-2.0
-2.5
-3.0
$Ln(L/L_0)$
CdS
T = 292K
LE
G
HE
INTRINSIC EDGE
IMPURITY TAIL
2.3
2.4
2.5
2.6
PHOTON ENERGY (E), eV

Fig 4·22

transitions and has been marked as the "intrinsic edge" whilst the low intensity sector is probably associated with impurities and has therefore been labelled as the impurity tail. The appearance in emission of two low energy exponential sectors has already been observed by Casey and Kaiser (1967) in GaAs and by Street et al. (1975) in chalcogenide glasses (see section 2.7.4). The different regions discussed above were observable for all (over a dozen) of the crystals examined and the values of the parameters of equation(16) were calculated for each region, at room temperature. In this way the slope $g = \sigma_L / kT$ of the "intrinsic" exponential ($\beta = 1$) edge of the LE region, the slopes $g = \tau^2$ of the asymmetric Gaussians ($\beta = 2$) ie the values τ_{LE} and τ_{HE} for the low and high energy Gaussians, and the slope $g = -\sigma_{H/kT}$ for the exponential ($\beta = 1$) HE region were obtained and are listed in table 5. The slope σ_i ($=gkT$) of the "impurity tail" varied markedly from sample to sample, and probably depends on the particular impurity present, its concentration, its state of ionization and its state of aggregation with other point defects. It was found that in all cases the magnitude of σ_L was less than that of $-\sigma_H$ and $\tau_{LE} < \tau_{HE}$. These relative magnitudes give the degree of asymmetry of the edge emission band.

The ZnS crystals studied here are known to contain various uncontrolled impurities (section 4.1.2,table 1). Below room temperature, very strong enhancement of the impurity-to-band recombination emission bands was observed for the

TABLE 5 Edge Emission band shape parameters; peak position $E_p = E_o$ in eV, full-width at half maximum H in eV, slope σ_L for LE "intrinsic edge"; slopes τ_{LE} and τ_{HE} ($g = \tau^2$) for Gaussian (G); slope $-\sigma_H$ for HE region. All values are at T = 292 K.

Crystal	E_p (eV)	H (eV)	σ_L	τ_{LE} (eV^{-1})	The range of validity of the low energy Gaussian region in eV	τ_{HE} (eV^{-1})	The range of validity of the high energy Gaussian region in eV	$-\sigma_H$
CdS	2.432	0.08	0.72	19.7	2.432 - 2.400	21.7	2.432 - 2.466	1.3
ZnS (Hex)	3.740	0.10	0.38	14.2	3.740 - 3.687	17.7	3.740 - 3.818	1.3
ZnS (Cub)	3.657	0.11	0.40	13.2	3.657 - 3.598	18.2	3.657 - 3.718	1.4

ZnS crystals (as shown in Figs. 4.20 and 4.21). At liquid nitrogen temperature in ZnS of both structures, the intrinsic or fundamental edge emission band is of lower maximum intensity than one or more nearby overlapping bands. Therefore unambigious determinations of the parameters of equation (16) was only possible for ZnS at room temperature. In some of the hexagonal ZnS samples the impurity band was even more dominant then in the typical specimens such as that shown in Fig. 4.20. This is probably due to higher concentrations of the impurities being present. Obviously the shape parameters and the half-width at room temperature are affected by impurity concentration so that in the extreme case values of $\sigma_L = 0.24$ and $H = 0.16$ eV were obtained compared to the values reported in table 5. This is similar to the observed effect of impurity concentration on both the slope of the exponential LE tail and the half-width (full-width at half maximum) of the edge emission band in the CL spectrum of GaAs (Casey and Kaiser 1967).

In CdS, the edge emission bands are less affected by impurities as seen from Fig. 4.19, in which the impurity band is well defined only at lower temperature. Also the impurity band maximum intensity is lower than the edge band intensity, unlike the case of either form of ZnS (Figs. 4.20 and 4.21). Therefore, it was possible to determine the emission band shape parameters for CdS at all temperatures. The temperature variation of both the low energy slope σ_L and the high

energy slope - σ_H for CdS is presented in Fig. 4.23. Many materials are known to exhibit the empirical Urbach's rule, according to which the absorption coefficient (α) in the low energy (ie longer wavelength) part of the fundamental absorption edge decays exponentially with the decrease of photon energy, $h\nu$ (see section 2.7.2 of this work). Mahr (1962) using a quantum mechanical one-coordinate oscillator model was able to show that for alkali halides the variation in the absorption coefficient (α) around the band maximum was of a Gaussian form. Furthermore it was found that the temperature dependence of the slope of absorption edges can usually be described by a function of the type $F \propto (2kT/\hbar\omega_o)$ tanh $(\hbar\omega_o/2kT)$. Such an expression extends the Boltzmann probability distribution of a classical oscillator to low temperatures where the zero-point oscillations of a quantum mechanical oscillator become important, ie the function (F) is a quantum mechanical correction factor. Furthermore, Mahr (1962) has shown that Urbach's expression has to be modified by this correction function to be compatible with low temperature optical absorption experimental results (see also Toyozawa 1959). An attempt to fit the experimental points to this equation for the present emission case, showed that the slope parameter does not have this form. Many more experimental and theoretical studies of additional materials will be necessary before the form of the temperature dependence of the edge emission band slopes can be established.

From a quantum mechanical treatment of the configuration

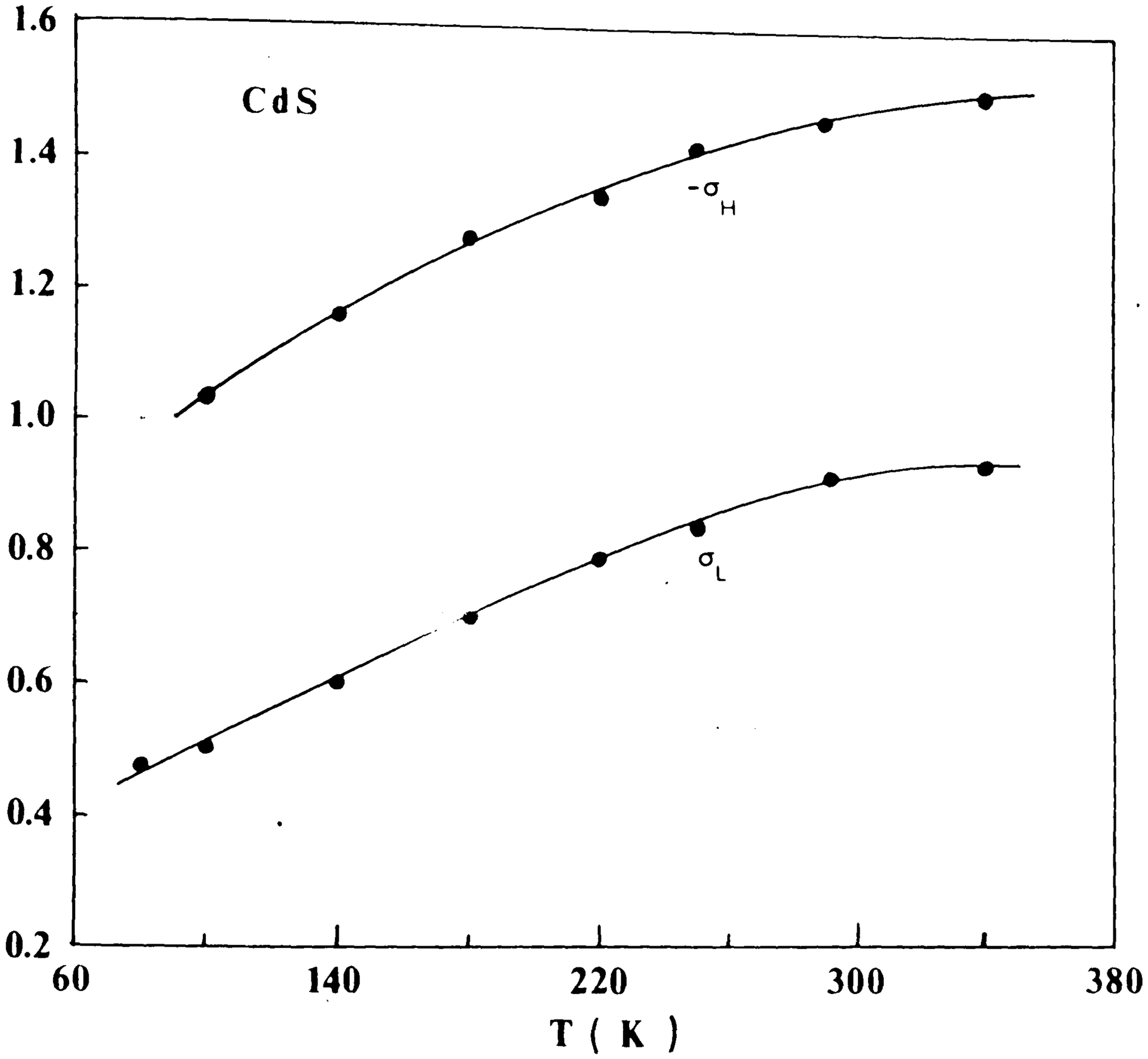


Fig. 4.23

Temperature dependence of the slopes σ_L (low energy region) and $-\sigma_H$ (high energy region) for CdS.

coordinate model (ie a one dimensional harmonic oscillator), it follows that the position of the peak $E_p = E_o$ of the edge emission band and the half-width H(T) should have the forms:

$$E_p = A + B \coth (\hbar\omega_o/2kT) \qquad (17)$$

and

$$H(T) = H(0) \left\{ \coth (\hbar\omega_o/2kT) \right\}^{\frac{1}{2}} \qquad (18)$$

c.f. equation (2) of section 2.7.1. Here $\hbar\omega_o$ is the energy of the "effective" phonon, ie that which is dominant at a given temperature. Derivations of the above equations have been outlined in section 2.7.1. However for a more rigorous mathematical theory on phonon-coupled emission, see Markham (1956) and Klick and Schulman (1957). To determine the type of lattice phonon (ie LO, LA, etc) participating at each temperature, the experimental values of $\hbar\omega_o$ were compared with those given in the literature (see for example values given in Marshall and Mitra 1964). In this way it was established that the best fit to equation (17) was obtained by using $\hbar\omega_o = \hbar\omega_{LO} = 0.038$ eV for the temperature range 140 to 340K and $\hbar\omega_o = \hbar\omega_{LA} = 0.0185$ eV below approximately 140K as plotted in Fig. 4.24. The values correspond to zone - boundary phonon energies (note that the LA zone centre phonon frequency is zero). A similar phonon related temperature dependence was observed for the half-width (H) of the edge emission band in CdS as shown in Fig. 4.25. Here again two different photons fit the data in different temperature ranges.

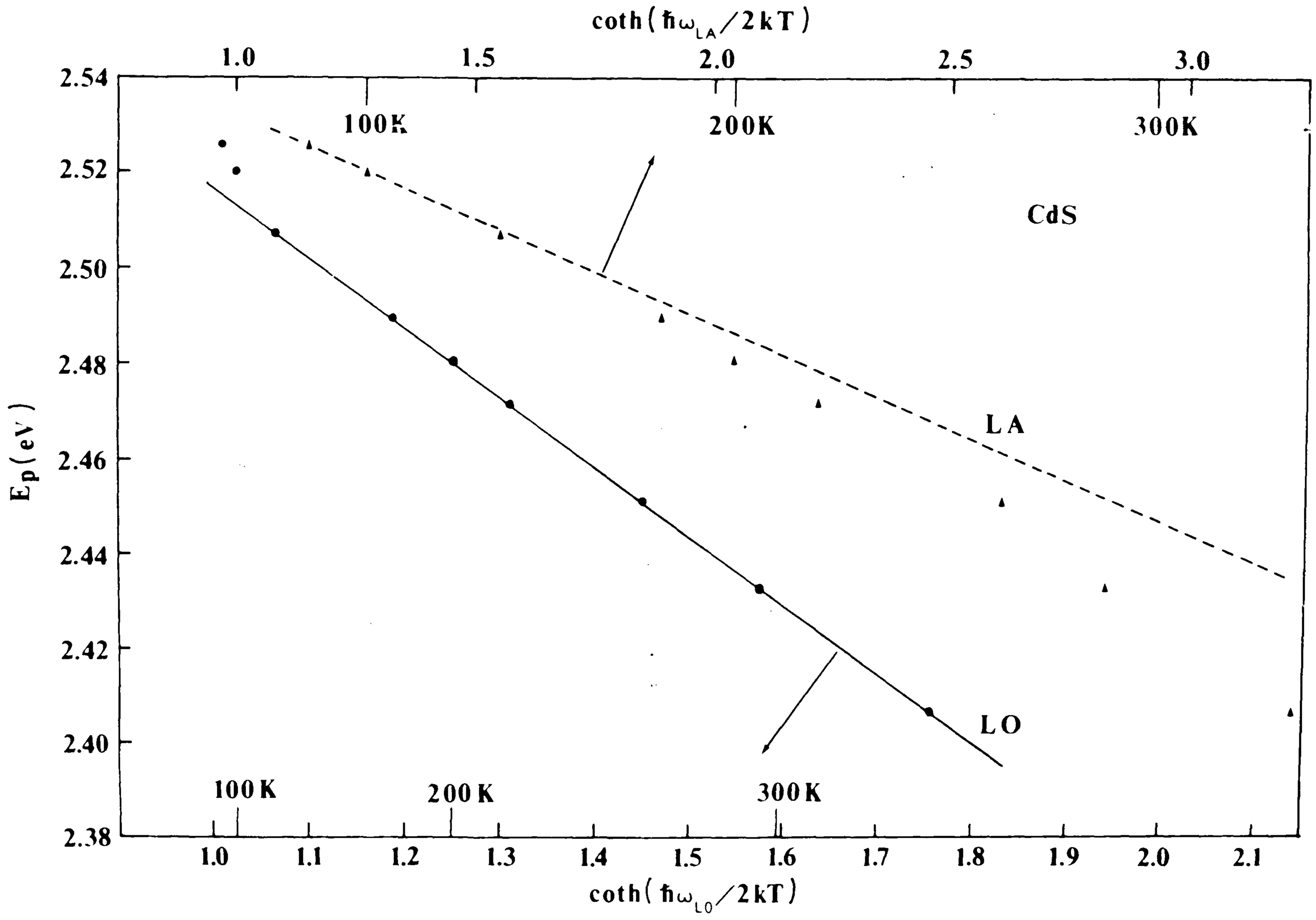


Fig. 4.24

Plots of peak position E_p versus coth ($\hbar\omega_{LA}/2kT$) (dashed line), and E_p versus coth ($\hbar\omega_{LO}/2kT$) (solid line) where $\hbar\omega_{LA}$ = 0.0185 eV and $\hbar\omega_{LO}$ = 0.038 eV.

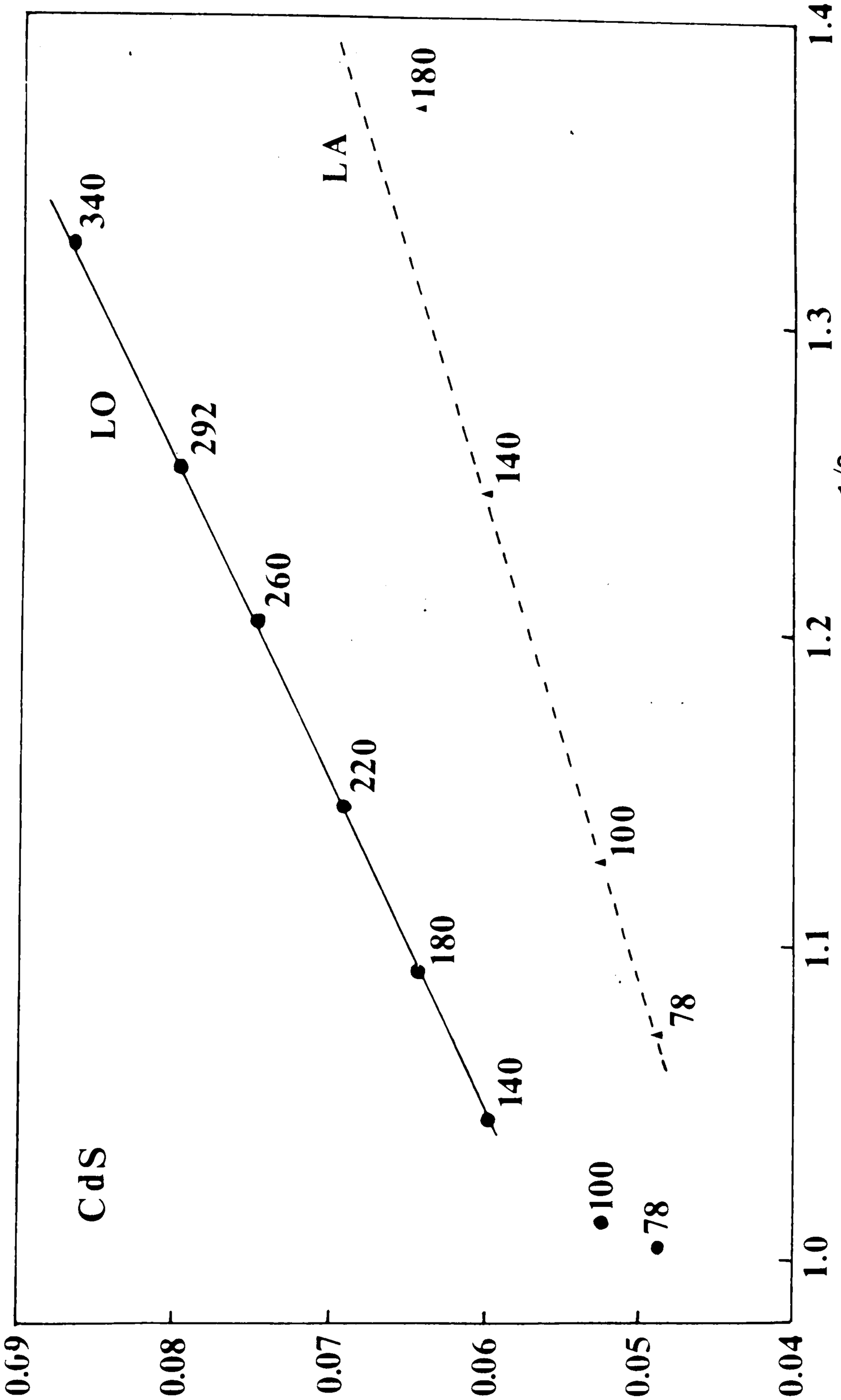


Fig. 4.25 Plot of halfwidth H versus $\left[\coth\left(\hbar\omega_o/2kT\right)\right]^{1/2}$ for both $\hbar\omega_O = \hbar\omega_{LO} = 0.038$ eV (solid line) and $\hbar\omega_O = \hbar\omega_{LA} = 0.0185$ eV (dashed line). Numbers at points represent temperatures in K.

Both H and E_p have similar dependences because for CdS the edge band is Gaussian down to the half - maximum height so that as far as the half-width (H) is concerned, it behaves like a Gaussian peak.

An analogous phenomenon was observed in optical absorption studies of ZnS crystals (Brada et al. 1975, **Yacobi** et al.1975 and Yacobi and Brada 1976). In that case both the slope parameter of the exponential absorption edge and the energy of the edge were found to fit the predictions with different phonons used for different temperature ranges. Infact in ZnS, at temperatures above 100K the LO phonon is predominate whereas below this temperature it is the LA phonon (Brada and Yacobi 1974).

4.4.3 DISCUSSION

It has already been discussed in some detail, that a configuration coordinate (or semiclassical Franck - Condon model) type model of electronic transitions coupled to the lattice vibrations predicts Gaussian shapes for both the optical absorption and emission bands (see section 2.7.1 and the many references therein). It was shown in the preceding section that the edge emission bands of CdS and ZnS are Gaussian only in a narrow range ("G") near the peak, and even then they are asymmetric. The exponential form of the emission band over most of the wavelength range must be understood in terms of some more complex model such as that of exponential tails

at the edges of otherwise parabolic valence and conduction bands (Pankove 1971) or the Dow and Redfield (1972) model. The assumption of exponential tails to the energy bands, as described by Pankove (1971) is only likely to apply to highly doped, degenerate semiconductors and is probably not relevant to the crystals examined here. The Dow and Redfield theory on the other hand (section 2.7.4) proposes that charged imperfections, such as ionized impurities, optical phonons or piezoelectric phonons create electrical microfields which facilitate the tunnelling of the electron away from the hole (ie internal Franz-Keldysh effect). This photon assisted tunnelling process is thought responsible for the exponential form of the low energy absorption tail (Urbach's rule). Their model is not, as yet, universally accepted but it does provide a unified quantitative explanation of most observations on the low energy tails of absorption edges in a very wide range of materials and it is thought to be the mechanism responsible for the exponential form of the "intrinsic" high intensity region of the low energy tails of the CdS and ZnS edge emission bands.

The interpretation of the "impurity" sector of the LE region of these bands is slightly uncertain as it could involve impurities either directly or indirectly. That is to say, what is involved could be either an impurity-to-energy band transition giving rise to an emission band which is concealed wholly or in part in the shoulder of the edge emission band or it could be that local electrical fields arising from

ionized impurities broaden the exciton levels to alter the form of the edge emission band tail. The forms of the bands shown in Figs. 4.19 to 4.21 strongly suggests the former interpretation. At 78K, in all cases, there are impurity-to-energy band emission bands which are well resolved from the edge emission band. This suggests that even when such a separate impurity band is not clearly resolved, as in CdS at 292K (Fig. 4.19a), the "impurity tail" of the edge emission band (Fig. 4.22) is the resultant of overlap with emission involving transitions from or to an impurity level. This would explain how it can be that the slope of the exponential impurity tail in Fig. 4.22 is greater than that of the intrinsic exponential edge.

The semiempirical form found for the edge emission bands in this work, ie $L(E) = L(E_o) \exp\left[g\ (E - E_o)^{\beta} \right]$, is similar to that obtained by Mahr (1962, 1963) for ionic crystals. However, the empirical expression proposed by him approximates to a Gaussian near the peak and to an exponential well out in the tail with a gradual transition between. Figure 4.22 indicates that in this work abrupt transitions from one form to the other was obtained. This behaviour is best represented by equation (16) proposed above, with the critical values listed in table 5. Dow et al. (1973) derived a similar expression for conduction band-to-acceptor emission but in their case the shape parameter β could have values in the range from 1 to 3/2.

The most significant general point arising from the results reported here is that the form of the low energy tail of the edge emission bands of ZnS and CdS is very like that of the absorption bands. This similarity between the optical absorption and emission bands has also been noted in GaAs. In that case it was shown that the dependence of the slope of the low intensity region on the impurity concentration was quantitatively similar in both emission (Casey and Kaiser 1967) and absorption (Dixon and Ellis 1961, Casey et al. 1975). This shows that phonons alone cannot account for the whole of the absorption or emission bands, as is assumed in a configurational coordinate model. The fact that both impurities and phonons must be taken into account, and that absorption and emission bands are closely related suggests strongly that the general approach of Dow and Redfield (1972) which is based on the effects of electrical fields occuring on a microscopical scale and arising from a variety of different causes is the most likely to provide an explanation of general applicability. In the two cases of edge absorption (Dow and Redfield 1972) and conduction band-to-acceptor emission (Dow et al. 1973), for which the detailed theory has been developed, the predictions have been found to be in agreement with experimental results. No detailed development of the model has appeared for the case of edge emission which is studied here.

It should be noted, that the monochromator (Bentham Instruments CF 44) used in this work gave linear wavelength dispersion throughout its range. However, in order for the data presented here and in the next section, to be consistent with the literature the near constant wavelength interval transmitted by a fixed slit monochromator has to be converted into constant energy transmission intervals. This basically means that a λ^2 correction term has to be applied to the spectral luminous intensity. There are two possible ways of doing this; (a) the monochromator slit width can be servoed for an equal energy interval as the photon energy varies, or (b) all spectra can be computer corrected. The latter was considered more suitable in this case because spectra in units of photon energy are not always required (c.f. section 4.3).

All the figures from (4.19) onwards in this section were obtained with a monochromator band width of 5 nm which gave spectral points every 1.25 nm. The beam voltage used was 30 KeV.

4.5 SHAPE ANALYSIS OF THE SELF-ACTIVATED CATHODOLUMINESCENCE BAND IN ZnS: Cl CRYSTALS

4.5.1 SYNOPSIS

The shape of the self-activated (SA) cathodoluminescence band of ZnS: Cl crystals was measured at temperatures in the range from liquid nitrogen to room temperature. The SA CL band was

found to be of Gaussian form only around the peak maximum, with exponential low and high energy tails. That is, as in the case of the fundamental edge emission band, the intensity of the self-activated cathodoluminescence band of ZnS can be expressed semiempirically by

$$L(E) = L(E_o) \quad \exp \left[g(E - E_o)^{\beta} \right],$$

where g and β are shape parameters, E and E_o are the photon energies at any wavelength and at the band maximum respectively (cf. section 4.4). The relevant shape parameters for the band are given in table 6 for both wurtzite - (hexagonal) and sphalerite - (cubic) structure material at several temperatures. The spectral correction procedure was employed to obtain the spectra in absolute terms (photons emitted per second) from the raw count-rate spectra and the vital importance of this correction will be emphasised.

When the temperature is decreased, as in well known (see Koda and Shionoya 1964), the peak of the uncorrected self-activated band shifts to lower energies (longer wavelengths). It was found in these experiments however that the peak of the corrected band shifts in the opposite direction; ie to higher energies (shorter wavelengths). The direction of shift with temperature is in agreement with that of the edge emission band (ie with the fact that the width of the forbidden energy band gap increases with decreasing temperature in ZnS, see section 4.4.2).

4.5.2 RESULTS AND ANALYSIS

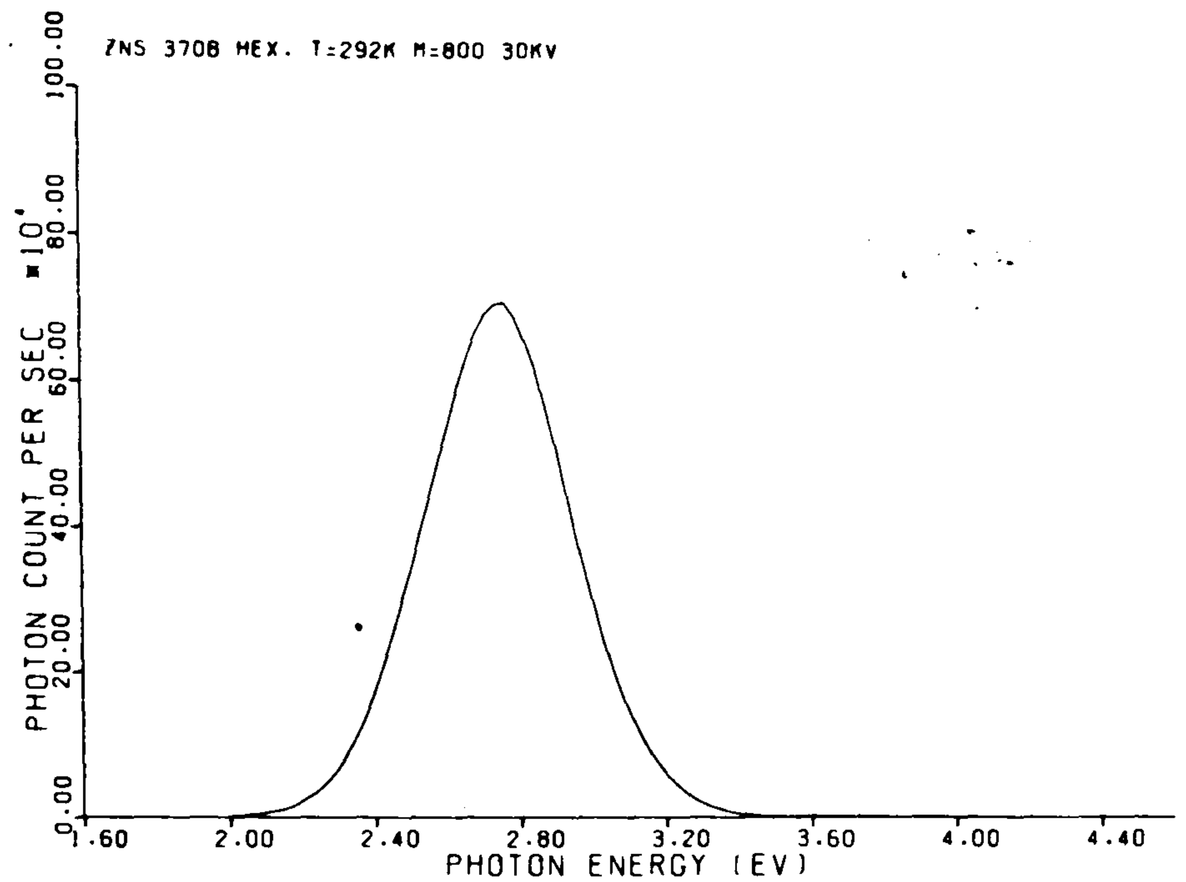
In the preceding section (4.4), it was shown that the edge emission bands (due to conduction to valence band transitions) of ZnS and CdS could best be described as Gaussian around the maximum with exponential tails on either side. A similar analysis of the form of the self-activated emission band in ZnS: Cl crystals (section 2.1.1) will be given below. Totally Gaussian optical absorption and emission band forms can be derived by considering the centre as a simple quantized one-dimensional harmonic oscillator as in the configuration co-ordinate model (see section 2.7.1 page 61 and the many references contained there). However, it has already been pointed out that departures from this ideal Gaussian band shape have often been observed experimentally but invariably left unexplained (see Klick and Schulman 1957). Furthermore, the presence of a low energy (longer wavelength) exponential tail (ie Urbach's rule) has been observed in a wide variety of materials in-cluding ZnS (section 2.7.2 page 68).

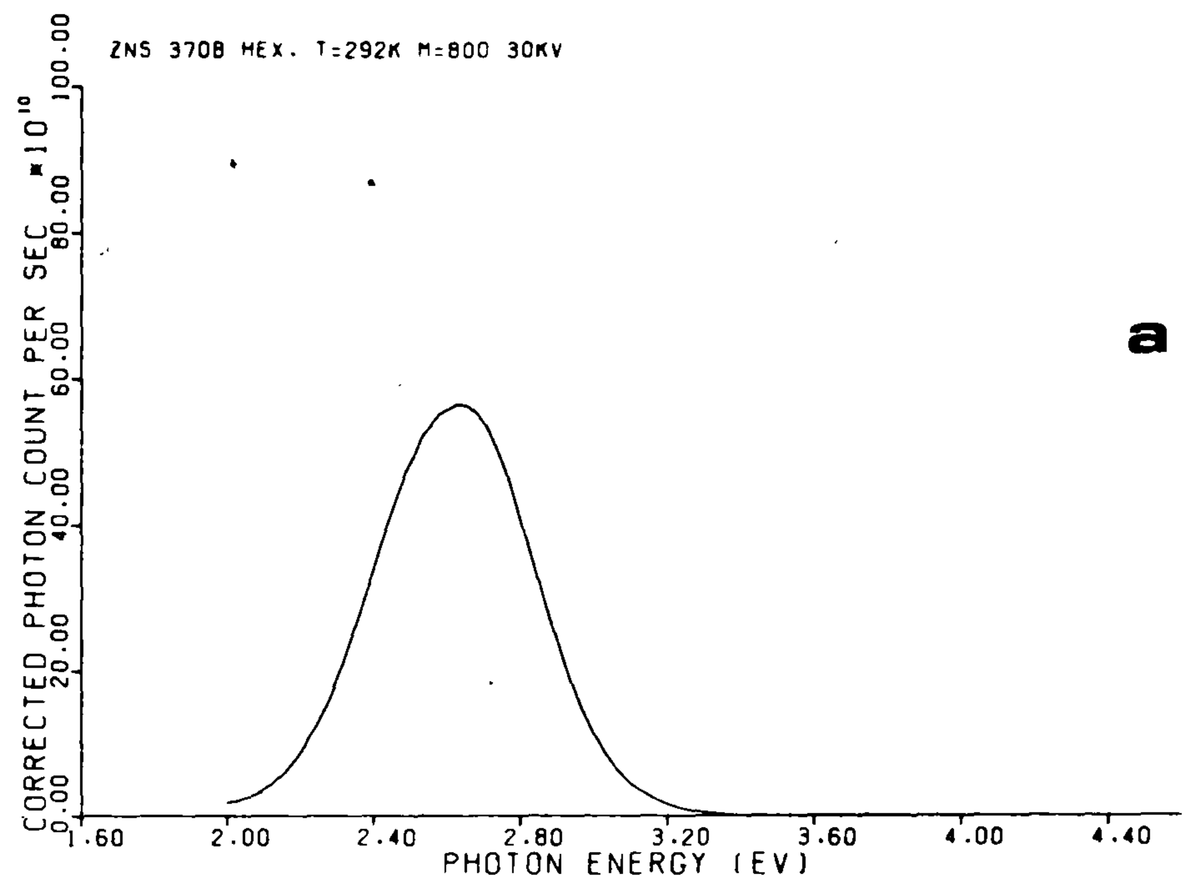
The reason for choosing the self-activated (SA) luminescence band in ZnS: Cl crystals, rather than any other, are two-fold. Firstly it is the most extensively studied and was thought to be the best understood of all the ZnS impurity bands (section 2.1.1). Secondly in the sample examined the SA CL emission band was found to be well defined and un-perturbed by any other impurity band in the wavelength range considered (300 to 600 nm), and the emission is of high intensity. So that accurate measurements could quickly be made.

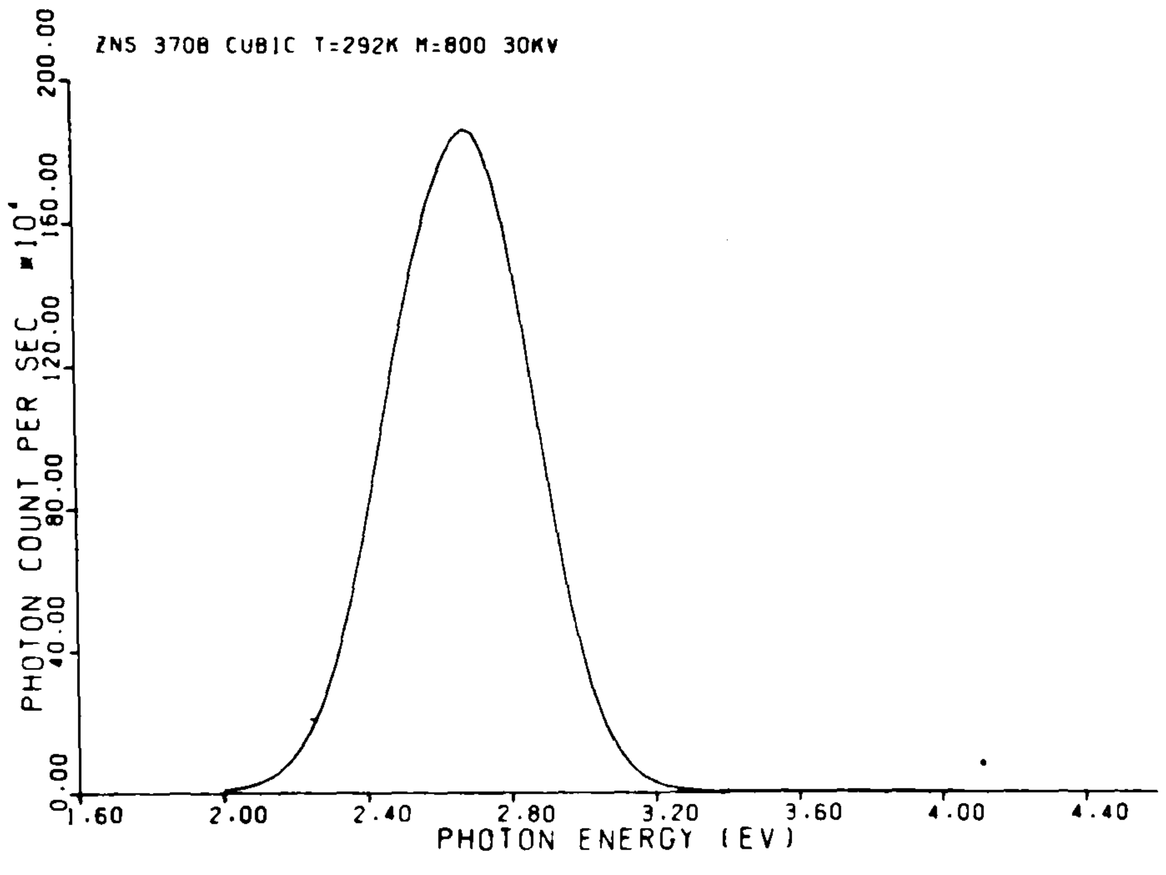
The ZnS platelets used, were of the type grown by sublimation in the presence of a mixture of argon and HCl (as described in section 3.2). In the temperature range investigated, 292 - 78K, the CL emission spectra from these ZnS: Cl crystals contained only one well defined, broad band of high photon emission in the visible region. Typical spectra are shown in Figs. 4.26 a and b for hexagonal and cubic structures at room temperature both uncorrected and corrected. From table 6, correction of the peak wavelength (E_i) due to the detector response (QEF), see section 3.6, amounts to approximately 18 nm (λ uncorrected $<$ λ corrected) and the observed shift between the hexagonal and cubic modifications is around 15 nm (λ hexagonal $<$ λ cubic; both corrected).

The different crystal regions investigated were identified from birefringence measurements as outlined earlier in section 3.3.

The failure of the simple configuration coordinate type model, predicting Gaussian band shapes, was clearly demonstrated in the last section. There it was shown that the edge emission band in hexagonal structure CdS and both hexagonal and cubic structure ZnS could best be described as being Gaussian only around the band peak maximum followed on either side by exponential tails. In the light of these results, it would seen reasonable to expect that the form of the ZnS SA cathodoluminescence band could also be expressed semiempirically as:







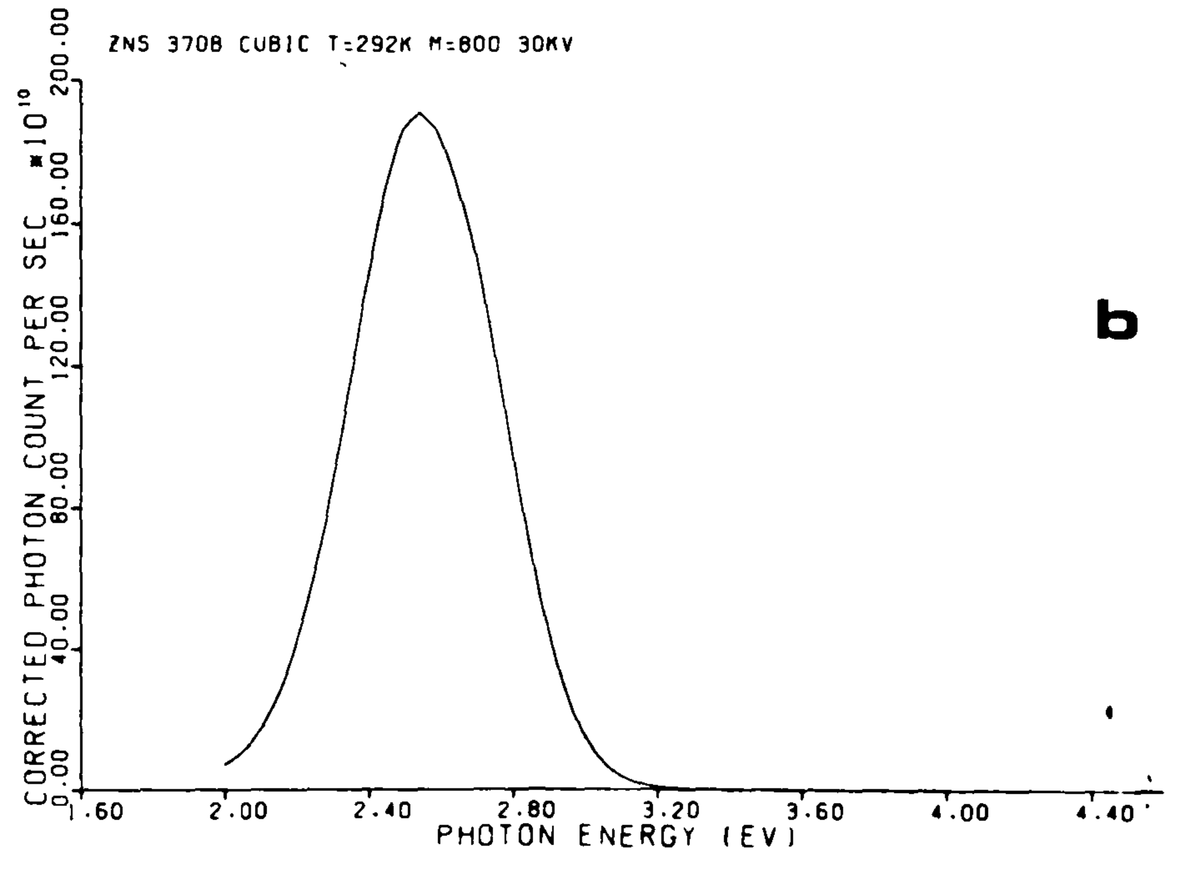


Fig. 4.26 Self-activated cathodoluminescence emission bands, of (a) hexagonal and (b) cubic structure in a ZnS: Cl crystal, both uncorrected and corrected at 292K.

$$L(E) = L(E_o) \exp \left[g(E - E_o)^{\beta} \right] \qquad (16)$$

Here L is the rate of photon emission, g and β are shape parameters, E the photon energy and E_o is the photon energy at the maximum of the band. Around the band peak $\beta = 2$ and therefore Gaussian, but for the low energy region of the band $\beta = 1$, ie the shape becomes exponential and Urbach's tail is obtained (cf. section 4.4.2.) The high energy region of the SA band was also found to be exponential. Then by plotting ln (L/L_o) against $(E - E_o)^2$, Fig. 4.27, and ln (L/L_o) against E, Fig. 4.28, it is possible to determine where the SA luminescence band shape is Gaussian and where it is exponential respectively. The straight line segments shown in Fig. 4.27 denote the range in which the band form is asymmetric Gaussian around the maximum and this region has been labelled as G(for Gaussian). The plot of ln (L/L_o) versus E, ie Fig. 4.28, also exhibits two straight line segments corresponding to the occurrence of exponential regions of the band. These regions have been labelled as the low energy (LE) and high energy (HE) tails in both Figs. 4.27 and 4.28. The appearance of the various regions discussed above were observed in all the samples examined (some half-a-dozen of each structure) and the values of the parameters of equation (16) were calculated for each region, at the different temperatures and are presented in table 6. Here the slope $g = \sigma_L/kT$ of the exponential ($\beta = 1$) LE region of the SA luminescence band, the slopes $g = \tau^2$ of the asymmetric Gaussians ($\beta = 2$) that is the values τ_{LEG}

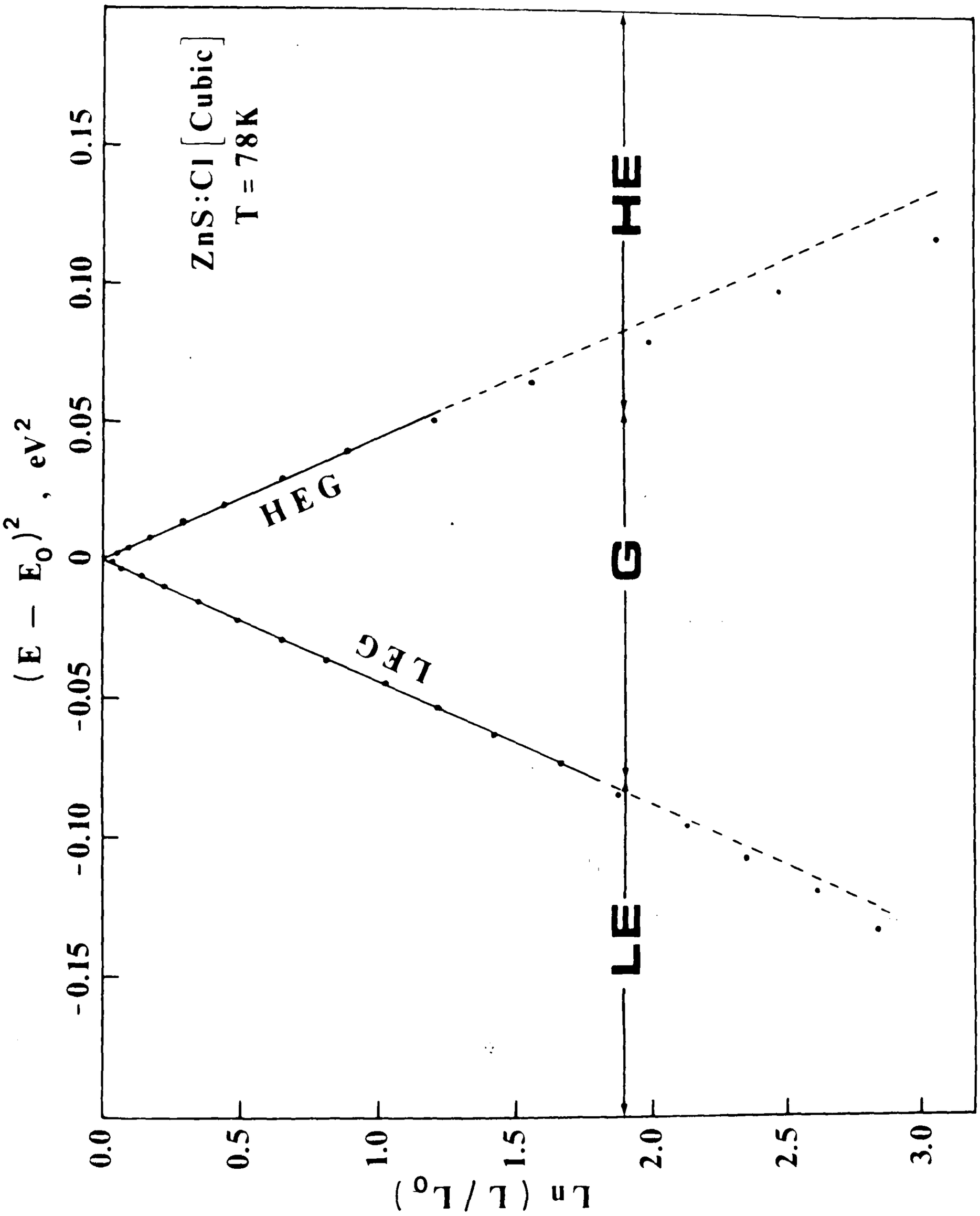


Fig. 4.27 Plots of the self-activated emission band data for a cubic structure ZnS: Cl crystal at 78K. The straight line segments show that in the region "G" around the maximum the band has an asymmetric Gaussian form.

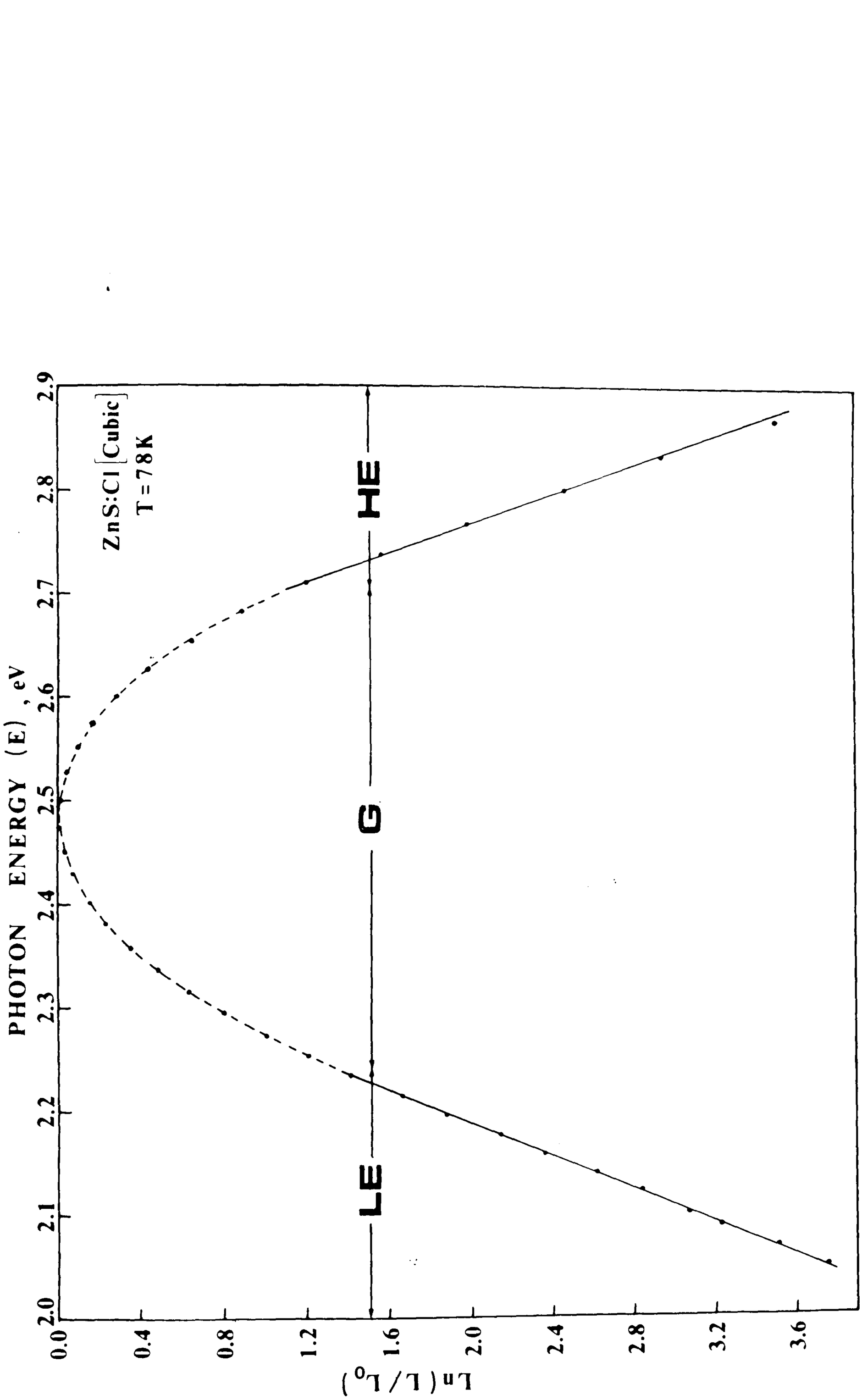


Fig. 4.28 Plots of the SA emission band for a cubic structure ZnS: Cl crystal at 78K. The straight lines show that in the low energy (LE) and high energy (HE) regions the form of the band is exponential.

TABLE 6 Cathodoluminescence ZnS: Cl (SA) band shape parameters; peak position $E_i = E_o$ in eV both uncorrected and corrected; ΔE_i the difference in peak value; full-width at half maximum H in eV; slopes τ_{LEG} and τ_{HEG} for Gaussian (G); slopes σ_L and $-\sigma_H$ for LE and HE exponential regions

Structure	Temperature (K)	E_i(eV) Uncorrected	E_i(eV) Corrected	$\Delta E_{i(eV)}$	H(eV)	σ_L	τ_{LEG} (eV^{-1})	*(LEG)	τ_{HEG} (eV^{-1})	**(HEG)	$-\sigma_H$
CUBIC (3C)	292	2.678(463nm)	2.539(488nm)	0.139	0.46	0.32	3.87	58%	3.99	48%	0.33
	200	2.670(464nm)	2.563(484nm)	0.107	0.39	0.57	4.14	69%	4.26	60%	0.62
	120	2.662(466nm)	2.580(481nm)	0.082	0.36	1.28	4.68	82%	4.76	77%	1.30
	78	2.654(467nm)	2.586(479nm)	0.068	0.35	1.95	4.77	87%	4.88	79%	2.30
HEXAGONAL (2H)	292	2.749(451nm)	2.634(471nm)	0.115	0.51	0.28	2.97	46%	3.61	34%	0.32
	78	2.728(454nm)	2.664(465nm)	0.064	0.39	1.57	4.18	56%	4.54	41%	1.61

NOTE: *(LEG) - Fraction of the Band which is Gaussian (LEG)

**(HEG) - Fraction of the Band which is Gaussian (HEG)

and τ_{HEG} for the low and high energy Gaussians respectively, and the slope $g = -\sigma_H/kT$ for the exponential ($\beta = 1$) HE region are given. From the results in table 6 it can be seen that in all cases $\sigma_L < -\sigma_H$ and also $\tau_{LEG} < \tau_{HEG}$. These relative magnitudes give the degree of asymmetry of the ZnS SA CL emission band. This behaviour is very similar to that reported earlier (section 4.4.2) for the edge (conduction to valence band) emission in these materials.

It must be stressed at this point that the actual values for σ_L and $-\sigma_H$ (for the exponential regions) should not be taken too literally. This is because all the emission spectra in this section were recorded using a fast stepper motor speed (which drives the monochromator grating)and a bandwidth of 5 nm at 30 KeV. This resulted in spectral points being recorded every 4.5 nm across the band rather than with the usual spacing of 1.25 nm (cf. section 4.4.3 on ZnS edge emission). It was believed initially, that since the SA band was about three times as intense compared to other impurity or edge emission peaks in ZnS, acquiring spectra with the above conditions would not produce adverse effects (ie. "jagged" spectra, cf. Figs 4.17 e, f, g and h in section 4.3.5). This belief is only justified when considering the spectra presented in Figs. 4.26 a and b of this section. However, when carrying out the shape analysis of the exponential LE and HE tails, especially of the latter, the problem of identification using widely spaced spectral points becomes a little difficult. From table 6 it can be

seen that the SA luminescence band is mostly Gaussian (> 60% of the total) in form with low intensity exponential LE and HE tails. In this low intensity region large intervals (ie 4.5 nm) between successive spectral points make detailed shape analysis less convincing. The problem becomes more pronounced at room temperature where the added complication of increased electron - phonon interactions cause a further deviation of the experimental points. There appears to be no room for doubt however, that exponential low and high energy tails do exist as demonstrated by Fig. 4.28.

The lower limiting point of the Gaussian region as a fraction of the peak emission is found to be a strong function of temperature. From table 6, it can be seen that at low temperature, the SA band is almost all Gaussian, but the low energy (LEG) and high energy (HEG) Gaussian ranges decrease with increasing temperature. Such a phenomenon can not be explained using the simple configuration coordinate model which predicts totally Gaussian band forms at all temperatures (see Klick and Schulman 1957 and section 2.7.1 of this thesis). With the increase in temperature the electron - phonon interaction becomes stronger which in turn affects the half-width H(eV) and the slope τ (eV^{-1}) of the Gaussians as expected but the LEG and HEG ranges should remain unchanged on the basis of the configuration coordinate model. The observed dependence is probably the effect of some factor which becomes more dominant at higher temperatures. For example, such behaviour could arise from the fact that in

going from lower to higher temperatures the number of ionized impurity states or other defects increase which could perturb the breaking point of the Gaussian via some internal electrical 'microfield' model (Dow et al. 1973). An extended review of the Dow and Redfield (1972) theory has been given in section 2.7.4. So far no theory has explained this type of behaviour for emission but a similar variation due to altered charge states of impurities has been observed in the optical absorption edge of ZnS (Yacobi and Brada 1976) and of GaAs (Redfield and Afromowitz 1967). In both cases the observed experimental results were shown to be fully consistent with the internal microfield Franz-Keldysh mechanism proposed by Dow and Redfield (1972) for absorption edges in such materials. This point was dealt with earlier in section 2.7.

It is worth noting here that in the hexagonal (2H) structure the ranges of the LEG and HEG at 78K are less wide than those observed for the cubic (3C) structure at the same temperature. This is probably the effect of slight faulting which is typical of hexagonal phase material in vapour grown platelets and was observed to be present, with a low density, even in the best areas selected. It may also explain why the SA CL photon emission from the hexagonal structure is less intense than that for cubic material, Figs. 4.26 a and b. Therefore it is not possible to draw any firm conclusions about the intrinsic relative rates of photon emission of the two structures. Choosing structurally - homogeneous regions was again important, as already dealt with in an earlier

section, since heavy faulting can change the shape as well as height of bands.

There is another possible reason why the cubic phase differs from the hexagonal phase in fitting the Gaussian function more closely at low temperatures. It is well established from electron spin resonance (ESR) work (Räuber and Schneider 1963, and Schneider et al. 1965) that there are two symmetries for the self-activated centre in the hexagonal phase and only one in the cubic phase. This centre has been identified as a group VII (eg Cl) impurity substituted for a S^{2-} ion adjacent to a Zn vacancy (see section 2.1.1). At liquid helium temperature a trapped hole in the excited SA centre is fixed at one S^{2-} ion, but at temperatures near 77K the hole hops rapidly among equivalent sulphur ions neighbouring the Zn vacancy. Schneider et al. (1963) have shown that the electron spin resonance spectra are all consistent with this model. In other words, at 77K the symmetry of the hole electron spin resonance spectrum was indicative of only partial localisation on a sulphur orbital and thus "hole-hopping" occurs.

More detailed experimental and theoretical work are needed before any final conclusions can be drawn, however.

Traditionally it seems that the peak energy E_i (eV), of the SA luminescence band in ZnS has always been reported to shift towards lower energies (longer wavelengths) with the decrease in temperature, which is the opposite direction of shift to

that of the edge emission band in this material. Infact, this temperature variation is considered to be one of the characteristics of the SA luminescence band (see section 2.1.1 page **26**), although detailed theoretical explainations have not been given. Also, the peak position is known to vary between 450 and 470 nm at room temperature, as the particular type of preparation is varied (Curie and Prener 1967).

In this work it was found that for the uncorrected signal, table 6, the peak energy E_i (eV) of the band does indeed shift to lower energies (longer wavelengths) with temperature decrease (Fig. 4.29 dashed curves). The experimental value for the peak of the uncorrected photomultiplier count rate band agrees fairly closely with those reported by Koda and Shionoya (1964), who used faulted cubic ZnS: Cl crystals. The difference of detail between these results can be explained as due to (a) faulting, since only homogeneous cubic regions were examined in this experiment and the fact that (b) CL and photoluminescence (PL) spectra are not identical (as pointed out by Norris et al. 1973).

It also seems that some of the inconsistency (not that due to lack of correction for different photomultipliers) in the peak position of the SA luminescence band reported in the literature is probably due to the variations in the initial excitation energy used in PL measurements, since recently, Grasser et al. (1971) and Georgobiani et al. (1973) have shown that changing the wavelength of excitation can shift

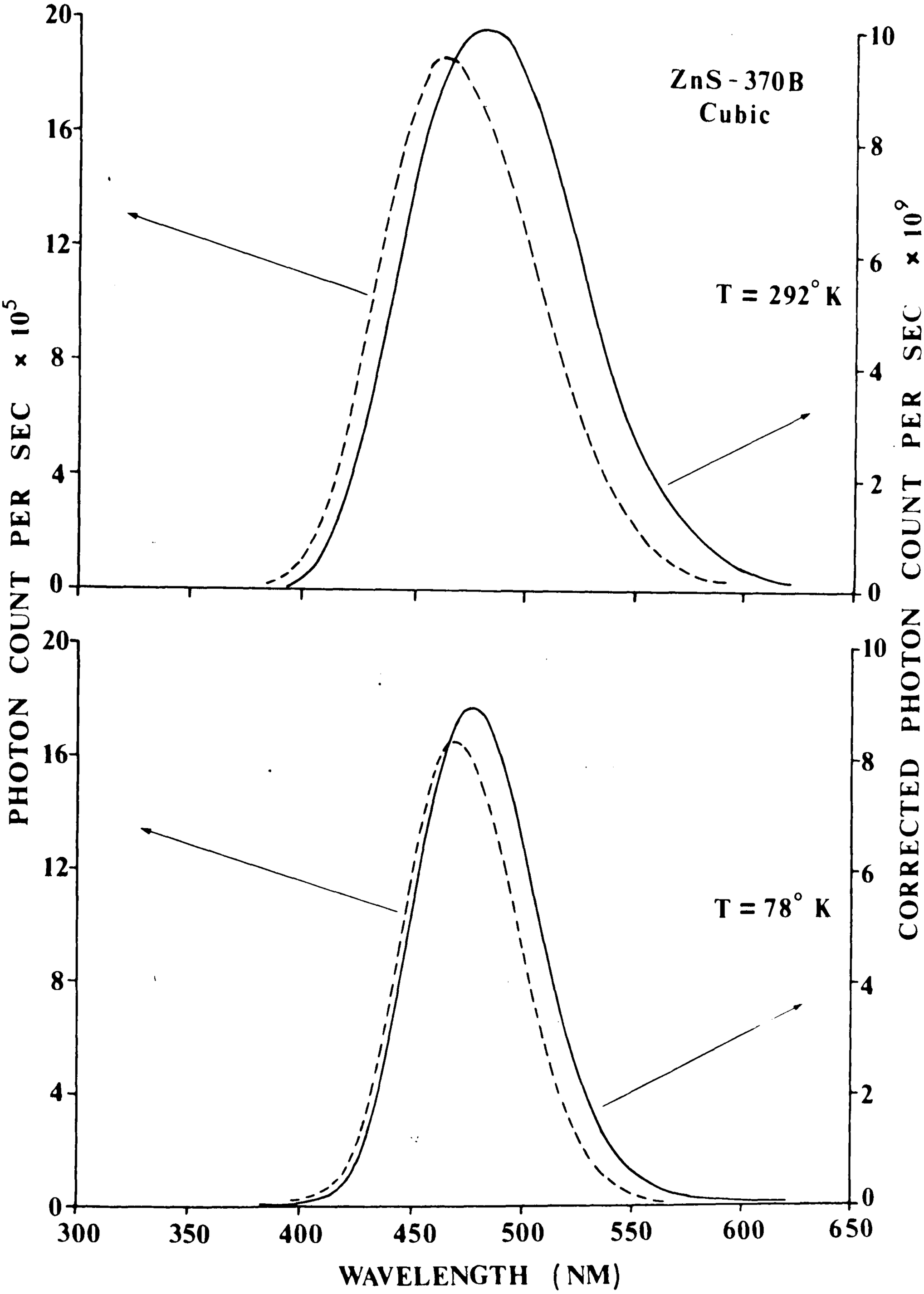


Fig. 4.29 Corrected (solid) and uncorrected (dashed) self-activated cathodoluminescence bands of cubic ZnS: Cl at room temperature and liquid nitrogen temperature.

peaks to either shorter or longer wavelengths depending on the wavelength of PL excitation.

If the CL emission spectrum is corrected, for reasons already discussed, then the peak energy E_i (eV) of the SA luminescence band is seen infact to shift towards higher energies (lower wavelengths) with the decrease in temperature (table 6 and Fig. 4.29, solid curves). This reversal in the direction of shift on correction is satisfying, eventhough it is in contradiction with the photoluminescence literature, because the edge CL band peak is known to shift towards higher energies as temperature is decreased and one would assume that the SA band would behave similarly.

It can be seen that the non-constancy of the CL detector response curve (Fig. 3.8 section 3.6 page 112) has a larger effect on broad bands at T = 292K, than on narrow bands at T = 78K (ΔE_i, table 6). The overall effect is that though the shift due to correction is unidirectional at all temperatures, it causes the broad band to move further than the narrow band as shown in Fig. 4.29, and the peak energy shift with temperature changes direction. Note also in Fig. 4.29 that the performance of the CL detection system is such that correction shows that the peak rate of photon emission of the SA luminescence band is really four orders of magnitude greater than that in the raw count-rate spectrum (dashed curve). These magnitudes and shape effects of correction

are so large that clearly correction is vital in this case (the CL calibration procedure is considered in section 3.6).

5. CONCLUSIONS

The scanning electron microscopy (SEM) cathodoluminescence (CL) results obtained in this work can be summarized as follows:

(a) The CL edge or fundamental emission (ie that arising from conduction band to valence band recombination emission) peak values (E_p), at room temperature, for hexagonal (2H), cubic (3C) and 4H polytypic structures of ZnS are given in table 2 section 4.2.3.

(b) The results of this work have shown that certain local CL variations in these complex striated ZnS platelets are specifically the effects of (i) structural changes, or (ii) impurity segregation, or (iii) internal electric fields. The first can be detected from the edge band peak position, the second from the observation of impurity bands together with the local structure and the third results in quenching of the CL at all wavelenghts.

(c) Panchromatic (all wavelengths) CL micrographs, monochromatic (one wavelength) micrographs and uncorrected spectra must all be intepreted with caution since they can be misleading. Infact only corrected spectra can be considered as truly indicative of the real CL emission properties of local regions of a sample.

(d) It has been shown that all emission spectra must be corrected for the rapid fall in the CL detector response curve (Fig. 3.8 section 3.6) in going from the blue (shorter wavelength) to the red (longer wavelength) end of the visible spectrum. This is mainly due to the steep fall in the quantum efficiency of S20 type (trialkali photocathode) photomultipliers over this range (see Fig. 3.7 in section 3.6).

Broad emission bands undergo larger correction effects than do narrower bands (cf. Fig. 4.29 section 4.5.2). A further example of this is the green - copper emission band (Fig.4.10a section 4.2.3) for which the uncorrected peak maximum appears at 523 nm (2.37 eV) but the real emission peak is found at 534nm(2.32eV) on correction (Fig.4.10b). On the other hand, the sharp red-tin band (Fig. 4.10d) only shifts by approximately 1.5 nm to 673 nm (1.84 eV) on correction, although it occurs in a wavelength range where the detector response is falling rapidly.

The rate of photon emission (corrected) can be many orders of magnitude greater than the (uncorrected) raw count rate. The effects of correction on peak shape as well as position can be large. Consequently the use of absolute (corrected) spectra rather than the commonly used "arbitary units" (uncorrected photomultiplier current or count rate) spectra is vital. Failure to correct spectra is still wide spread in the luminescence literature and could account for many of the quantitative discrepancies so often reported. It may

well be that much of the irreproducibility in the literature is not entirely a consequence of uncontrolled variability in the luminescent properties of the materials studied, but at least partly due to the use, uncorrected, of detector systems, especially photomultipliers, of different response characteristics (cf. Fig. 3.7 section 3.6). Luminescence may not be as irreproducible as it appears.

(e) The method of colour synthesis, in which a series of black-and-white micrographs were photographed onto colour film, was demonstrated (section 4.3) to give significant information about the luminescent properties of these complex ZnS platelets. Such CL micrographs in colour (Fig. 4.16 and 4.18) can be produced systematically with very little extra cost. The success of the method depends largely on (a) the colour filter set (Kodak Ltd) being properly balanced and (b) the initial black-and-white positives should be of a high photographic quality.

(f) The fundamental edge emission bands of hexagonal (2H) CdS and both hexagonal (2H) and cubic (3C) structure ZnS were found to be Gaussian near the intensity maximum only and exhibited an exponential form in both the low and high energy tails of the band.

(g) The form of the edge band can be expressed semiempirically by the equation:

$$L(E) = L(E_o) \quad \exp \left[g(E - E_o)^{\beta} \right] \qquad (16)$$

where L is the intensity, g and β are shape parameters, E and E_o are the photon energies at a particular wavelength and at the band maximum respectively. When β = 2, ie around the band maximum, the shape is Gaussian. However, when β =1, the low energy region of the band becomes exponential and the Urbach tail is obtained. The high energy tail was found to be exponential also (see Fig. 4.22 section 4.4.2). The quantitative values of the parameters of equation (16) are given in table 5 section 4.4.2.

(h) In the case of CdS it was found that the position of the band maximum and its half-width (H, eV) varied with temperature as theoretically expected since both are determined by the Gaussian region, and the LA phonon was the effective one in the temperature range 78K to 140K, while from 140K to 340K it was the LO phonon (see Fig. 4.24 and 4.25 in section 4.4.2).

(i) The variation with temperature of the slopes of the exponential low (σ_L) and high ($-\sigma_H$) energy tails of CdS was found to be of similar form as shown in Fig. 4.23 section 4.4.2, but no theoretical interpretation of this dependence has been found.

(j) Similar shape analysis of the self-activated cathodoluminescence band of both hexagonal and cubic structure ZnS: Cl crystals at various temperatures revealed a Gaussian band form around the intensity maximum only, followed by low and high energy exponential tails. The salient SA band parameters are give in table 6 in section 4.5.2.

(k) The vital importance of choosing structurally homogeneous regions for CL measurements has been emphasized throughout this work since stacking faults or structure changes alter the efficiency of photon emission, half-width, peak photon energy, slope parameter and other related quantities. This may also be a contributary cause of the fact that the peak photon energy values reported in the luminescence literature are so diverse for the same band. Non-correction for detector (especially photomultiplier) response characteristics, and a dependence of photoluminescence (PL) results on the wavelength of the exciting radiation are other important causes of discrepancies in the literature.

(l) The self-activated (SA) band was found to shift towards shorter wavelengths (higher energies) with the decrease in temperature for corrected spectra and in the opposite direction when uncorrected.

REFERENCES

Alexander E, Kalman Z H, Mardix S and Steinberger I T (1970) Phil. Mag. 21 1237

Apple E F (1959) J. Electrochem. Soc. 106 271

Auger P (1925) J. Phys. Radium 6 205

Aven M and Potter R M (1958) J. Electrochem. Soc. 105 134

Barrett C and Massalski T B (1966) in Structure of Metals (McGraw Hill, New York)

Baum F J and Darnell F J (1962) J. Electrochem. Soc. 109 165

Baumhauer H (1912) Z. Kristallogr. 50 33

Bearden J A (1964) U.S. Atomic Energy Commission, Oak Ridge, Tennesse, NYO - 10586

Belk J A (1974) in Quantitative Scanning Electron Microscopy, eds. Holt D B, Muir M D, Grant P R and Boswarva I M (Academic Press, London) 389

Bernard R, Davoine F and Pinard P (1959) C. R. Acad. Sci 248 2564

Bishop H E (1974) in Quantitative Scanning Electron Microscopy, eds. Holt D B, Muir M D, Grant P R and Boswarva I M (Academic Press, London) 41

Blick H, Riehl N and Sizmann R (1961) Z. Phys. 163 594

Bond E F, Beresford D and Haggis G H (1974) J. Microscopy 100 271

Bowers R and Melamed N T (1955) Phys. Rev. 99 1781

Brada Y, Steinberger I T and Stone B (1972) Phys. Lett. 38A 263

Brada Y and Yacobi B G (1974) in Proceedings of the Twelfth International Conference on the Physics of Semiconductors ed. Pilkuln M H (Teubner, Stuttgart) 1212

Brada Y, Yacobi B G and Peled A (1975) Sol. State Comm. 17 193

Brafman O, Alexander E, Fraenkel B S, Kalman Z H and Steinberger I T (1964) J. Appl. Phys. 35 1855

Brafman O, Shachar G and Steinberger I T (1965) J. Appl. Phys. 36 668

Brafman O and Steinberger I T (1965) Appl. Phys. Lett. 7 110

Brafman O and Steinberger I T (1966) Phys. Rev. 143 501

Carlsson L and Van Essen C G (1974) J. Phys. E., Scientific Instruments 7 98

Casey H C and Kaiser R H (1967) J. Electrochem. Soc. 114 149

Casey H C, Sell D D and Wecht K W (1975) J. Appl. Phys. 46 250

Casey H C and Stern F (1976) J. Appl. Phys. 47 631

Chopra K L and Bahl S K (1972) Thin Solid Films 11 377

Cingolani A, Levialdi A and Perillo P (1966) Phys. Lett. 21 24

Cingolani A, Levialdi A and Romeo N (1967) Nuovo Cim. 51 210

Curie D and Prener J S (1967) in Physics and Chemistry of II - VI Compounds, eds. Aven M and Prener J S (North - Holland, Amsterdam) 433

Davey J P (1966) in Optique des Rayons X et Microanalyse (Herman, Paris) 436

Davidson S M and Rasul A (1977) J. Phys. E., Scientific Instruments 10 43

Dean P J (1969) App. Solid State Sci. 1 1

De Bruin S H, Dieleman J, and Van Doorn C Z (1964) Acta. Phys. Polon. 26 579

De Mets M (1974) in Principles and Technique of SEM, ed. Hayet. M A (Van Nostrand Reinhold) 2 1

Dexter D L (1967) Phys. Rev. Letts. 19 1383

Dixon J R and Ellis J M (1961) Phys. Rev. 123 1560

Dow J D, Bowen M, Bray R, Spears D L and Hess K (1974) Phys. Rev. B10 4305

Dow J D and Redfield D (1970) Phys. Rev. B1 3358

Dow J D and Redfield D (1972) Phys. Rev. 5B 594

Dow J D, Smith D L and Lederman F L (1973) Phys. Rev. 8B 4612

Dutton D (1958) Phys. Rev. 112 785

Echlin P and Hyde P J W (1972) in Proceedings of the Vth Ann. SEM. Symposium IITRI, Chicago, USA. 137

Elliott R J (1957) Phys. Rev. 108 1384

Elliott R J, Gibson A F (1974) in An Introduction to Solid State Physics and its Application (Macmillan Press Ltd, London)

Ellis S G, Hermann F, Loebner E E, Merz W J, Struck C W and White J G (1958) Phys. Rev. 109 1860

Era K, Shionoya S and Washizawa Y (1968a) J. Phys. Chem. Solids 29 1827

Era K, Shionoya S, Washizawa Y and Ohmatsu H (1968b) J. Phys. Chem. Solids 29 1843

Everhart T E and Thornley R F M (1960) J. Sci. Inst. 37 246

Fan H Y (1951) Phys. Rev. 82 900

Foord R, Jones R, Oliver C J and Pike E R (1969) Appl. Optics 8 1975

Franz W (1958) Z. Naturforsch. 13A 484

Froelich H C (1953) J. Electrochem. Soc. 100 280

Garrod D K and Bray R (1972) in Proceedings of the 11th International Conference on the Physics of Semiconductors (PWN - Polish Scientific, Warsaw) 1167

Gedcke D A (1974) in Quantitative Scanning Electron Microscopy, eds. Holt D B, Muir M D, Grant P R and Boswarva I M (Academic Press, London) 403

Georgobiani A N, Blazhevich A I, Ozerov Yu V, Panasjuk E I, Todua P A and Friedrich H (1973) in Proceedings of the International Conference on Luminescence, Leningrad, ed. Williams F (Plenum Press, New York) 239

Giles P L (1975) J. Microscopie Biol. Cell. 22 357

Goldberg P (1966) in Luminescence of Inorganic Solids (Academic Press, New York)

Goldstein J I and Yakowitz H (1975) in Practical Scanning Electron Microscopy (Plenum Press, New York)

Goodhew P J (1975) in Electron Microscopy and Analysis (Wykeham Publications Ltd, London) 117

Gopinath A (1974) in Quantitative Scanning Electron Microscopy, eds. Holt D B, Muir M D, Grant P R and Boswarva I M (Academic Press, London) 95

Grasser R, Roth G and Scharmann A (1971) Z. Phys. 249 91

Guild J (1931) Phil. Trans. Roy. Soc. London. Ser. A. 230 149

Gurney R W and Mott N F (1939) Trans. Faraday Soc. 35 69

Hachenberg O and Brauer W (1959) in Advances in Electronics and Electron Physis, ed. Marton L (Academic Press, New York) 11 413

Haupt U (1959) Z. Physik 157 232

Heinrich K F J (1965) in IV International Congress on X-Ray Optics and Microanalysis, Orsay, eds. Castaing R, Deschamps P and Philibert J (Herman, Paris) 159

Hohler G (1949) Ann. Phys. (Leipz) 4 371

Holt D B and Culpan M (1970) J. Mater. Sci. 5 546

Holt D B (1974) in Quantitative Scanning Electron Microscopy, eds. Holt D B, Muir M D, Grant P R and Boswarva I M (Academic Press, London) 335

Holt D B, Steyn J B and Giles P L (1975) in Developments in Electron Microscopy and Analysis (Proc. EMAG 75) ed. Venables J A (Academic Press, London) 111

Hoogenstraaten W (1953) J Electrochem. Soc. 100 356

Hörl E M (1972) Micron 3 540

Hörl E M and Mügschl E (1972) in Proceedings of the 5th Eur. Congr. Elect. Microsc. (EMCON 1972), ed. Cosslett V E (Institute of Physics, London and Bristol) 502

Hutson A R (1961) Bull. Amer. Phys. Soc. 6 110

Invi T and Uemura Y (1950) Progr. Theoret. Phys. 5 395

Johnson P D and Studer F J (1951) Phys. Rev. 82 976

Jones G A C, Nag B R and Gopinath A (1973) in Proceedings of the VIth Ann. SEM Symposium IITRI, Chicago, USA, 309

Jones G A C, Nag B R and Gopinath A (1974) J. Phys. D: Appl. Phys. 7 183

Jones M P, Gavrilovic J and Beaven C H J (1966) Trans. Inst. Mining and Met. (Sec B) 75 B274

Kawai H, Kuboniwa S and Hoshina T (1974) Japan J. Appl. Phys. 13 1593

Keldysh L V (1958) J E T P. 7 788

Kiflawi I, Kalman Z H, Mardix S and Steinberger I T (1972) Acta. Cryst. 24B 2110

Klasens H A (1953) J. Electrochem. Soc. 100 72

Klick C C (1952) Phys. Rev. 85 154

Klick C C and Schulman J H (1957) Solid State Phys. eds. Seitz F and Turnbull D (Academic Press, New York) 5 97

Koda T and Shionoya S (1964) Phys. Rev. 136A 541

Konitzer J D and Markham J J (1960) J. Chem. Phys. 32 843

Kroger F A and Dikhoff J (1950) Physica 16 297

Kroger F A and Hellingham J E (1948) J. Electrochem. Soc. 93 156

Kroger F A and Hellingham J E (1949) J. Electrochem. Soc. 95 68

Krolevets N M, Lepsveridze D S, Salkov E A and Shepelskii G A (1974) JETP Letters 20 24

Lax M (1952) J. Chem Phys. 20 1752

Lehmann W (1966a) J. Electrochem. Soc. 113 449

Lehmann W (1966b) J. Electrochem. Soc. 113 788

Lenard P (1910) Ann. der Phys. 31 461

Lennartz G and Laffolie H (1967) Mikrochimica Acta, Suppl. II 279

Leverenz H W (1950) in An Introduction to Luminescence of Solids (J Wiley and Son, Inc.).

Lorenz M R and Orton A (1970) in Proceedings of the 10th International Conference on the Physics of Semiconductors, Cambridge, Mass. USA. (IBM Watson Research Centre) 444

Lütz F and Gebhardt Z (1962) Z. Physik 169 475

Mahr H (1962) Phys. Rev. 125 1510

Mahr H (1963) Phys. Rev. 132 1880

Mandel G (1964) Phys. Rev. 134 A 1073

Mardix S, Kalman Z H and Steinberger I T (1968) Acta. Cryst. 24A 464

Mardix S and Steinberger I T (1970) J. Appl. Phys. 41 5339

Mardix S, Lang A R and Blech I (1971) Phil. Mag. 24 683

Markham J J (1959) Rev. Mod. Phys. 31 956

Markham J J (1966) Solid State Phys. Suppl. 8 (Academic Press, New York and London)

Marshall R and Mitra S S (1964) Phys. Rev. 134 A1019

Martienssen W (1957) J. Phys. Chem. Solids 2 257

McKeag A H and Ranby P W (1949) J. Electrochem. Soc. 96 85

Meijer H J G and Polder D (1953) Physica 19 255

Merz W J (1958) Helv. Phys. Acta 31 625

Mita Y (1964) Japan. J. Appl. Phys. 3 366

Mita Y (1965) J. Phys. Soc. Japan. 20 1822

Mita Y and Sugibuchi K (1966) in Proceedings of the International Conference on Luminescence, Budapest. ed. Szigeti G (Akadémiai Kiadó, Budapest) 1158

Möglich F, Riehl N and Rompe R (1940) Z. Tech. Phys. 21 128

Morehead F F and Title R S (1963) J. Phys. Chem. Solids 24 719

Morgan T N (1965) Phys. Rev. 139 A 343

Morozova N K, Gamosov L V and Lakin E E (1974) Opt. Spektrosk. 37 1116

Mott N F and Gurney R W (1940) in Electronic Process in Ionic Crystals (Oxford University Press, London and New York)

Muir M D, Grant P R, Hubbard G and Mundell J (1971) in Proceedings of the IVth Ann. SEM. Symposium IITRI, Chicago, USA, 401

Muir M D and Holt D B (1974) in Proceedings of the VII Ann. SEM. Symposium IITRI, Chicago, USA. 135

Muir M D (1974) in Quantitative Scanning Electron Microscopy eds. Holt D B, Muir M D, Grant P R and Boswarva I M (Academic Press, London) 3

Muir M D and Grant P R (1974) in Quantitative Scanning Electron Microscopy, eds. Holt D B, Muir M D, Grant P R and Boswarva I M (Academic Press, London) 287

Murray H D (1952) in Colour: in Theory and Practice (Chapman and Hall Ltd. London)

Neumark G P (1962) Phys. Rev. 125 838

Norris C B, Barnes C E and Beezhold W (1973) J. Appl. Phys. 44 3209

Oatley C W (1972) in The Scanning Electron Microscope: Part 1 - The Instrument (C U P)

Oliver C J and Pike E R (1968) J. Phys. D. 1 1459

Paige E G S and Rees H D (1966) Phys. Rev. Letts 16 444

Patterson D A and Klick C C (1957) Phys. Rev. 105 401

Pankove J I (1965) Phys. Rev. 140 A 2056

Pankove J I (1971) in Optical Processes in Semiconductors (Prentice - Hall: Englewood Cliffs, New Jersey)

Pease R F W and Hayes T L (1966) Nature 210 1049

Piper W W (1953) Phys. Rev. 92 23

Piper W W, Marple D T F and Johnson P D (1958) Phys. Rev. 110 323

Piper W W, Johnson P D and Marple D T F (1959) J. Phys. Chem. Solids. 8 457

Prener J S (1951) J. Electrochem. Soc. 98 406

Prener J S and Williams F E (1956) J. Electrochem. Soc. 103 342

Queisser H J and Heim U (1974) Ann. Rev. Mater. Sci. 4 125

Radkowski A (1948) Phys. Rev. 73 749

Rasul A and Davidson S M (1977) in Proceedings of the Xth Ann. SEM Symposium IITRI, Chicago, USA, to be published

Räuber A and Schneider J (1963) Phys. Letts. 3 230

Redfield D (1963a) Phys. Rev. 130 914

Redfield D (1963b) Phys. Rev. 130 916

Redfield D (1964) Trans. N. Y. Acad. Sci. 26 590

Redfield D and Afromowitz M A (1967) Appl. Phys. Lett. 11 138

Röppischer H (1968) in Proceeding of the International Conference on Luminescence 2, Budapest ed. Szigeti G (Akadémiai Kiadó, Budapest) 1855

Rose A (1973) in Vision: Human and Electronic (Plenum Press, New York and London)

Russell G A and Klick C C (1956) Phys. Rev. 101 1473

Samelson H and Lempicki A (1962) Phys. Rev. 125 901

Schneider J, Holton W C, Estle T L and Räuber A (1963) Phys. Letts. 5 312

Schneider J, Räuber A, Dischler B, Estle T L and Holton W C (1965) J. Chem. Phys. 42 1839

Schön M (1948) Ann. Physik Series 6 3 343

Schrader R E and Larach S (1956) Phys. Rev. 103 1899

Shachar G (1966) Appl. Phys. Letts. 8 282

Shachar G and Brada Y (1968) J. Appl. Phys. 39 1701

Shachar G and Brada Y (1970) J. Appl. Phys 41 3127

Shachar G, Brada Y, Alexander E and Yacobi Y (1970a) J. Appl. Phys. 41 723

Shachar G, Brada Y and Steinberger I T (1970b) J. Appl. Phys. 41 4938

Shachar G, Brada Y and Steinberger I T (1971) J. Appl. Phys. 42 872

Sheppard J J (1968) in Human Colour Perception: A Critical Study of the Experimental Foundation(American Elsevier Pub. Co., New York)

Shionoya S, Koda T, Era K and Fujiwara H (1962) in Luminescence of Organic and Inorganic Materials, eds. Kallman H P and Spruce, G M (J Wiley and Sons, Inc.) 355

Shionoya S, Koda T, Era K and Fujiwara H (1963) J. Phys. Soc. Japan, Supplement II. 18 299

Shionoya S, Koda T, Era K and Fujiwara H (1964) J. Phys. Soc. Japan 19 1157

Shionoya S, Kobayashi Y and Koda T (1965) J. Phys. Soc. Japan 20 2046

Shionoya S, Era K and Washizawa Y (1966a) J. Phys. Soc. Japan 21 1624

Shionoya S, Urabe K, Koda T, Era K and Fujiwara H (1966b) J. Phys. Chem. Solid. 27 865

Shionoya S (1967) in Proceedings of the International Conference on II - VI Semiconducting Compounds, Providence, USA. ed. Thomas D G (Benjamin Inc., New York) 1

Shionoya S (1970) J. Luminescence 1,2 17

Sidot M (1866) C. R. Acad. Sci. 63 188

Smith K C A and Oatley C W (1955) Brit. J. Appl. Phys. 6 391

Steinberger I T and Mardix S (1967) in Proceedings of the International Conference on II - VI Semiconducting Compounds, Providence, USA. ed. Thomas D G (Benjamin Inc., New York) 167

Steinberger I T, Alexander E, Brada Y, Kalman Z H, Kiflawi I and Mardix S (1972) J. Cryst. Growth 13/14 285

Steinberger I T, Kiflawi I, Kalman Z H and Mardix S (1973) Phil. Mag. 27 159

Steyn J B and Holt D B (1973) in Scanning Electron Microscopy: Systems and Applications (I O P Conference Series No.18, London and Bristol) 272

Steyn J B, Giles P L and Holt D B (1976) J. Microscopy 107 107

Street R A, Searle T M and Austin I G (1975) Phil. Mag. 32 431

Sugibuchi K (1967) Phys. Rev. 153 404

Sugibuchi K and Mita Y (1966) Phys. Rev. 147 355

Sugimoto H and Maruyama T (1967) J. Phys. Soc. Japan. 23 44

Suzuki A and Shionoya S (1971) J. Phys. Soc. Japan. 31 1455, 1462

Tauc T (1959) J. Phys. Chem. Solids 11 345

Thomas D G (1968) Phys. Today. 21 43

Thorne Lady A P (1974) in Spectrophysics (Chapman and Hall, London) 144

Thornton P R (1968) in Scanning Electron Microscopy (Chapman and Hall, London)

Toyozawa Y (1959) Progr. Thoret. Phys. 22 455

Urabe K and Shionoya S (1968) J. Phys. Soc. Japan. 24 543

Urabe K, Shionoya S and Suzuki A (1968) J. Phys. Soc. Japan. 25 1611

Urbach F (1953) Phys. Rev. 92 1324

Van Gool W and Cleiren A P (1960) Philips Res. Repts. 15 238

Van Gool W, Cleiren A P and Heijliger H J M (1960) Philips Res. Repts. 15 254

Van Gool W (1961) Philips Res. Repts. Suppl. 3

Van Roosbroeck W and Shockley W (1954) Phys. Rev. 94 1558

Vavilov V S and Britsyn K I (1961) Soviet Phys: Solid State. 2 1746

Verma A R and Krishna P (1966) in Polymorphism and Polytypism in Crystals. (J Wiley and Sons, Inc., New York)

Verneuil (1888) C.R. Acad. Sci. 106 1106

Vlasenko N A and Khomchenko V S (1973) Phys. Stat. Sol.(a) 19 K137

Von Hippel A (1936) Z. Phys. 101 680

Watkins G D (1973) Solid State Comm. 12 589

Watkins G D (1976) in Radiation Effects in Semiconductors, eds. Urli N B and Corbett J W (IOP Series No. 31, London 1977) 95

Wells O C (1974) in Scanning Electron Microscopy (McGraw-Hill, New York)

Williams F E (1951a) J. Chem. Phys. 19 457

Williams F E (1951b) Phys. Rev. 82 281

Williams F E (1957) J. Opt. Soc. America 47 869

Williams F E (1960) J. Phys. Chem. Solids. 12 265

Williams R (1962) Phys. Rev. 126 442

Williams F E and Hebb M H (1951) Phys. Rev. 84 1181

Williams P M and Yoffe A D (1968) Phil. Mag. 18 555

Williams P M and Yoffe A D (1969a) Nature 221 952

Williams P M and Yoffe A D (1969b) Radiation Effects 1 61

Williams P M and Yoffe A D (1971) in Radiation Effects in Semiconductors, eds. Corbett J W and Watkins G D (Gordon and Breach, New York) 399

Wright W D (1928) Trans. Opt. Soc. London. 30 141

Yacobi B G and Brada Y (1974) Phys. Rev. 10B 665

Yacobi B G, Brada Y, Lachish U and Hirsch C (1975) Phys. Rev. 11B 2990

Yacobi B G and Brada Y (1976) Sol. State. Comm. 18 135

Yakowitz H and Heinrich K F J (1969) J. Res. NBS. A: Phys. Chem. 73A 113

Yakowitz H (1974) in Proceedings of the VIIth Ann. SEM Symposium IITRI, Chicago. 1029

Yoffe A D, Howlett K J and Williams P M (1973) in Proceedings of the VIth Ann. SEM Symposium IITRI, Chicago, USA. 301